Novel Structures in Scattering Amplitudes and Other Boundary Correlators

by

Aidan Herderschee

A dissertation submitted in partial fulfillment
of the requirements for the degree of
Doctor of Philosophy
(Physics)
in the University of Michigan
2023

Doctoral Committee:

Professor Henriette Elvang, Chair
Professor Thomas Lam
Professor Finn Larsen
Professor James Liu
Professor Aaron Pierce

"The significance and joy in my science comes in those occasional moments of discovering something new and saying to myself, 'So that's how God did it.' My goal is to understand a little corner of God's plan."

-Henry F. Schaefer, III

Aidan Herderschee

aidanh@umich.edu

ORCID iD: 0000-0002-9957-7998

ACKNOWLEDGMENTS

TABLE OF CONTENTS

LIST OF FIGURES

LIST OF TABLES

TABLE

LIST OF APPENDICES

LIST OF ACRONYMS

YM Yang-Mills

SYM super Yang-Mills

pSYM planar super Yang-Mills

KK Kleiss-Kuijf

BCJ Bern-Carrasco-Johansson

KLT Kawai-Lewellen-Tye

LSZ Lehmann-Symanzik-Zimmermann.

WZW Wess–Zumino–Witten

CHY Cachazo-He-Yuan

DDM Duca-Dixon-Maltoni

CWI Conformal Ward Identity

HD Higher Derivative

AdS Anti-de Sitter

BCFW Britto–Cachazo–Feng–Witten

BAS Bi-Adjoint Scalar

GR General Relativity

MHV Maximal Helicity Violating

NSD Next to Self-Dual

SD Self-Dual

QFT Quantum Field Theory

EFT Effective Field Theory

Eq Equation

Ref Reference

ABSTRACT

In this dissertation, I discuss some novel structures found in the computation of scattering amplitudes and other boundary correlators. First, I describe the connection between singularities of planar amplitudes in $\mathcal{N} = 4$ super-Yang-Mills and the boundary structure of the positive kinematic region in kinematic space. I use wall-crossing to study different compactifications of the positive kinematic region and illustrate how algebraic coordinate transformations emerge from infinite sequences of rational coordinate transformations. Second, I shift to studying the double copy, an algorithm for computing scattering amplitudes in uncolored theories, such as gravity, using planar amplitudes in colored theories, such as Yang-Mills. I extend the double copy algorithm to include higher derivative corrections in the input and output amplitudes. In particular, I develop an algorithm termed the Kawai-Lewellen-Tye bootstrap to systematically determine the space of effective field theories (EFT) that can be double-copied and study how the higher derivative operators map under the double copy. Finally, I conclude by studying how these amplitude structures generalize to boundary correlators in anti-de Sitter space (AdS). I use the differential representation, where the AdS boundary correlator is represented as a collection of (non-local) differential operators acting on a contact diagram, to generalize color-kinematics duality and certain techniques for evaluating higher loop Feynman diagrams to AdS.

CHAPTER 1

Introduction

1.1 Scattering Amplitudes

Scattering is a common phenomenon in everyday life. The scattering of light allows us to see the world around us, and the scattering of sounds waves is used in echolocation. Therefore, it is natural that scattering is at the core of much fundamental physics research. For example, the scattering of high energy particles at colliders, such as the Large Hadron Collider, provides an important probe of sub-atomic physics. Additionally, scattering processes that occurred during inflation are imprinted on the cosmological microwave background and can be measured using powerful telescopes. Scattering processes relevant to colliders and cosmology are often studied using quantum field theory (QFT). QFT is a theoretical framework that synthesizes special relativity and quantum mechanics, where particles are expressed as excited states of an underlying quantum field. The QFTs of interest in this thesis are characterized by a Lagrangian, which describes the matter content and all possible interactions among the fields.

Scattering amplitudes are given by the formula

$$\mathcal{A}(i \to f) = \lim_{\substack{t_f \to \infty \\ t_i \to -\infty}} \langle f | U(t_f, t_i) | i \rangle - \langle f | i \rangle \tag{1.1}$$

where $U(t_f, t_i)$ is the time-evolution operator from t_i to t_f. We have subtracted the initial overlap between the states before time-evolving. The primary benefit of taking the limits in Eq. (1.1) is that the initial and final states can be treated as free. Significant effort has been devoted to developing better computational tools for computing scattering amplitudes. In curved spacetimes, such as anti-de Sitter space (AdS), scattering amplitudes generalize to boundary correlators. Boundary correlators are position space correlation functions where the operators are inserted on the boundary of the space. Such a generalization is natural from interpreting scattering amplitudes as position space correlation functions on the null boundary of Minkowski space. Scattering amplitudes have traditionally been computed by summing over all Feynman diagrams associated with a

given process:

$$\mathcal{A} \quad \sim \quad \text{(diagram)} \quad + \quad \text{(diagram)} \quad + \quad \text{(diagram)} \quad + \quad \ldots \tag{1.2}$$

Similarly, one sums Witten diagrams when computing boundary correlators in curved space-times:

$$\mathcal{A} \quad \sim \quad \text{(diagram)} \quad + \quad \text{(diagram)} \quad + \quad \text{(diagram)} \quad + \quad \ldots \tag{1.3}$$

Witten diagrams are graphically distinguished from Feynman diagrams by the circle at the boundary. Qualitatively, the above diagrams correspond to different virtual processes that can occur at intermediate times. The external states of the diagrams correspond to the final and initial states and are called on-shell states. The terms in these diagram expansions can be organized by the power of the coupling, which is equivalent to organizing the diagrams by the number of internal loops.

Although a generic scattering process corresponds to summing over many Feynman diagrams, the final result is often remarkably simple. However, this simplicity only becomes manifest in the correct representation. For example, in spinor-helicity notation, the tree-level scattering amplitude of Yang-Mills (YM) in four dimensions with 2 positive helicity states and $(n-2)$ negative helicity states,[1] the maximal helicity violating (MHV) sector, has a closed-form solution [1]:

$$\mathcal{A}[1^+ \ldots i^- \ldots j^- \ldots n^+] = \frac{\langle i, j \rangle^4}{\langle 1, 2 \rangle \langle 2, 3 \rangle \ldots \langle n, 1 \rangle} \ , \tag{1.4}$$

where $\langle i, j \rangle$ is roughly the square-root of $2p_i \cdot p_j$. However, the number of contributing Feynman diagrams to this process grows exponentially in the multiplicity, n, of the external states. The remarkable simplicity of the final result compared to the complexity of the Feynman diagram computation indicates there should be a more efficient approach to computing such amplitudes. There are highly efficient recursion relations for computing tree amplitudes and loop integrands in specific theories [2–4]. This pattern of complex calculations yielding simple solutions has led to the discovery of many novel structures of both mathematical and physical relevance. For example, amplitudes in $\mathcal{N} = 4$ super-Yang-Mills (SYM) can be written as volume forms of an abstract geometrical object called the Amplituhedron [5]. Alternatively, symmetries of the underlying theory can manifest as the amplitude exhibiting universal behavior in the limit that external momentum is taken to be soft [6–10]. In addition to improving computational efficiency, there is the tentative

---

[1]Helicity is the projection of spin along the direction of momentum assuming all states are outgoing.

hope that these underlying mathematical structures could also point to fundamentally new physics in the same way special relativity was hidden in Maxwell's equations.

One approach to research is to study interesting phenomena in the simplest possible setting and slowly add more complexity. In this vein, I first study the simplest scattering amplitudes known to me: scattering amplitudes in $\mathcal{N} = 4$ planar super Yang-Mills (pSYM). $\mathcal{N} = 4$ pSYM is the most supersymmetric theory that does not contain massless particles with spin greater than one, and the considerable level of symmetry is reflected in the simplicity of its amplitudes. For example, MHV $\mathcal{N} = 4$ pSYM can be written as sums of generalized polylogarithms, a particularly simple class of functions [11–17] up to seven loop order at 6-points [18], four loop at 7-point [19] and three loop order at 8-point [20]. I leverage computational control of these amplitudes to make conjectures about their singularity structure at all loop orders in chapter 2, which, along with appendix A, is adapted from my paper Ref. [21]. I then turn to the double copy, an algorithm for converting planar amplitudes into amplitudes in theories without color structure, such as general relativity (GR), in chapter 3. I generalize known double-copy algorithms to a large class of effective field theories (EFT). Chapter 3, along with appendix B, is adapted from Ref. [22], which I wrote with collaborators Huan-Hang Chi, Henriette Elvang, Callum R. T. Jones, and Shruti Paranjape. Finally, I go beyond flat space and study the boundary correlators of colored and uncolored theories in AdS using a novel differential representation in chapter 4. Using the differential representation, I show how many structures discovered in flat space generalize to boundary correlators in AdS, both at tree-level and one-loop. Chapter 4 is adapted from Ref. [23], which I wrote with collaborators Pranav Diwakar, Radu Roiban, and Fei Teng, and my paper Ref. [24]. Other works completed during my time in graduate school, Refs. [25–31], which were written in collaboration with various authors, are not included in this thesis.

1.2   The Singularity Structure of Planar Amplitudes

Planar amplitudes are natural objects in theories where the external states transform under a global or gauge group, such as YM and the non-linear sigma model. For such theories, the amplitude is a function of color-structures and kinematic data. To isolate the planar amplitudes, one expands all color-structures into sums of traces. For example, the product of structure constants, $f^{abc} f^{cde}$, is expanded as

$$f^{abc} f^{cde} \rightarrow \text{Tr}[T^a T^b T^d T^e] - \text{Tr}[T^b T^a T^d T^e] - \text{Tr}[T^a T^b T^e T^d] + \text{Tr}[T^b T^a T^e T^d] \,. \qquad (1.5)$$

The coefficients of the traces correspond to the color-ordered amplitudes:

$$\mathcal{A}^{a_1, a_2, \ldots a_n} = \sum_{\alpha \in S_{n-1}} \text{Tr}[T^{a_{\alpha_1}} T^{a_{\alpha_2}} \ldots T^{a_{\alpha_n}}] \mathcal{A}[\alpha_1, \alpha_2, \ldots, \alpha_n] \tag{1.6}$$

where S_{n-1} is the set of all permutations of $(n-1)$ external states and the $\mathcal{A}[\alpha_1, \alpha_2, \ldots, \alpha_n]$ are the color-ordered amplitudes. Importantly, only planar Feynman diagrams contribute to planar amplitudes. For a given graph to be planar under a given ordering, none of its legs must cross when the external points are ordered. For example, three trivalent tree graphs contribute to a general 4-point amplitude:

$$\tag{1.7}$$

However, the last graph has crossed lines when the external points are ordered as $\{1234\}$. Therefore, this graph is not planar under the $\{1234\}$ ordering of external states. In general, there are many more Feynman diagrams than planar diagrams. For example, the number of planar and unordered cubic tree graphs up to 7-point are

Multiplicity (n)	3	4	5	6	7
planar	1	2	5	14	42
unordered	1	3	12	75	450

It is natural to expect that planar amplitudes exhibit a simplified structure compared to amplitudes without any color-structure. However, even planar amplitudes in generic theories can be very complicated. To further simplify the problem, we restrict ourselves to planar amplitudes in $\mathcal{N} = 4$ super-Yang Mills (SYM). Due to the large amount of symmetry, amplitudes in $\mathcal{N} = 4$ SYM are very simple compared to more generic theories. For example, the theory is superconformal at the origin of moduli space, so the behavior of the theory does not change at different energy scales. The planar amplitudes of $\mathcal{N} = 4$ SYM form a closed sub-sector termed $\mathcal{N} = 4$ pSYM. Furthermore, there has been a lot of research into pushing higher loop calculations in $\mathcal{N} = 4$ pSYM, so there is a large amount of 'theoretical' data available on planar loop amplitudes at high order in perturbation theory.

We are interested in better understanding the analytic structure of planar $\mathcal{N} = 4$ pSYM amplitudes. Scattering amplitudes can be considered complex-analytic functions on kinematic space and the analytic structure of scattering amplitudes contains essential information about the underlying theory. Detailed knowledge of the analytic structure of the Feynman amplitude can significantly streamline higher loop computations. For example, the requirement that the amplitude is analytic

greatly restricts what functions can, and cannot, appear at a given loop order in perturbation theory. Higher loop amplitudes can sometimes be bootstrapped solely given knowledge of what functions can appear, their singularity structure, and some reality conditions. For example, such techniques have been used to evaluate the 6-point $\mathcal{N} = 4$ pSYM amplitude through seven loops [18].

The full analytic structure of the amplitude is beyond the scope of this dissertation and we instead focus on studying the singularity structure of the amplitude. The poles and branch-cuts of the amplitude correspond to single and multi-particle intermediate states. Locality implies that amplitudes factorize on their poles into products of lower point amplitudes. This factorization corresponds to the intermediate, single-particle state associated with the pole going on-shell. The story is similar for branch-cut singularities. As an example, consider the bubble diagram of a scalar with mass m in two dimensions interacting via a 4-point vertex:

$$
\begin{aligned}
\text{(bubble diagram)} &= \int \frac{d^2 l}{i\pi} \frac{1}{[l^2 - m^2 + i\epsilon][(l + p_1 + p_2)^2 - m^2 + i\epsilon]} \\
&= \begin{cases}
\dfrac{4 \arctan\left[\sqrt{\frac{s}{4m^2 - s}}\right]}{\sqrt{s(4m^2 - s)}} & \text{for } s < 4m^2 \\[2ex]
\dfrac{4 \arctan\left[\sqrt{\frac{s}{s - 4m^2}}\right]}{\sqrt{s(s - 4m^2)}} + \dfrac{2\pi i}{\sqrt{s(s - 4m^2)}} & \text{for } s > 4m^2
\end{cases}, \quad s = (p_1 + p_2)^2 .
\end{aligned}
\tag{1.8}
$$

The branch-cut starting at $s = 4m^2$ corresponds to the production of a 2-particle intermediate state, which naturally appears if we "cut" the bubble:

$$\tag{1.9}$$

Unlike single-particle states, multi-particle states can have any energy above a certain threshold because the particles have relative momentum contributing to their total energy. The threshold mass, in this case $4m^2$, corresponds to the branch-cut singularity. The more general l-loop sunset graphs

$$\tag{1.10}$$

have branch-cuts starting at $s = ((l+1)m)^2$, which corresponds to the mass-threshold of the $(l+1)$-particle intermediate state. These examples show how the dynamics of the multi-particle states are contained in the branch-cut structure of the amplitudes. There has been significant interest

in developing techniques to compute the singularity structure of n-point scattering amplitudes at generic loop order without directly computing the amplitude. This was a trivial exercise for the Feynman diagrams studied above but becomes much more difficult for generic Feynman diagrams, even for $\mathcal{N} = 4$ pSYM.

We study the singularity structure of planar amplitudes in $\mathcal{N} = 4$ pSYM using a conjectured connection between the singularity structure of planar amplitudes and the boundary structure of a particular region in kinematic space called the positive kinematic region. The positive kinematic region is an unphysical kinematic region where planar amplitudes are conjectured to have no poles or branch-cuts. Furthermore, all simple poles and branch-cut singularities of planar gauge amplitudes are conjectured to lie on the boundaries of the positive kinematic region. The physical significance of the positive kinematic is mysterious; there is no good physical justification for why the amplitudes' singularities should only lie on the boundary of some kinematic region. However, the positive kinematic region implicitly appears in many computations. For example, the integrands that appear in open superstring scattering amplitudes are generically divergent unless evaluated in the positive kinematic region [32, 33]. Therefore, when evaluating superstring integrands without using string field theory techniques or taking sophisticated Pochhammer contours in the string moduli space [34], one must implicitly work in the positive kinematic region, only taking an analytic continuation to generic momentum configurations at the end of the calculation.

As a simple example, consider the 4-point amplitude of the planar scalar theory:

$$\mathcal{L} = \int d^d x [\frac{1}{2}(\partial_\mu \phi^a)(\partial^\mu \phi^a) + \frac{g}{6} d^{abc} \phi^a \phi^b \phi^c] \, , \tag{1.11}$$

where the scalars transform in the adjoint representation of $SU(N)$ and $d^{abc} = \text{Tr}[T^a \{T^b, T^c\}]$. This scalar theory is not well defined non-perturbatively because its energy is not bounded from below. However, its scattering amplitudes are perturbatively well-defined and suitable as an illustrative example. The 4-point scattering amplitude is a function of Mandelstam variables s_{12}, s_{23}, and s_{13}, where

$$s_I = (\sum_{i \in I} p_i^\mu)^2 \, , \tag{1.12}$$

which are related by momentum conservation,

$$s_{12} + s_{23} + s_{13} = 0 \, . \tag{1.13}$$

The positivity conditions,

$$s_{12} > 0, \quad s_{23} > 0 \, , \tag{1.14}$$
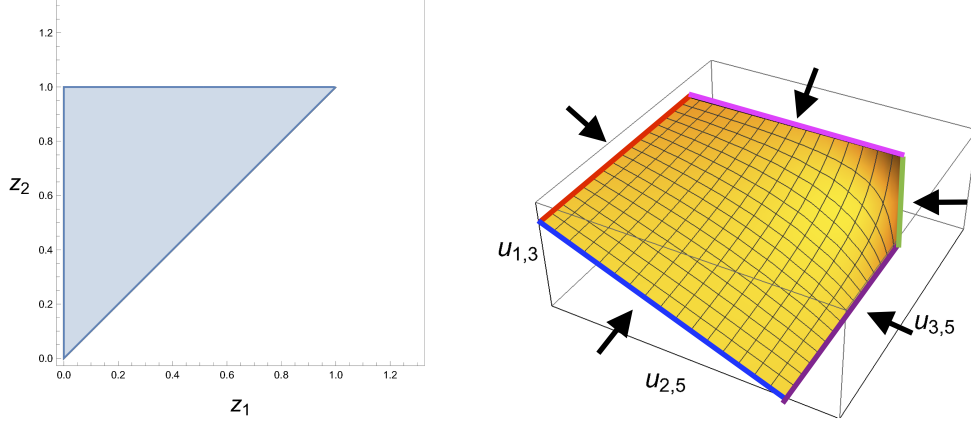
Figure 1.1: Different parameterizations of $Gr_+(2,5)/T$. In the z-variable parameterization, only three boundaries are manifest. However, the u-variable parameterization makes all five boundaries manifest.
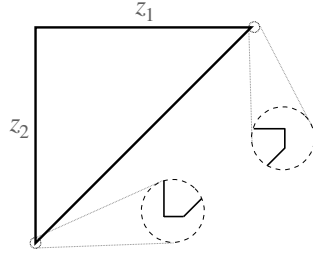
Figure 1.2: Schematic picture of blowup of $Gr_+(2,5)/T$ in the z_1, z_2 coordinates.

define the positive kinematic region. The planar 4-point tree-level amplitude is

$$\mathcal{A}[1234] = g^2(\frac{1}{s_{12}} + \frac{1}{s_{23}}) . \tag{1.15}$$

The above amplitude has simple poles at $s_{12}, s_{23} = 0$, which are precisely the boundaries of the positive region. The planar structure of the amplitude is crucial for defining the positive kinematic region. In a generic 4-point amplitude with cubic vertices, there are s_{12}, s_{23}, and s_{13} poles. However, these Mandelstam variables are related by momentum conservation (1.13).[2] At one-loop, in dimensional regularization, one continues to find branch-cut singularities at $s_{12}, s_{23} = 0$, but no other types of singularities. For example, there is no s_{13}-channel branch-cut, which would violate the conjecture.

The positive kinematic region is well studied in $\mathcal{N} = 4$ pSYM. For $\mathcal{N} = 4$ pSYM, there is even a conjecture for the positive kinematic region for all amplitudes in the maximal helicity

---

[2]It is impossible to define a convex region of the 4-point kinematic space that has boundaries at $s_{12} = 0$, $s_{23} = 0$, and $s_{13} = 0$.

violating sector (MHV), but its boundary structure is poorly understood. The kinematic space corresponds to a particular quotient of the Grassmannian, $Gr(k, n)$, the space of all k-dimensional subspaces of $\mathbb{R}^n$. $Gr(k, n)$ can be parameterized as the space of $k \times n$ matrices modulo $GL(k, \mathbb{R})$ transformations. Taking the quotient is equivalent to all the k-columns being identified under projective re-scalings. The positive regions of MHV $\mathcal{N} = 4$ pSYM amplitudes correspond to $Gr(4, n)/T$, where T corresponds to the quotient described previously, and the positive region corresponds to enforcing that all ordered minors are positive [15, 35, 36].[3] To see why studying the boundary structure of the positive region is difficult, consider the positive region of $Gr(2, 5)/T$ as a toy model. From above, $Gr(2, 5)$ corresponds to the space of 2×5 matrices

$$\mathbf{C} \sim \begin{pmatrix} a_{11} & a_{12} & a_{13} & a_{14} & a_{15} \\ a_{21} & a_{22} & a_{23} & a_{24} & a_{25} \end{pmatrix} \tag{1.16}$$

modulo $GL(2, \mathbb{R})$ transformations,

$$\forall c_{ij} \in \mathbb{R} : \quad \mathbf{C} \sim \begin{pmatrix} c_{11} & c_{12} \\ c_{21} & c_{12} \end{pmatrix} \cdot \mathbf{C} . \tag{1.17}$$

where the $\sim$ means that the left and right hand side are identified. Modding out by T corresponds to taking all the columns to be identified under projection:

$$\forall \lambda_i \in \mathbb{R}^+ : \quad \begin{pmatrix} a_{11} & a_{12} & a_{13} & a_{14} & a_{15} \\ a_{21} & a_{22} & a_{23} & a_{24} & a_{25} \end{pmatrix} \sim \begin{pmatrix} \lambda_1 a_{11} & \lambda_2 a_{12} & \lambda_3 a_{13} & \lambda_4 a_{14} & \lambda_5 a_{15} \\ \lambda_1 a_{21} & \lambda_2 a_{22} & \lambda_3 a_{23} & \lambda_4 a_{24} & \lambda_5 a_{25} \end{pmatrix} \tag{1.18}$$

The positive region corresponds to imposing that all ordered minors are positive:

$$\forall i, j \in \{1, 2, 3, 4, 5\},\ i < j : \quad \langle i, j \rangle > 0 , \tag{1.19}$$

where $\langle i, j \rangle$ denotes a minor of columns i and j. The angle brackets in eq. (1.19) should not be identified with the spinor products in eq. (1.4). Given eqs. (1.17), (1.18), and (1.19), a natural parameterization of $\mathbf{C}$ is

$$\mathbf{C} \sim \begin{pmatrix} 1 & 1 & 1 & 1 & 0 \\ 0 & z_1 & z_2 & 1 & 1 \end{pmatrix} , \tag{1.20}$$

where taking all ordered minors to be positive requires that $0 < z_1 < z_2 < 1$. This region is plotted in Fig. 1.1. Only three boundaries appear at $z_2 = 1$, $z_1 = 0$, and $z_2 = z_1$. However, consider the

---

[3]The positive kinematic region of MHV $\mathcal{N} = 4$ pSYM amplitudes is reviewed in section 2.1.1.

alternate parameterization

$$u_{i,j} = \frac{\langle i, j-1 \rangle \langle i-1, j \rangle}{\langle i, j \rangle \langle i-1, j-1 \rangle} \ . \tag{1.21}$$

The positive region corresponds to imposing $0 < u_{i,j} < 1$. These $u_{i,j}$ variables obey the non-linear relations:

$$u_{1,3} = 1 - u_{2,4} u_{2,5}, \quad \text{(Cyclic permutations)}, \tag{1.22}$$

The second plot of the positive region in Fig. 1.1 using u-variables shows that there are five boundaries, not three, which are denoted by the arrows. Each boundary corresponds to one of the $u_{i,j}$ going to zero, corresponding to either $\langle i, j-1 \rangle$ or $\langle i-1, j \rangle$ going to zero. In the parameterization given by eq. (1.20), the two additional boundaries have been shrunk to points, as visualized in Fig. 1.2. The underlying problem with eq. (1.20) is that a single set of coordinates, unless chosen very carefully, will not manifest all possible boundaries of the positive region. When we define the positive kinematic region, we denote what boundaries are included, which corresponds to choosing a particular compactification of the positive kinematic region. To denote the compactified space, we add a bar and remove the positive sign, so $Gr_+(k,n)/T$ becomes $\overline{Gr(k,n)/T}$.

The positive kinematic regions of 4-, 5-, 6- and 7-point amplitudes in $\mathcal{N} = 4$ pSYM are well understood. The maximally compactified positive kinematic region has a finite number of boundaries, and the amplitude exhibits a finite number of singularities. Furthermore, all the singularities can be simultaneously rationalized. For example, while Eq. (1.8) seems to contain a square-root branch-cut, a simple coordinate transformation removes the square-root:

$$s \rightarrow \frac{4\alpha m^2}{1 + \alpha^2} \ . \tag{1.23}$$

This coordinate transform makes manifest that only the logarithmic branch cut actually matters. However, these properties no longer hold at 8-point. At 8-point, there are algebraic branch-cuts that cannot be simultaneously rationalized with any coordinate transformation. In addition, one finds an infinite number of boundaries when one considers the maximal compactification of the 8-point positive kinematic region.

To study compactifications of the positive kinematic region, we must systematically consider all possible coordinate systems of the positive kinematic space. Performing a non-linear coordinate transformation generically leads to a discontinuous change in what boundaries are manifest. In my paper Ref. [21], I used wall-crossing to systematically study different coordinate systems and how distinct boundaries appear and disappear under coordinate transformations. The core idea is to associate a fan, called a scattering diagram, with the positive kinematic region. Each chamber in the scattering diagram is identified with a particular coordinate system that manifests some subset of the boundaries. Combining the chambers into a fan corresponds to systematically "sewing"
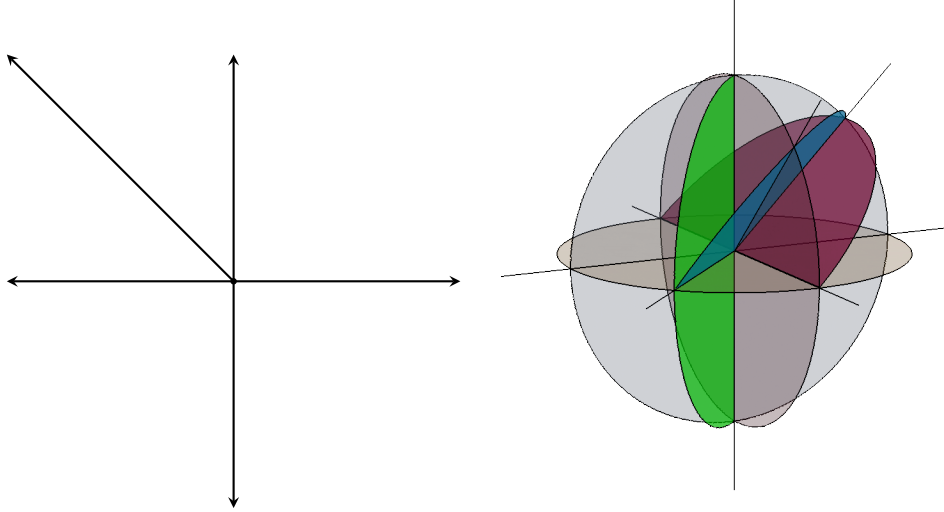
Figure 1.3: Pictures of the scattering diagrams corresponding to $\overline{Gr(2,5)/T}$ (left) and $\overline{Gr(2,6)/T}$ (right).

these coordinate systems by elementary transformations. Importantly, each chamber corresponds to a unique coordinate choice, but the *path* between non-adjacent chambers is not unique. Imposing that all paths between two chambers yield the same coordinate transform places stringent restrictions on the scattering diagram.

In chapter 2, I show how algebraic branch-cuts naturally emerge from taking particular infinite sequences of chambers, as visualized in Fig. 2.4. I develop the notion of asymptotic chambers and study these asymptotic chambers in detail, finding that algebraic coordinates naturally appear. One benefit of the wall-crossing framework is that it yields a coordinate system that simultaneously rationalizes a large subset of branch-cuts. It is possible that terms in the Feynman amplitude can be broken into different sectors for which all branch cuts can be simultaneously rationalized. However, although the notion of asymptotic chambers explains the appearance of algebraic branch-cuts, it does not explain why only a finite subset of boundaries/chambers should be relevant for the amplitude. Given that only a finite number of singularities are expected to appear at 8-point [37], we expect that the physical positive kinematic region does not correspond to a maximal compactification of the space. Unfortunately, it does not seem like the wall-crossing framework provides much insight into what partial compactification we should consider. I discuss possible prescriptions for determining which partial compactification should be chosen but do not provide any conclusive results. In particular, I propose the notion of a degenerate scattering diagram, where a subset of chambers is truncated.
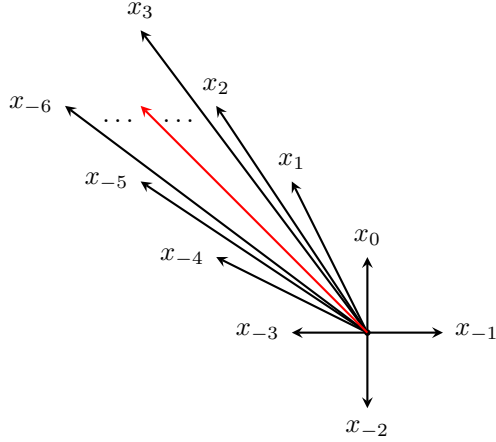
Figure 1.4: An example of a scattering fan with an infinite number of chambers
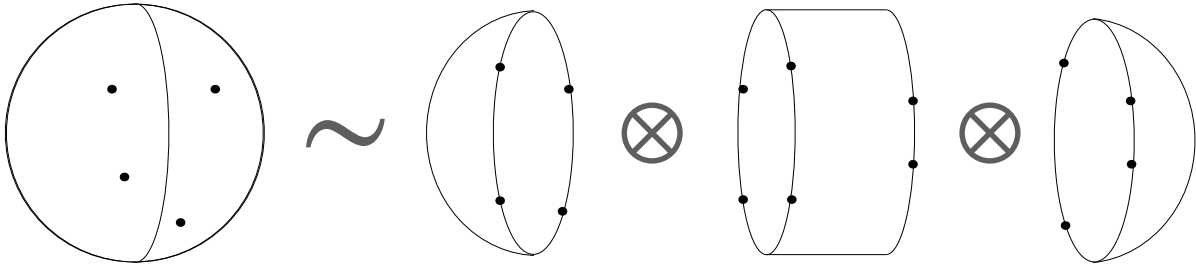
Figure 1.5: Schematic picture of the string double copy, where a closed string amplitude is derived by sewing two open string amplitudes.

1.3   Beyond Planar Amplitudes: Nonplanar Amplitudes from Double Copy

In the previous section, we discussed the singularity structure of planar amplitudes. However, many interesting amplitudes do not have any kind of color structure, such as GR amplitudes. GR amplitudes are much more difficult to compute than planar YM amplitudes because one needs to sum over all graphs, not just planar graphs. The double copy alleviates this issue by providing an algorithm for converting observables in colored theories to observables in uncolored theories, such as from YM to GR. In chapter 3, I study the double copy in the context of EFTs.

The double copy was originally found in string theory as a relation between open and closed string amplitudes as visualized in Fig. 1.5. An explicit example is illustrative. In spinor-helicity

11

notation, one 4-point gauge open string amplitude in Type-I string theory is

$$\mathcal{A}_4^{\text{Type-I}}[1^-2^-3^+4^+] = -\alpha'^2\langle 1,2\rangle^2[3,4]^2\frac{\Gamma[-\alpha's_{12}]\Gamma[-\alpha's_{23}]}{\Gamma[1-\alpha's_{12}-\alpha's_{23}]} \tag{1.24}$$

and 4-point graviton closed string amplitude in Type-IIB superstring theory is

$$\mathcal{M}_4^{\text{Type-IIB}}[1^-2^-3^+4^+] = \pi\langle 1,2\rangle^4[3,4]^4\frac{\Gamma[-\alpha's_{12}]\Gamma[-\alpha's_{23}]\Gamma[-\alpha's_{13}]}{\Gamma[1+\alpha's_{12}]\Gamma[1+\alpha's_{23}]\Gamma[1+\alpha's_{13}]} , \tag{1.25}$$

where α' corresponds to the string tension and the $\pm$ superscript denotes the helicity of the external state. The string Kawai-Lewellen-Tye (KLT) double copy is the relation

$$\mathcal{M}_4^{\text{Type-IIB}}[1^-2^-3^+4^+] = -\sin(\pi\alpha's_{12})\mathcal{A}_4^{\text{Type-I}}[1^-2^-3^+4^+]\mathcal{A}_4^{\text{Type-I}}[1^-2^-4^+3^+] , \tag{1.26}$$

which can be verified by explicit computation [38]. The KLT double copy can be derived by considering the closed-string amplitude as an integral over the moduli space of the Riemann sphere and performing a particular contour deformation.

Even though string theory is very interesting, we are interested in the structure of amplitudes in field theory. Taking the limit in which α' is asymptotically small, Eq. (1.26) leads to the field theory incarnation of the double copy

$$\mathcal{M}_4^{\text{GR}}[1^-2^-3^+4^+] = -s\mathcal{A}_4^{\text{YM}}[1^-2^-3^+4^+]\mathcal{A}_4^{\text{YM}}[1^-2^-4^+3^+] \tag{1.27}$$

where $\mathcal{M}_n^{\text{GR}}$ and $\mathcal{A}_n^{\text{YM}}[\ldots]$ are GR and planar YM amplitudes respectively,

$$\mathcal{A}_4^{\text{YM}}[1^-2^-3^+4^+] = \frac{-\langle 1,2\rangle^2[3,4]^2}{s_{12}s_{23}}, \quad \mathcal{M}_4^{\text{GR}}[1^-2^-3^+4^+] = \frac{\langle 1,2\rangle^4[3,4]^4}{s_{12}s_{23}s_{13}} . \tag{1.28}$$

The general intuition is that open string amplitudes correspond to planar amplitudes while closed string amplitudes correspond to uncolored amplitudes. Since sewing open strings yields closed strings, it is natural that uncolored amplitudes in certain theories can be written in terms of planar amplitudes.

This story generalizes to higher point amplitudes; eq. (1.26) becomes

$$\mathcal{A}_n^{L\otimes R} = \sum_{\alpha\in B_L,\beta\in B_R}\mathcal{A}_n^L[\alpha]S_n^{\alpha'}[\alpha|\beta]\mathcal{A}_n^R[\alpha] \tag{1.29}$$

at n-point, where the sum is over two choices of $(n-3)!$ orderings, B_L and B_R. The kernel, $S^{\alpha'}[\alpha|\beta]$, is defined as the inverse of the $(n-3)! \times (n-3)!$ double partial amplitudes matrix

whose elements are denoted as $m^{\alpha'}[\alpha|\beta]$ [39]:

$$S_3^{\alpha'}[123|123] = (m_3^{\alpha'}[123|123])^{-1}$$

$$S_4^{\alpha'}[1234|1234] = (m_4^{\alpha'}[1234|1234])^{-1},$$ (1.30)

$$\begin{bmatrix} S_4^{\alpha'}[12345|12345] & S_4^{\alpha'}[12345|12435] \\ S_4^{\alpha'}[12435|12345] & S_4^{\alpha'}[12435|12435] \end{bmatrix} = \begin{bmatrix} m_4^{\alpha'}[12345|12345] & m_4^{\alpha'}[12435|12345] \\ m_4^{\alpha'}[12345|12435] & m_4^{\alpha'}[12435|12435] \end{bmatrix}^{-1}.$$

Double partial amplitudes are defined by taking a *double* color-trace decomposition of the full amplitude:

$$\mathcal{A}_n = \sum_{\alpha,\beta \in S_{n-1}} \text{Tr}[T^{a_{\alpha_1}} T^{a_{\alpha_2}} \ldots] \text{Tr}[\tilde{T}^{a_{\beta_1}} \tilde{T}^{a_{\beta_2}} \ldots] m_n^{\alpha'}[\alpha|\beta] .$$ (1.31)

In the limit α' goes to zero, the $m^{\alpha'}[\alpha|\beta]$ reduce to amplitudes of the cubic bi-adjoint scalar (BAS) theory

$$\mathcal{L}_{\text{BAS}} = -\frac{1}{2}(\partial \phi^{aa'})^2 + \frac{1}{6} f^{abc} \tilde{f}^{a'b'c'} \phi^{aa'} \phi^{bb'} \phi^{cc'} .$$ (1.32)

Like eq. (1.11), the BAS theory in eq. (1.32) is not well-defined non-perturbatively, but its scattering amplitudes are perturbatively well-defined, at least at tree-level. At 3-, 4- and 5-point,

$$m_3[123|123] = g, \quad m_3[123|132] = -g ,$$

$$m_4[1234|1234] = \frac{g^2}{s_{12}} + \frac{g^2}{s_{23}}, \quad m_4[1234|1243] = \frac{-g^2}{s_{12}} ,$$ (1.33)

$$m_5[12345|12345] = \frac{g^3}{s_{12}s_{34}} + \frac{g^3}{s_{23}s_{45}} + \frac{g^3}{s_{34}s_{15}} + \frac{g^3}{s_{45}s_{12}} + \frac{g^3}{s_{15}s_{23}} .$$

In its field theory incarnation, the double copy has dramatically simplified higher-loop amplitude computations and found application in a wide range of areas. Again, the crucial point is that $\mathcal{A}^{\text{YM}}[\alpha]$ is significantly easier to compute than $\mathcal{M}^{\text{GR}}$ and the double provides an algorithm to compute $\mathcal{M}^{\text{GR}}$ from $\mathcal{A}^{\text{YM}}[\alpha]$.

The double copy applies to a large class of theories, with examples given in table 1.1. In the paper Ref. [22], which I wrote with collaborators Huan-Hang Chi, Henriette Elvang, Callum R. T. Jones, and Shruti Paranjape, we aimed to generalize the double copy to generic EFTs. The underlying principle of EFT is that one can make quantitative predictions for many systems without knowing the precise underlying theory. For example, fluid mechanics is a type of EFT. Fluid mechanics makes quantitative predictions for the behavior of fluids without referencing the subatomic nature of the fluids under study. However, fluid mechanics is only valid for low energy scales as the fluid approximation of atoms breaks down at high energies. We can take the same approach to compute scattering amplitudes in the EFT approximation. In the EFT approximation of a given scattering amplitude, contributions from physics at a high energy scale Λ, to the scattering

L / R	BAS	χPT	YM	$\mathcal{N} = 4$ pSYM
BAS	BAS	χPT	YM	$\mathcal{N} = 4$ pSYM
χPT	χPT	sGal	BI	$\mathcal{N} = 4$ sDBI
YM	YM	BI	NS-NS gravity	$\mathcal{N} = 4$ SG
$\mathcal{N} = 4$ pSYM	$\mathcal{N} = 4$ pSYM	$\mathcal{N} = 4$ sDBI	$\mathcal{N} = 4$ SG	$\mathcal{N} = 8$ SG

Table 1.1: The table shows the tree-level double-copy L $\otimes$ R for a selection of different choices of L and R models. The single-color models are χPT = chiral perturbation theory, YM, and $\mathcal{N} = 4$ pSYM. These theories double-copy as shown to: the special Galileon (sGal), Born-Infeld theory (BI), $\mathcal{N} = 4$ supersymmetric Dirac-Born-Infeld theory (sDBI), and and NS-NS gravity which is the $\alpha' \to 0$ limit of the NS-NS sector of superstring theory describing Einstein gravity coupled to a dilaton and a 2-form gauge field (in 4d the latter is dualized to an axion). Finally, SG stands for supergravity.

process at a lower energy E, are represented by a low-energy series expansion in E/Λ. When E is much less than Λ, the EFT scattering amplitude is a good approximation of the "true" scattering amplitude. For example, the small s_{12}, s_{23} expansion of the string amplitudes in eqs. (1.24) and (1.25) can be interpreted as amplitudes in particular EFTs that approximate string theory. From the perspective of the EFT Lagrangian, the low-energy expansion implies the addition of interaction terms to the Lagrangian that are arranged systematically in $1/\Lambda$ powers and incorporate an increasing number of fields and derivatives. The Wilson coefficients of these higher-order interactions encode high-energy physics. For example, at low energies, the string kernel amplitudes $m^{\alpha'}[\alpha|\beta]$ can be interpreted as amplitudes in the cubic BAS of eq. (1.32) plus some particular collection of higher derivative operators [39] where Λ corresponds to the string scale, $\Lambda^{-2} = \alpha'$. Many of the theories given in table 1.1, such as GR, are EFTs with particular choices of Wilson coefficients. The question is whether the double copy can be generalized to generic EFTs. This problem is not simply a formality but has far-reaching implications. Infinite counterterms are necessary to regulate UV divergences and finite counterterms are important for determining the (existence of) regularization schemes that preserve certain symmetries. In gravitational-wave calculations, higher-dimension operators account for finite-size corrections [40, 41].

In chapter 3, I derive a systematic extension of the double copy to include higher derivative operators. To derive a generalization of the KLT double copy, I re-interpret the double copy as an algebra on the space of theories:

$$\text{EFT}^{\text{L} \otimes \text{R}} = \text{EFT}^{\text{L}} \otimes \text{EFT}^{\text{R}} . \tag{1.34}$$

Crucially, this algebra contains an identity model which obeys

$$\mathbb{1} \otimes \mathbb{1} = \mathbb{1} \,, \tag{1.35}$$

$$L \otimes \mathbb{1} = L \,, \quad \mathbb{1} \otimes R = R \,. \tag{1.36}$$

I then recognize the identity model of interest to be cubic BAS, eq. (1.32), plus higher derivative (h.d.) operators:

$$\mathcal{L}_{\text{BAS+h.d.}} = \mathcal{L}_{\text{BAS}} + \sum_i \frac{c_i}{\Lambda^{\Delta_i - d}} \mathcal{O}_i \,. \tag{1.37}$$

Note that I do not fix c_i to their string values. The goal of the KLT bootstrap is to find higher derivative corrections to the cubic BAS theory in eq. (1.37) that are consistent with Eq. (1.35). Remarkably, eq. (1.35) implies both that the identity model is identified with the kernel and that the rank of the double partial amplitudes matrix is $(n-3)!$, which I call the minimal rank condition. The leading higher-dimension operators compatible with the minimal rank condition are

$$
\begin{aligned}
\mathcal{L} \supset & -\frac{a_{\text{L}} + a_{\text{R}}}{2\Lambda^4} f^{abx} f^{cdx} f^{a'b'x'} f^{c'd'x'} (\partial_\mu \phi^{aa'})(\partial^\mu \phi^{bb'}) \phi^{cc'} \phi^{dd'} \\
& + \frac{a_{\text{L}}}{\Lambda^4} f^{abx} f^{cdx} d^{a'b'x'} d^{c'd'x'} (\partial_\mu \phi^{aa'}) \phi^{bb'} (\partial^\mu \phi^{cc'}) \phi^{dd'} \\
& + \frac{a_{\text{R}}}{\Lambda^4} d^{abx} d^{cdx} f^{a'b'x'} f^{c'd'x'} (\partial_\mu \phi^{aa'}) \phi^{bb'} (\partial^\mu \phi^{cc'}) \phi^{dd'} + \dots \,.
\end{aligned}
\tag{1.38}
$$

One can show higher derivative corrections that are compatible with minimal rank lead to a kernel that is manifestly free of spurious poles.

Given the most general kernel, I also study how higher derivative operators map under the kernel. For a theory to be compatible with a given identity model under the KLT algebra, its planar amplitudes must obey linear relations that depend on the kernel. Such relations impose that the double copy formula in Eq. (1.29) is independent of B_L and B_R. Alternatively, these constraints can also be derived from imposing eq. (1.36). For BAS without any higher derivative corrections, the corresponding linear relations are the Kleiss-Kuijf (KK) and Bern-Carrasco-Johansson (BCJ) relations. At 4-point, these take the form

$$0 = \mathcal{A}_4[1234] + \mathcal{A}_4[1342] + \mathcal{A}_4[1423] \,, \tag{1.39}$$

$$0 = s_{12} \mathcal{A}_4[1234] - s_{13} \mathcal{A}_4[1324] \,, \tag{1.40}$$

15

along with the trace reversal identities

$$0 = \mathcal{A}_4[1234] - \mathcal{A}_4[1432] \,,$$
$$0 = \mathcal{A}_4[1342] - \mathcal{A}_4[1243] \,, \tag{1.41}$$
$$0 = \mathcal{A}_4[1423] - \mathcal{A}_4[1324] \,.$$

Eqs. (1.39), (1.40) and (1.41) are sufficient for the field theory double copy to be basis independent. For the string theory kernel, eqs. (1.39) and (1.40) becomes the string monodromy relations:

$$0 = \mathcal{A}_4[2134] + \cos(\alpha' s_{12})\mathcal{A}_4[1234] + \cos(\alpha' s_{13})\mathcal{A}_4[1324] \,.$$
$$0 = \sin(\alpha' s_{12})\mathcal{A}_4[1234] - \sin(\alpha' s_{13})\mathcal{A}_4[1324] \,. \tag{1.42}$$

For a generic kernel, the relations required by basis invariance are called the generalized KKBCJ relations. Therefore, to study how higher derivative operators in YM map to higher derivative operators in GR, I first impose that the amplitudes obey generalized KKBCJ relations. I then use the KLT double copy to compute the corresponding higher derivative operators in the resulting gravity theory. We found a number of interesting results. In our examples with the generalized KLT kernel based on BAS+h.d., we found that the double-copy contains the same operators as the standard field theory double copy, but with shifts in some of their Wilson coefficients, a phenomenon which I call "kernel equivalence."

The KLT bootstrap was further studied in Refs. [30, 31], which were written in collaboration with Henriette Elvang and Alan Shih-Kuan Chen. The detailed results of Refs. [30, 31] are beyond the scope of this dissertation, but worth summarizing to give the upshot of the program proposed in chapter 3. Refs. [30, 31] shows that constraints from the KLT bootstrap at 6-point severely constrain the kernel at 4-point. Using constraints from the KLT bootstrap at 6-point, Refs. [30, 31] give a conjecture for the most general KLT kernel compatible with the minimal rank constraint, which has a number of interesting implications. In particular, at 4-point, the minimal rank constraints fix the generalized KKBCJ relations to string monodromy relations or the field theory KK & BCJ relations. This is unexpected because the monodromy relations are intrinsically stringy and the KLT bootstrap corresponds to imposing low-energy constraints; this result points to the intrinsically stringy nature of the double-copy. The construction also clarifies the "kernel equivalence" phenomenon described above.

1.4   Beyond Flat Space: Boundary Correlators in Anti-de Sitter

We now go beyond flat space by studying boundary correlators in AdS. Boundary correlation functions in AdS space provide an important laboratory for studying quantum field theory and quantum
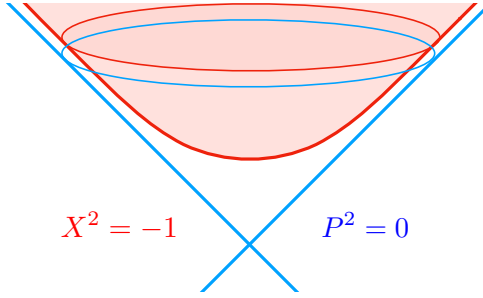
Figure 1.6: A visualization of the embedding of Euclidean AdS_2 into $\mathbb{R}^{2,1}$.

gravity. For example, boundary correlators in AdS correspond to correlation functions of gauge-invariant operators in unitary CFTs [42–45], providing a concrete realization of the holographic principle [46, 47]. AdS is arguably the simplest curved space background one can consider and is analogous to putting the theory in a box. However, AdS boundary correlators are still significantly harder to compute than scattering amplitudes. A particularly fruitful approach to searching for new methods for computing AdS boundary correlators has been generalizing established techniques for computing scattering amplitudes. In this chapter, we show that several of the properties of scattering amplitudes discussed in section 1.3 generalize to AdS boundary correlators. Using a novel representation of the AdS boundary correlator termed the differential representation, we find that KKBCJ relations generalize to planar AdS boundary correlators and that certain techniques for computing 1-loop scattering amplitudes also generalize.

The computation of boundary correlators in AdS is similar to flat space. $(d+1)$-dimensional AdS can be realized as a hyperboloid in $\mathbb{R}^{d+1,1}$ where the boundary of AdS (BAdS) corresponds to the lightcone in $\mathbb{R}^{d+1,1}$ modulo projective re-scaling

$$\text{AdS}_{d+1}: \quad (X^0)^2 - (X^1)^2 - (X^2)^2 - \ldots - (X^{d+1})^2 = R^2, \quad X^A \in \mathbb{R}^{d+1,1} . \tag{1.43}$$

$$\text{BAdS}_{d+1}: \quad (P^0)^2 - (P^1)^2 - (P^2)^2 - \ldots - (P^{d+1})^2 = 0, \quad P^A \sim \lambda P^A, \quad P^A \in \mathbb{R}^{d+1,1} .$$

which is visualized for $d = 2$ in Fig. 1.6. To compute a boundary correlator, one sums all possible graphs associated with the given scattering process. Each graph is associated with a term in the perturbative expansion of the amplitude where

- Each vertex is associated with an integration over the bulk of AdS.

- Each internal edge corresponds to a bulk-to-bulk propagator.

- Each external edge corresponds to a bulk-to-boundary propagator.

We denote boundary position coordinates as P_i. A standard Green's function differential equation

defines the propagators. For example, a cubic 4-point scalar Witten diagram can be written as

$$\begin{gathered}\Delta_2 \quad \Delta_3 \\ \Delta \\ \Delta_1 \quad \Delta_4 \end{gathered} = \int_{\text{AdS}} dX\, dY\, E_{\Delta_3}(X, P_3) E_{\Delta_4}(X, P_4) G_\Delta(X, Y) E_{\Delta_1}(Y, P_1) E_{\Delta_2}(Y, P_2)\,, \quad (1.44)$$

where $E_\Delta(X, P)$ and $G_\Delta(X, Y)$ correspond to bulk-to-boundary and bulk-to-bulk propagators respectively for a state with mass $m^2 R^2 = \Delta(\Delta - d)$. Here, R is the length scale of AdS, which we set to 1 for the remainder of this thesis.

The problem with the above procedure is that, even at tree-level, one must perform multiple non-trivial integrals over the bulk of AdS to evaluate a single Witten diagram. Tree-level scattering amplitudes, on the other hand, can be computed without any integration. The key is that we are computing the AdS correlators in position space while scattering amplitudes are almost always computed in momentum space. However, unlike flat space, Fourier transforming to momentum space does not trivialize the AdS bulk integrals. Instead, the natural analogs of momentum variables for AdS are differential operators acting on a contact diagram [48]. For example, the integral representation of the Witten diagram in eq. (4.42) can be re-written as a non-local differential operator acting on an AdS contact diagram:

$$\begin{gathered}\Delta_2 \quad \Delta_3 \\ \Delta \\ \Delta_1 \quad \Delta_4 \end{gathered} = \frac{1}{(D_1 + D_2)^2 + \Delta(\Delta - d)} \mathcal{C}_4\,, \quad \text{where} \quad \mathcal{C}_n = \begin{gathered}\Delta_3 \quad \Delta_4 \\ \Delta_2 \quad \vdots \\ \Delta_1 \quad \Delta_n \end{gathered} \quad (1.45)$$

and the D_i are conformal generators and $\mathcal{C}_n$ is the n-point AdS contact diagram. Eq. (1.45) is the same as the corresponding flat space amplitude, except that the Mandelstam variable has been replaced with a differential operator acting on the AdS contact diagram:

$$\left(\sum_{i \in I} p_i\right)^2 \to \left(\sum_{i \in I} D_i\right)^2\,. \quad (1.46)$$

In flat space, the contact diagram is simply the momentum-conserving delta-function which is universal to all amplitudes:

$$\mathcal{C}_n\big|_{\text{flat space}} = \int_{\mathbb{R}^d} d^d x \prod_i e^{ix \cdot \sum p_i} = \delta^d\left(\sum p_i^\mu\right)\,. \quad (1.47)$$

In AdS, the contact diagram is instead a non-trivial function of position coordinates

$$\left(\prod_{i=1}^{n} \frac{\Gamma(\Delta_i)}{2\pi^{d/2}\Gamma(\Delta_i - d/2 + 1)} \right) D_{\Delta_1 \ldots \Delta_n}(P_i) \qquad (1.48)$$

where the $D_{\Delta_1 \ldots \Delta_n}(P_i)$ is a D-function [49]. Such contact diagrams are simple at 3-point, but are non-trivial hypergeometric functions for generic Δ_i at 4-point and beyond.

Generalizing Eq. (1.45), the natural analog of momentum space in AdS is the differential representation

$$\mathcal{A}_n = \hat{\mathcal{A}}_n \mathcal{C}_n \,, \qquad (1.49)$$

where $\hat{\mathcal{A}}$ is a function of differential operators. For example, at 5-point,

$$= \hat{\mathcal{A}}_5^{\text{exp}} \mathcal{C}_5, \quad \hat{\mathcal{A}}_5^{\text{exp}} = \frac{1}{(D_1 + D_2)^2 (D_3 + D_4)^2} \qquad (1.50)$$

for internal states with $\Delta = d$. The primary difference between AdS and flat space is then that AdS kinematic space is non-commutative because conformal generators do not commute:

$$j \neq k : \quad [(D_i + D_j)^2, (D_i + D_k)^2] \neq 0. \qquad (1.51)$$

Therefore, the differential representation implies that AdS boundary correlators should be interpreted as functions on a non-commutative kinematic space. However, for the computations in this dissertation, this non-commutativity issue does not appear.

The differential representation of the AdS boundary correlator first appeared in stringy formulas of AdS boundary correlators in Refs. [48, 50]. In chapter 4, I provide a systematic study of the differential representation from a field theory perspective. In particular, I show that many properties of flat space scattering amplitude immediately generalize to AdS correlators using the differential representation. For example, I discussed in the previous section that YM scattering amplitudes obey KKBCJ relations, such as eq. (1.40). Given the differential representation in Eq. (1.49), I conjecture that the AdS analog of Eq. (1.40) is

$$(D_1 + D_2)^2 \mathcal{A}_4[1234] = (D_1 + D_3)^2 \mathcal{A}_4[1324] \,. \qquad (1.52)$$

I explicitly checked that Eq. (1.52) holds for YM in AdS by direct calculation. Therefore, YM

in AdS obeys some version of color-kinematics duality, at least at 4-point. I further point to the possibility of an AdS double copy using the differential representation.

In addition to showing that the differential representation simplifies computations at tree-level, I also generalize the differential representation to one-loop. The one-loop generalization of the differential representations involves developing the notion of integrating over a differential operator

$$\int [\mathcal{D}D_Q](\ldots) , \tag{1.53}$$

which I claim is the AdS generalization of the loop momentum integral

$$\int d^d l(\ldots) . \tag{1.54}$$

For example, in this framework, the bubble integral is denoted as

$$\vcenter{\hbox{}} \; = \int [\mathcal{D}D_Q] \frac{1}{(D_Q^2 - \Delta_l(d - \Delta_l))(D_{Q3}^2 - \Delta_l(d - \Delta_l))} . \tag{1.55}$$

I demonstrate the computational benefits of the one-loop differential representation by computing the bubble and triangle scalar Witten diagrams using flat-space techniques. I compared the bubble computation to a position space computation, finding agreement. To my knowledge, closed-form expressions for the triangle Witten diagram in general dimension were previously unknown [51]. These results open the door to generalizing standard techniques for evaluating flat-space higher-loop amplitudes, such as differential equations [52–55] and integration-by-parts identities [56–58], to AdS boundary correlators. The hope is such techniques can also be generalized to de Sitter without significant difficulty. For example, in Ref. [59], the differential representation at tree-level and for scalars externals was generalized from AdS to generic symmetric manifolds.

1.5   Summary

This dissertation discusses novel structures in amplitudes and AdS boundary correlators, starting from the simple theory of $\mathcal{N} = 4$ pSYM in flat-space and generalizing to more generic EFTs and boundary correlators in AdS. The positive kinematic region, color-kinematics duality, and double copy structures are studied. Color-kinematics duality is found to generalize to AdS boundary correlators at 4-point. However, even the simplest double-copy formulas do not immediately generalize to YM and GR in AdS. Future research could involve studying the AdS analog of the positive kinematic region for planar AdS boundary correlators using operator-valued integrals.

CHAPTER 2

The Positive Kinematic Region of Planar Amplitudes in $\mathcal{N} = 4$ super-Yang Mills

2.1 Overview

Amplitudes in $\mathcal{N} = 4$ pSYM are an ideal testing ground for exploring the analytic structure of planar scattering amplitudes. For instance, amplitudes in $\mathcal{N} = 4$ pSYM have a finite number of branch points associated with solutions to the Landau equations and are expected to have a finite radius of convergence in perturbation theory [37]. Significant progress has been made in understanding the structure of $\mathcal{N} = 4$ pSYM amplitudes beyond Feynman diagrams. At weak coupling, deep geometric structures, such as the amplituhedron, have emerged that provide both powerful computational techniques for computing integrands at any loop order and a radically different perspective on the nature of locality and unitarity [5, 14, 35, 60, 61]. At strong coupling, holographic calculations provide non-trivial predictions for the behavior of $\mathcal{N} = 4$ pSYM amplitudes in the form of the BDS-ansatz [62–64] and its generalizations [65, 66]. Other formalisms motivated by the duality between Wilson loops and scattering amplitudes have also emerged [67–74].

MHV amplitudes in $\mathcal{N} = 4$ pSYM are particularly simple and have been useful litmus tests for conjectures. MHV n-point amplitudes are transcendental functions of fixed weight at each loop order that can be expressed in terms of multi-polylogarithms (MPLs) at all orders calculated to date [11–17].[1] These transcendental functions of weight W, F_W, are the generalizations of logarithms that obey extremely nice properties. Primarily, the *symbol* provides a map from the amplitude to a sum of W-fold tensor products:

$$F \to \sum F_0^{\phi_{\alpha_1}, \phi_{\alpha_2}, \dots, \phi_{\alpha_W}} \left[\log(\phi_{\alpha_1}) \otimes \log(\phi_{\alpha_2}) \otimes \dots \otimes \log(\phi_{\alpha_W}) \right], \tag{2.1}$$

---

[1]Using the Grassmannian form of $\mathcal{N} = 4$ pSYM loop integrands, one can directly show all integrals in the MHV (and NMHV) sector can be written as iterated integrals of $d\log$-forms [14]. Unfortunately, this does not necessarily mean they integrate to a function that can be written in terms of MPLs [75].

where F_0 are rational numbers. Each factor in the tensor product behaves similarly to a logarithm, leading to properties like

$$[\ldots \otimes \log(\phi_1\phi_2) \otimes \ldots] = [\ldots \otimes \log(\phi_2) \otimes \ldots] + [\ldots \otimes \log(\phi_1) \otimes \ldots] . \tag{2.2}$$

The ϕ_i in eq. (2.1) are functions of external kinematic data and correspond to branch points of F_W. The set of all ϕ that can appear in eq. (2.1) is called the symbol alphabet of F_W.

The symbol provides a very transparent understanding of the analytic structure of F_W. We will focus on finding a minimal symbol alphabet, a set of multiplicatively independent letters that all letters in the original symbol alphabet can be written as monomials of. For example, consider the initial symbol alphabet $\{\phi_1, \phi_2, \phi_1\phi_2\}$. One minimal symbol alphabet is $\{\phi_1, \phi_2\}$ as $\phi_1\phi_2$ factors into ϕ_1 and ϕ_2. An alternative minimal symbol alphabet is $\{\phi_2, \phi_1\phi_2\}$, as $\phi_1 = (\phi_1\phi_2)/\phi_2$. Given a minimal symbol alphabet, one can use eq. (2.2) to construct a complete basis of possible tensors. Finding a minimal symbol alphabet of the 8-point MHV amplitude would be a major achievement and open up the possibility of bootstrapping 8-point MHV higher loop amplitudes. We take an important step towards this goal by proposing a minimal symbol alphabet for algebraic letters.

2.1.1 The Positive Kinematic Region

Scattering amplitudes are functions on kinematic space. The positive kinematic region is a region of kinematic space where planar gauge theory amplitudes are conjectured to have no poles or branch cuts. More precisely, in all examples studied to date, the Landau equations admit no solutions when the external data is taken to be in the positive kinematic region. The positive kinematic region for a given ordering of externals, $\alpha \in \text{Perm}[1, 2, \ldots, n]$, is associated with the region where all planar variables are positive definite,

$$X_{i,j} = \left(\sum_{a=i}^{j-1} p_{\alpha(a)} \right)^2 > 0 , \tag{2.3}$$

Since we are studying the positive kinematic region of massless planar gauge theory amplitudes in 4 dimensions, we parameterize our external kinematic data using momentum twistors [15]; Z_i^A is the momentum twistor of state i and the A index transforms in the fundamental representation of the dual conformal algebra, $SU(2,2)$. Individual momentum twistors are projective:

$$Z_i^A \sim t_i Z_i^A . \tag{2.4}$$

Therefore, the kinematic space of the n-point amplitude can be interpreted as a quotient of the Grassmannian, $Gr(4, n)/T$, where T acts on columns by a re-scaling. The positive kinematic region is then a quotient of the positive Grassmannian, $Gr_+(4, n)/T$, cut out by the inequalities

$$0 < \langle i, j, k, l \rangle \text{ when } i < j < k < l \,, \tag{2.5}$$

where $\langle \ldots \rangle$ corresponds to a minor of columns "...".[2] As explained in section 1.2, we need to consider a particular compactification of this space.

2.1.2 Critically Positive Coordinates and Cluster Algebras

Previous research into the connection between the positive kinematic region and $\mathcal{N} = 4$ pSYM amplitudes has generally focused on the cluster algebra structure of the positive kinematic region [15, 18, 76–87].[3] More concretely, the positive kinematic region of MHV $\mathcal{N} = 4$ pSYM amplitudes corresponds to a $\mathcal{X}$-type cluster algebra[4] which associates to the positive kinematic region a set of *critically positive* coordinates called $\hat{y}$-variables. A coordinate that is critically positive vanishes on at least one boundary of the positive region. Although each cluster parameterization makes only a sub-set of boundaries manifest, considering all cluster parameterizations together allows one to study all the possible boundaries. At 6-point and 7-point, the symbol alphabet, the ϕ_i in eq. (2.1), consists solely of the $\hat{y}$-variables, implying that $\hat{y}$-variables correspond to logarithmic branch cuts! Calculations are further simplified by considering a minimal multiplicative basis of $\hat{y}$-variables instead of the set of $\hat{y}$-variables themselves. Given an initial cluster, one minimal multiplicative basis consists of the $\hat{y}$-variables of an initial cluster, $\hat{y}_i$, along with some non-factorable Laurent polynomials of $\hat{y}_i$. We denote this set of non-factorable Laurent polynomials as $\mathcal{O}(\mathcal{X})$.

Starting at 8-point, two problematic features appear in the cluster algebra approach:

- There are an infinite number of $\hat{y}$-variables in the cluster algebra.

- Algebraic letters start to appear in the symbol alphabet.

Several approaches to tackling these problems have appeared in the literature and significant progress has been made.

---

[2]This is only true in the MHV sector. Beyond MHV, the kinematic region is most naturally interpreted as bundles over $Gr(4, n)/T$ [35, 36].

[3]Note that alternate approaches have also been very successful without directly referencing the cluster algebra structure of the positive kinematic region. The $\bar{\mathcal{Q}}$ approach in particular has been extremely useful in probing $n \geq 8$ higher loop amplitudes [88–90]. Computations with irrational Yangian invariants provide a very clever probe of the algebraic letters [91–93]. Finally, studying branch points using Landau-equations and the amplitudhedron have allowed direct computations of the singularity structure at high loop order [94–96].

[4]A quick introduction to cluster algebras is provided in appendix A.1.
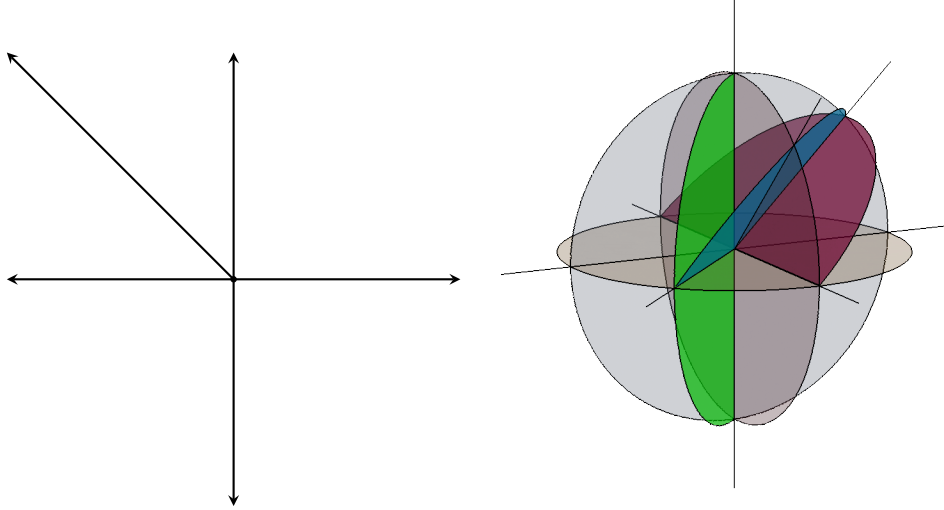
Figure 2.1: Pictures of the scattering diagrams corresponding to $\overline{Gr(2,5)/T}$ (left) and $\overline{Gr(2,6)/T}$ (right).

The first problem is troublesome because a key restriction for calculations at 6-point and 7-point is that the symbol alphabet is finite. Upon finding that the cluster algebra is infinite at 8-point, one might be tempted to assume that the symbol alphabet at 8-point is also infinite. However, it has been proven that the n-point amplitude in $\mathcal{N} = 4$ pSYM has a finite number of branch points associated with solutions to the Landau equations [37], implying that the symbol alphabet could also be finite. Following this train of thought, several truncation procedures have been proposed, motivated by connections between stringy canonical forms and compactifications of configuration spaces [36, 97–100].

The second problem has proven a major obstacle for interpreting letters as cluster variables because cluster variables are rational by construction. Multiple methods have been developed to extract algebraic functions from cluster algebras and then match these functions with algebraic letters that appear in direct calculations [36, 91, 92, 101, 102]. We use the term cluster algebraic letters as an umbrella term for all such cluster-like variables that are algebraic.[5] However, no unified picture has emerged that provides a systematic understanding of these cluster algebraic functions.

---

[5]Notably, the initial definition of cluster algebraic functions in Ref. [36] only included 2 algebraic letters for each limiting ray in the $\overline{Gr(4,8)/T}$ g-vector fan. However, at least 18 algebraic letters seem to appear in the MHV 3-loop amplitude at 8-point [20, 89].

2.1.3 Scattering Diagrams and Asymptotic Chambers

In this chapter, we propose wall crossing, and scattering diagrams more specifically, as a useful framework to address these issues [103–108]. Wall crossing has found applications in a number of research areas, such as the moduli spaces of $\mathcal{N} = 2$ gauge theories and black hole entropy formulas [109–114]. However, we are not studying any kind of entropy formula or moduli space, but instead compactifications of the positive kinematic region, $\overline{Gr(4, n)/T}$. The application of wall crossing and scattering diagrams to partial compactifications is best understood in the context of mirror symmetry [103, 108, 115], but such a discussion is unfortunately beyond the scope of this chapter.[6] Instead, we take a more practical approach, giving a computational definition of a scattering diagram with examples and then making the connection to cluster algebras. We argue that scattering diagrams, which represent a more general mathematical framework than cluster algebras, are useful for studying cluster algebraic functions that appear in the symbol alphabet of $\mathcal{N} = 4$ pSYM.

The scattering diagram of a rank N cluster algebra corresponds to a fan in $\mathbb{Z}^N$, where each cone in the fan corresponds to a different coordinate system for $\mathcal{X}$. Cones of the scattering diagram correspond to clusters of the cluster algebra. In the case of finite cluster algebras, crossing between adjacent cones in the scattering diagram always corresponds to a cluster mutation. For example, the scattering diagrams of $\overline{Gr(2, 5)/T}$ and $\overline{Gr(2, 6)/T}$ are provided in fig. 2.1. Crucially, the scattering diagram perspective motivates an alternate set of coordinates for $\mathcal{X}$, denoted as $\hat{y}_\gamma$-variables. For a given cone/cluster, the $\hat{y}_\gamma$-variables can be written as monomials of the $\hat{y}$-variables and vice-versa. Therefore, the $\hat{y}_\gamma$-variables and $\hat{y}$-variables have the same multiplicative basis.

In the finite case, the walls corresponding to cluster mutations define a complete scattering diagram. In some sense, the finite scattering diagram is simply a rewriting of the cluster algebra and contains no new information. In the infinite case, where there are an infinite number of cones, scattering diagrams are a genuine generalization of the cluster algebra framework. In particular, infinite sequences of cones appear in the scattering diagrams that asymptotically approach limiting rays, as schematically drawn in fig. 2.2. We use these infinite sequences of cones to define the notion of asymptotic chambers: cones that are asymptotically close to the limiting ray. Although there are always an *infinite* number of walls as you approach the limiting ray, we argue that walls not intersecting the limiting ray can be ignored when calculating relations between the $\hat{y}_\gamma$-variables in this asymptotic limit. For example, there are 6 asymptotic chambers in fig. 2.2 as only three

---

[6]The schematic connection between mirror symmetry and cluster algebras is as follows. We can interpret $\mathcal{X}$ as the blow-up of an associated toric geometry. Cluster transformations correspond to changing the blow up description by an elementary transformation. Scattering diagrams provide a framework to systematically "sew" these different parameterizations together using a fan defined by tropical points of the dual mirror manifold, $\mathcal{A}^\vee$. This framework is famous for giving a geometric interpretation of the connection between tropical points of $\mathcal{A}^\vee$ and regular functions on $\mathcal{X}$ using mirror symmetry.
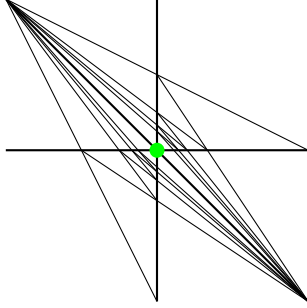
Figure 2.2: A schematic representation of the cone structure near the limiting ray in some 3-dimensional scattering diagram. We are looking down on the limiting ray, which corresponds to the green dot.

walls intersect the limiting ray. We can calculate relations between the $\hat{y}_\gamma$-variables of distinct asymptotic chambers using the wall crossing framework.

The initial motivation for asymptotic chambers actually came from $\mathcal{N} = 2$ super-symmetric gauge theories. For specific $\mathcal{N} = 2$ gauge theories on $\mathbb{R}^3 \times S^1$, the moduli space corresponds to a $\mathcal{X}$-type cluster algebra [110]. This connection between cluster algebras and $\mathcal{N} = 2$ gauge theories led to a number of interesting results, such as a connection between canonical bases of the cluster algebra and the set of simple line defects in the theory [113]. The concept of an asymptotic chamber was proposed in Ref. [110], although initial calculations were first performed in Section 5.9 of Ref. [109] using different terminology. Later generalizations made connections between asymptotic chambers and Fenchel-Nielsen coordinates of (higher) Teichmuller spaces [116–118]. However, to our knowledge, the notion of asymptotic chambers in the context of higher dimension scattering diagrams has been largely unstudied for general $\mathcal{X}$ spaces.

Crucially, although the $\hat{y}$-variables often diverge in the asymptotic limit, the $\hat{y}_\gamma$-variables themselves remain finite. These "asymptotic" $\hat{y}_\gamma$-variables correspond to the algebraic letters that appear in the 8-point symbol alphabet! Using scattering diagrams and the notion of asymptotic chambers, we conjecture a complete multiplicative basis for all algebraic letters that could appear in the $\mathcal{N} = 4$ pSYM symbol alphabet at 8-point. Remarkably, we found at most 52 multiplicatively independent algebraic letters associated with the asymptotic chambers. This result systematizes the techniques in refs. [101, 102], which effectively analyzed a particular subset of asymptotic chambers and did not study the relations between the algebraic letters of different asymptotic chambers.

The scattering diagram approach also offers a new perspective on proposed truncation procedures for $\hat{y}$-variables. We take a similar philosophy to refs. [36, 101, 102], arguing that the positive kinematic region is not maximally compactified, so not all boundaries appear. However, in contrast to refs. [36, 101, 102], which argue for a truncation of the x-variables, we instead argue for a truncation of clusters in the cluster algebra, or equivalently cones in the scattering diagram. We further

argue that such a truncation naturally leads to the notion of asymptotic chambers and algebraic critical coordinates.

2.1.4 Notation

We denote the cluster variables associated with $\mathcal{A}$ and $\mathcal{X}$ as x and $\hat{y}$ respectively. This notation differs from refs. [36, 101], which denote cluster variables associated with $\mathcal{A}$ and $\mathcal{X}$ as a and x respectively. Furthermore, we denote mutations of the kth node as μ_k. For example, $x_i = \mu_k x_i$ if $i \neq k$. Finally, we often denote cluster algebras using the notation $A_{p_1,p_2,\ldots,p_n}$, because these cluster algebras correspond to the Teichmuller space of bordered Riemann surfaces. The cluster algebra $A_{p_1,p_2,\ldots,p_n}$ corresponds to the Teichmuller space of a Riemann surface with n borders and p_i punctures on border i. For those unfamiliar with the connection between cluster algebra and surfaces, this notation is unimportant for our applications to $\mathcal{N} = 4$ pSYM but is nice for organizational purposes.

2.2 Wall crossing, Cluster Algebras, and Asymptotic Chambers

In this section, we develop the notion of scattering diagrams and asymptotic chambers. We begin with a short introduction to g-vectors before giving a relation between the scattering diagram and the g-vector fan of the cluster algebra. We then develop the notion of asymptotic chambers, using the $A_{1,1}$ cluster algebra as our guide.

2.2.1 Principal Quivers and the g-vector Fan

Our goal is to find a minimal multiplicative basis of the $\hat{y}$-variables that parameterize the positive region of $\mathcal{X}$. Unfortunately, the set of $\hat{y}$-variables is very difficult to study for a cluster algebra with generic frozen variables. For example, $\hat{y}$-variables will not always be independent. To see the problem, consider the initial quiver,

$$x_1 \longrightarrow x_2 \longleftarrow x_3$$

so

$$\hat{y}_1 = \frac{1}{x_2}, \quad \hat{y}_2 = x_1 x_3, \quad \hat{y}_3 = \frac{1}{x_2} . \tag{2.6}$$

Without any frozen nodes, we trivially see that $\hat{y}_1 = \hat{y}_3$. However, suppose we include the frozen node

$$
\begin{array}{c}
y_1 \\
\downarrow \\
x_1 \longrightarrow x_2 \longleftarrow x_3 \;,
\end{array}
$$

so $\hat{y}_1 = y_1/x_2$ and $\hat{y}_1 \neq \hat{y}_3$. From this example, it is clear that the frozen nodes play a crucial role in distinguishing $\hat{y}$-variables. One approach to this problem is to simply add frozen nodes until the $\hat{y}$-variables are maximally disambiguated [119, 120]. Only a finite, albeit large, number of frozen nodes are necessary to maximally disambiguate the $\hat{y}$-variables.

However, we are not interested in the set of all $\hat{y}$-variables but instead finding a multiplicatively independent basis. Given that any $\hat{y}$-variable can be written as a monomial of x-variables, we only need to maximally disambiguate x-variables of the cluster algebra, not the $\hat{y}$-variables. We are therefore motivated to consider a cluster algebra with a principal quiver [119]. To construct a principal quiver, consider an initial quiver without any frozen nodes. Then add a frozen node, y_i, to each non-frozen node, x_i, with an edge pointing from the frozen node to the mutable node. For example, the quiver

$$
\begin{array}{cc}
y_1 & y_2 \\
\downarrow & \downarrow \\
x_1 \longrightarrow & x_2
\end{array}
\tag{2.7}
$$

is a principle quiver of the A_2 cluster algebra. Remarkably, the frozen nodes of a principal quiver are enough to maximally disambiguate all x-variables! Details of this statement are provided in appendix A.2. We subsequently study cluster algebras with principle quivers to study the multiplicative basis of $\hat{y}$-variables of cluster algebras with arbitrary frozen nodes. Furthermore, we can choose any quiver of our cluster algebra to be the principal quiver. is a principle quiver of the A_2 cluster algebra. Remarkably, the frozen nodes of a principal quiver are enough to maximally disambiguate all x-variables! Details of this statement are provided in appendix A.2. We subsequently study cluster algebras with principle quivers to study the multiplicative basis of $\hat{y}$-variables of cluster algebras with arbitrary frozen nodes. Furthermore, we can choose any quiver of our cluster algebra to be the principal quiver.

We now turn to the problem of understanding the relation between $\hat{y}$-variables and x-variables for a cluster algebra with a principal quiver. Although we cannot write a direct map from $\hat{y}$ to x, attempting to do so allows us to associate a canonical vector to each x-variable. Suppose we start with the principal quiver. Any x-variable in the cluster algebra can be written as a Laurent polynomial of the x-variables and y-variables of the principle quiver. It is not generally possible to re-write this Laurent polynomial entirely in terms of $\hat{y}$-variables. However, it can be written as a polynomial of $\hat{y}$-variables of the principle quiver up to a monomial of x-variables of the principle

x_i	F_i	g_i
x_1	1	$(1, 0)$
x_2	1	$(0, 1)$
x_3	$1 + \hat{y}_1$	$(-1, 1)$
x_4	$1 + \hat{y}_1 + \hat{y}_1 \hat{y}_2$	$(-1, 0)$
x_5	$1 + \hat{y}_2$	$(0, -1)$

Table 2.1: The $F(\hat{y}_i)$ polynomials and g-vectors of the A_2 cluster algebra.

quiver:

$$x = x^{\vec{g}} F(\hat{y}_i), \quad x^{\vec{g}} = \prod_i x_i^{g_i} , \tag{2.8}$$

where $F(\hat{y}_i)$ is a Laurent polynomial in $\hat{y}$-variables of the principal quiver, which we denote as $\hat{y}_i$. No two x-variables share the same g-vector, allowing us to associate a canonical g-vector to each element of the cluster algebra. As an illustrative example, again consider the A_2 cluster algebra. The $\hat{y}$-variables of (2.7) are

$$\hat{y}_1 = y_1 x_2^{-1}, \quad \hat{y}_2 = y_2 x_1 . \tag{2.9}$$

Upon mutating x_1, we find

$$x_3 = \frac{y_1 + x_2}{x_1} = \frac{x_2}{x_1}(1 + \hat{y}_1)$$
$$\rightarrow \vec{g} = (-1, 1), \quad F(\hat{y}_i) = 1 + \hat{y}_1 . \tag{2.10}$$

Mutating through all clusters yields all $F(\hat{y}_i)$ polynomials and g-vectors of the A_2 cluster algebra, which are provided in table 2.1. Each cluster defines a cone bounded by the g-vectors of the x-variables in the cluster. Remarkably, the cones associated with distinct clusters are nonoverlapping, which is not at all obvious from the above definition. The collection of these cones defines a (sometimes incomplete) fan.

In summary, we reduced the problem of finding a multiplicative basis of the $\hat{y}$-variables of a cluster algebra with generic frozen variables to finding a multiplicative basis of the $\hat{y}$-variables of a cluster algebra with a principal quiver. We then used the $\hat{y}$-variables of the principle quiver to find a map from x-variables to g-vectors.

2.2.2 Scattering Diagrams and Wall Crossing

In this section, we introduce the notion of scattering diagrams and wall crossing, following the review in Ref. [121]. We then show how cluster algebras fit into the wall crossing framework,

using the A_2 cluster algebra as our primary example.

A scattering diagram is defined on a lattice, $\mathbb{Z}^N$. We denote vectors as γ and basis vectors as γ_i.[7] A scattering diagram requires three pieces of input data:

- A collection of cones bounded by co-dimension 1 walls. Each wall in the scattering diagram is associated with a scalar function, $f(y)$.

- N coordinates on $\mathcal{X}$, denoted as $\hat{y}_{\gamma_i}$. Each coordinate corresponds to a basis vector.[8]

- A skew-symmetric matrix, $B^0_{i,j}$, that defines a skew-symmetric[9] product for the γ,

$$\langle \gamma_i, \gamma_j \rangle = \gamma_i \cdot B^0 \cdot \gamma_j \, . \tag{2.11}$$

Each cone in the fan is associated with a particular parameterization of $\mathcal{X}$ similar to how the $\hat{y}$-variables of a cluster correspond to a particular parameterization of $\mathcal{X}$. Crossing a wall between two cones corresponds to a coordinate transformation.

We now describe the coordinate transformation. Each co-dimension one wall is associated with a vector, $\gamma^\perp$, perpendicular to the wall,

$$\gamma^\perp = a_i \gamma_i \, . \tag{2.12}$$

The sign of $\gamma^\perp$ is chosen so $\gamma^\perp$ points opposite the direction one is mutating across the wall. Furthermore, the magnitude of $\gamma^\perp$ is chosen so that all of its components, the a_i in eq. (2.12), are integers whose least common denominator is 1. Finally, we associate a unique monomial, $\hat{y}_{\gamma^\perp}$, to each $\gamma^\perp$:

$$\hat{y}_{\gamma^\perp} = \left(\prod \hat{y}_{\gamma_i}^{a_i} \right)^{\text{Sign}(\gamma^\perp \cdot \vec{N})} \, , \tag{2.13}$$

$$\vec{N} = (1, 1, \ldots, 1) \, . \tag{2.14}$$

For example, for a wall with the perpendicular vector $\gamma^\perp = (0, \ 1, \ 1)$, the associated monomial is

$$\hat{y}_{(0, \ 1, \ 1)} = \hat{y}_{\gamma_2} \hat{y}_{\gamma_3} \, . \tag{2.15}$$

Due to the $\text{Sign}(\gamma^\perp \cdot \vec{N})$ exponent, the perpendicular vector $\gamma^\perp = (0, \ -1, \ -1)$ is associated with

---

[7]For example, if $N = 3$, then $\gamma_1 = (1, \ 0, \ 0)$, $\gamma_2 = (0, \ 1, \ 0)$ and $\gamma_3 = (0, \ 0, \ 1)$.

[8]We use the notation $\hat{y}_{\gamma_i}$, instead of $\hat{y}_i$, to distinguish them from $\hat{y}$-variables.

[9]The scattering diagram framework can also be applied when the product is skew-symmetrizable instead of just skew-symmetric, but the following formulas requires modifications. See Ref. [110].

the same monomial,

$$\hat{y}_{(0,\,-1,\,-1)} = \hat{y}_{\gamma_2}\hat{y}_{\gamma_3} \; . \tag{2.16}$$

This makes sense as $(0,\,-1,\,-1)$ and $(0,\,1,\,1)$ correspond to the same wall and should therefore be associated with the same monomial. Although $\gamma^\perp$ flips sign depending on the direction you are mutating across the wall, $\hat{y}_{\gamma^\perp}$ is the same due to the $\text{Sign}(\gamma^\perp \cdot \vec{N})$ exponent. The mutation relation for $\hat{y}_{\gamma_i}$ across a wall is

$$\hat{y}_{\gamma_i} \to \hat{y}_{\gamma_i} f(\hat{y}_{\gamma^\perp})^{\langle \gamma_i, \gamma^\perp \rangle} \; , \tag{2.17}$$

which gives the $\hat{y}_{\gamma_i}$ of the new cone in terms of $\hat{y}_{\gamma_i}$ of the initial cone. To see eq. (2.17) in an explicit example, suppose we are crossing from cone C_1 to cone C_2 in fig. 2.3a, where we fix,

$$B^0_{i,j} = \begin{bmatrix} 0 & 1 \\ -1 & 0 \end{bmatrix} , \tag{2.18}$$

and $f(y) = 1 + y$ for all walls. The perpendicular vector for the relevant wall is $\gamma^\perp = (0,1)$, so $\hat{y}_{\gamma^\perp} = \hat{y}_{\gamma_2}$. Applying eq. (2.17), the $\hat{y}_{\gamma_i}$ of chamber C_2 are then

$$\begin{aligned}
\hat{y}_{\gamma_1} &= \hat{y}^{\mathrm{I}}_{\gamma_1}(1 + \hat{y}^{\mathrm{I}}_{\gamma_2})^{(1,0)\cdot B^0\cdot(0,1)} = \hat{y}^{\mathrm{I}}_{\gamma_1}(1 + \hat{y}^{\mathrm{I}}_{\gamma_2}) \; , \\
\hat{y}_{\gamma_2} &= \hat{y}^{\mathrm{I}}_{\gamma_2}(1 + \hat{y}^{\mathrm{I}}_{\gamma_2})^{(0,1)\cdot B^0\cdot(0,1)} = \hat{y}^{\mathrm{I}}_{\gamma_2} \; ,
\end{aligned} \tag{2.19}$$

where $\hat{y}^{\mathrm{I}}_{\gamma_i}$ corresponds to the $\hat{y}_{\gamma_i}$ of cone C_1.

For a scattering diagram to be self-consistent, the relations between the $\hat{y}_{\gamma_i}$ of any two cones should be path independent. To see why self-consistency is non-trivial, again consider the scattering diagram in fig. 2.3a with the same $B^0_{i,j}$ and $f(y)$. Applying eq. (2.17) to each path in fig. 2.3a, we find

$$\begin{aligned}
\begin{pmatrix} \hat{y}^{\mathrm{I}}_{\gamma_1} \\ \hat{y}^{\mathrm{I}}_{\gamma_2} \end{pmatrix} &\to \begin{pmatrix} \hat{y}^{\mathrm{I}}_{\gamma_1} \\ \frac{\hat{y}^{\mathrm{I}}_{\gamma_2}}{\hat{y}^{\mathrm{I}}_{\gamma_1}+1} \end{pmatrix} \to \begin{pmatrix} \hat{y}^{\mathrm{I}}_{\gamma_1}\left(\frac{\hat{y}^{\mathrm{I}}_{\gamma_2}}{\hat{y}^{\mathrm{I}}_{\gamma_1}+1}+1\right) \\ \frac{\hat{y}^{\mathrm{I}}_{\gamma_2}}{\hat{y}^{\mathrm{I}}_{\gamma_1}+1} \end{pmatrix} , \\[2mm]
\begin{pmatrix} \hat{y}^{\mathrm{I}}_{\gamma_1} \\ \hat{y}^{\mathrm{I}}_{\gamma_2} \end{pmatrix} &\to \begin{pmatrix} \hat{y}^{\mathrm{I}}_{\gamma_1}\left(\hat{y}^{\mathrm{I}}_{\gamma_2}+1\right) \\ \hat{y}^{\mathrm{I}}_{\gamma_2} \end{pmatrix} \to \begin{pmatrix} \hat{y}^{\mathrm{I}}_{\gamma_1}\left(\hat{y}^{\mathrm{I}}_{\gamma_2}+1\right) \\ \frac{\hat{y}^{\mathrm{I}}_{\gamma_2}}{\hat{y}^{\mathrm{I}}_{\gamma_1}\left(\hat{y}^{\mathrm{I}}_{\gamma_2}+1\right)+1} \end{pmatrix} ,
\end{aligned} \tag{2.20}$$

where $\hat{y}^{\mathrm{I}}_{\gamma_i}$ again corresponds to the $\hat{y}_{\gamma_i}$ of the initial cone, C_1. The scattering diagram in fig. 2.3a is inconsistent as the $\hat{y}_{\gamma_i}$ associated with C_3 are not path independent. To make the scattering diagram self-consistent, we must include the additional wall $\gamma^\perp = (1,1)$, leading to the scattering diagram
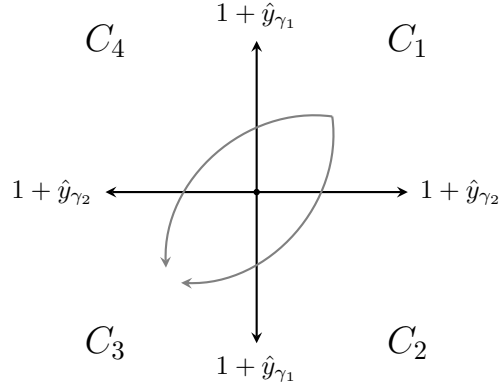
(a) Inconsistent scattering diagram.
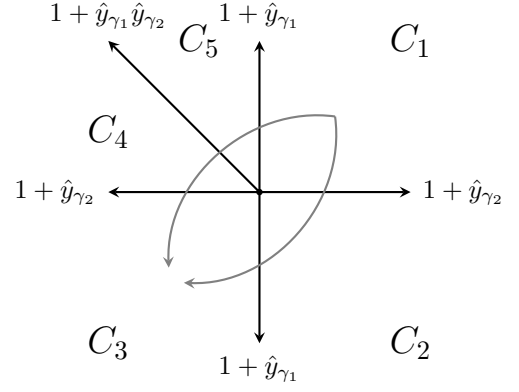
(b) Self-consistent scattering diagram.

Figure 2.3: Two examples of scattering diagrams. The scattering diagram on the left is inconsistent if $B_{i,j}^0$ equals eq. (2.18). The relations between $\hat{y}_\gamma$ is not path independent, as shown in eq. (2.20). The scattering diagram on the right is path-independent and can be identified with the A_2 cluster algebra.

in fig. 2.3b. Including this second wall, the first line in eq. (2.20) becomes

$$
\begin{pmatrix} \hat{y}_{\gamma_1}^{\mathrm{I}} \\ \hat{y}_{\gamma_2}^{\mathrm{I}} \end{pmatrix} \rightarrow \begin{pmatrix} \hat{y}_{\gamma_1}^{\mathrm{I}} \\ \frac{\hat{y}_{\gamma_2}^{\mathrm{I}}}{\hat{y}_{\gamma_1}^{\mathrm{I}}+1} \end{pmatrix} \rightarrow \begin{pmatrix} \hat{y}_{\gamma_1}^{\mathrm{I}} \left(\frac{\hat{y}_{\gamma_1}^{\mathrm{I}} \hat{y}_{\gamma_2}^{\mathrm{I}}}{\hat{y}_{\gamma_1}^{\mathrm{I}}+1} + 1 \right) \\ \frac{\hat{y}_{\gamma_2}^{\mathrm{I}}}{\hat{y}_{\gamma_1}^{\mathrm{I}} \left(\hat{y}_{\gamma_2}^{\mathrm{I}}+1 \right)+1} \end{pmatrix} \rightarrow \begin{pmatrix} \hat{y}_{\gamma_1}^{\mathrm{I}} \left(\hat{y}_{\gamma_2}^{\mathrm{I}} + 1 \right) \\ \frac{\hat{y}_{\gamma_2}^{\mathrm{I}}}{\hat{y}_{\gamma_1}^{\mathrm{I}} \left(\hat{y}_{\gamma_2}^{\mathrm{I}}+1 \right)+1} \end{pmatrix} , \tag{2.21}
$$

which now matches the second line of eq. (2.20).

We now describe the connection between cluster algebras and scattering diagrams. The relation between scattering diagrams and cluster algebras is that the g-vector fan defines a scattering diagram where each cluster is dual to a cone in the scattering diagram. The $B_{i,j}^0$ matrix that defines the skew-symmetric product in eq. (2.11) corresponds to the exchange matrix of the principal quiver. For a cluster algebra with a finite number of cones, each wall corresponds to a cluster mutation and we fix

$$
f(y) = 1 + y \tag{2.22}
$$

for all walls. We call the walls that correspond to cluster mutations, *cluster walls*. The $\hat{y}$-variables of a given cone are the $\hat{y}_{\gamma^\perp}$ associated with each wall that bounds the cone,

$$
\hat{y}_j = \prod \hat{y}_{\gamma_i}^{a_i^j}, \quad \gamma_j^\perp = a_i^j \gamma_i , \tag{2.23}
$$

where $\gamma_i^\perp$ is the $\gamma^\perp$ associated with $\hat{y}_i$. Note that $\gamma_j^\perp$ points inward from the cone in this convention.

Furthermore, the exchange matrix of the quiver associated with a cone is

$$B_{i,j} = \langle \gamma_i^\perp, \gamma_j^\perp \rangle \,. \tag{2.24}$$

For example, for the cone associated with the principle quiver, the principle cone, we have

$$\gamma_i^\perp \big|_{\text{Principle Cone}} = \gamma_i \tag{2.25}$$

so

$$\hat{y}_{\gamma_i}\big|_{\text{Principle Cone}} = \hat{y}_i, \quad B_{i,j}\big|_{\text{Principle Cone}} = \gamma_i \cdot B^0 \cdot \gamma_j = B^0_{i,j} \,. \tag{2.26}$$

The cluster mutation in eq. (A.11) corresponds to both a wall crossing transform, eq. (2.17), and a mutation in the $\gamma_i^\perp$. To see this, again consider the cluster algebra associated with the quiver

$$
\begin{array}{ccc}
y_1 & & y_2 \\
\downarrow & & \downarrow \\
x_1 & \longrightarrow & x_2 \,.
\end{array}
$$

The explicit computation of the g-vectors in table 2.1 reveals that it is the same as fig. 2.3b. Consider a mutation from cone C_1 to C_2. The $\hat{y}_{\gamma_i}$ mutation is given by eq. (2.19) and the $\gamma_i^\perp$ mutate as

$$
\begin{aligned}
\gamma_1^\perp &= (1,0) \to \gamma_1^\perp = (1,0) \,, \\
\gamma_2^\perp &= (0,1) \to \gamma_2^\perp = (0,-1) \,.
\end{aligned}
\tag{2.27}
$$

Combining eqs. (2.19) and (2.27), the mutation relation for $\hat{y}_i$ is

$$
\begin{pmatrix} \hat{y}_1 \\ \hat{y}_2 \end{pmatrix} \to \begin{pmatrix} \hat{y}_1(1+\hat{y}_2) \\ \frac{1}{\hat{y}_2} \end{pmatrix} \,,
\tag{2.28}
$$

which exactly matches the mutation relation for $\hat{y}$-variables. Again, note that it was a combination of mutating $\gamma_i^\perp$ and $\hat{y}_{\gamma_i}$ that gave the cluster mutation relation for the $\hat{y}$-variables.

We can also consider the scattering diagrams of more complex cluster algebras, such as the A_3 cluster algebra

$$
\begin{array}{ccccc}
y_1 & & y_2 & & y_3 \\
\downarrow & & \downarrow & & \downarrow \\
x_1 & \longrightarrow & x_2 & \longrightarrow & x_3 \,,
\end{array}
$$

which is associated with $\overline{Gr(2,6)/T}$. Since the cluster algebra is rank 3, the associated scattering
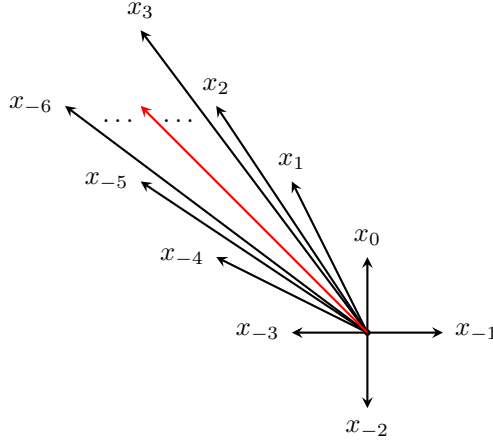
Figure 2.4: g-vector fan associated with the $A_{1,1}$ cluster algebra. There are an infinite number of cluster variables whose g-vectors approach a limiting ray, $\vec{g}_{lim} = (-1, 1)$. The explicit form of the g-vectors is provided in eq. (2.31).

diagram is 3 dimensional. From direct calculation, we found the scattering diagram given in fig. 2.1 in the Introduction. The walls are now 2 dimensional and defined by the span of two g-vectors. To find the wall associated with the $\hat{y}$-variable of a specific quiver, consider all the g-vectors bounding the dual cone except the g-vector of the x variable associated with the same node as the $\hat{y}$-variable. The span of these two g-vectors defines the wall associated with the $\hat{y}$-variable.

In summary, scattering diagrams are a useful framework that provide a nice way to study canonical coordinate transformations on $\mathcal{X}$. Finding self-consistent scattering diagrams is naively quite hard since you need to check that the relations between the $\hat{y}_{\gamma_i}$ of any two cones are path independent. The g-vector fans of finite cluster algebras provide a class of self-consistent scattering diagrams where cluster mutations correspond to a very specific type of wall crossing.

2.2.3 Asymptotic Chambers and Limiting Walls

We now turn to infinite cluster algebras. We will show how the scattering diagram framework provides a systematic way to study the multiplicative basis of $\hat{y}_i$ even when the $\hat{y}_i$ themselves go to infinity. Although $|\gamma_i^\perp| \to \infty$ in certain limits, so $\hat{y}_i \to \{\infty, 0\}$, the $\hat{y}_\gamma$-variables remain finite.

We first show that the g-vector fans of infinite cluster algebras need to include additional walls that do not correspond to cluster mutations. Furthermore, we will find the functions attached to these walls are not elements of the cluster algebra and can be identified with the mysterious cluster

algebraic functions of Ref. [36]. We will study the cluster algebra defined by the principal quiver

$$
\begin{array}{ccc}
y_{-1} & & y_0 \\
\downarrow & & \downarrow \\
x_{-1} & \Longrightarrow & x_0 \ ,
\end{array}
$$

as our motivating example. A review of relevant derivations and formulas for this cluster algebra are provided in appendix A.3. The key results are a closed form solution for x_i with $i > 0$,

$$
\begin{aligned}
x_i &= \frac{1}{2^{i+2}}[(x_{-1} + B_+ \sqrt{\triangle})(\mathcal{P} + \sqrt{\triangle})^{i+1} + (x_{-1} - B_+ \sqrt{\triangle})(\mathcal{P} - \sqrt{\triangle})^{i+1}] \ , \\
\mathcal{P} &= \frac{y_{-1}}{x_{-1}x_0} + \frac{x_0}{x_{-1}} + \frac{x_{-1}y_{-1}y_0}{x_0} \ , \\
B_+ &= \frac{2x_0 - x_{-1}\mathcal{P}}{\triangle} \ , \\
\triangle &= \mathcal{P}^2 - 4y_{-1}y_0 \ ,
\end{aligned}
\tag{2.29}
$$

and an equation for $\hat{y}_{2n-1}$ and $\hat{y}_{2n}$ in terms of x-variables after $2n$ mutations,

$$
\hat{y}_{2n-1} = y_0^n y_{-1}^{2n+1} x_{2n}^{-2}, \quad \hat{y}_{2n} = y_0^{1-2n} y_{-1}^{-2n} x_{2n-1}^2 \ .
\tag{2.30}
$$

The g-vectors, denoted by black arrows in fig. 2.4, are

$$
\vec{g}_i = \begin{cases} (-i, i+1) & i \geq -1 \\ (2+i, -i-3) & i \leq -2 \end{cases} \ .
\tag{2.31}
$$

We will now show that the self-consistency of the scattering diagram requires the existence of a new wall associated with the limiting ray that does not correspond to a standard cluster mutation.

Consider cones that are asymptotically close to the limiting ray. Importantly, the $\hat{y}_i$ variables go to 0 or ∞ as we approach the limiting ray, which can be seen from eqs. (2.29) and (2.30). To calculate $\hat{y}_{\gamma_i}$ in this limit, we first express $\hat{y}_{\gamma_i}$ in terms of monomials of $\hat{y}$-variables. From the scattering diagram in fig. 2.4, the $\gamma_i^\perp$ associated with the $\hat{y}_i$ in eq. (2.30) are

$$
[\gamma_{-1}^\perp]^{2n} = (1 + 2n, 2n), \quad [\gamma_0^\perp]^{2n} = (-2n, 1 - 2n) \ ,
\tag{2.32}
$$

where $[\gamma_i^\perp]^{2n}$ is the perpendicular vector to the wall associated with node x_i after $2n$ mutations. We subsequently found that

$$
\begin{aligned}
\gamma_1 &= (1 - 2n)[\gamma_{-1}^\perp]^{2n} - 2n[\gamma_0^\perp]^{2n} \ , \\
\gamma_2 &= 2n[\gamma_{-1}^\perp]^{2n} + (2n + 1)[\gamma_0^\perp]^{2n} \ .
\end{aligned}
\tag{2.33}
$$

35
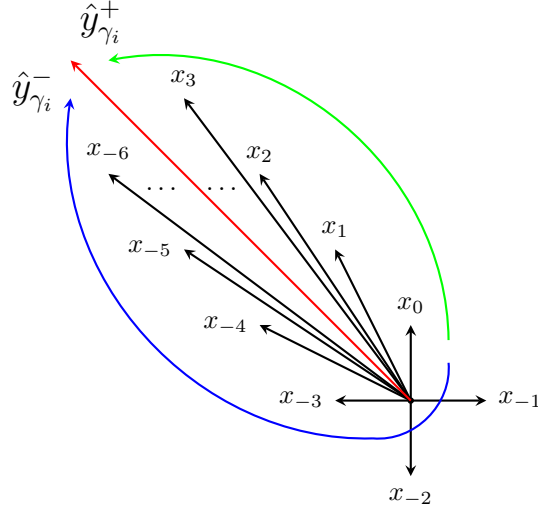
Figure 2.5: g-vector fan associated with the $A_{1,1}$ cluster algebra. There are two paths to cones asymptotically close to the limiting ray (red), which are green and blue respectively. The green path leads to the $\hat{y}_{\gamma_i}^+$ expressions while taking the blue path leads to the $\hat{y}_{\gamma_i}^-$ expressions.

Combining eqs. (2.23) and (2.33) gives a formula for $\hat{y}_{\gamma_i}$ in the asymptotic limit, denoted as $\hat{y}_{\gamma_i}^+$,

$$
\begin{aligned}
\hat{y}_{\gamma_1}^+ &= \lim_{n\to\infty} (\hat{y}_{2n-1})^{1-2n}(\hat{y}_{2n})^{-2n} = 16y_{-1}(x_{-1} + B_+\sqrt{\triangle})^{-2}(\mathcal{P} + \sqrt{\triangle})^{-2} \,, \\
\hat{y}_{\gamma_2}^+ &= \lim_{n\to\infty} (\hat{y}_{2n-1})^{2n}(\hat{y}_{2n})^{2n+1} = \frac{y_0}{4}(x_{-1} + B_+\sqrt{\triangle})^2 \,.
\end{aligned}
\tag{2.34}
$$

We used the explicit formulas for $\hat{y}_i$ in eqs. (2.29) and (2.30) to write the final expressions for $\hat{y}_{\gamma_1}^+$ and $\hat{y}_{\gamma_2}^+$ in terms of our initial cluster variables: y_{-1}, y_0, x_{-1} and x_0. The final expressions in eq. (2.34) are finite and provide a multiplicative basis for the $\hat{y}$-variables asymptotically close to the limiting wall if one approaches from the right. A visualization of the path is given by the green line in fig. 2.5. We then repeated the same calculation, but following the blue line in fig. 2.5. If one approaches from the left, the asymptotic limits of $\hat{y}_{\gamma_i}$, denoted as $\hat{y}_{\gamma_i}^-$, are

$$
\begin{aligned}
\hat{y}_{\gamma_1}^- &= \hat{y}_{\gamma_1}^+ \left(1 - \frac{\mathcal{P} - \sqrt{\mathcal{P}^2 - 4y_{-1}y_0}}{\mathcal{P} + \sqrt{\mathcal{P}^2 - 4y_{-1}y_0}}\right)^{-4} \,, \\
\hat{y}_{\gamma_2}^- &= \hat{y}_{\gamma_2}^+ \left(1 - \frac{\mathcal{P} - \sqrt{\mathcal{P}^2 - 4y_{-1}y_0}}{\mathcal{P} + \sqrt{\mathcal{P}^2 - 4y_{-1}y_0}}\right)^4 \,.
\end{aligned}
\tag{2.35}
$$

The fact that eqs. (2.34) and (2.35) are not equal indicates that the scattering diagram must include another wall to be self-consistent. However, eq. (2.35) can be re-written into the suggestive form

$$
\hat{y}_{\gamma_i}^- = \hat{y}_{\gamma_i}^+ (1 - \hat{y}_{\gamma^\perp})^{-2\langle\gamma_i,\gamma^\perp\rangle}, \quad \hat{y}_{\gamma^\perp} = \hat{y}_{\gamma_1}^+\hat{y}_{\gamma_2}^+ = \hat{y}_{\gamma_1}^-\hat{y}_{\gamma_2}^-, \quad \gamma^\perp = (1,1)\,,
\tag{2.36}
$$

which can be matched to eq. (2.17) by requiring $f(\hat{y}) = (1 - \hat{y})^{-2}$. Eq. (2.36) shows that we must include a *limiting wall* with $\gamma^\perp = (1, 1)$ for the scattering diagram to be self-consistent. The $\hat{y}_{\gamma^\perp}$ associated with the limiting wall,

$$
\begin{aligned}
\hat{y}_{\gamma^\perp} &= \hat{y}_{\gamma_1}^+ \hat{y}_{\gamma_2}^+ \,, \\
&= \frac{\mathcal{P} - \sqrt{\mathcal{P}^2 - 4y_{-1}y_0}}{\mathcal{P} + \sqrt{\mathcal{P}^2 - 4y_{-1}y_0}} \,,
\end{aligned}
\tag{2.37}
$$

takes exactly the right form for eq. (2.36) to be matched with eq. (2.17). The limiting wall corresponds to the red line in figs. 2.4 and 2.5. Performing a mutation across this limiting wall cannot be identified with a cluster mutation in the $A_{1,1}$ scattering diagram. From the perspective of the cluster algebra, these cones are separated by an infinite number of cluster mutations. Finally, the $\hat{y}_{\gamma^\perp}$ of the limiting wall obeys the bound $0 < \hat{y}_{\gamma^\perp} < 1$ in contrast to normal $\hat{y}$-variables which are just positive definite.

We now briefly compare our result to previous computations in the literature. Notably, one multiplicative basis of $\hat{y}_{\gamma_i}^\pm$ is the three algebraic functions identified in Ref. [102] for a given $A_{1,1}$ cluster algebra. Furthermore, due to the bound $0 < \hat{y}_{\gamma^\perp} < 1$, the cluster algebraic function attached to the limiting walls seem more like the u-variables identified in refs. [98, 122], which obey similar bounds, than standard $\hat{y}$-variables. Finally, note that the $\hat{y}_{\gamma^\perp}$ attached to the limiting wall is a ratio of the cluster algebraic functions defined in Ref. [36].

Moving beyond $A_{1,1}$, we now turn to a more general discussion. We define asymptotic chambers as cones asymptotically close to the limiting ray that are separated by walls intersecting the limiting ray. For higher dimension scattering diagrams, both limiting walls and cluster walls intersect the limiting ray. Furthermore, there are always cluster walls asymptotically close to the limiting ray which do not intersect the limiting ray and become more parallel to the limiting walls as one approaches the limiting ray. These walls are *asymptotic walls*. An example is sketched in fig. 2.6 [123]. For our definition of asymptotic chambers to be self-consistent, we must be able to ignore asymptotic walls if we are infinitesimally close to the limiting ray. If the $\hat{y}_{\gamma_i}$ associated with asymptotic chambers transformed non-trivially when crossing an asymptotic wall, the $\hat{y}_{\gamma_i}$ of asymptotic chambers would not be well defined. For example, consider the asymptotic chambers C_2 and C_5 in fig. 2.6. If $\hat{y}_{\gamma_i}$ transformed non-trivially across the asymptotic walls, it would be ambiguous which $\hat{y}_{\gamma_i}$ was associated with the asymptotic chamber.

To see whether asymptotic walls are relevant when infinitesimally close to the limiting ray, let us consider crossing one of these asymptotic walls. From the definition of asymptotic walls, the
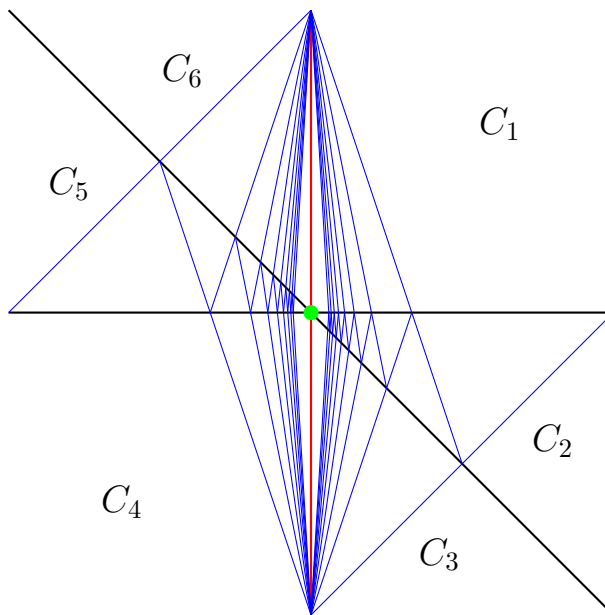
Figure 2.6: A schematic representation of the cone structure near the limiting ray of $A_{2,1}$, a rank 3 cluster algebra. The full scattering diagram is 3 dimensional and we are looking down on the limiting ray, which is indicated by the green dot. The red line corresponds to the limiting wall. The black lines correspond to cluster walls that intersect the limiting ray. The blue lines correspond to asymptotic walls, cluster walls that do not intersect the limiting wall and become more parallel with a limiting wall as one approaches the limiting ray. There are 6 asymptotic chambers, each labeled by C_i.

$\gamma^\perp$ of the asymptotic wall asymptotes to

$$\gamma^\perp \to \lim_{n\to\infty} n \times \gamma^\perp_{lim} \, , \tag{2.38}$$

where $\gamma^\perp_{lim}$ is the $\gamma^\perp$ of the limiting wall that the asymptotic wall approaches. Therefore, the wall crossing formula for the asymptotic wall reduces to

$$\hat{y}_{\gamma_i} \to \lim_{n\to\infty} \hat{y}_{\gamma_i} (1 + \hat{y}^n_{\gamma^\perp_{lim}})^{n\langle\gamma_i, \gamma^\perp_{lim}\rangle} \, , \tag{2.39}$$

which naively diverges. However, in the previous example, we found that $0 < \hat{y}_{\gamma^\perp_{lim}} < 1$ for $A_{1,1}$. If this bound holds for general $\hat{y}_{\gamma^\perp_{lim}}$, then eq. (2.39) becomes trivial and the asymptotic walls can be ignored when asymptotically close to the limiting ray. We therefore conjecture the bound

$$0 < \hat{y}_{\gamma^\perp_{lim}} < 1 \, , \tag{2.40}$$

in $\mathcal{X}$ for all asymptotic chambers, not just those adjacent to the limiting wall. Eq. (2.40) is a very remarkable bound and a key conjecture of this chapter. We explicitly checked that eq. (2.40) held for all examples studied in section 2.4.

In summary, the key insight is that the $\hat{y}_{\gamma_i}$ associated with asymptotic chambers are finite and can be algebraic functions of our initial coordinates. Furthermore, these $\hat{y}_{\gamma_i}$ obey the wall crossing formula as we mutate around the limiting ray. To find all the $\hat{y}_{\gamma_i}$ associated with a limiting ray, we simply need to find all the walls in the g-vector fan that intersect the limiting ray and then use the wall crossing formula in eq. (2.17). The primary difficulty is finding all the walls that intersect the limiting ray.

2.3 Algorithm for Finding Asymptotic Chambers from $A_{1,1}$ Subalgebra

We now outline a search algorithm we used to find the asymptotic chambers associated with a limiting ray. In normal search algorithms for finite cluster algebras, one performs sequences of mutations until one finds all the cones in the fan, defining a cone by its associated g-vectors. This method does not work well for infinite cluster algebras where there are an infinite number of cones, even asymptotically close to the limiting ray. We partially circumvented this issue by defining a new equivalence class of cones arbitrarily close to the limiting ray called *pre-asymptotic* chambers.

We first mutate the initial quiver until we find a quiver containing an $A_{1,1}$ subalgebra:

$$x_i \Longrightarrow x_j \,,$$

which we define as the principal quiver. To calculate the g-vectors and walls of adjacent cones, we use the g-vector mutation formula originally derived in Ref. [119]:

$$\mu_k \vec{g}_i = \begin{cases} \vec{g}_i & \text{if } i \neq k \\ -\vec{g}_i + \sum_{m=1}^{N} [B_{m,k}]_+ \vec{g}_m - \sum_{m=1}^{N} [B_{N+m,k}]_+ \vec{b}_m & \text{if } i = k \end{cases} , \qquad (2.41)$$

where $[x]_+ = \max(x, 0)$ and $\vec{b}_m$ is column m of the initial $B_{i,j}$ matrix. This formula can be derived by combining eq. (A.9) in appendix A.1,

$$\mu_k x_i = \begin{cases} \frac{1}{x_i} (\prod_{j \to i} x_j + \prod_{j \leftarrow i} x_j) & i = k \\ x_i & i \neq k \end{cases} , \qquad (2.42)$$

with eq. (2.8) in section 2.2.1:

$$x = x^{\vec{g}} F(\hat{y}_i), \quad x^{\vec{g}} = \prod_i x_i^{g_i} . \qquad (2.43)$$

This allowed us to compute the g-vectors of adjacent cones in the g-vector fan very efficiently. Using eq. (2.41), we calculated the g-vectors of cones associated with repeated mutations on nodes x_i and x_j. The g-vectors of the x_i and x_j nodes asymptotically approached a limiting ray, $\vec{g}_{lim}$. In principle, we could now perform a brute force search, performing random mutations asymptotically close to the limiting ray until we found no new walls intersecting the limiting ray. However, this approach would be highly inefficient as there are always an infinite number of cones asymptotically close to the limiting ray. Although we did perform a brute-force search, we partially streamlined the algorithm by defining a new equivalence class of cones: pre-asymptotic chambers.

Consider the schematic scattering diagram in fig. 2.6, which corresponds to the $A_{2,1}$ cluster algebra. Suppose we mutate to one of the cones in the sequence that approaches the asymptotic chamber C_1. Mutating across an asymptotic wall toward or away from the limiting ray does not give us any new information. In some sense, the sequence of cones approaching C_1 are equivalent, and therefore redundant, for the purposes of trying to find walls intersecting the limiting ray. We wish to find some criterion that allows us to avoid mutating into these redundant cones. To see what this criterion should be, we first note that the sequence of g-vectors along the black cluster wall generically obey the relation

$$\vec{g}(x_n) - \vec{g}(x_{n-1}) = \vec{g}_{lim} . \qquad (2.44)$$

Therefore, it is natural to consider the projection of the g-vectors onto the hyperplane perpendicular to the limiting ray, such that

$$\mathbf{P}_\perp(\vec{g}(x_n) - \vec{g}(x_{n-1})) = \mathbf{P}_\perp \vec{g}_{lim} = \vec{0} \,. \tag{2.45}$$

If we define equivalence classes of cones by considering the projection of their g-vectors, not the g-vectors themselves, the sequence of cones approaching C_1 correspond to the same cone under this projection. This is true for the sequences of cones approaching C_3, C_4, and C_6 as well. For C_2 and C_5, we find two classes of cone upon taking the projection. To see why, let us focus on C_2. Denoting the projection of the g-vectors on the two bordering cluster walls as g_a and g_b, the two classes of cones are defined by the sets $\{g_a, g_a, g_b\}$ and $\{g_a, g_b, g_b\}$. Turning to more general cluster algebras, we define pre-asymptotic chambers as the equivalence classes of cones defined by the projection of g-vectors onto the hyperplane perpendicular to the limiting ray. Certain infinite sequences of cones approaching the same asymptotic chamber correspond to the same equivalence class under this projection.

The final subtlety to consider is that we found only a subset of the asymptotic chambers when we performed our initial search of pre-asymptotic chambers asymptotically close to the limiting ray. We could not find all pre-asymptotic chambers from a single search because we cannot use the mutation rule in eq. (2.41) to mutate across limiting walls. Fortunately, the asymptotic scattering diagrams considered have only one limiting wall each. We checked how many limiting walls appear by studying the asymptotic walls that appear in our brute force search. For a limiting wall to appear, asymptotic walls almost parallel the limiting wall should appear during the brute force search of cones asymptotically close to the limiting ray. However, all asymptotic walls associated with the same limiting ray search were asymptotically parallel to the same limiting wall. We subsequently assumed that only one limiting wall appears in the asymptotic scattering diagram. Furthermore, we found that the limiting wall fully divides the asymptotic scattering diagram. In other words, there is no "short-cut" around the limiting wall. Therefore, we performed two searches of the pre-asymptotic chambers, one on each side of the limiting wall.

2.4   Explicit Calculations of Asymptotic Chambers

Our goal is to compute a minimal multiplicative basis for $\hat{y}_{\gamma_i}$ asymptotically close to limiting rays, the *asymptotic symbol alphabet*. We now describe an algorithm for finding the asymptotic symbol alphabet associated with a limiting ray. A brute force search algorithm for finding asymptotic chambers is given in appendix 2.3. Once we found all the asymptotic chambers associated with a given limiting ray, the calculation for finding the associated symbol alphabet proceeded as follows:

1. Starting from the initial quiver, we performed mutations until we found a quiver with an $A_{1,1}$ subalgebra. We chose the quiver with the $A_{1,1}$ subalgebra as the principal quiver for the purposes of defining the scattering diagram and g-vectors.

2. Repeating the computation in section 2.2.3 for the $A_{1,1}$ subalgebra, we computed the $\hat{y}_{\gamma_i}$ of an initial asymptotic chamber in terms of the $\hat{y}_i$ of the principal quiver. We denote the $\hat{y}_{\gamma_i}$ of the initial asymptotic chamber as $\hat{y}^0_{\gamma_i}$.

3. We computed the $\hat{y}_{\gamma_i}$ of all other asymptotic chambers in terms of the $\hat{y}^0_{\gamma_i}$ using wall crossing.

4. We found a complete multiplicative basis of the asymptotic chambers' $\hat{y}_{\gamma_i}$ in terms of $\hat{y}^0_{\gamma_i}$.

The multiplicative basis calculated in the final step is the asymptotic symbol alphabet associated with the limiting ray. Although each element of the multiplicative basis will be a rational function of $\hat{y}^0_{\gamma_i}$, the $\hat{y}^0_{\gamma_i}$ will themselves often be algebraic functions of $\hat{y}_i$.

For the remainder of this section, we study a variety of cluster algebras using the above algorithm. We first dissect some lower rank cluster algebras, discussing a variety of phenomena that appear. We then move onto $\overline{Gr(4,8)/T}$, conjecturing a complete algebraic symbol alphabet for the 8-point MHV amplitude. We conclude this section by commenting on how we may need to modify the above algorithm when faced with more general types of limiting rays.

2.4.1 Lower Rank Cluster Algebras

We now consider the asymptotic chambers of some lower rank cluster algebras, finding several interesting phenomena:

- $A_{2,1}$: Both cluster walls and limiting walls can intersect the limiting ray, leading to more non-trivial cluster algebraic functions.

- $A_{2,2}$: The scattering diagram associated with the limiting ray is not simple. A simple fan is an N-dimensional fan for which all cones are bound by N walls.[10]

- $A_{1,1,1}$: There can be multiple limiting rays and each limiting ray is associated with its own discriminant.

---

[10]Alternatively, a simple fan is a fan whose dual polytope is simple.

2.4.1.1 Example: $A_{2,1}$

We will examine the $A_{2,1}$ cluster algebra in detail, so the algorithm is clear. The $A_{2,1}$ cluster algebra corresponds to the initial quiver,

$$
\begin{array}{c}
b \\
\uparrow \quad \searrow \\
z_{-1} \longrightarrow z_0 \ ,
\end{array}
$$
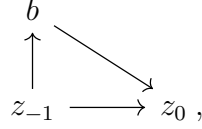
where b, z_{-1} and z_0 are x-variables and frozen variables have been suppressed. To find the limiting ray, we performed a mutation on b, finding the new quiver

$$
\begin{array}{c}
x_1 : \ b' \\
\downarrow \quad \nwarrow \\
x_2 : \ z_{-1} \ \Longrightarrow \ x_3 : \ z_0 \ ,
\end{array}
$$
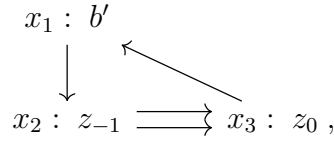
which we chose to be the principal quiver. The "x_i :" denotes which basis vector each x-variable of the principle quiver corresponds to. The corresponding exchange matrix is

$$
B_{i,j}^0 = \begin{bmatrix} 0 & 1 & -1 \\ -1 & 0 & 2 \\ 1 & -2 & 0 \end{bmatrix} . \tag{2.46}
$$

Identifying the $A_{1,1}$ subalgebra, we performed repeated mutations on the x_2 and x_3 nodes, just as in section 2.2.3, to approach the limiting ray. After repeatedly mutating the x_2 and x_3 nodes, the g-vectors of the x-variables associated with these nodes asymptotically approached

$$
g_{lim} = (0, -1, 1) \ , \tag{2.47}
$$

which we identified as the limiting ray. Using the algorithm in appendix 2.3, we found all the walls that intersect the limiting ray:

$$
\begin{aligned}
\gamma_a^\perp &= (1, 0, 0) \ , \\
\gamma_b^\perp &= (1, 1, 1) \ , \\
\gamma_c^\perp &= (0, 1, 1) \ ,
\end{aligned} \tag{2.48}
$$

where γ_c corresponds to a limiting wall. A visualization of these walls is provided in fig. 2.7, where we have taken a projection of the scattering diagram onto the plane perpendicular to the limiting ray. This projection of the scattering diagram is the asymptotic scattering diagram.

The $\hat{y}_{\gamma_i}$ of the initial asymptotic chamber, $\hat{y}_{\gamma_i}^0$, were then calculated using the same techniques
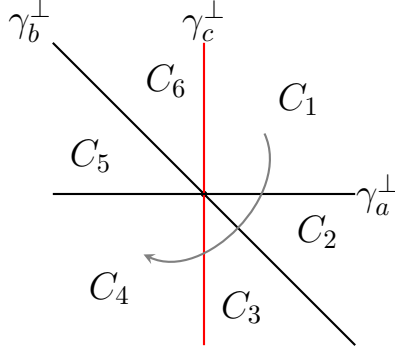
Figure 2.7: The scattering diagram of asymptotic chambers near the limiting ray in the $A_{2,1}$ cluster algebra. We projected down onto the plane perpendicular to the limiting ray, $g_{lim} = (0, -1, 0)$, and labeled the walls.

as those in section 2.2.3. The $\gamma_i^\perp$ of the cone associated with the $2n$-th quiver in the sequence,

are

$$
\begin{aligned}
[\gamma_1^\perp]^{2n} &= (1, 0, 0) \,, \\
[\gamma_2^\perp]^{2n} &= (0, 2n + 1, 2n) \,, \\
[\gamma_3^\perp]^{2n} &= (0, -2n, 1 - 2n) \,.
\end{aligned}
\tag{2.49}
$$

$[\gamma_i^\perp]^{2n}$ is the perpendicular vector of the wall associated with the node x_i after $2n$ mutations and the limit $n \to \infty$ corresponds to our initial asymptotic chamber. Eq. (2.49) implies

$$
\begin{aligned}
\gamma_1 &= [\gamma_1^\perp]^{2n} \,, \\
\gamma_2 &= (1 - 2n)[\gamma_2^\perp]^{2n} - 2n[\gamma_3^\perp]^{2n} \,, \\
\gamma_3 &= (2n)[\gamma_2^\perp]^{2n} + (2n + 1)[\gamma_3^\perp]^{2n} \,,
\end{aligned}
\tag{2.50}
$$

so

$$\hat{y}^0_{\gamma_1} = \lim_{n\to\infty} [\hat{y}_1]^{2n} = \hat{y}_1 \frac{1}{2} \left(1 + \hat{y}_3\hat{y}_2 + \hat{y}_2 + \sqrt{\triangle'} \right) ,$$

$$\hat{y}^0_{\gamma_2} = \lim_{n\to\infty} ([\hat{y}_2]^{2n})^{1-2n}([\hat{y}_3]^{2n})^{-2n} = \frac{4\hat{y}_2\triangle'}{\left(1 - \hat{y}_3\hat{y}_2 + \hat{y}_2 + \sqrt{\triangle'}\right)^2} ,$$

$$\hat{y}^0_{\gamma_3} = \lim_{n\to\infty} ([\hat{y}_2]^{2n})^{2n}([\hat{y}_3]^{2n})^{2n+1} = \frac{1}{4}\hat{y}_3 \left(1 + \frac{1 - \hat{y}_2(\hat{y}_3 + 1)}{\sqrt{\triangle'}} \right)^2 ,$$

$$\triangle' = (\hat{y}_3\hat{y}_2 + \hat{y}_2 + 1)^2 - 4\hat{y}_2\hat{y}_3 ,$$

(2.51)

where $[\hat{y}_i]^{2n}$ is the $\hat{y}$-variable associated with the x_i node after $2n$ mutations. Eq. (2.51) relates the $\hat{y}_{\gamma_i}$ of our initial asymptotic chamber to the $\hat{y}_i$ of our principal quiver. The formulas for $\hat{y}^0_{\gamma_2}$ and $\hat{y}^0_{\gamma_3}$ are exactly the same as eq. (2.34), except that we wrote the expression in terms of $\hat{y}$-variables of the principle quiver instead of x-variables. The formula for $\hat{y}^0_{\gamma_1}$ was derived using the closed form solution for the x-variables of the $A_{1,1}$ subalgebra in appendix A.3 and noting that b' never mutates.

With the asymptotic chambers and eq. (2.51), we can mutate around the asymptotic scattering diagram to find all cluster algebraic functions associated with the limiting ray. For example, going along the path given in fig. 2.7, the $\hat{y}_{\gamma_i}$ mutate as

$$\begin{pmatrix} \hat{y}^0_{\gamma_1} \\ \hat{y}^0_{\gamma_2} \\ \hat{y}^0_{\gamma_3} \end{pmatrix} \to \begin{pmatrix} \hat{y}^0_{\gamma_1} \\ \frac{\hat{y}^0_{\gamma_2}}{\hat{y}^0_{\gamma_1}+1} \\ \left(\hat{y}^0_{\gamma_1} + 1\right)\hat{y}^0_{\gamma_3} \end{pmatrix} \to \begin{pmatrix} \hat{y}^0_{\gamma_1} \\ \frac{\hat{y}^0_{\gamma_2}\left(\hat{y}^0_{\gamma_1}\hat{y}^0_{\gamma_2}\hat{y}^0_{\gamma_3}+1\right)}{\hat{y}^0_{\gamma_1}+1} \\ \frac{\left(\hat{y}^0_{\gamma_1}+1\right)\hat{y}^0_{\gamma_3}}{\hat{y}^0_{\gamma_1}\hat{y}^0_{\gamma_2}\hat{y}^0_{\gamma_3}+1} \end{pmatrix} \to \begin{pmatrix} \hat{y}^0_{\gamma_1} \\ \frac{\hat{y}^0_{\gamma_2}\left(\hat{y}^0_{\gamma_1}\hat{y}^0_{\gamma_2}\hat{y}^0_{\gamma_3}+1\right)}{\left(1-\hat{y}^0_{\gamma_2}\hat{y}^0_{\gamma_3}\right)^4(\hat{y}^0_{\gamma_1}+1)} \\ \frac{\left(\hat{y}^0_{\gamma_1}+1\right)\left(1-\hat{y}^0_{\gamma_2}\hat{y}^0_{\gamma_3}\right)^4\hat{y}^0_{\gamma_3}}{\left(\hat{y}^0_{\gamma_1}\hat{y}^0_{\gamma_2}\hat{y}^0_{\gamma_3}+1\right)} \end{pmatrix} .$$

(2.52)

Again, the jump across the limiting wall corresponds to a generalized cluster mutation. Calculating the $\hat{y}_{\gamma_i}$ of all asymptotic chambers, we found the multiplicative basis

$$\hat{y}^0_{\gamma_1}, \ \hat{y}^0_{\gamma_2}, \ \hat{y}^0_{\gamma_3}, \ (1 + \hat{y}^0_{\gamma_1}), \ (1 - \hat{y}^0_{\gamma_2}\hat{y}^0_{\gamma_3}), \ (1 + \hat{y}^0_{\gamma_1}\hat{y}^0_{\gamma_2}\hat{y}^0_{\gamma_3}) .$$

(2.53)

Eq. (2.53) corresponds to all the algebraic functions associated with the limiting ray in the $A_{2,1}$ cluster algebra. Although the expressions in eq. (2.53) look rational, remember that the $\hat{y}^0_{\gamma_i}$ are algebraic functions of $\hat{y}_i$. They are all algebraic in terms of $\hat{y}_i$ due to the presence of the quadratic root, $\sqrt{\triangle'}$.
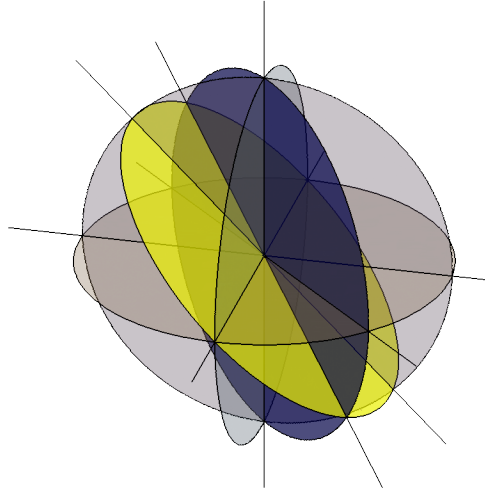
Figure 2.8: The scattering diagram associated with the asymptotic chambers of the $A_{2,2}$ cluster algebra.

2.4.1.2 Example: $A_{2,2}$

We now continue to the $A_{2,2}$ cluster algebra. The $A_{2,2}$ cluster algebra includes a cluster with the quiver
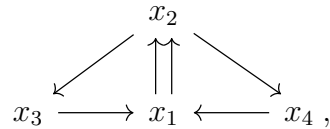
which was chosen as our principal quiver. The asymptotic scattering diagram is slightly more complex than the $A_{2,1}$ cluster algebra, but the algorithm is the same. The limiting ray is

$$g_{lim} = (-1, 1, 0, 0) . \tag{2.54}$$

The scattering walls are

$$\gamma^\perp \in \{(0, 0, 1, 0), \ (0, 0, 0, 1), \ (1, 1, 1, 0), \\ (1, 1, 0, 1), \ (1, 1, 0, 0)\} , \tag{2.55}$$

where the last element corresponds to the limiting wall. To visualize this scattering diagram, we project down to 3 dimensions using the basis,

$$
\begin{aligned}
\hat{e}_1' &= (1, 1, 0, 0)\,, \\
\hat{e}_2' &= (0, 0, 1, 0)\,, \\
\hat{e}_3' &= (0, 0, 0, 1)\,,
\end{aligned}
\tag{2.56}
$$

giving the asymptotic scattering diagram in fig. 2.8. Note that the asymptotic scattering diagram associated with $A_{2,2}$ is not simple as there are cones bounded by 4 walls instead of 3.

We then calculated the $\hat{y}_{\gamma_i}^0$ variables of the initial asymptotic chamber in terms of the $\hat{y}$-variables of the principle quiver. The derivation is almost exactly as in section 2.4.1.1, so we will not write it out here. The final result is,

$$
\begin{aligned}
i \in \{3, 4\} : \hat{y}_{\gamma_i}^0 &= \frac{\hat{y}_i}{2}\left(1 + \hat{y}_2\hat{y}_1 + \hat{y}_1 + \sqrt{\triangle'}\right)\,, \\
\hat{y}_{\gamma_1}^0 &= \hat{y}_1 \frac{4\triangle'}{\left(1 - \hat{y}_2\hat{y}_1 + \hat{y}_1 + \sqrt{\triangle'}\right)^2}\,, \\
\hat{y}_{\gamma_2}^0 &= \frac{\hat{y}_2}{4}\left(1 + \frac{1 - \hat{y}_1\left(\hat{y}_2 + 1\right)}{\sqrt{\triangle'}}\right)^2\,, \\
\triangle' &= \left(\hat{y}_2\hat{y}_1 + \hat{y}_1 + 1\right)^2 - 4\hat{y}_1\hat{y}_2\,.
\end{aligned}
\tag{2.57}
$$

Due to the number of cones, we will not show the $\hat{y}_{\gamma_i}$ of each cone. A complete multiplicative basis in terms of the $\hat{y}_{\gamma_i}^0$ is

$$
\hat{y}_{\gamma_1}^0,\ \hat{y}_{\gamma_2}^0,\ \hat{y}_{\gamma_3}^0,\ \hat{y}_{\gamma_4}^0,\ (\hat{y}_{\gamma_1}^0\hat{y}_{\gamma_2}^0\hat{y}_{\gamma_3}^0 + 1),\ (\hat{y}_{\gamma_1}^0\hat{y}_{\gamma_2}^0\hat{y}_{\gamma_4}^0 + 1),\ (\hat{y}_{\gamma_3}^0 + 1),\ (\hat{y}_{\gamma_4}^0 + 1),\ (1 - \hat{y}_{\gamma_1}^0\hat{y}_{\gamma_2}^0)\,. \tag{2.58}
$$

Again, $\hat{y}_{\gamma_i}^0$ are the $\hat{y}_{\gamma_i}$ associated with the initial asymptotic chamber approached by repeated mutations on the x_1 and x_2 nodes in the initial quiver.

2.4.1.3 Example: $A_{1,1,1}$

Our final example before moving onto $\overline{Gr(4, 8)/T}$ is $A_{1,1,1}$. The $A_{1,1,1}$ cluster algebra includes a cluster with the quiver
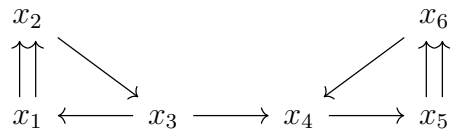
which was chosen as our principle quiver. Unlike the previous examples, there are actually two limiting rays:

$$g_{lim}^1 = (-1, 1, 0, 0, 0, 0) \,,$$
$$g_{lim}^2 = (0, 0, 0, 0, -1, 1) \,. \tag{2.59}$$

First consider the limiting ray g_{lim}^1, which is approached by performing repeated mutations on the x_1 and x_2 nodes. The formulas for $\hat{y}_{\gamma_i}^0$ are then:

$$i \in \{4, 5, 6\} : \hat{y}_{\gamma_i}^0 = \hat{y}_i,$$
$$\hat{y}_{\gamma_3}^0 = \frac{\hat{y}_3}{2} \left(1 + \hat{y}_2 \hat{y}_1 + \hat{y}_1 + \sqrt{\triangle'} \right) \,,$$
$$\hat{y}_{\gamma_1}^0 = \hat{y}_1 \frac{4 \triangle'}{\left(1 - \hat{y}_2 \hat{y}_1 + \hat{y}_1 + \sqrt{\triangle'} \right)^2} \,,$$
$$\hat{y}_{\gamma_2}^0 = \frac{\hat{y}_2}{4} \left(1 + \frac{1 - \hat{y}_1 (\hat{y}_2 + 1)}{\sqrt{\triangle'}} \right)^2 \,,$$
$$\triangle' = (\hat{y}_2 \hat{y}_1 + \hat{y}_1 + 1)^2 - 4 \hat{y}_1 \hat{y}_2 \,. \tag{2.60}$$

However, upon applying the algorithm in appendix 2.3, we found that there are actually an infinite number of asymptotic chambers. Rather, an infinite number of cluster walls intersect the limiting ray. It is unsurprising that this phenomenon eventually occurs as an infinite number of walls intersect a single ray even in the $A_{2,1}$ cluster algebra. We ignored this phenomenon in section 2.4.1.1 because none of the rays in $A_{2,1}$ with infinitely many intersecting walls are limiting rays.

Now consider the second limiting ray in eq. (2.59), which we approached by performing repeated mutations on the x_5 and x_6 nodes. As we approach the second limiting ray, the limits of $\hat{y}_{\gamma_i}$, denoted as $\hat{y}_{\gamma_i}^{0'}$, are

$$i \in \{1, 2, 3\} : \hat{y}_{\gamma_i}^{0'} = \hat{y}_i,$$
$$\hat{y}_{\gamma_4}^{0'} = \frac{\hat{y}_4}{2} \left(1 + \hat{y}_6 \hat{y}_5 + \hat{y}_5 + \sqrt{\triangle'} \right) \,,$$
$$\hat{y}_{\gamma_5}^{0'} = \hat{y}_5 \frac{4 \triangle'}{\left(1 - \hat{y}_6 \hat{y}_5 + \hat{y}_5 + \sqrt{\triangle'} \right)^2} \,,$$
$$\hat{y}_{\gamma_6}^{0'} = \frac{\hat{y}_6}{4} \left(1 + \frac{1 - \hat{y}_5 (\hat{y}_6 + 1)}{\sqrt{\triangle'}} \right)^2 \,,$$
$$\triangle' = (\hat{y}_6 \hat{y}_5 + \hat{y}_5 + 1)^2 - 4 \hat{y}_5 \hat{y}_6 \,. \tag{2.61}$$

We again found an infinite number of asymptotic chambers. Note that the discriminant, $\triangle'$, of the $\hat{y}_{\gamma_i}^{0'}$ variables is different than that of the $\hat{y}_{\gamma_i}^0$ variables. Rather, the discriminant of the algebraic

letters associated with a given set of asymptotic chambers seems to be determined by the associated limiting ray.

It is not particularly interesting for us to further study the cluster algebraic functions associated with $A_{1,1,1}$ as the asymptotic scattering diagrams contain an infinite number of asymptotic chambers. However, one could take a doubly asymptotic limit to find a 4 dimensional scattering diagram that could be finite. More concretely, one could first find the 5 dimensional asymptotic scattering diagram associated with the limiting ray g_{lim}^1 and then find the 4 dimensional asymptotic scattering diagram associated with the limiting ray of this 5 dimensional asymptotic scattering diagram. The resulting 4 dimensional asymptotic scattering diagram could be finite. We leave studying such doubly asymptotic limits to future work.

2.4.2 $\overline{Gr(4,8)/T}$ and Algebraic Letters

We now consider the algebraic letters associated with the 8-point MHV amplitude in $\mathcal{N} = 4$ pSYM. Two classes of known algebraic letters are known to emerge in the $\mathcal{N} = 4$ pSYM symbol alphabet at 8-point and they are related by a cyclic shift: $\langle i, j, k, l \rangle \rightarrow \langle i+1, j+1, k+1, l+1 \rangle$ [89, 90]. Notably, each class of algebraic letters is associated with a unique discriminant. Since each limiting ray seems to be associated with a unique discriminant, $\triangle'$, a reasonable conjecture is that the asymptotic chambers of only two limiting rays are relevant for the 8-point MHV amplitude. Furthermore, we only need to analyze the asymptotic chambers of one of these limiting rays since we can derive the algebraic letters associated with the other limiting ray by applying a cyclic shift.[11]

We first briefly review the positive kinematic region before summarizing the computation of the algebraic letters. We parameterize kinematic space using momentum twistors, Z_i^A. Due to dual conformal symmetry, we can identify $Z_i^A \in Gr(4, n)$. Furthermore, since the Z_i^A are projective under a "little group" transform, $Z_i^A \rightarrow t_i Z_i^A$, we can identify $Z_i^A \in Gr(4, n)/T$. The positive kinematic region corresponds to a compactification of the positive Grassmannian, $\overline{Gr(4, n)/T}$. The cluster algebra structure of $\overline{Gr(k, n)/T}$ is well known. In particular, there is a famous initial parameterization that corresponds to the quiver in fig. 2.9 at 8-point, where boxed elements in the

---

[11]Refs. [36, 101, 102] have pointed out that additional types of limiting rays might be relevant for studying the symbol alphabet at higher loop. However, Ref. [36] also pointed out at least some of these additional limiting rays are related by a braid group [124] to the limiting rays we study in this section. Therefore, even if the algebraic letters associated with these other limiting rays appear in the 8-point MHV symbol alphabet, it seems plausible they could be derived through braid transformations of the symbol alphabet derived in this section.
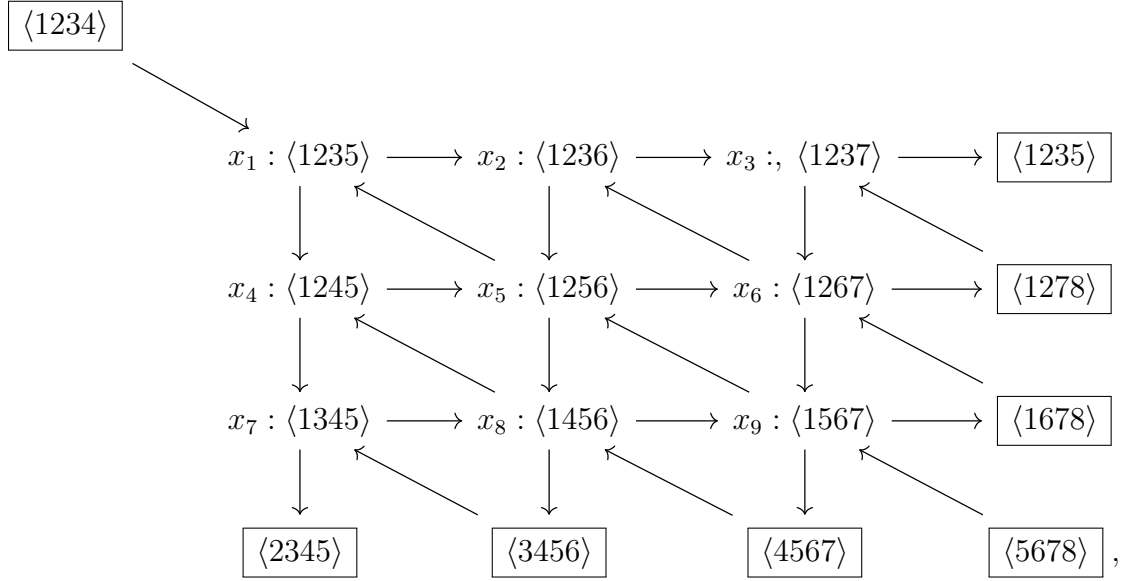
Figure 2.9: The initial quiver for the $\overline{Gr(4,8)}$ cluster algebra.

quiver correspond to frozen variables. The $\hat{y}$-variables associated with the quiver are

$$\hat{y}_1^{\mathrm{I}} = \frac{\langle 1234 \rangle \langle 1256 \rangle}{\langle 1236 \rangle \langle 1245 \rangle} \qquad \hat{y}_2^{\mathrm{I}} = \frac{\langle 1235 \rangle \langle 1267 \rangle}{\langle 1237 \rangle \langle 1256 \rangle} \qquad \hat{y}_3^{\mathrm{I}} = \frac{\langle 1236 \rangle \langle 1278 \rangle}{\langle 1238 \rangle \langle 1267 \rangle}$$

$$\hat{y}_4^{\mathrm{I}} = \frac{\langle 1235 \rangle \langle 1456 \rangle}{\langle 1256 \rangle \langle 1345 \rangle} \qquad \hat{y}_5^{\mathrm{I}} = \frac{\langle 1236 \rangle \langle 1245 \rangle \langle 1567 \rangle}{\langle 1235 \rangle \langle 1456 \rangle \langle 1267 \rangle} \qquad \hat{y}_6^{\mathrm{I}} = \frac{\langle 1237 \rangle \langle 1256 \rangle \langle 1678 \rangle}{\langle 1236 \rangle \langle 1567 \rangle \langle 1278 \rangle}$$

$$\hat{y}_7^{\mathrm{I}} = \frac{\langle 1245 \rangle \langle 3456 \rangle}{\langle 1456 \rangle \langle 2345 \rangle} \qquad \hat{y}_8^{\mathrm{I}} = \frac{\langle 1256 \rangle \langle 1345 \rangle \langle 4567 \rangle}{\langle 1245 \rangle \langle 3456 \rangle \langle 1567 \rangle} \qquad \hat{y}_9^{\mathrm{I}} = \frac{\langle 1267 \rangle \langle 1456 \rangle \langle 5678 \rangle}{\langle 1256 \rangle \langle 4567 \rangle \langle 1678 \rangle} \,, \qquad (2.62)$$

where the "I" super-script denotes how these $\hat{y}$-variables are associated with the initial quiver. Note that the quiver in fig. 2.9 was not chosen as the principal quiver for our scattering diagram. Instead, we mutated to the quiver

$$(2.63)$$

which was chosen to be the principal quiver, by mutating the nodes $\{1, 2, 4, 1, 6, 8\}$ of the initial

50

quiver from left to right. As argued in section 2.2.1, no information is lost or gained by choosing different principle quivers. An explicit map from the $\hat{y}$-variables of our initial quiver to those of the chosen principal quiver is

$$
\begin{aligned}
\hat{y}_1 &= \frac{\left(\hat{y}_6^{\mathrm{I}} + \hat{y}_1^{\mathrm{I}}\left(\hat{y}_4^{\mathrm{I}} + 1\right)\left(\left(\hat{y}_2^{\mathrm{I}} + 1\right)\hat{y}_6^{\mathrm{I}} + 1\right) + 1\right)}{\hat{y}_1^{\mathrm{I}}\hat{y}_2^{\mathrm{I}}\hat{y}_4^{\mathrm{I}}} \\
&\quad \times \left(\hat{y}_8^{\mathrm{I}} + \hat{y}_1^{\mathrm{I}}\left(\hat{y}_2^{\mathrm{I}} + 1\right)\left(\left(\hat{y}_4^{\mathrm{I}} + 1\right)\hat{y}_8^{\mathrm{I}} + 1\right) + 1\right) , \\
\hat{y}_2 &= \frac{\hat{y}_4^{\mathrm{I}}\hat{y}_8^{\mathrm{I}}}{\hat{y}_8^{\mathrm{I}} + \hat{y}_1^{\mathrm{I}}\left(\hat{y}_2^{\mathrm{I}} + 1\right)\left(\left(\hat{y}_4^{\mathrm{I}} + 1\right)\hat{y}_8^{\mathrm{I}} + 1\right) + 1} , \\
\hat{y}_3 &= \frac{\hat{y}_1^{\mathrm{I}}\hat{y}_2^{\mathrm{I}}\hat{y}_3^{\mathrm{I}}}{\hat{y}_1^{\mathrm{I}}\left(\hat{y}_2^{\mathrm{I}} + 1\right) + 1} , \\
\hat{y}_4 &= \frac{\hat{y}_2^{\mathrm{I}}\hat{y}_6^{\mathrm{I}}}{\hat{y}_6^{\mathrm{I}} + \hat{y}_1^{\mathrm{I}}\left(\hat{y}_4^{\mathrm{I}} + 1\right)\left(\left(\hat{y}_2^{\mathrm{I}} + 1\right)\hat{y}_6^{\mathrm{I}} + 1\right) + 1} , \\
\hat{y}_5 &= \frac{\hat{y}_1^{\mathrm{I}}\hat{y}_2^{\mathrm{I}}\hat{y}_4^{\mathrm{I}}\hat{y}_5^{\mathrm{I}}}{\hat{y}_1^{\mathrm{I}}\left(\hat{y}_2^{\mathrm{I}} + 1\right)\left(\hat{y}_4^{\mathrm{I}} + 1\right) + 1} , \\
\hat{y}_6 &= \frac{\hat{y}_1^{\mathrm{I}}\left(\hat{y}_4^{\mathrm{I}} + 1\right) + 1}{\left(\hat{y}_1^{\mathrm{I}}\left(\hat{y}_2^{\mathrm{I}} + 1\right)\left(\hat{y}_4^{\mathrm{I}} + 1\right) + 1\right)\hat{y}_6^{\mathrm{I}}} , \\
\hat{y}_7 &= \frac{\hat{y}_1^{\mathrm{I}}\hat{y}_4^{\mathrm{I}}\hat{y}_7^{\mathrm{I}}}{\hat{y}_1^{\mathrm{I}}\left(\hat{y}_4^{\mathrm{I}} + 1\right) + 1} , \\
\hat{y}_8 &= \frac{\hat{y}_1^{\mathrm{I}}\left(\hat{y}_2^{\mathrm{I}} + 1\right) + 1}{\left(\hat{y}_1^{\mathrm{I}}\left(\hat{y}_2^{\mathrm{I}} + 1\right)\left(\hat{y}_4^{\mathrm{I}} + 1\right) + 1\right)\hat{y}_8^{\mathrm{I}}} , \\
\hat{y}_9 &= \frac{\left(\hat{y}_1^{\mathrm{I}}\left(\hat{y}_2^{\mathrm{I}} + 1\right)\left(\hat{y}_4^{\mathrm{I}} + 1\right) + 1\right)^2\hat{y}_6^{\mathrm{I}}\hat{y}_8^{\mathrm{I}}\hat{y}_9^{\mathrm{I}}}{\left(\hat{y}_6^{\mathrm{I}} + \hat{y}_1^{\mathrm{I}}\left(\hat{y}_4^{\mathrm{I}} + 1\right)\left(\left(\hat{y}_2^{\mathrm{I}} + 1\right)\hat{y}_6^{\mathrm{I}} + 1\right) + 1\right)} \\
&\quad \times \frac{1}{\left(\hat{y}_8^{\mathrm{I}} + \hat{y}_1^{\mathrm{I}}\left(\hat{y}_2^{\mathrm{I}} + 1\right)\left(\left(\hat{y}_4^{\mathrm{I}} + 1\right)\hat{y}_8^{\mathrm{I}} + 1\right) + 1\right)} .
\end{aligned}
\tag{2.64}
$$

Combining eqs. (2.62) and (2.64) gives explicit expressions of the principal quivers' $\hat{y}$-variables in terms of external kinematic data.

We now analyze the initial asymptotic chamber using the $A_{1,1}$ subalgebra of the principal quiver. After performing an infinite number of mutations on the x_1 and x_9 nodes, the g-vectors of the x_1 and x_9 nodes approached

$$
g_{lim} = (-1, 0, 0, 0, 0, 0, 0, 0, 1) ,
\tag{2.65}
$$

which we identified as the limiting ray. We then found expressions for the $\hat{y}^0_{\gamma_i}$ in terms of the $\hat{y}_i$:

$$
\begin{aligned}
i \in \{2,3,4,7\} &: \hat{y}^0_{\gamma_i} = \hat{y}_i\,, \\
i \in \{5,6,8\} &: \hat{y}^0_{\gamma_i} = \hat{y}_i f(\hat{y}_1, \hat{y}_9)\,, \\
\hat{y}^0_{\gamma_1} &= \frac{4\hat{y}_1 \triangle'}{\left(1 - \hat{y}_9\hat{y}_1 + \hat{y}_1 + \sqrt{\triangle'}\right)^2}\,, \\
\hat{y}^0_{\gamma_9} &= \frac{\hat{y}_9}{4}\left(1 + \frac{1 - \hat{y}_1(\hat{y}_9 + 1)}{\sqrt{\triangle'}}\right)^2\,,
\end{aligned}
\tag{2.66}
$$

where

$$
\begin{aligned}
f(\hat{y}_1, \hat{y}_9) &= \frac{1}{2}\left(1 + \hat{y}_9\hat{y}_1 + \hat{y}_1 + \sqrt{\triangle'}\right)\,, \\
\triangle' &= (\hat{y}_9\hat{y}_1 + \hat{y}_1 + 1)^2 - 4\hat{y}_1\hat{y}_9\,.
\end{aligned}
\tag{2.67}
$$

Unlike the $A_{2,1}$ and $A_{2,2}$ cluster algebras, not all the $\hat{y}^0_{\gamma_i}$ are algebraic function of the $\hat{y}_i$. Although difficult to see immediately, one can show that the discriminant, $\triangle'$, is proportional to

$$
\begin{aligned}
\sqrt{\triangle'} &\propto \sqrt{A^2 - 4B}\,, \\
A &= \langle 1256\rangle\langle 3478\rangle - \langle 1278\rangle\langle 3456\rangle - \langle 1234\rangle\langle 5678\rangle\,, \\
B &= \langle 1234\rangle\langle 3456\rangle\langle 5678\rangle\langle 1278\rangle\,,
\end{aligned}
\tag{2.68}
$$

which corresponds to the limiting ray g_1 in Ref. [36]. The limiting ray in eq. (2.65) looks different than the limiting ray in Ref. [36] because we chose a different principal quiver to define the g-vector fan. While we chose the quiver in (2.63) as our principal quiver, the authors of Ref. [36] chose the initial quiver in fig. 2.9 as their principal quiver.

We employed the algorithm in section 2.3 to find all the walls that intersect the limiting ray. However, using pre-asymptotic chambers did not completely remove undesirable redundancies, because a single asymptotic chamber can correspond to multiple pre-asymptotic chambers. This redundancy is not a problem for lower rank cluster algebras where the number of pre-asymptotic chambers is small and finite. For the asymptotic scattering diagrams of $A_{2,1}$ and $A_{2,2}$, one can prove that the number of asymptotic chambers is finite simply by showing that the number of pre-asymptotic chambers is finite. However, for $\overline{Gr(4,8)/T}$, we found that the number of pre-asymptotic chambers is infinite, or so large it is effectively infinite, while the number of asymptotic chambers is finite. If the number of pre-asymptotic chambers is infinite, brute force mutation procedures cannot prove that you have found all asymptotic chambers. Instead, one must perform mutations on pre-asymptotic chambers until no new asymptotic chambers appear after a large number of mutations. Specifically, we found that all the discovered asymptotic chambers were
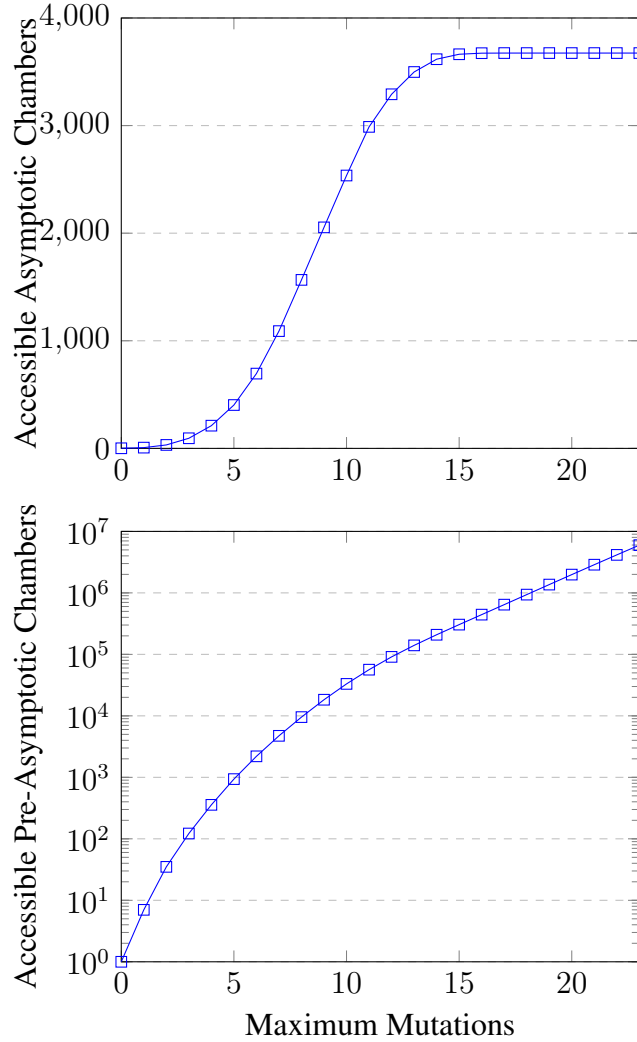
Figure 2.10: Number of accessible asymptotic and pre-asymptotic chambers after a maximum of X mutations from the initial pre-asymptotic chamber. Note that we are only considering (pre-)asymptotic chambers on one side on the limiting wall.

within 18 mutations of our initial pre-asymptotic chamber and checked all pre-asymptotic chambers within 23 mutations of our initial pre-asymptotic chamber. Fig. 2.10 is a plot of the number of asymptotic and pre-asymptotic chambers, Y, accessible after a maximum of X mutations on the initial pre-asymptotic chamber given in section 2.4.2.

We eventually found 26 cluster walls:

$$\gamma^{\perp} \in \{(0, 1, 0, 0, 0, 0, 0, 0, 0),\ (0, 0, 1, 0, 0, 0, 0, 0, 0),$$
$$(0, 0, 0, 1, 0, 0, 0, 0, 0),\ (0, 0, 0, 0, 1, 0, 0, 0, 0),$$
$$(0, 0, 0, 0, 0, 1, 0, 0, 0),\ (0, 0, 0, 0, 0, 0, 1, 0, 0),$$

$$(0, 1, 0, 0, 0, 0, 0, 1, 0), \quad (0, 1, 1, 0, 0, 0, 0, 0, 0),$$
$$(0, 0, 0, 0, 0, 0, 0, 1, 0), \quad (0, 0, 0, 1, 0, 1, 0, 0, 0),$$
$$(0, 0, 0, 1, 0, 0, 1, 0, 0), \quad (0, 1, 1, 0, 0, 0, 0, 1, 0),$$
$$(0, 0, 0, 1, 0, 1, 1, 0, 0), \quad (1, 0, 0, 0, 1, 0, 0, 0, 1),$$
$$(1, 0, 0, 0, 0, 1, 0, 0, 1), \quad (1, 0, 0, 0, 0, 0, 0, 1, 1),$$
$$(1, 1, 0, 0, 0, 0, 0, 1, 1), \quad (1, 0, 0, 1, 0, 1, 0, 0, 1),$$
$$(1, 1, 1, 0, 0, 0, 0, 1, 1), \quad (1, 1, 0, 0, 0, 0, 0, 2, 1),$$
$$(1, 0, 0, 1, 0, 1, 1, 0, 1), \quad (1, 0, 0, 1, 0, 2, 0, 0, 1),$$
$$(1, 2, 1, 0, 0, 0, 0, 2, 1), \quad (1, 1, 1, 0, 0, 0, 0, 2, 1),$$
$$(1, 0, 0, 1, 0, 2, 1, 0, 1), \quad (1, 0, 0, 2, 0, 2, 1, 0, 1),$$
$$(1, 0, 0, 0, 0, 0, 0, 0, 1)\} \,,$$

$$(2.69)$$

where the last element corresponds to the limiting wall. An extensive computer search found a complete multiplicative basis of the $\hat{y}_{\gamma_i}$ consists of 27 non-trivial polynomials of $\hat{y}_{\gamma_i}^0$,

$$f_1 = \hat{y}_{\gamma_2}^0 + 1 \,,$$
$$f_2 = \hat{y}_{\gamma_3}^0 + 1 \,,$$
$$f_3 = \hat{y}_{\gamma_4}^0 + 1 \,,$$
$$f_4 = \hat{y}_{\gamma_5}^0 + 1 \,,$$
$$f_5 = \hat{y}_{\gamma_6}^0 + 1 \,,$$
$$f_6 = \hat{y}_{\gamma_7}^0 + 1 \,,$$
$$f_7 = \hat{y}_{\gamma_8}^0 + 1 \,,$$
$$f_8 = \hat{y}_{\gamma_2}^0 \hat{y}_{\gamma_3}^0 + \hat{y}_{\gamma_3}^0 + 1 \,,$$
$$f_9 = \hat{y}_{\gamma_8}^0 \hat{y}_{\gamma_2}^0 + \hat{y}_{\gamma_2}^0 + 1 \,,$$
$$f_{10} = \hat{y}_{\gamma_6}^0 \hat{y}_{\gamma_4}^0 + \hat{y}_{\gamma_4}^0 + 1 \,,$$
$$f_{11} = \hat{y}_{\gamma_4}^0 \hat{y}_{\gamma_7}^0 + \hat{y}_{\gamma_7}^0 + 1 \,,$$
$$f_{12} = \hat{y}_{\gamma_2}^0 \hat{y}_{\gamma_3}^0 + \hat{y}_{\gamma_2}^0 \hat{y}_{\gamma_8}^0 \hat{y}_{\gamma_3}^0 + \hat{y}_{\gamma_3}^0 + 1 \,,$$
$$f_{13} = \hat{y}_{\gamma_4}^0 \hat{y}_{\gamma_7}^0 + \hat{y}_{\gamma_4}^0 \hat{y}_{\gamma_6}^0 \hat{y}_{\gamma_7}^0 + \hat{y}_{\gamma_7}^0 + 1 \,,$$
$$f_{14} = \hat{y}_{\gamma_1}^0 \hat{y}_{\gamma_5}^0 \hat{y}_{\gamma_9}^0 + 1 \,,$$
$$f_{15} = \hat{y}_{\gamma_1}^0 \hat{y}_{\gamma_6}^0 \hat{y}_{\gamma_9}^0 + 1 \,,$$
$$f_{16} = \hat{y}_{\gamma_1}^0 \hat{y}_{\gamma_8}^0 \hat{y}_{\gamma_9}^0 + 1 \,,$$
$$f_{17} = \hat{y}_{\gamma_1}^0 \hat{y}_{\gamma_8}^0 \hat{y}_{\gamma_9}^0 \hat{y}_{\gamma_2}^0 + \hat{y}_{\gamma_2}^0 + 1 \,,$$

$$(2.70)$$

$$f_{18} = \hat{y}^0_{\gamma_1} \hat{y}^0_{\gamma_6} \hat{y}^0_{\gamma_9} \hat{y}^0_{\gamma_4} + \hat{y}^0_{\gamma_4} + 1 \,,$$

$$f_{19} = \hat{y}^0_{\gamma_1} \hat{y}^0_{\gamma_4} \hat{y}^0_{\gamma_9} \left(\hat{y}^0_{\gamma_6}\right)^2 + \hat{y}^0_{\gamma_4} \hat{y}^0_{\gamma_6} + \hat{y}^0_{\gamma_1} \hat{y}^0_{\gamma_4} \hat{y}^0_{\gamma_9} \hat{y}^0_{\gamma_6} + \hat{y}^0_{\gamma_4} + 1,$$

$$f_{20} = \hat{y}^0_{\gamma_1} \hat{y}^0_{\gamma_2} \hat{y}^0_{\gamma_9} \left(\hat{y}^0_{\gamma_8}\right)^2 + \hat{y}^0_{\gamma_2} \hat{y}^0_{\gamma_8} + \hat{y}^0_{\gamma_1} \hat{y}^0_{\gamma_2} \hat{y}^0_{\gamma_9} \hat{y}^0_{\gamma_8} + \hat{y}^0_{\gamma_2} + 1,$$

$$f_{21} = \hat{y}^0_{\gamma_2} \hat{y}^0_{\gamma_3} + \hat{y}^0_{\gamma_1} \hat{y}^0_{\gamma_2} \hat{y}^0_{\gamma_8} \hat{y}^0_{\gamma_9} \hat{y}^0_{\gamma_3} + \hat{y}^0_{\gamma_3} + 1,$$

$$f_{22} = \hat{y}^0_{\gamma_3} \left(\hat{y}^0_{\gamma_2}\right)^2 + \hat{y}^0_{\gamma_3} \hat{y}^0_{\gamma_8} \left(\hat{y}^0_{\gamma_2}\right)^2 + \hat{y}^0_{\gamma_1} \hat{y}^0_{\gamma_3} \left(\hat{y}^0_{\gamma_8}\right)^2 \hat{y}^0_{\gamma_9} \left(\hat{y}^0_{\gamma_2}\right)^2$$
$$+ \hat{y}^0_{\gamma_1} \hat{y}^0_{\gamma_3} \hat{y}^0_{\gamma_8} \hat{y}^0_{\gamma_9} \left(\hat{y}^0_{\gamma_2}\right)^2 + 2\hat{y}^0_{\gamma_3} \hat{y}^0_{\gamma_2} + \hat{y}^0_{\gamma_3} \hat{y}^0_{\gamma_8} \hat{y}^0_{\gamma_2} + \hat{y}^0_{\gamma_1} \hat{y}^0_{\gamma_3} \hat{y}^0_{\gamma_8} \hat{y}^0_{\gamma_9} \hat{y}^0_{\gamma_2} + \hat{y}^0_{\gamma_2} + \hat{y}^0_{\gamma_3} + 1,$$

$$f_{23} = \hat{y}^0_{\gamma_1} \hat{y}^0_{\gamma_2} \hat{y}^0_{\gamma_3} \hat{y}^0_{\gamma_9} \left(\hat{y}^0_{\gamma_8}\right)^2 + \hat{y}^0_{\gamma_2} \hat{y}^0_{\gamma_3} \hat{y}^0_{\gamma_8} + \hat{y}^0_{\gamma_1} \hat{y}^0_{\gamma_2} \hat{y}^0_{\gamma_3} \hat{y}^0_{\gamma_9} \hat{y}^0_{\gamma_8} + \hat{y}^0_{\gamma_2} \hat{y}^0_{\gamma_3} + \hat{y}^0_{\gamma_3} + 1,$$

$$f_{24} = \hat{y}^0_{\gamma_6} \hat{y}^0_{\gamma_7} \left(\hat{y}^0_{\gamma_4}\right)^2 + \hat{y}^0_{\gamma_7} \left(\hat{y}^0_{\gamma_4}\right)^2 + \hat{y}^0_{\gamma_1} \left(\hat{y}^0\right)^2_{\gamma_6} \hat{y}^0_{\gamma_7} \hat{y}^0_{\gamma_9} \left(\hat{y}^0_{\gamma_4}\right)^2$$
$$+ \hat{y}^0_{\gamma_1} \hat{y}^0_{\gamma_6} \hat{y}^0_{\gamma_7} \hat{y}^0_{\gamma_9} \left(\hat{y}^0_{\gamma_4}\right)^2 + \hat{y}^0_{\gamma_6} \hat{y}^0_{\gamma_7} \hat{y}^0_{\gamma_4} + 2\hat{y}^0_{\gamma_7} \hat{y}^0_{\gamma_4} + \hat{y}^0_{\gamma_1} \hat{y}^0_{\gamma_6} \hat{y}^0_{\gamma_7} \hat{y}^0_{\gamma_9} \hat{y}^0_{\gamma_4} + \hat{y}^0_{\gamma_4} + \hat{y}^0_{\gamma_7} + 1,$$

$$f_{25} = \hat{y}^0_{\gamma_4} \hat{y}^0_{\gamma_7} + \hat{y}^0_{\gamma_1} \hat{y}^0_{\gamma_4} \hat{y}^0_{\gamma_6} \hat{y}^0_{\gamma_9} \hat{y}^0_{\gamma_7} + \hat{y}^0_{\gamma_7} + 1,$$

$$f_{26} = \hat{y}^0_{\gamma_1} \hat{y}^0_{\gamma_4} \hat{y}^0_{\gamma_7} \hat{y}^0_{\gamma_9} \left(\hat{y}^0_{\gamma_6}\right)^2 + \hat{y}^0_{\gamma_4} \hat{y}^0_{\gamma_7} \hat{y}^0_{\gamma_6} + \hat{y}^0_{\gamma_1} \hat{y}^0_{\gamma_4} \hat{y}^0_{\gamma_7} \hat{y}^0_{\gamma_9} \hat{y}^0_{\gamma_6} + \hat{y}^0_{\gamma_4} \hat{y}^0_{\gamma_7} + \hat{y}^0_{\gamma_7} + 1 \,,$$

$$f_{27} = 1 - \hat{y}^0_{\gamma_1} \hat{y}^0_{\gamma_9} \,,$$

and the 9 $\hat{y}^0_{\gamma_i}$, giving a symbol alphabet of 36 independent letters. When computing eqs. (2.69) and (2.70), we found 7348 asymptotic chambers, in comparison to the 64 asymptotic chambers studied in Ref. [102] using slightly different methods.[12] Although we are confident we found all asymptotic chambers, we were not able to rigorously prove it as we did for $A_{2,1}$ and $A_{2,2}$. A complete search of all asymptotic chambers is very computationally challenging for $\overline{Gr(4,8)/T}$ for reasons beyond its high rank. However, any missing asymptotic chambers should not change eqs. (2.69) or (2.70). Interestingly, only a subset of less than 1000 asymptotic chambers was required to find both a complete multiplicative basis for the $\hat{y}_{\gamma_i}$ and all the relevant walls in the asymptotic scattering diagrams.

Combining eqs. (2.62), (2.64), (2.66) and (2.70) gives explicit expressions for the algebraic letters in terms of momentum twistors. We have explicitly checked that the algebraic letters of Ref. [90] are monomials of $\hat{y}^0_{\gamma_i}$ and f_i. Interestingly, note that many of the letters are obviously not algebraic. From eq. (2.66), $\hat{y}^0_{\gamma_2}$, $\hat{y}^0_{\gamma_3}$, $\hat{y}^0_{\gamma_4}$, and $\hat{y}^0_{\gamma_7}$ are rational, so any f_i that is solely a function of these variables will also be rational. From this criterion alone, the algebraic alphabet is reduced from 36 to 26 letters. Additional numerical checks show that some of these algebraic letters can further simplify to rational functions for certain momentum configurations.

These results are remarkable. There is no reason to expect that there are a finite number of asymptotic chambers associated with any limiting ray of the $\overline{Gr(4,8)/T}$ cluster algebra. In section 2.4.1.3, we saw an explicit example of a limiting ray with an infinite number of asymptotic

---

[12]Each origin cluster corresponds to two asymptotic chambers. Further discussion on the techniques in Ref. [102] is given in appendix A.5.

chambers. Furthermore, although the number of asymptotic chambers is extremely large, the multiplicative basis has rank 36 for the relevant limiting rays! We can further discard letters that are clearly not algebraic, reducing the rank of the algebraic alphabet from 72 to 52. We can now conjecture that we have found ALL algebraic letters that could appear in the $\mathcal{N} = 4$ pSYM 8-point amplitude. Our $\hat{y}^0_{\gamma_i}$ coordinates show how the relations between the algebraic letters associated with the same limiting ray are inherently rational, even though the $\hat{y}^0_{\gamma_i}$ are generically algebraic functions of our initial coordinates, $\hat{y}^I_i$. Finally, in all examples studied in this chapter, the rank of the asymptotic symbol alphabet has been equal to the number of cluster walls plus the rank of the cluster algebra. More precisely, there seems to be a correspondence between walls in the asymptotic scattering diagram, $\gamma^\perp$ in eq. (2.69), and polynomial letters in the asymptotic symbol alphabet, f_i in eq. (2.70). At present, it is unclear to us whether this relation holds for more general cluster algebras or is a red herring.

2.4.3 Beyond $A_{1,1}$ Subalgebras

Although this chapter focuses on limiting rays associated with quadratic cluster algebraic functions, we expect that cubic cluster algebraic functions will also be relevant for studying the symbol alphabet of $\mathcal{N} = 4$ pSYM beyond 8-point. Quadratic (cubic) algebraic functions are algebraic functions that are products of roots of quadratic (cubic) polynomials. To see why cubic letters should appear, note that algebraic letters can at least partially be derived from *irrational* Yangian invariants, as shown in refs. [91, 92]. Using the duality between on-shell super-space variables and differentials on kinematic space,

$$\eta^A_i \leftrightarrow dZ^A_i \, , \tag{2.71}$$

where η^A_i are the on-shell superspace variable associated with state i [35, 125], Yangian invariants in $\mathcal{N} = 4$ pSYM can be written in a manifestly dlog form:

$$\text{Yangian Invariant} \rightarrow \prod_i d\log(\alpha_i) \, , \tag{2.72}$$

where α_i correspond to functions of external data, Z^A_i, that are not necessarily rational. The α_i can be interpreted as "letters" of the Yangian invariant and correspond to singularities. Since we expect the branch points of N^kMHV amplitudes to match onto branch points of MHV amplitudes, we can therefore probe the symbol alphabet of MHV amplitudes by studying the α_i that appear in Yangian invariants associated with N^kMHV amplitudes. Starting at 11-point, we start to see irrational Yangian invariants that include *cubic* algebraic letters. Therefore, we expect to find cluster algebraic functions that are cubic at 11-point.

The problem with cubic cluster algebraic functions is that it may not be possible to probe their

associated asymptotic chambers using an $A_{1,1}$ subalgebra as in section 2.4.1. If at least one asymptotic chamber of a limiting ray can be approached by repeated mutations on an $A_{1,1}$ subalgebra, then the asymptotic symbol alphabet must consist of quadratic cluster algebraic letters. To see this, note that the generating function for cluster variables in an $A_{1,1}$ subalgebra always takes the form

$$G_{n>0}(t) = \frac{x_0 - x_{-1}\mathcal{F}t}{1 - \mathcal{P}t + \mathcal{F}t^2} = \sum_{n=0}^{\infty} x_n t^n \,, \tag{2.73}$$

where $\mathcal{F}$ is some product of cluster variables outside the $A_{1,1}$ subalgebra. Taking limits of x_i generated by the above relation, such as

$$\lim_{i \to \infty} x_i/x_{i-1}, \tag{2.74}$$

will always generate a function that is either rational or quadratic, but not cubic. Since wall crossing mutations around limiting rays are always rational transformations, this means all $\hat{y}_{\gamma_i}$ must be either rational or quadratic.[13] Therefore, we must identify more general mutation sequences in order to approach asymptotic chambers associated with cubic algebraic functions. Such mutation sequences could correspond to generating functions with higher-order polynomials in the denominator, such that specific limits of x_i generate cubic cluster algebraic functions. We expect the methods and results in Ref. [126] may be useful for pursuing this direction.

2.5 Degenerate Scattering Diagrams and Tropicalization

We now study speculative truncations of $\hat{y}$-variables from the perspective of scattering diagrams. We will first motivate and define the notion of a degenerate scattering diagram, commenting on the specific connection to $\mathcal{N} = 4$ pSYM. Although we did not find a definite algorithm for truncating $\hat{y}$-variables, we did find that the notion of asymptotic chambers naturally emerges from degenerate scattering diagrams.

2.5.1 Scattering Diagrams from Tropicalization of the Dual Cluster Algebra

In this section, we relate the g-vector fan to tropicalization of the *dual* cluster algebra. We then motivate degenerate fans using tropicalization arguments.

We now give a brief review of tropicalization. Since all elements of $\mathcal{O}(\mathcal{X})$ are positive Laurent polynomials where the minus operation never appears, we can consider the tropicalization of such

---

[13]There is a small loophole in this argument. If the asymptotic scattering diagram itself contains a limiting ray, one could take a doubly asymptotic limit as suggested at the end of section 2.4.1.3. However, it seems unlikely to us that such doubly asymptotic limits could generate cubic algebraic letters.

functions. Tropicalization naturally emerges from studying the behavior of geometric spaces at small (or large) values of their coordinates. For example, given a function $f(a_1, a_2, \ldots, a_n)$, the tropical function is defined as

$$\text{Trop}[f(a_1, a_2, \ldots, a_n)] = \lim_{\epsilon \to \infty} \frac{-1}{\epsilon} \log[f(e^{-\epsilon a_1}, e^{-\epsilon a_2}, \ldots, e^{-\epsilon a_n})] . \tag{2.75}$$

The tropicalization of a function effectively amounts to the replacements

$$
\begin{aligned}
a \times b &\to a + b , \\
a + b &\to \min(a, b) , \\
1 &\to 0 ,
\end{aligned}
\tag{2.76}
$$

where a and b now take values on a semifield. For example,

$$
\begin{aligned}
\text{Trop}[1 + x] &= \min(0, x) , \\
\text{Trop}[1 + x + xy] &= \min(0, x, x + y) .
\end{aligned}
\tag{2.77}
$$

Tropicalization has many applications, ranging from mirror symmetry to intersection theory. We will now review one aspect of the connection with cluster algebras.

In our tropicalization arguments, we do not consider the $\mathcal{O}(\mathcal{X})$ associated with our initial principal quiver. Instead, we consider the *dual* principal quiver and the associated dual cluster algebra, $\mathcal{X}^\vee$. The dual principal quiver is given by the initial quiver except that we flip all arrows between mutable nodes. As an example, given the initial quiver

$$
\begin{array}{ccc}
y_1 & & y_2 \\
\downarrow & & \downarrow \\
x_1 & \longrightarrow & x_2 ,
\end{array}
$$

the dual quiver is

$$
\begin{array}{ccc}
y_1^\vee & & y_2^\vee \\
\downarrow & & \downarrow \\
x_1^\vee & \longleftarrow & x_2^\vee .
\end{array}
$$

We now study $\mathcal{O}(\mathcal{X}^\vee)$. For example, in the case of the A_2 cluster algebra, $\mathcal{O}(\mathcal{X}^\vee)$ consists of

$$
\begin{aligned}
f_1 &= 1 + \hat{y}_1^\vee , \\
f_2 &= 1 + \hat{y}_2^\vee , \\
f_3 &= 1 + \hat{y}_2^\vee + \hat{y}_2^\vee \hat{y}_1^\vee .
\end{aligned}
\tag{2.78}
$$

(a) Trop$[1 + \hat{y}_1^\vee]$ (b) Trop$[1 + \hat{y}_2^\vee]$ (c) Trop$[1 + \hat{y}_2^\vee + \hat{y}_1^\vee \hat{y}_2^\vee]$
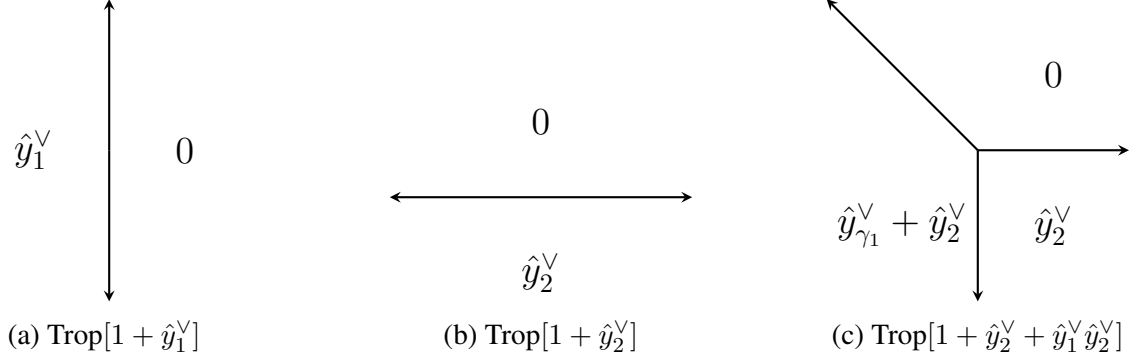
Figure 2.11: The fan associated with the tropicalization of functions in eq. (2.79).

Any $\hat{y}$-variable in $\mathcal{X}^\vee$ can be written as a product of functions in eq. (2.78) and $\hat{y}_i^\vee$.

The tropicalization of each $f \in \mathcal{O}(\mathcal{X}^\vee)$ defines a fan that splits $\mathbb{Z}^N$ into regions where Trop$[f(\hat{y})]$ is constant. We simply state without proof that all such fans together give the scattering diagram in the finite case [98, 106, 107]. For example, again consider the A_2 cluster algebra and the tropicalization of functions in eq. (2.78):

$$
\begin{aligned}
f_1 = 1 + \hat{y}_1^\vee &\rightarrow \text{Trop}[f_1] = \min(0, \hat{y}_1^\vee) \,, \\
f_2 = 1 + \hat{y}_2^\vee &\rightarrow \text{Trop}[f_2] = \min(0, \hat{y}_2^\vee) \,, \\
f_3 = 1 + \hat{y}_2^\vee + \hat{y}_1^\vee \hat{y}_2^\vee &\rightarrow \text{Trop}[f_3] = \min(0, \hat{y}_2^\vee, \hat{y}_1^\vee + \hat{y}_2^\vee) \,.
\end{aligned}
\tag{2.79}
$$

The tropicalization of each f_i defines a fan in $\mathbb{Z}^2$, which are given in fig. 2.11. In this example, one can immediately see that the combination of all fans defined by tropicalization of $f_i \in \mathcal{O}(\mathcal{X}^\vee)$ is equivalent to the scattering diagram for $\mathcal{X}$.[14]

We now motivate degenerate scattering diagrams. Suppose we do not tropicalize all regular functions in $\mathcal{O}(\mathcal{X}^\vee)$, but only a subset. For example, suppose we only considered the tropicalization of f_2 and f_3 in eq. (2.79). We would find only 4 walls in the scattering diagram. Naively, this does not correspond to a well-defined scattering diagram if we assume the walls are single cluster walls. However, one might conjecture that it corresponds to a *degenerate scattering diagram*, where certain walls are combined so certain chambers are inaccessible.

2.5.2 Degenerate Scattering Diagrams

We now introduce the notion of degenerate scattering diagrams to motivate this truncation. Suppose that we want to truncate some cones from the scattering diagram while keeping others. Rather

---

[14]The relation between the scattering diagram of $\mathcal{X}$ and $\mathcal{O}(\mathcal{X}^\vee)$ is easier to understand from a mirror symmetry perspective. $\mathcal{A}^\vee$ is dual to $\mathcal{X}$ under mirror symmetry [108].

(a) Non-degenerate scattering diagram corresponding to A_2.

(b) A degenerate scattering diagram
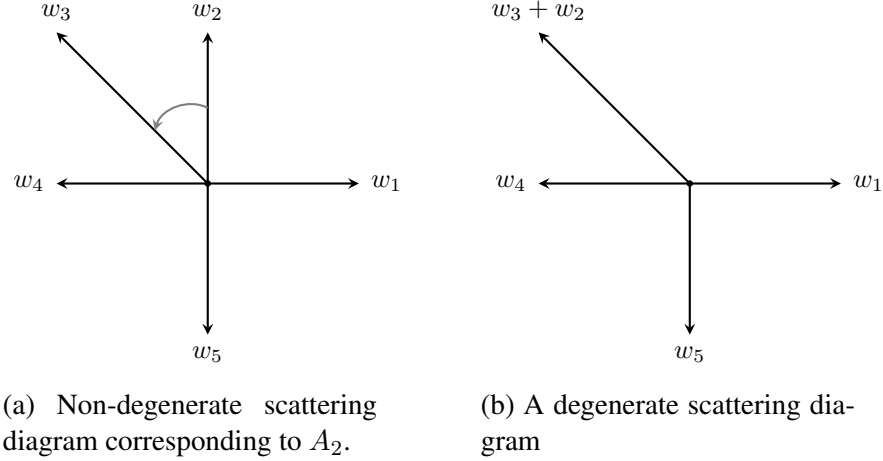
Figure 2.12: A demonstration of how to derive a degenerate scattering diagram from the non-degenerate scattering diagram for the A_2 cluster algebra.

we want to enforce certain conditions of the form: "If you cross wall A, you must also cross wall B and vice-versa." This is a well-defined procedure if we combine walls in the scattering diagram. For example, again consider the scattering diagram associated with A_2. Suppose we consider the fan derived by only tropicalizing f_3 and f_2 in eq. (2.79), leading to the degenerate fan in fig. 2.12b. We can derive this fan from a wall combination procedure by combining walls w_2 and w_3 in the full scattering diagram in fig. 2.12a. We can view this procedure as a "wall combination procedure" or "cone truncation" procedure. However, by combining walls, we lose several nice properties associated with the original scattering diagram. First, multiple functions are associated with a single degenerate wall, so wall crossing across a degenerate wall takes the form:

$$\mu_{\gamma^\perp} \hat{y}_{\gamma_i} = \hat{y}_{\gamma_i} \prod_a f_a(\hat{y}_{\gamma_a^\perp})^{\langle \gamma_i, \gamma_a^\perp \rangle} \ . \tag{2.80}$$

Second, the functions f_a in eq. (2.80) change depending on whether you are mutating forward or backward across a degenerate wall. For instance, the functions associated with the degenerate wall in fig. 2.12b take the form:

$$\mu_{\gamma^\perp=(1,1)}^+ \hat{y}_{\gamma_i} = \hat{y}_{\gamma_i}(1 + \frac{\hat{y}_{\gamma_1}\hat{y}_{\gamma_2}}{1 + \hat{y}_{\gamma_1}})^{\langle \gamma_i, \gamma_2 \rangle}(1 + \hat{y}_{\gamma_1} + \hat{y}_{\gamma_1}\hat{y}_{\gamma_2})^{\langle \gamma_i, \gamma_1 \rangle} \ ,$$
$$\mu_{\gamma^\perp=(1,1)}^- \hat{y}_{\gamma_i} = \hat{y}_{\gamma_i}(1 + \hat{y}_{\gamma_1}\hat{y}_{\gamma_2})^{-\langle \gamma_i, \gamma_2 \rangle}(1 + \hat{y}_{\gamma_1} + \hat{y}_{\gamma_1}\hat{y}_{\gamma_2})^{-\langle \gamma_i, \gamma_1 \rangle} \ , \tag{2.81}$$

where the $+(-)$ indicates if you going counter-clockwise (clockwise) around the scattering diagram.

Although the degenerate walls are useful for motivating asymptotic chambers, there is signifi-

cant ambiguity in their construction. Primarily, given an arbitrary fan, we do not have a procedure for associating a unique degenerate scattering diagram to this fan. For example, again consider the fan in fig. 2.12. We could construct this fan by combining wall w_2 with walls w_3 or w_1. Given only the fan, there is no canonical choice without additional input.

2.5.3 Asymptotic Chambers from Degenerate Scattering Diagrams

We now consider the above procedure when the number of cones is infinite. We work with the degenerate cluster polytope instead of the degenerate scattering diagram.[15] Note that if one only tropicalizes a finite subset of $\mathcal{O}(\mathcal{X}^\vee)$, one often finds that the associated degenerate cluster polytope includes a facet corresponding to a limiting ray.[16] For example, consider the following principle quiver:

$$
\begin{array}{ccc}
y_1 & \longrightarrow & x_1 \\
& & \uparrow \quad \searrow \\
y_2 \longrightarrow & x_2 & \longrightarrow x_3 \longleftarrow y_3 \;,
\end{array}
$$

which corresponds to the $A_{2,1}$ cluster algebra, and its dual quiver,

$$
\begin{array}{ccc}
y_1^\vee & \longrightarrow & x_1^\vee \\
& & \downarrow \quad \nwarrow \\
y_2^\vee \longrightarrow & x_2^\vee & \longleftarrow x_3^\vee \longleftarrow y_3^\vee \;.
\end{array}
$$

Now consider the tropicalization of the following subset of regular functions of $A_{2,1}^\vee$:

$$
\begin{aligned}
f_1 &= \hat{y}_1^\vee + 1 \;, \\
f_2 &= \hat{y}_2^\vee + 1 \;, \\
f_3 &= \hat{y}_3^\vee + 1 \;, \\
f_4 &= \hat{y}_3^\vee \hat{y}_1^\vee + \hat{y}_3^\vee + 1 \;, \\
f_5 &= \hat{y}_2^\vee \hat{y}_1^\vee + \hat{y}_1^\vee + 1 \;, \\
f_6 &= \hat{y}_3^\vee \hat{y}_2^\vee + \hat{y}_3^\vee + 1 \;.
\end{aligned}
\tag{2.82}
$$

The corresponding polytope is given in fig. 2.13, where the facet corresponding to the limiting ray is highlighted in red. We argue that the vertices containing this facet correspond to asymptotic chambers in the degenerate scattering diagram. Such a conjecture naturally explains the appearance

---

[15]Working with the degenerate cluster polytope is purely for visualization purposes and contains equivalent combinatorial information to the degenerate scattering diagram. A review of the map is provided in appendix A.4.

[16]In some sense, this facet would not appear if we tropicalized all functions in $\mathcal{O}(\mathcal{X}^\vee)$ as the facet would be pushed to infinity.
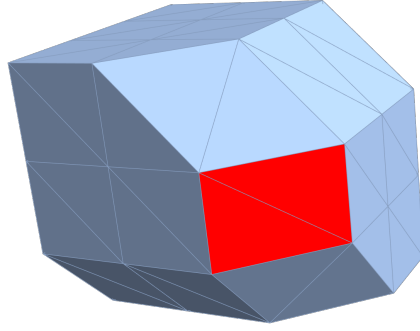
Figure 2.13: A degenerate cluster polytope of $A_{2,1}$ corresponding to the tropicalization of polynomials in eq. (2.82). The red facet corresponds to the limiting ray.
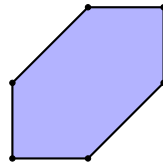
Figure 2.14: The dual polytope of the asymptotic scattering diagram in fig. 2.7. Each asymptotic chamber corresponds to a vertex and walls between asymptotic chambers correspond to 1-dim edges.

of algebraic letters found at 8-point. Note that the facet associated with the limiting ray is not dual to the asymptotic scattering diagram given in section 2.4.1.1, whose associated cluster polytope is given in fig. 2.14. This is because even the asymptotic scattering diagram is degenerate.[17]

There have been several proposals for deriving degenerate scattering diagrams. Such proposals amount to choosing finite subsets of $\mathcal{O}(\mathcal{X}^{\vee})$ to tropicalize. For example, the authors of Ref. [36] proposed that the desirable subset of $\mathcal{O}(\mathcal{X}^{\vee})$ corresponds to the smallest subset of minors closed under parity: $\langle i, i+1, j, j+1 \rangle$ and $\langle i, j-1, j, j+1 \rangle$. These functions can be identified with some subset of $\mathcal{O}(\mathcal{X}^{\vee})$ using the "web-variables" originally given in Ref. [127]. Several alternate subsets have been proposed [36, 100–102, 128]. However, in contrast to our conjecture, which motivates a truncation of the clusters, these proposals argue for a truncation of the x-variables. In the finite case, the authors identify a subset of x-variables whose g-vectors are in bijection with facets of the degenerate cluster polytope and conjecture that this subset acts as a complete multiplicative basis for the desired $\hat{y}$-variables. In the infinite case, where facets corresponding to limiting rays appear, they conjecture the limiting rays correspond to cluster algebraic functions. It may turn

---

[17]It seems that the facet associated with the limiting ray will always be degenerate unless you include F-polynomials associated with points on the limiting ray. These polynomials are not elements of $\mathcal{O}(\mathcal{X}^{\vee})$ as they are not critically positive [36]. In our example, you need to include the F-polynomial associated with the generalization of $\mathcal{P}$ in appendix A.3, even though $\mathcal{P}$ is not an x-variable of the dual cluster algebra.

out these conjectures are equivalent to our proposal. To make any definite conclusion, one would have to find a more precise procedure for isolating the correct degenerate scattering diagram, as the procedure provided here is still ambiguous.

2.6 Discussion

The structure of scattering amplitudes beyond Feynman diagrams has undergone intense study in several contexts over the past 60 years. This program has been very successful at tree level, where numerous bottom-up approaches have almost completely circumvented the Lagrangian approach [129–137]. However, a systematic understanding of how locality, causality and unitarity are precisely encoded at all orders in scattering amplitudes remains surprisingly elusive. Many approaches, ranging from topological strings on twistor space [138] to flat space holography [139–141], have given partial answers to this problem. For example, the infrared structure of scattering amplitudes is famously connected to the vacuum structure of the theory and asymptotic symmetries [142–145]. Recent research suggests that the underlying structure of scattering amplitudes is deeply connected to geometric and combinatorial notions such as total positivity and motives [14, 15, 32, 35, 80, 146]. The amplituhedron provides a precise geometric description of integrands in $\mathcal{N} = 4$ pSYM at all-loop orders. However, although the amplituhedron has led to many interesting results in the study of scattering amplitudes, it is a fundamentally perturbative description of the underlying physics. The ultimate goal of this program is a geometric description of the integrated all-loop amplitude independent of the chosen perturbation method, a "non-perturbative geometry" [36].

One possible manifestation of this non-perturbative geometry is the connection between boundaries of the positive kinematic region and logarithmic branch points of integrated MHV amplitudes in $\mathcal{N} = 4$ pSYM. This conjecture is more subtle than it initially appears due to ambiguities in the precise definition of the positive kinematic region, such as the chosen compactification. In this chapter, we focused on studying the positive kinematic region of the MHV sector and proposed that scattering diagrams are a useful mathematical framework to study the boundary structure of the positive kinematic region. Furthermore, we developed the notion of asymptotic chambers to explain the appearance of algebraic letters in the symbol alphabet of MHV amplitudes. Interestingly, the asymptotic diagram approach provides manifestly rational relations for the asymptotic $\hat{y}_\gamma$-variables associated with the same limiting ray.

As a proof of concept, we used scattering diagrams to study the branch point structure of the 8-point MHV amplitude. Using the scattering diagram framework, we made a conjecture for all possible algebraic letters that could appear in the 8-point symbol alphabet. We confirmed that the algebraic letters found in explicit computations could be written as monomials of letters in our

alphabet. We also developed the notion of degenerate scattering diagrams and commented on a possible truncation procedure for $\hat{y}$-variables, following the philosophy of refs. [36, 101, 102].

Our results are especially interesting in the context of the Landau equations [147, 148]. The Landau equations provide a direct link between the structure of the integrand and the branch points of the integrated amplitude. In particular, the branch points of amplitudes at high multiplicity and loop order have been calculated by applying the Landau equations to the amplituhedron [94–96]. However, although the Landau equations provide a non-trivial probe of the integrated amplitudes' branch points, knowledge of the branch points is not enough to uniquely determine the symbol alphabet (see section 7 of Ref. [95]). For example, although some letters in the alphabet may take the schematic form

$$\phi \sim \frac{f - \sqrt{\triangle'}}{f + \sqrt{\triangle'}} \tag{2.83}$$

where f and $\triangle'$ are rational functions of external kinematic data, the Landau equations only predict branch points of the form $\triangle' = 0$. This mismatch results from how the solution to the Landau equations corresponds to the algebraic branch cut from the square-root in ϕ_i instead of the full logarithmic branch point. A related mismatch also occurs for rational branch points. Similar to how cluster algebras provide the missing link between Landau singularities and the symbol alphabet at 6-point and 7-point, asymptotic chambers provide the missing link between the algebraic symbol alphabet and specific solutions to the Landau equations at 8-point. It has been argued that the branch points of $\mathcal{N} = 4$ pSYM associated with solutions to Landau equations are universal to all gauge theories. It would be interesting to understand whether the logarithmic branch points, which contain more information than the solutions to the Landau equations, retain any degree of universality.

The notion of degenerate scattering diagrams has applications beyond planar gauge theories, specifically higher loop integrands of ϕ^3. However, it is instead the cluster polytope picture that is more interesting for studying higher loop integrands of ϕ^3 [149, 150] and generalized scattering amplitudes [151–157]. Both the higher loop integrands of ϕ^3 and generalized scattering amplitudes can be identified with the canonical rational function of the (degenerate) cluster polytopes discussed in section 2.5 [128]. Each vertex in the cluster polytope can be mapped to a specific Feynman diagram. However, multiple vertices correspond to the same Feynman diagram, and considering all vertices in the full cluster polytope generically overcounts certain Feynman diagrams. Therefore, it is instead more natural to consider degenerate cluster polytopes, where redundant vertices have been truncated. For example, the degenerate cluster polytope associated with $A_{2,1}$, fig. 2.15, is associated with the multi-trace, 1-loop 3-point integrand of ϕ^3 theory [150]. This degenerate polytope can be derived from the tropicalization of f_5 and f_6 in eq. (2.82) along with
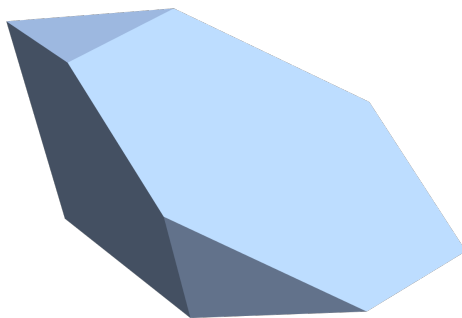
Figure 2.15: A degenerate cluster polytope of $A_{2,1}$ corresponding to the tropicalization of f_4 and f_5 in eq. (2.82) along with eq. (2.84).

the polynomial

$$f_{\mathcal{P}} = 1 + \hat{y}_3^\vee + \hat{y}_1^\vee \hat{y}_2^\vee \hat{y}_3^\vee \, , \tag{2.84}$$

which is the F-polynomial of the generalization of $\mathcal{P}$ in appendix A.3 to $A_{2,1}$. Although the motivation for truncating the unwanted vertices is very different, the notion of truncating undesirable vertices (cones) from the degenerate cluster polytope (scattering diagram) is the same as section 2.5.

Finally, the notion of asymptotic chambers has applications outside of scattering amplitudes, such as studying coordinate systems of (higher) Teichmuller spaces. Specifically, when the cluster algebra corresponds to the (higher) Teichmuller space of a Riemann surface, one can identify cluster algebraic functions with Fenchel-Nielsen coordinates [116]. Non-trivial relations obeyed by Fenchel-Nielsen coordinates, and their generalizations, have been studied in the context of spectral networks [117, 118]. However, to our knowledge, no one has systematically studied relations between Fenchel-Nielsen coordinates in the context of scattering diagrams and cluster mutations.

CHAPTER 3

Double Copy and Effective Field Theory

3.1 Overview

We have previously restricted ourselves to studying planar scattering amplitudes. However, many interesting amplitudes do not have any color structure and therefore don't have the same simplifications. It is important to develop better techniques to compute such amplitudes. Beginning with the pioneering discovery of Kawai-Lewellen-Tye (KLT) [38], the existence of a multiplicative structure, called the *double-copy*, on the space of relativistic field theories and string theories has become an indispensable tool for the computation of uncolored scattering amplitudes. The double copy is playing an increasingly important role in modern gravity computations; for example, one of the recent exciting applications is to gravitational-wave physics [41, 158–165]. However, a fully systematic understanding of the double-copy is still an open question. We will study the double-copy in the context of higher dimension operators.

The significance of EFTs was discussed in section 1.3. Although several procedures for double-copying higher dimension operators have been developed [166–169], no pattern had previously emerged for which local counterterms can and cannot be derived from the double-copy. This chapter consists of a technical derivation of the KLT bootstrap, the algorithm for computing higher derivative corrections to the double copy map, and the application of the generalized KLT double copy to YM with higher derivative operators to compute amplitudes in GR with higher derivative corrections.

To illustrate our methodology, we examine the KLT bootstrap at 4-point. At 4-point, the sum in eq. (3.1) is over just a single choice of color-orderings α and β. For a specific choice for orderings, the 4-point KLT formula for the identity model, $\mathbb{1} \otimes \mathbb{1} = \mathbb{1}$, becomes

$$m_4[\gamma|\delta] = m_4[\gamma|\alpha] \, S_4[\alpha|\beta] \, m_4[\beta|\delta] \,|_{\gamma=\beta, \delta=\alpha}. \tag{3.1}$$

which simplifies to

$$S_4[\alpha|\beta] = 1/m_4[\beta|\alpha] \,. \tag{3.2}$$

Therefore, the KLT formula for the identity implies the kernel of the double-copy is determined by the double-partial amplitudes of the identity mode. For generic orderings, the double-copy bootstrap equation $\mathbb{1} \otimes \mathbb{1} = \mathbb{1}$ becomes

$$m_4[\gamma|\delta] = m_4[\gamma|\alpha] \frac{1}{m_4[\beta|\alpha]} m_4[\beta|\delta] \,. \tag{3.3}$$

Rearranging eq. (3.3), it says

$$\det \begin{pmatrix} m_4[\beta|\alpha] & m_4[\beta|\delta] \\ m_4[\gamma|\alpha] & m_4[\gamma|\delta] \end{pmatrix} = 0 \,. \tag{3.4}$$

Since this holds for all choices of the $(n-1)! = 6$ color-orderings $\alpha, \beta, \gamma, \delta$, this says that all such 2×2 minors vanish. In other words, the 6×6 matrix of doubly color-ordered zeroth-copy tree amplitudes m_4 must have rank 1. The determinant in eq. (3.4) trivially vanishes for amplitudes of the cubic BAS model, but once higher-derivative operators are included, eq. (3.4) becomes a non-trivial constraint. This is an example of how $\mathbb{1} \otimes \mathbb{1} = \mathbb{1}$ becomes a bootstrap equation for the zeroth copy and hence for the double-copy kernel. We solve eq. (3.3) perturbatively in the momentum expansion, and subject to additional constraints from locality, we find the most general allowed higher-derivative corrections to the BAS model consistent with bootstrap constraints at 4- and 5-point.

Using the generalized KLT kernel, we study how higher dimension operators in YM map to operators in GR. To do so, we perturbatively impose the generalized KKBCJ equations discussed in section 1.3 and then double-copy the resulting theory using the generalized kernel. At 4-point, we study how generic operators in YM are constrained by the generalized KKBCJ relations and map to operators in GR. At 5-point, due to the complexity of calculations, we restrict the external polarization vectors to a particular configuration called the self-dual sector to simplify expressions. Remarkably, at both 4-point and 5-point, we find that the double-copy contains the same operators as the standard field theory double copy, but with shifts in some of their Wilson coefficients.

We largely focus on generalizations of the double-copy that arise from adding higher-derivative operators to the BAS model, but one can also look for other types of solutions to the KLT bootstrap equations. In section 3.7, we initiate a search for zeroth copies at various ranks. The central property we examine is whether the rank R_n determinant has zeroes in unphysical locations that could lead to spurious singularities in the double-copy amplitudes *unless* additional cancellations take place. The locality constraints are again essential and indicate that minimal rank $(n-3)!$ may play a special role for generalizations of the double-copy.

3.2 Double-Copy Bootstrap

We have previously outlined the ideas of the double-copy bootstrap. The purpose of this section is to make each step of the procedure precise.

3.2.1 Double-Copy Kernel and Zeroth-Copy Models: Bootstrap $\mathbb{1} \otimes \mathbb{1} = \mathbb{1}$

In the KLT double-copy formula,

$$\mathcal{A}_n^{\text{L}\otimes\text{R}} = \sum_{\alpha,\beta} \mathcal{A}_n^{\text{L}}[\alpha] \, S_n[\alpha|\beta] \, \mathcal{A}_n^{\text{R}}[\beta], \tag{3.5}$$

the L (R) sector refers to field theories with all states in the adjoint representation of color groups G_L (G_R), which could for example be $SU(N)$ ($SU(\tilde{N})$). The single-copy amplitudes $\mathcal{A}_n^{\text{L}}[\alpha]$ ($\mathcal{A}_n^{\text{R}}[\beta]$) are color-ordered with respect to a single-trace of n generators of G_L (G_R). The structure of eq. (3.5) shows that the double-copy kernel S_n has a color-structure associated with the product $G_L \times G_R$. As we indicated in the Introduction, the kernel is the inverse of a submatrix of doubly color-ordered m_n amplitudes, so they must have a color-structure $G_R \times G_L$. The candidates for the zeroth-copy models are local field theories with a single scalar field $\phi^{aa'}$ that transforms in the adjoint of each group factors.

At n-point there are $n!$ possible color-orderings for each color-group factor, but only $(n-1)!$ are independent under the cyclicity of each color-trace. We use $\mathbf{m}_n$ to denote the $(n-1)! \times (n-1)!$ matrix of color-ordered tree amplitudes of the zeroth copy. For example, at 4-point we choose the ordering $\{1234, 1243, 1324, 1342, 1423, 1432\}$ and the 6×6 matrix of zeroth-copy tree amplitudes is then

$$\mathbf{m}_4 = \begin{pmatrix} m_4[1234|1234] & m_4[1234|1243] & m_4[1234|1324] & \cdots & m_4[1234|1432] \\ m_4[1243|1234] & m_4[1243|1243] & m_4[1243|1324] & \cdots & m_4[1243|1432] \\ \vdots & \vdots & \vdots & & \vdots \\ m_4[1432|1234] & m_4[1432|1243] & m_4[1432|1324] & \cdots & m_4[1432|1432] \end{pmatrix}. \tag{3.6}$$

We do not make any assumptions a priori about the properties of the color-ordered amplitudes m_n. For example, we do *not* assume trace-reversal, so in general

$$m[\beta|\alpha^T] \neq m[\beta|\alpha] \quad \text{or} \quad m[\beta^T|\alpha] \neq m[\beta^T|\alpha], \tag{3.7}$$

where for example $\{1234\}^T = \{4321\} = \{1432\}$. Also, we do *not* assume that the $\mathbf{m}_n$ is symmetric, i.e. in general we have

$$m_4[\beta|\alpha] \neq m_4[\alpha|\beta]. \tag{3.8}$$

For the BAS or string zeroth-copy models, the rank of the matrix $\mathbf{m}_n$ is $(n-3)!$; this is what we call *minimal rank*. Moreover, in those two cases, trace-reversal does hold and $\mathbf{m}_n$ is symmetric. Allowing for generalizations makes it possible to incorporate more 'heterotic' double-copies in which the L and R constraints are genuinely distinct.

Suppose more generally that, for some integer R_n, there are invertible $R_n \times R_n$ submatrices of $\mathbf{m}_n$. We label such submatrices by a specification of a choice of a subset of R_n orderings for the rows and columns in $\mathbf{m}_n$. We denote the row or *R basis* as $B_R = \{\beta_1, ..., \beta_{R_n}\}$ and the column or *L basis* as $B_L = \{\alpha_1, ..., \alpha_{R_n}\}$. In matrix notation, we then have

$$
\mathbf{m}_n(B_R, B_L) \equiv
\begin{bmatrix}
m_n[\beta_1|\alpha_1] & \cdots & m_n[\beta_1|\alpha_{R_n}] \\
\vdots & \ddots & \vdots \\
m_n[\beta_{R_n}|\alpha_1] & \cdots & m_n[\beta_{R_n}|\alpha_{R_n}]
\end{bmatrix}.
\tag{3.9}
$$

The condition that the zeroth copy is the identity element under the double-copy multiplication rule, $\mathbb{1} \otimes \mathbb{1} = \mathbb{1}$, is that the tree amplitudes copy to themselves using the double-copy kernel; in matrix notation, this is the requirement

$$
\mathbb{1} \otimes \mathbb{1} = \mathbb{1}: \quad \mathbf{m}_n\left(B_R', B_L\right) \mathbf{S}_n\left(B_L, B_R\right) \mathbf{m}_n\left(B_R, B_L'\right) = \mathbf{m}_n\left(B_R', B_L'\right).
\tag{3.10}
$$

Now set $B_L' = B_L$ and $B_R' = B_R$ in eq. (3.10) and multiply on both the L and R by $\left(\mathbf{m}_n\left(B_R, B_L\right)\right)^{-1}$. It then follows that

$$
\mathbf{S}_n(B_L, B_R) \equiv \left(\mathbf{m}_n(B_R, B_L)\right)^{-1}.
\tag{3.11}
$$

Thus, requiring the zeroth copy to be an identity element under the double-copy inevitably links its tree amplitudes to the double-copy kernel.

This, however, does not exhaust the contents of eq. (3.10). Using eq. (3.11), we have

$$
\text{bootstrap eq:} \quad \mathbf{m}_n\left(B_R', B_L\right) \left(\mathbf{m}_n\left(B_R, B_L\right)\right)^{-1} \mathbf{m}_n\left(B_R, B_L'\right) = \mathbf{m}_n\left(B_R', B_L'\right),
\tag{3.12}
$$

This equation is non-trivial for elements of B_L' that are not in B_L and elements of B_R' not in B_R. As such, it constrains the zeroth-copy amplitudes m_n: thus eq. (3.12) is our double-copy bootstrap equation.

To interpret the constraint eq. (3.12), consider for a given basis choice, B_L and B_R, the extension

of $\mathbf{m}_n(B_R, B_L)$ to the $(R_n + 1) \times (R_n + 1)$ submatrix

$$M = \left[\begin{array}{ccc|c} m_n[\beta_1|\alpha_1] & \cdots & m_n[\beta_1|\alpha_{R_n}] & m_n[\beta_1|\delta] \\ \vdots & \ddots & \vdots & \vdots \\ m_n[\beta_{R_n}|\alpha_1] & \cdots & m_n[\beta_{R_n}|\alpha_{R_n}] & m_n[\beta_{R_n}|\delta] \\ \hline m_n[\gamma|\alpha_1] & \cdots & m_n[\gamma|\alpha_{R_n}] & m_n[\gamma|\delta] \end{array} \right], \tag{3.13}$$

where $\alpha_i \in B_L$ and $\beta_i \in B_R$ while $\delta \notin B_L$ and $\gamma \notin B_R$. Using that the determinant of a block matrix with $\det A \neq 0$ can be expressed as

$$\det \left[\begin{array}{c|c} A & B \\ \hline C & D \end{array} \right] = \det(A) \det \left(D - CA^{-1}B \right), \tag{3.14}$$

we can write the determinant of eq. (3.13) as

$$\det(M) = \det \left(\mathbf{m}_n \left(B_R, B_L \right) \right) \times \left(m_n[\gamma|\delta] - \mathbf{m}_n[\gamma|B_L] \left(\mathbf{m}_n \left(B_R, B_L \right) \right)^{-1} \mathbf{m}_n[B_R|\delta] \right), \tag{3.15}$$

By eq. (3.11), the (negative of the) second factor can be written

$$\sum_{\alpha \in B_L, \beta \in B_R} m_n[\gamma|\alpha] \, \mathbf{S}_n \left(B_L, B_R \right) [\alpha|\beta] \, m_n[\beta|\delta] - m_n[\gamma|\delta]. \tag{3.16}$$

The vanishing of this condition is exactly the same as the written-out matrix multiplication of eq. (3.12). Thus we learn that ***the "self-copy"*** $\mathbb{1} \otimes \mathbb{1} = \mathbb{1}$ ***condition (3.12) is equivalent to the requirement that the full*** $(n-1)! \times (n-1)!$ ***matrix*** $\mathbf{m}_n$ ***of zeroth-copy amplitudes has rank*** $\mathbf{R_n}$. This means that *the rank R_n of the double-copy kernel must be equal to the rank of the full matrix* $\mathbf{m}_n$.

3.2.2 Single-Copy Models: Generalized KKBCJ from $\mathbb{1} \otimes \mathbf{R} = \mathbf{R}$ and $\mathbf{L} \otimes \mathbb{1} = \mathbf{L}$

It is convenient also to use a matrix notation to represent the single-copy amplitudes with orderings restricted to a given choice of basis

$$\mathbf{A}_n^{\mathrm{L}}(B_L) \equiv \left(\mathcal{A}_n^{\mathrm{L}}[\alpha_1] \quad \cdots \quad \mathcal{A}_n^{\mathrm{L}}[\alpha_{R_n}] \right)^\top, \qquad \mathbf{A}_n^{\mathrm{R}}(B_R) \equiv \left(\mathcal{A}_n^{\mathrm{R}}[\beta_1] \quad \cdots \quad \mathcal{A}_n^{\mathrm{R}}[\beta_{R_n}] \right)^\top, \tag{3.17}$$

where $^\top$ denotes transpose. In this notation, the double-copy formula (3.5) can be written as a simple matrix product

$$\mathcal{A}_n^{\text{L}\otimes\text{R}} = \left(\mathbf{A}_n^{\text{L}}\left(B_L\right)\right)^\top \mathbf{S}_n(B_L, B_R)\, \mathbf{A}_n^{\text{R}}\left(B_R\right). \tag{3.18}$$

and the generalized KKBCJ relations arise from the KLT algebra:

$$\mathbb{1}\otimes\text{R}=\text{R}: \qquad \mathbf{m}_n\left(B_R', B_L\right)\mathbf{S}_n\left(B_L, B_R\right)\mathbf{A}_n^{\text{R}}\left(B_R\right) = \mathbf{A}_n^{\text{R}}\left(B_R'\right), \tag{3.19}$$

$$\text{L}\otimes\mathbb{1}=\text{L}: \qquad \left(\mathbf{A}_n^{\text{L}}\left(B_L\right)\right)^\top \mathbf{S}_n\left(B_L, B_R\right)\mathbf{m}_n\left(B_R, B_L'\right) = \left(\mathbf{A}_n^{\text{L}}\left(B_L'\right)\right)^\top. \tag{3.20}$$

These conditions are non-trivial only for elements in B_R' (B_L') that are not in B_R (B_L).

The relations eqs. (3.19) and (3.20) are the *generalized KKBCJ conditions*. They ensure that the result of the double-copy is independent of the choice of bases B_L and B_R. To see this, rewrite eq. (3.19) as

$$\mathbf{S}_n\left(B_L, B_R\right)\mathbf{A}_n^{\text{R}}\left(B_R\right) - \mathbf{S}_n\left(B_L, B_R'\right)\mathbf{A}_n^{\text{R}}\left(B_R'\right) = 0. \tag{3.21}$$

When multiplied from the left by $\left(\mathbf{A}_n^{\text{L}}\left(B_L\right)\right)^\top$, eq. (3.21) states that the double copy resulting from the two basis choices of B_R and B_R' are the same. Similarly, eq. (3.20) ensures that the double-copy is independent of the choice of L-basis. Without basis independence, we cannot think of the double-copy as a map between field theories.

When the m_n are the amplitudes of the BAS model, the generalized KKBCJ conditions become the standard KKBCJ relations discussed in the Introduction. Likewise, they are equivalent to the string monodromy relations when the m_n are the amplitudes of the string zeroth copy.

When the full matrix $(n-1)! \times (n-1)!$ of zeroth-copy amplitudes $\mathbf{m}_n$ has non-maximal rank R_n, it must have $(n-1)! - R_n$ null vectors n_i^{L} and n_i^{R} for multiplication from the left and right, respectively. We show in Appendix 3.2.5 that these null vectors precisely encode the generalized KKBCJ relations as

$$\sum_{\text{all }\beta} n_i^{\text{R}}[\beta]\, \mathcal{A}_n^{\text{R}}[\beta] = 0 \quad \text{and} \quad \sum_{\text{all }\alpha} \mathcal{A}_n^{\text{L}}[\alpha]\, n_i^{\text{L}}[\alpha] = 0 \tag{3.22}$$

for each $i = 1, 2, \ldots, (n-1)! - R_n$. The relation between null vectors and BCJ conditions was introduced previously in the context of a massive double-copy formalism in [170]. They are useful for understanding how the generalized KKBCJ relations modify the regular field theory KKBCJ relations.

3.2.3 Roadmap for the Generalized Double-Copy

Let us summarize how the double-copy bootstrap proceeds:

1. Choose a candidate for a zeroth-copy model, i.e. a local field theory with a bi-adjoint scalar field $\phi^{aa'}$ and some choice of interactions. Compute its color-ordered tree amplitudes $m_n[\alpha|\beta]$.

2. Subject the matrix of these amplitudes to the double-copy bootstrap equation $\mathbb{1} \otimes \mathbb{1} = \mathbb{1}$ in the form eq. (3.12) with some choice of rank R_n, possibly restricting the couplings in the model. Inverting the resulting rank R_n matrices gives the generalized double-copy kernel S_n via eq. (3.11).

3. Tree amplitudes of L and R single-copy local models are then subjected to the generalized KKBCJ relations $L \otimes \mathbb{1} = L$ and $\mathbb{1} \otimes R = R$ in the form of eqs. (3.19) and (3.20).

4. Double-copy using eq. (3.18).

Along the way, locality constraints must be imposed. In particular, we have pointed out that zeroes of $\det(\mathbf{m}_n(B_R, B_L))$ may signal issues with spurious poles in the double-copy.

A particularly prominent example is the bootstrap of a zeroth-copy model based on BAS with higher-derivative corrections, so let us comment more on this.

3.2.4 Perturbative KLT Bootstrap

To study a double-copy kernel based on BAS + higher-derivative (HD) operators, let $m_n^{(0)}$ denote the BAS amplitudes and $\mathcal{A}_n$ the single-copy amplitudes that obey the regular field theory KKBCJ relations associated with the BAS zeroth copy. We can then write the BAS + HD amplitudes and single-copy amplitudes (suppressing L and R superscripts) as

$$m_n[\beta|\alpha] = m_n^{(0)}[\beta|\alpha] + m_n^{(1)}[\beta|\alpha] + \dots,$$
$$\mathcal{A}_n[\alpha] = \mathcal{A}_n^{(0)}[\alpha] + \mathcal{A}_n^{(1)}[\alpha] + \dots,$$
$$(3.23)$$

where $m^{(i)}[\beta|\alpha]$ and $\mathcal{A}_n^{(i)}[\alpha]$ with $i > 0$ are the contributions from higher-dimension operators. They are systematically organized by increasing powers in $1/\Lambda$ of the UV scale of BAS+HD EFT such that the limits

$$\lim_{\Lambda \to \infty} m_n[\beta|\alpha] = m_n^{(0)}[\beta|\alpha], \quad \lim_{\Lambda \to \infty} \mathcal{A}_n[\alpha] = \mathcal{A}_n^{(0)}[\alpha] \qquad (3.24)$$

Double-Copy
w/ BAS+HD

YM+HD $\longrightarrow$ Gravity+HD

UV Decoupling   UV Decoupling
$\Lambda \to \infty$ $\Lambda \to \infty$

Double-Copy
w/ BAS

YM $\longrightarrow$ Gravity
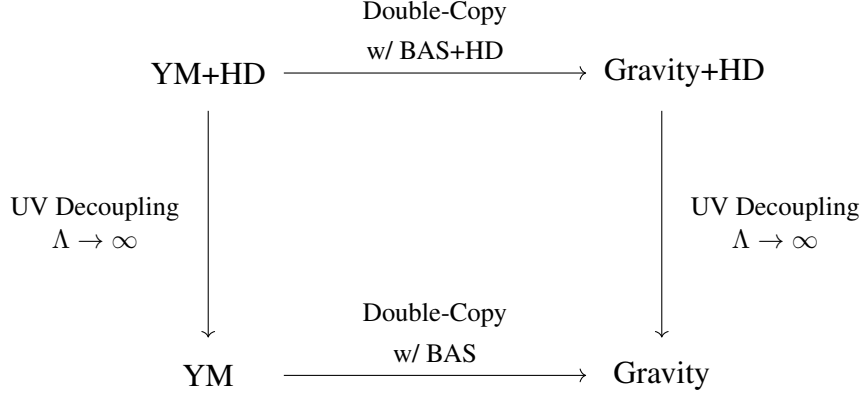
Figure 3.1: Illustration of the physical meaning of the perturbative double-copy. Physics at the UV scale Λ decouples in both the single- and double-copies as $\Lambda \to \infty$ (i.e. this diagram commutes) only if the rank of the higher-derivative corrected BAS is the same as the rank of the uncorrected BAS.

are smooth. This is the expected behavior in a physical EFT where the Λ corresponds to the scale of some, perhaps unknown, UV physics which decouples from the IR dynamics in an appropriate limit.[1]

Taking the double-copy to be perturbative in $1/\Lambda$ means that the double-copy amplitude also has an expansion in $1/\Lambda$. For example, the double copy of YM+HD with itself should give NS-NS gravity plus higher dimension operators and the contributions from these operators should go smoothly to zero as $\Lambda \to \infty$. This physically sensible requirement has implications for the rank of the double-copy kernel. Generic deformations of cubic BAS will increase the rank from $(n-3)!$ of BAS. Since the double-copy kernel is the inverse of a rank R_n matrix of BAS+HD amplitudes, the kernel would be divergent in the limit $\Lambda \to \infty$ where the cubic BAS amplitudes are recovered. This would imply that the double-copy amplitudes do not have sensible $\Lambda \to \infty$ limits and then we can no longer identify $\Lambda \to \infty$ as the limit of decoupling UV physics.

To avoid a situation of unnatural UV-IR mixing in the double-copy, we must therefore require that the rank of the zeroth copy *does not change* as a function of Λ.[2] This means that to study the most general double-copy kernel based on BAS+HD we must work with the rank $R_n = (n-3)!$.

The double-copy bootstrap with rank $(n-3)!$ is studied at 3-, 4-, and 5-point in Sections 3.3-3.6. In Section 3.7 we consider examples of models with rank $R_n > (n-3)!$ that are not UV deformations of the BAS model.

---

[1]We are not considering mass-deformations of the BAS model. See [170] for a discussion of double-copy construction with masses.

[2]Of course, it is logically possible that the UV dynamics may not fully decouple, and we are free to entertain the possibility of a discontinuity in the rank of the zeroth copy. Curiously, for all examples studied in this chapter, relaxing this naturalness assumption also leads to spurious poles in the double-copy.

3.2.5 Generalized KKBCJ Relations as Null Vectors

We now show that the $\text{BAS} \times \text{BAS}$ bootstrap equation and deformed BCJ relation yield that vectors orthogonal to $\mathcal{A}^{\text{R}}[\alpha]$ span the kernel of the column space of $m[\alpha|\beta]$, thereby proving that there are only $(n-1)! - R_n$ linearly independent generalized KKBCJ relations. A similar argument holds for $\mathcal{A}^{\text{L}}[\alpha]$, whose orthogonal vectors span the nullspace, or the kernel of the row space, of $m[\alpha|\beta]$.

We can choose the $(n-1)!$ color orderings as

$$\{\text{all } (n-1)! \text{ color-orderings}\} = B_R \bigcup \bar{B}_R \,, \tag{3.25}$$

where B_R is some BCJ basis and $\bar{B}_R$ is the complement of B_R in the $(n-1)!$ color orderings. And $B_R \bigcup \bar{B}_R$ means B_R occupies the first R_n slots, while $\bar{B}_R$ takes the remaining $(n-1)! - R_n$ slots, of the $(n-1)!$ color-orderings.

Then, an explicit basis for these $(n-1)! - R_n$ different null vectors take the form

$$\vec{n}_i^{\text{R}} = \left(\mathbf{m}_n[\alpha_i, B_{\text{L}}] \mathbf{S}_n[B_L, B_R], \quad 0, \quad \cdots, \quad -1, \quad \cdots \right)$$

$$\equiv \left(\mathbf{m}_n[\alpha_i, B_{\text{L}}] \mathbf{S}_n[B_L, B_R], \quad -\mathbf{1}_{\alpha_i} \right), \tag{3.26}$$

where α_i corresponds to some color-ordering in $\bar{B}_R$ and the -1 entry is at the corresponding position of α_i in eq. (3.25). So the defined vector $-\mathbf{1}_{\alpha_i}$ takes value -1 at the corresponding position of α_i and 0 elsewhere. And different choices of the dummy BCJ basis B_L will give the same null vectors.

Taking the product of $\vec{n}_i^{\text{R}}$ with $\mathbf{m}_n$ and $\mathcal{A}^{\text{R}}$, one finds

$$\vec{n}_i^{\text{R}} \cdot \mathbf{m}_n \left[B_R \bigcup \bar{B}_R, B_L' \bigcup \bar{B}_L' \right]$$

$$= \left(\mathbf{m}_n[\alpha_i, B_{\text{L}}] \mathbf{S}_n[B_L, B_R], \quad -\mathbf{1}_{\alpha_i} \right) \cdot \left(\frac{\mathbf{m}_n[B_R, B_L'] \,\big|\, \mathbf{m}_n[B_R, \bar{B}_L']}{\mathbf{m}_n[\bar{B}_R, B_L'] \,\big|\, \mathbf{m}_n[\bar{B}_R, \bar{B}_L']} \right)$$

$$= \left(\begin{matrix} \mathbf{m}_n[\alpha_i, B_{\text{L}}] \mathbf{S}_n[B_L, B_R] \mathbf{m}_n[B_R, B_L'] - \mathbf{m}_n[\alpha_i, B_L'], \\ \mathbf{m}_n[\alpha_i, B_{\text{L}}] \mathbf{S}_n[B_L, B_R] \mathbf{m}_n[B_R, \bar{B}_L'] - \mathbf{m}_n[\alpha_i, \bar{B}_L'] \end{matrix} \right)^{\text{T}}$$

$$= \vec{0}, \tag{3.27}$$

and

$$\vec{n}_i^{\text{R}} \cdot \mathbf{A}^{\text{R}} \left[B_R \bigcup \bar{B}_R \right]$$
$$= \left(\mathbf{m}_n[\alpha_i, B_{\text{L}}] \mathbf{S}_n[B_L, B_R], \quad -\mathbf{1}_{\alpha_i} \right) \cdot \left(\mathbf{A}^{\text{R}}[B_R], \quad \mathbf{A}^{\text{R}}[\bar{B}_R] \right)$$
$$= \mathbf{m}_n[\alpha_i, B_{\text{L}}] \mathbf{S}_n[B_L, B_R] \mathbf{A}^{\text{R}}[B_R] - \mathbf{A}^{\text{R}}[\alpha_i]$$
$$= 0, \tag{3.28}$$

where we used the bootstrap equation and the deformed KKBCJ relations, and B'_L is some BCJ basis and $\bar{B}'_L$ is its complement in the $(n-1)!$ color orderings. A different choice of B'_L corresponds to a trivial rearrangement of column vectors of $\mathbf{m}_n \left[B_R \bigcup \bar{B}_R, B'_L \bigcup \bar{B}'_L \right]$. Eq. (3.27) explicitly shows that $\vec{n}_i^{\text{R}}$ is orthogonal to column vectors of the $(n-1)! \times (n-1)!$ $\mathbf{m}_n$ matrix, and to $\mathbf{A}^{\text{R}}$ as well.

The $\vec{n}_i^{\text{R}}$'s are manifestly linearly independent due to the different locations of -1 entry in each vector, so the $\vec{n}_i^{\text{R}}$'s correspond to a complete basis for the kernel of the column space of $\mathbf{m}_n$, and also the space of the generalized KKBCJ relations of $\mathbf{A}^{\text{R}}$. Since there are only $(n-1)! - R_n$ linearly independent null vectors of $\mathbf{m}_n$, there are olny $(n-1)! - R_n$ linearly independent generalized KKBCJ relations of $\mathbf{A}^{\text{R}}$.[3]

3.3 KLT Bootstrap at 3-Point

Let us begin at 3-point as an informative warm-up for the higher-point analysis. In 3-particle kinematics, all Mandelstam variables vanish on-shell, so it is impossible for an on-shell 3-point scalar amplitude to have momentum dependence. At the level of the Lagrangian, this means that any higher-derivative corrections at 3-point can be moved into higher-point by a field redefinition. Thus we only need to consider *constant* 3-point scalar amplitudes.

By cyclic symmetry, there are two independent options for the double color ordered bi-adjoint scalar amplitudes and we parameterize them using couplings g and λ_3 as

$$m_3[123|123] = g + \lambda_3, \qquad m_3[123|132] = -g + \lambda_3. \tag{3.29}$$

---

[3]If we have reversal identity for the BAS theory, $m_n[\alpha|\beta^T] = (-1)^{x_1} m_n[\alpha|\beta]$ and $m_n[\alpha^T|\beta] = (-1)^{x_2} m_n[\alpha|\beta]$, for signs determined by possibly n-dependent integers x_1 and x_2, we also have corresponding reversal identity for the L and R sector of the single copy theory.

These amplitudes arise from Lagrangian interactions of the form[4]

$$\mathcal{L}_3 = -\frac{g}{6} f^{abc} \tilde{f}^{a'b'c'} \phi^{aa'} \phi^{bb'} \phi^{cc'} + \frac{\lambda_3}{6} d^{abc} \tilde{d}^{a'b'c'} \phi^{aa'} \phi^{bb'} \phi^{cc'}. \tag{3.30}$$

The first term is the cubic interaction from the cubic BAS model (1.32) and the second one is its fully symmetric counterpart. In terms of generators, we have

$$i f^{abc} = \text{Tr} \left[T^a [T^b, T^c] \right], \qquad d^{abc} = \text{Tr} \left[T^a \{T^b, T^c\} \right]. \tag{3.31}$$

The invariant d^{abc} is sometimes called the anomaly coefficient and it is non-zero for generic representations of $SU(N)$ groups with $N > 2$.

The general 2×2 bi-adjoint scalar matrix labeled by the $(n-1)! = 2$ independent color-orderings $\{123, 132\}$ is then

$$\mathbf{m}_3 = \begin{pmatrix} m_3[123|123] & m_3[123|132] \\ m_3[132|123] & m_3[132|132] \end{pmatrix} = \begin{pmatrix} g + \lambda_3 & -g + \lambda_3 \\ -g + \lambda_3 & g + \lambda_3 \end{pmatrix}, \tag{3.32}$$

and its determinant is

$$\det(\mathbf{m}_3) = 4g\lambda_3. \tag{3.33}$$

Thus, for non-zero values of g and λ_3 the matrix $\mathbf{m}_3$ has rank 2, however, whenever one of the two couplings vanishes, the rank is reduced to 1. In Section 3.7, we show that the model with $\lambda_3 \neq 0$ does not satisfy the minimal-rank condition at 4-point and it leads to a generalized KLT kernel with spurious poles at 5-point. For this reason, we set

$$\lambda_3 = 0 \tag{3.34}$$

in our studies of generalizations of the KLT double-copy. This in particular means that the null vectors of $\mathbf{m}_3$ are $\{1, 1\}$, which via eq. (3.22) imply the usual 3-point KK relation

$$\mathcal{A}_3[132] + \mathcal{A}_3[123] = 0 \tag{3.35}$$

on the L and R sector 3-point amplitudes.

---

[4]A mixed term , $f^{abc} \tilde{d}^{a'b'c'} \phi^{aa'} \phi^{bb'} \phi^{cc'} = 0$, vanishes due to the symmetric-antisymmetric index contractions.

3.4 KLT Bootstrap at 4-Point

In this section, we solve the KLT bootstrap equation at 4-point for minimal rank $(n-3)! = 1$. The general solution can be written in terms of a single function and we derive from it the generalized KKBCJ relations. Next, we use these results to find the most general higher-derivative corrections to the BAS model at 4-points subject to constraints of locality and minimal rank. This gives a generalized KLT formula for double-copying single-color EFTs at 4-point. We compare the result to the string KLT kernel and comment in general properties of the result.

3.4.1 4-Point Bootstrap Equations

The KLT bootstrap for minimal rank $(n-3)! = 1$ imposes that all 2-by-2 minors of the matrix $\mathbf{m}_4$ in eq. (3.6) must vanish,

$$m_4[\alpha|\beta]m_4[\delta|\gamma] = m_4[\alpha|\gamma]m_4[\delta|\beta], \tag{3.36}$$

for any choice of $\alpha, \beta, \gamma, \delta \in \{1234, 1243, 1324, 1342, 1423, 1432\}$.

Using cyclic symmetry and momentum relabeling, the six different doubly color-ordered 4-point amplitudes m_4 can be expressed in terms of three functions, f_1, f_2, and f_6, as follows:

$$
\begin{aligned}
m_4[1234|1234] &= f_1(s,t) \quad \text{with} \quad f_1(s,t) = f_1(u,t)\,, \\
m_4[1234|1243] &= f_2(s,t)\,, \\
m_4[1234|1324] &= f_3(s,t) = f_2(u,t)\,, \\
m_4[1234|1342] &= f_4(s,t) = f_2(s,t)\,, \\
m_4[1234|1423] &= f_5(s,t) = f_2(u,t)\,, \\
m_4[1234|1432] &= f_6(s,t) \quad \text{with} \quad f_6(s,t) = f_6(u,t)\,.
\end{aligned}
\tag{3.37}
$$

where here and in the following it is always understood that $s + t + u = 0$. For example, to obtain the 3rd line, we use that

$$
\begin{aligned}
f_3(s,t) &= m_4[1234|1324] = m_4[4123|4132] = m_4[1234|1243]\Big|_{1\to4\to3\to2\to1} \\
&= f_2(s,t)\Big|_{1\to4\to3\to2\to1} = f_2(u,t)\,.
\end{aligned}
\tag{3.38}
$$

We allow for the possibility that $m_n[\beta|\alpha] \neq m_n[\alpha|\beta]$ and we do not assume trace reversal symmetry, e.g. $m_n[\alpha|\beta^T]$ is not necessarily related to $m_n[\alpha|\beta]$. In terms of f_1, f_2, and f_6, the matrix $\mathbf{m}_4$

of eq. (3.6) then takes the form

$$
\mathbf{m}_4 =
\begin{pmatrix}
f_1(s,t) & f_2(s,t) & f_2(u,t) & f_2(s,t) & f_2(u,t) & f_6(s,t) \\
f_2(s,u) & f_1(s,u) & f_2(t,u) & f_6(s,u) & f_2(t,u) & f_2(s,u) \\
f_2(u,s) & f_2(t,s) & f_1(t,s) & f_2(t,s) & f_6(t,s) & f_2(u,s) \\
f_2(s,u) & f_6(t,u) & f_2(t,u) & f_1(t,u) & f_2(t,u) & f_2(s,u) \\
f_2(u,s) & f_2(t,s) & f_6(u,s) & f_2(t,s) & f_1(u,s) & f_2(u,s) \\
f_6(u,t) & f_2(s,t) & f_2(u,t) & f_2(s,t) & f_6(u,t) & f_2(u,t)
\end{pmatrix}.
\tag{3.39}
$$

Generically this matrix has rank 6, so we must impose the rank 1 bootstrap condition by setting all 2-by-2 minor to zero. This can be done very simply. Consider the vanishing of the 2-by-2 minor of eq. (3.39) with rows 1 and 2 and columns 1 and 6:

$$
\big(f_1(s,t) - f_6(s,t)\big) f_2(s,u) = 0.
\tag{3.40}
$$

This implies[5]

$$
\boxed{f_6(s,t) = f_1(s,t).}
\tag{3.41}
$$

Next, the 2-by-2 minor of eq. (3.39) with rows 1 and 3 and columns 1 and 2 vanishes when

$$
0 = f_1(s,t) f_2(t,s) - f_2(s,t) f_2(u,s),
\tag{3.42}
$$

while the vanishing of the minor with rows 1 and 2 and columns 1 and 3 requires

$$
0 = f_1(s,t) f_2(t,u) - f_2(s,u) f_2(u,t).
\tag{3.43}
$$

It follows from eq. (3.42) that f_1 is fixed in terms of f_2 as

$$
\boxed{f_1(s,t) = \frac{f_2(s,t) f_2(u,s)}{f_2(t,s)},}
\tag{3.44}
$$

and combining eqs. (3.42) and (3.43) gives a final self-consistency condition for f_2,

$$
\boxed{f_2(s,t) f_2(u,s) f_2(t,u) = f_2(t,s) f_2(u,t) f_2(s,u).}
\tag{3.45}
$$

When the three equations eqs. (3.41), (3.44), and (3.45) are imposed, the matrix (3.39) has rank 1, as desired; thus, these three conditions are the **4-point KLT bootstrap equations**.

---

[5]When $f_2 = 0$, the other rank 1 conditions set $f_1 = f_6 = 0$. So we assume f_2 to be non-zero.

The cubic bi-adjoint scalar amplitudes in eq. (1.32) have

$$f_1^{\text{BAS}}(s,t) = f_6^{\text{BAS}}(s,t) = \frac{g^2}{s} + \frac{g^2}{u}, \quad f_2^{\text{BAS}}(s,t) = -\frac{g^2}{s}, \tag{3.46}$$

and it is easy to see that they solve the three 4-point bootstrap equations eqs. (3.41), (3.44), and (3.45). They are likewise solved by the string theory 4-point amplitudes of Mizera which have [39]

$$f_1^{\text{string}}(s,t) = f_6^{\text{string}}(s,t) = \frac{1}{\tan(\alpha'\pi s)} + \frac{1}{\tan(\alpha'\pi u)}, \quad f_2^{\text{string}}(s,t) = -\frac{1}{\sin(\alpha'\pi s)}. \tag{3.47}$$

As we shall see, the bootstrap equations are not quite sufficient to guarantee that the amplitudes in eq. (3.37) correspond to doubly color-ordered amplitudes of a local theory, i.e. that the only singularities in the amplitudes correspond to physical poles. This is a nontrivial constraint. For example, $f_2(s,t) = s$ solves eq. (3.45), but gives $f_1(s,t) = su/t$ which has a t-pole not permitted by the color structure of $m_4[1234|1234] = f_1(s,t)$. Therefore, locality constraints on f_1 and f_2 generally further restrict the solution.

3.4.2 Generalized KKBCJ Conditions

Eqs. (3.41), (3.44), and (3.45) ensure that the 6×6 matrix has rank 1. Hence it must have five null vectors under left and right multiplication. One can directly verify that

$$(1,0,0,0,0,-1), \quad (0,1,0,-1,0,0), \quad (0,0,1,0,-1,0), \tag{3.48}$$

are null vectors under both left and right multiplication for any solution f_2. Via eq. (3.22), the null vectors imply the following relations among both L and R sector single-copy amplitudes:

Trace reversal: $\mathcal{A}_4[1234] = \mathcal{A}_4[1432], \quad \mathcal{A}_4[1243] = \mathcal{A}_4[1342], \quad \mathcal{A}_4[1324] = \mathcal{A}_4[1423].$ (3.49)

These are exactly the three 4-point KK relations (1.41) that are not the $U(1)$-decoupling relation. This means that any L or R sector amplitudes must satisfy the trace-reversal identity

$$\mathcal{A}_4[\alpha] = \mathcal{A}_4[\alpha^T], \tag{3.50}$$

where the α^T denotes the color-ordering that has the reverse ordering of α, for example $(1234)^T = (4321)$.

Under right multiplication, the two remaining null vectors can be written as

$$\left(1, 1, 0, 0, -\frac{f_2(s,t)}{f_2(u,t)} - \frac{f_2(s,u)}{f_2(t,u)}, 0\right), \quad \left(1, -\frac{f_2(u,s)}{f_2(t,s)}, 0, 0, 0, 0\right). \tag{3.51}$$

By eq. (3.22), they imply

L generalized $U(1)$: $\mathcal{A}_4^{\mathrm{L}}[1234] + \mathcal{A}_4^{\mathrm{L}}[1243] - \left(\frac{f_2(s,t)}{f_2(u,t)} + \frac{f_2(s,u)}{f_2(t,u)}\right)\mathcal{A}_4^{\mathrm{L}}[1423] = 0$, (3.52)

L generalized BCJ: $\mathcal{A}_4^{\mathrm{L}}[1234] - \frac{f_2(u,s)}{f_2(t,s)}\mathcal{A}_4^{\mathrm{L}}[1243] = 0$. (3.53)

When $f_2(s,t) = -g^2/s$, these relations reduce to the familiar $U(1)$-decoupling relation (1.39) and BCJ conditions (1.40). Note that if one *insists* that the usual BCJ relation (1.40) hold, i.e. if we impose

$$\frac{f_2(u,s)}{f_2(t,s)} = \frac{t}{u}, \tag{3.54}$$

then eq. (3.52) reduces to the usual $U(1)$ decoupling identity (1.39) after using $s + t + u = 0$. This is natural; the BCJ relation can be derived from color-kinematics duality [171] in which the color-structures are all generated by the structure constants f^{abc} and therefore $U(1)$-decoupling must hold. Our generalized KKBCJ relations (3.49) allow for more general color-structures, such as d^{abc} and d^{abcd} in the higher-derivative operators and therefore they modify the $U(1)$ decoupling identity and the BCJ relations.

For the R sector, if follows from the left-multiplication null vectors that

R generalized $U(1)$: $\mathcal{A}_4^{\mathrm{R}}[1234] + \mathcal{A}_4^{\mathrm{R}}[1243] - \left(\frac{f_2(s,t)}{f_2(t,s)} + \frac{f_2(s,u)}{f_2(u,s)}\right)\mathcal{A}_4^{\mathrm{R}}[1423] = 0$, (3.55)

R generalized BCJ: $\mathcal{A}_4^{\mathrm{R}}[1234] - \frac{f_2(u,t)}{f_2(t,u)}\mathcal{A}_4^{\mathrm{R}}[1243] = 0$. (3.56)

The generalized R and L sector KKBCJ relations are generally distinct. This differs from the usual field theory KKBCJ relations or the string monodromies.[6] In particular, this means that the criteria for being a valid input for the KLT relations are different for the R and L sector models. For example, the higher-derivative corrections allowed for YM may be different for the R and L sectors. We discuss the generalized KKBCJ further in Section 3.4.5.

---

[6]Note that the modified $U(1)$ decoupling relations above are not exactly the same as the string theory monodromy relations for the choice (3.47); rather the string monodromy relations arise from combinations of our general KKBCJ relations with f_2 chosen as in eq. (3.47).

3.4.3 Perturbative Solution

We now determine the most general local higher-derivative corrections to the BAS model that are compatible with the minimal rank condition at 4-point. We begin with an ansatz for f_2 whose leading term is the usual bi-adjoint s-pole. Since there can be no higher-derivative corrections to the 3-point amplitudes, there can be no other pole terms and hence any higher-derivative corrections at 4-point must be a power-expansion in s and t. The most general ansatz for f_2 is, therefore,[7]

$$f_2(s,t) = -\frac{g^2}{s} + \sum_{k=0}^{N}\sum_{r=0}^{k} \frac{a_{k,r}}{\Lambda^{2(k+1)}} \, s^r \, t^{k-r} \ , \tag{3.57}$$

where N is the highest power in Mandelstams used in the expansion and $a_{k,r}$ are coefficients that encode the higher-derivative corrections. We use Λ as a mass-dimension parameter that keeps track of the power-expansion such that we reduce to the BAS model in the limit $\Lambda \to \infty$.

Using the ansatz for f_2 in eq. (3.44), we find

$$f_1(s,t) = \frac{g^2}{s} - \frac{g^2}{s+t} + \frac{2a_{0,0}}{\Lambda^2}\frac{t^2}{s(s+t)} + \dots \ , \tag{3.58}$$

The t-dependent residue of the s and u poles is not possible in a pure scalar theory, so we must set $a_{0,0} = 0$. Going to higher orders in the power-expansion, one finds unphysical poles with coefficients $a_{2r,2r}$, so we must take

$$a_{2r,2r} = 0 \quad \text{for any } r = 0,1,2,3,\dots \tag{3.59}$$

With this choice, f_1 only has physical poles.

Imposing the bootstrap condition in eq. (3.45) on the ansatz in eq. (3.57) with eq. (3.59), we find that

$$a_{2,1} = a_{2,0} \ , \qquad a_{4,3} = a_{4,2} - a_{4,1} + a_{4,0} + \dots \ , \tag{3.60}$$

---

[7]The analysis is valid in d-dimensions and as such we leave g to have mass-dimension $3 - d/2$. To keep Λ mass-dimension 1 dimension-counting parameter then implies that the coefficients $a_{k,r}$ have mass-dimension $6 - d$.

so that the result for f_2 is

$$
\begin{aligned}
f_2(s,t) = & -\frac{g^2}{s} + \frac{1}{\Lambda^4}(a_{1,0}t + a_{1,1}s) + \frac{a_{2,0}}{\Lambda^6}t(s+t) + \\
& + \frac{1}{\Lambda^8}\left[a_{3,0}t^3 + a_{3,1}st^2 + a_{3,2}s^2t + a_{3,3}s^3\right] + \\
& + \frac{1}{\Lambda^{10}}\left[a_{4,0}t^4 + a_{4,1}st^3 + a_{4,2}s^2t^2 + (a_{4,0} - a_{4,1} + a_{4,2})s^3t\right] \\
& + \frac{1}{\Lambda^{12}}\left[a_{5,0}t^5 + a_{5,1}st^4 + a_{5,2}s^2t^3 + a_{5,3}s^3t^2 \right.\\
& \left. + \left(\frac{a_{1,0}a_{1,1}(a_{1,0} - a_{1,1})}{g^4} + \frac{a_{1,1}(a_{3,1} - a_{3,2}) - a_{1,0}(a_{3,0} - a_{3,2} + a_{3,3})}{g^2}\right.\right.\\
& \left.\left. + a_{5,0} - a_{5,1} + a_{5,3}\right)s^4t + a_{5,5}s^5\right] + O\left(\frac{1}{\Lambda^{14}}\right),
\end{aligned}
\tag{3.61}
$$

and for f_1 we then have,

$$
\begin{aligned}
f_1(s,t) = & \; g^2\left(\frac{1}{s} - \frac{1}{s+t}\right) + \frac{a_{1,0} - 2a_{1,1}}{\Lambda^4}t - \frac{a_{2,0}}{\Lambda^6}t^2 \\
& - \frac{1}{\Lambda^8}\left[\left(2a_{3,3} - a_{3,2} + a_{3,1} - a_{3,0} - g^{-2}a_{1,1}(a_{1,1} - a_{1,0})\right)st(s+t)\right.\\
& \left. + \left((4a_{3,3} - 2a_{3,2} + a_{3,0}) + 2g^{-2}a_{1,1}(a_{1,1} - a_{1,0})\right)t^3\right] + O\left(\frac{1}{\Lambda^{10}}\right).
\end{aligned}
\tag{3.62}
$$

Eqs. (3.61) and (3.62) correspond to the most general solution to the bootstrap equations assuming that the leading contribution to the partial amplitudes is cubic BAS.

3.4.4 Comparison with String Theory

The results for the bi-adjoint 4-point amplitude with higher-derivative corrections are more general than the string kernel result [39]. Let us now expand the string functions (3.47) in small α',

$$
\begin{aligned}
f_1^{\text{string}}(s,t) & = \frac{1}{\alpha'\pi s} + \frac{1}{\alpha'\pi u} + \frac{1}{3}\alpha't - \frac{1}{45}\alpha'^3\pi^3(s^3 + u^3) + O(\alpha'^5) \\
f_2^{\text{string}}(s,t) & = -\frac{1}{\alpha'\pi s} - \frac{1}{6}\alpha'\pi s - \frac{7}{360}(\alpha'\pi s)^3 + O(\alpha'^5).
\end{aligned}
\tag{3.63}
$$

Setting $g^2 = 1/(\pi\alpha')$ and identifying $\Lambda^2 = 1/(\pi\alpha')$, we compare f_2^{string} with our f_2 in eq. (3.61)

and find the choice of $a_{i,j}$'s that reproduce the string result, namely:

$$a_{2k,i} = 0 \text{ for all } k, i,$$

$$a_{k,i} = 0 \text{ for } k > i, \tag{3.64}$$

$$a_{1,1} = -\frac{1}{6\pi\alpha'}, \quad a_{3,3} = -\frac{7}{360\pi\alpha'}, \quad a_{5,5} = -\frac{31}{15120\pi\alpha'}, \quad a_{7,7} = -\frac{127}{604800\pi\alpha'}, \dots.$$

We use this to compare our results for generalized KLT to that of string theory.

3.4.5 Comments on Perturbative Solution

Consider the lowest orders of the higher-derivative bi-adjoint 4-point amplitudes

$$m_4[1234|1234] = f_1(s,t) = \frac{g^2}{s} + \frac{g^2}{u} + \frac{a_{1,0} - 2a_{1,1}}{\Lambda^4} t - \frac{a_{2,0}}{\Lambda^6} t^2 + \dots,$$

$$\tag{3.65}$$

$$m_4[1234|1243] = f_2(s,t) = -\frac{g^2}{s} + \frac{a_{1,0}}{\Lambda^4} t + \frac{a_{1,1}}{\Lambda^4} s - \frac{a_{2,0}}{\Lambda^6} tu + \dots.$$

These matrix elements derive from a Lagrangian of the form[8]

$$
\begin{aligned}
\mathcal{L} = \; & \mathcal{L}_{\text{BAS}} \\
& - \frac{a_{\text{L}} + a_{\text{R}}}{2\Lambda^4} f^{abx} f^{cdx} f^{a'b'x'} f^{c'd'x'} (\partial_\mu \phi^{aa'})(\partial^\mu \phi^{bb'}) \phi^{cc'} \phi^{dd'} \\
& + \frac{a_{\text{L}}}{\Lambda^4} f^{abx} f^{cdx} d^{a'b'x'} d^{c'd'x'} (\partial_\mu \phi^{aa'}) \phi^{bb'} (\partial^\mu \phi^{cc'}) \phi^{dd'} \\
& + \frac{a_{\text{R}}}{\Lambda^4} d^{abx} d^{cdx} f^{a'b'x'} f^{c'd'x'} (\partial_\mu \phi^{aa'}) \phi^{bb'} (\partial^\mu \phi^{cc'}) \phi^{dd'} \\
& - \frac{a_{2,0}}{2\Lambda^6} f^{abx} f^{cdx} f^{a'b'x'} f^{c'd'x'} (\partial_\nu \partial_\mu \phi^{a,a'} \partial^\nu \partial^\mu \phi^{b,b'} \phi^{c,c'} \phi^{d,d'} + \partial_\nu \partial_\mu \phi^{a,a'} \partial^\mu \phi^{b,b'} \partial^\nu \phi^{c,c'} \phi^{d,d'}) \\
& + \dots,
\end{aligned}
\tag{3.66}
$$

where

$$a_{\text{L}} = \frac{1}{4}(a_{1,1} - a_{1,0}), \quad a_{\text{R}} = \frac{1}{4} a_{1,1}. \tag{3.67}$$

There are no ϕ^4 operators; they are simply not permitted by the rank 1 bootstrap equations at 4-point. That is consistent with the example in the Introduction, where including a ϕ^4 operator led to non-minimal rank. The lowest dimension operators allowed by the KLT bootstrap are of the form $\partial^2 \phi^4$.

At 2-derivative order, the effective action has two independent couplings, a_{R} and a_{L}, that encode different color-structures in the L and R sectors. This reflects that generalized KLT kernel built

---

[8]The normalization is chosen such that $\sum_a \text{Tr}[XT^a]\text{Tr}[YT^a] = \text{Tr}[XY]$.

from the m_4-amplitudes is not symmetric: it treats the L and R sectors separately and it is in this sense "heterotic". If we insist on a symmetric kernel, this requires $\mathbf{m}_4$ in eq. (3.39) to be symmetric which is achieved by taking $f_2(s, u) = f_2(s, t)$; this is one particular solution to the bootstrap equation (3.45). It is solved perturbatively by $a_{1,0} = 0$, i.e. $a_R = a_L$, while $a_{2,0}$ can remain non-zero. Thus we see that the string solution (3.64) is an example of a symmetric kernel, but it is not the most general one.

It is clear from the effective action in eq. (3.66) that the contribution at order $\partial^2 \phi^4$ is necessssarily linked to violation of the $U(1)$-decoupling relation due to the presence of the symmetric d^{abc} color-structures. It is explicitly a_L that is responsible for the leading-order modifications of the BCJ and $U(1)$-decoupling identities in the L sector; and likewise a_R that is responsible for the modifications in the R sector, e.g.

$$
\begin{aligned}
0 =& \mathcal{A}_4^R[1234] + \mathcal{A}_4^R[1243] + \left(1 - \frac{12a_R}{g^2 \Lambda^4} tu + O(\Lambda^{-8})\right) \mathcal{A}_4^R[1423] \,, \\
0 =& \mathcal{A}_4^R[1234] - \left(\frac{t}{u} - \frac{4a_R}{g^2 \Lambda^4} \frac{st(t-u)}{u} + O(\Lambda^{-8})\right) \mathcal{A}_4^R[1243] \,.
\end{aligned}
\tag{3.68}
$$

The $1/\Lambda^6$ term in eq. (3.66) controlled by $a_{2,0}$ does not modify the BCJ and $U(1)$-decoupling identities. If we wanted a generalized KLT kernel that preserved the $U(1)$-decoupling identity, we would set $a_R = a_L = 0$ while keeping $a_{2,0}$. The KKBCJ constraints generalize the string theory monodromy relations and allow the L and R sector amplitudes to be distinct.

3.5 Example: Higher-Derivative YM to Gravity

In this section we present the double-copy of YM plus higher dimension operators at 3- and 4-point as an illustrative example of our generalized double-copy. Another interesting example is chiral perturbation theory (χPT) with higher-derivative operators: we give results for that its double copy with itself and YM+HD in Appendix B.1.

3.5.1 3-Point

Up to the choice of coupling constants, 3-point amplitudes are uniquely fixed by little group scaling and locality. For gluons, there are only two options: the MHV and anti-MHV helicity amplitudes arising from the usual YM 3-point vertex of $\text{Tr}F^2$ and the all-minus and all-plus amplitudes of $\text{Tr}F^3$. We have

$$
\mathcal{A}_3[1_g^- 2_g^- 3_g^+] = g_{YM} \frac{\langle 12 \rangle^3}{\langle 23 \rangle \langle 31 \rangle} \,, \qquad \mathcal{A}_3[1_g^- 2_g^- 3_g^-] = \frac{g_{F^3}}{\Lambda^2} \langle 12 \rangle \langle 23 \rangle \langle 13 \rangle \,.
\tag{3.69}
$$

We write out only the mostly-minus amplitudes explicitly; the conjugate amplitudes are obtained by exchanging angle brackets with square brackets. These amplitudes satisfy the rank-1 KKBCJ relations in eq. (3.35).

The double-copy of YM with itself gives gravity coupled to the dilaton φ and the antisymmetric 2-form. In 4d, the latter can be dualized to an axion-scalar B with a shift-symmetry, $B \to B + \text{constant}$. The precise map of the 4d on-shell states is

$$
\begin{array}{ccc}
 & \text{L} & \text{R} \\
h^+ & + & + \\
h^- & - & - \\
Z & + & - \\
\bar{Z} & - & +
\end{array}
\tag{3.70}
$$

where $\pm$ denote the L and R sector gluon helicity states, $h^\pm$ are the graviton helicity states, and the complex scalar is $Z = \frac{1}{\sqrt{2}}(\varphi + iB)$.

Using eq. (3.69) and the map in eq. (3.70), we construct all possible 4d gravity-dilaton-axion 3-point amplitudes arising from the double-copy relation

$$
\mathcal{M}_3(123) = \frac{1}{g}\mathcal{A}_3^{\text{L}}[123]\mathcal{A}_3^{\text{R}}[123] \, ,
\tag{3.71}
$$

The pure graviton amplitudes

$$
\mathcal{M}_3\left(h^- h^- h^+\right) = \kappa \frac{\langle 12 \rangle^6}{\langle 23 \rangle^2 \langle 31 \rangle^2} \, ,
\tag{3.72}
$$

$$
\mathcal{M}_3\left(h^- h^- h^-\right) = \frac{\kappa_{R^3}}{\Lambda^4} \langle 12 \rangle^2 \langle 23 \rangle^2 \langle 13 \rangle^2 \, .
\tag{3.73}
$$

and their conjugates correspond to the 3-point interactions of $\sqrt{g}R$ and $\sqrt{g}R^3$, respectively. We have identified the couplings as

$$
\kappa \equiv \frac{g_{\text{YM}}^{\text{R}} g_{\text{YM}}^{\text{L}}}{g} \, , \qquad \kappa_{R^3} \equiv \frac{g_{F^3}^{\text{R}} g_{F^3}^{\text{L}}}{g} .
\tag{3.74}
$$

Note that we are allowing for the possibility that the YM and F^3 couplings are different in the L and R sectors.

The double-copy of the leading-order YM amplitudes also includes the coupling of the dilaton to the graviton. Specifically, in the MHV sector we get

$$
\mathcal{M}_3(-Z\bar{Z}) = \kappa \frac{\langle 12 \rangle^2 \langle 13 \rangle^2}{\langle 23 \rangle^2} \, ,
\tag{3.75}
$$

85

and its anti-MHV conjugate. These amplitudes simply represent the canonical coupling of the complex scalars coupled to gravity via the kinetic term $g^{\mu\nu}\partial_\mu Z \partial_\nu \bar{Z}$. The corresponding non-zero axion-dilaton amplitudes are

$$\mathcal{M}_3(-\varphi\varphi) = \mathcal{M}_3(-BB) = \kappa \frac{\langle 12\rangle^2 \langle 13\rangle^2}{\langle 23\rangle^2}\,, \tag{3.76}$$

and similarly with square brackets for the corresponding amplitudes of a positive helicity graviton.

Since 3-point special kinematics means that either only angle-brackets *or* only square brackets are nonvanishing, the amplitudes $\mathcal{M}_3(\pm ZZ) = g^{-1}\mathcal{A}_3^{\mathrm{L}}[\pm + +]\mathcal{A}_3^{\mathrm{L}}[\pm - -]$ vanish identically. Likewise, 3-scalar amplitudes vanish.

In the double-copy of YM with itself, dilaton- and axion-parity ($\varphi \to -\varphi$ and independently $B \to -B$) emerge from the double-copy. However, when higher-derivative corrections are included, this is no longer the case. In the generic double-copy, where the L and R sector couplings can be distinct, dilaton- and axion-parity is broken already at 3-point by the F^3 operator. To see this, note that the double-copy (3.71) gives

$$\mathcal{M}_3(--Z) = \frac{g_{\mathrm{YM}}^{\mathrm{L}} g_{F^3}^{\mathrm{R}}}{g\Lambda^2}\langle 12\rangle^4\,, \quad \mathcal{M}_3(--\bar{Z}) = \frac{g_{F^3}^{\mathrm{L}} g_{\mathrm{YM}}^{\mathrm{R}}}{g\Lambda^2}\langle 12\rangle^4\,, \tag{3.77}$$

and their conjugates. The single axion and dilaton amplitudes are then

$$\mathcal{M}_3(--\varphi) = \frac{\kappa_\varphi}{\Lambda^2}\langle 12\rangle^4\,, \quad \mathcal{M}_3(--B) = -i\frac{\kappa_B}{\Lambda^2}\langle 12\rangle^4\,, \tag{3.78}$$

where we have defined

$$\kappa_\varphi = \frac{g_{\mathrm{YM}}^{\mathrm{L}} g_{F^3}^{\mathrm{R}} + g_{F^3}^{\mathrm{L}} g_{\mathrm{YM}}^{\mathrm{R}}}{\sqrt{2}g}\,, \quad \kappa_B = \frac{g_{\mathrm{YM}}^{\mathrm{L}} g_{F^3}^{\mathrm{R}} - g_{F^3}^{\mathrm{L}} g_{\mathrm{YM}}^{\mathrm{R}}}{\sqrt{2}g}\,. \tag{3.79}$$

The couplings κ, κ_{R^3}, κ_φ, and κ_B are not independent, but satisfy

$$\kappa_\varphi^2 - \kappa_B^2 = 2\kappa\kappa_{R^3}\,. \tag{3.80}$$

In previous studies [166] of the double-copy of YM with higher-derivative operators, the L and R sector couplings were chosen to be the same and that choice results in $g_B = 0$. In that case, axion-parity holds, while dilaton-parity is violated even at 3-point by the inclusion of the F^3 operator. Note that F^3 is not compatible with supersymmetry, so in a supersymmetric context, the amplitudes in eqs. (3.77) and (3.78) all vanish.

In superstring theory, dilaton-parity is violated by α'-corrections. This does not happen at 3-point due to supersymmetry, as discussed above, but it can be seen directly from the $\alpha'^3 e^{-6\varphi}R^4$

effective operator. In type-IIA superstring theory dimensionally reduced to 4d, axion-parity, $B \rightarrow -B$, continues to hold to all orders in α'. From a double-copy point of view, this is related to the fact that the couplings of the open string in the L and R sectors are identical and the KLT kernel is symmetric. Conversely, as can be seen from eq. (3.79), for a non-L-R symmetric or *heterotic* double-copy, axion- or B-parity is generically broken. Such hhB interactions arise in the effective action of the heterotic superstring [172] from the modification of the B field strength tensor by a Lorentz Chern-Simons term and play an important role in the Green-Schwarz anomaly cancellation mechanism [173].

We now turn to 4-point, where the 3-point amplitudes above are needed for identifying the pole terms correctly, both in the L and R sector amplitudes and in the resulting gravitational amplitude.

3.5.2 4-Gluon MHV Amplitude and Generalized KKBCJ

The starting point is to construct the most general ansatz for the tree-level MHV amplitude in YM + higher derivative operators. We write it as

$$
\begin{aligned}
\mathcal{A}_4[1^+2^+3^-4^-] &= [12]^2\langle 34\rangle^2 \left(\frac{g_{\text{YM}}^2}{su} - \frac{g_{F3}^2}{\Lambda^4}\frac{t}{s} + \sum_{k=2}^{N}\sum_{r=1}^{k-1} \frac{e_{k,r}}{\Lambda^{2k}} s^{r-1}t^{k-r-1} \right) , \\
\mathcal{A}_4[1^+3^-2^+4^-] &= [12]^2\langle 34\rangle^2 \left(\frac{g_{\text{YM}}^2}{tu} + \sum_{k=2}^{N}\sum_{r=1}^{k-1} \frac{h_{k,r}}{\Lambda^{2k}} s^{r-1}t^{k-r-1} \right) .
\end{aligned}
\tag{3.81}
$$

The terms with g_{YM}^2 arise from the pole terms with two regular YM vertices whereas the s-pole term with g_{F3}^2 is from two insertions of F^3. There can be no other pole terms in the MHV sector. Contributions from local operators at 4-point are parameterized as polynomial terms in the ansatz with general coefficients $e_{k,r}$ and $h_{k,r}$. We have explicitly checked (to all orders we are using) that any local contribution to the MHV amplitudes can be written in the form given in eq. (3.81). The choice of Mandelstam basis in eq. 3.81 is equivalent to choosing a particular basis of higher-dimension operators in the Lagrangian. The local contributions at $O(\Lambda^{-4})$ with coefficients $e_{2,1}$ and $h_{2,1}$ correspond to the combination of $\text{Tr}[F^4]$ operators that contribute to the MHV amplitude. The terms at $O(\Lambda^{-6})$ correspond to operators of the schematic form $\text{Tr}[D^2F^4]$.

The 4 other arrangements of the external lines are obtained from the above two by cyclic sym-

metry and momentum relabeling:

$$\mathcal{A}_4[1^+2^+4^-3^-] = \mathcal{A}_4[1^+2^+3^-4^-]\Big|_{3\leftrightarrow4}$$

$$\mathcal{A}_4[1^+3^-4^-2^+] = \mathcal{A}_4[2^+1^+3^-4^-] = \mathcal{A}_4[1^+2^+3^-4^-]\Big|_{1\leftrightarrow2}$$

$$\mathcal{A}_4[1^+4^-2^+3^-] = \mathcal{A}_4[1^+3^-2^+4^-]\Big|_{3\leftrightarrow4}$$

$$\mathcal{A}_4[1^+4^-3^-2^+] = \mathcal{A}_4[2^+1^+4^-3^-] = \mathcal{A}_4[1^+2^+3^-4^-]\Big|_{1\leftrightarrow2,3\leftrightarrow4} = \mathcal{A}_4[1^+2^+3^-4^-].$$

(3.82)

Naturally, one expects the coefficients $e_{k,r}$ and $h_{k,r}$ in eq. (3.81) to be related since these amplitudes should arise from a Lagrangian with a color-group structure and — as we shall see — indeed this is the case: the generalized KKBCJ relations will fix the $h_{k,r}$ completely in terms of the $e_{k,r}$ and the kernel coefficients $a_{k,r}$ and they impose additional constraints on the $e_{k,r}$.

The generalized KKBCJ constraints are imposed using the trace-reversal identities in eq. (3.49) as well as the L and R sector identities in eqs. (3.52)-(3.53) or eqs. (3.55)-(3.56). The result in the **L sector** is

$$\mathcal{A}_4^{\mathsf{L}}[1^+2^+3^-4^-] = [12]^2\langle34\rangle^2\left[\frac{(g_{\mathrm{YM}}^{\mathsf{L}})^2}{su} - \frac{(g_{F^3}^{\mathsf{L}})^2}{\Lambda^4}\frac{t}{s} + \frac{(g_{\mathrm{YM}}^{\mathsf{L}})^2}{g^2\Lambda^4}(a_{1,1} - a_{1,0}) + \frac{e_{3,1}^{\mathsf{L}}}{\Lambda^6}t\right.$$
$$\left. + \frac{1}{\Lambda^8}\left\{\frac{(g_{\mathrm{YM}}^{\mathsf{L}})^2}{g^2}\tilde{a}_{3,3}\,s^2 + \alpha^{\mathsf{L}}\,t^2 + e_{4,2}^{\mathsf{L}}\,st\right\} + \ldots\right],$$

$$\mathcal{A}_4^{\mathsf{L}}[1^+3^-2^+4^-] = [12]^2\langle34\rangle^2\left[\frac{(g_{\mathrm{YM}}^{\mathsf{L}})^2}{tu} + \frac{1}{\Lambda^4}\left(\frac{(g_{\mathrm{YM}}^{\mathsf{L}})^2}{g^2}(a_{1,1} - a_{1,0}) - (g_{F^3}^{\mathsf{L}})^2\right) + \frac{e_{3,1}^{\mathsf{L}}}{\Lambda^6}s\right.$$
$$+ \frac{1}{\Lambda^8}\left\{-\left(\frac{(g_{\mathrm{YM}}^{\mathsf{L}})^2}{g^2}\tilde{a}_{3,3} + \frac{(g_{F^3}^{\mathsf{L}})^2}{g^2}(a_{1,1} - a_{1,0})\right)tu+\right.$$
$$\left.\left. + \left(\alpha^{\mathsf{L}} - \frac{(g_{\mathrm{YM}}^{\mathsf{L}})^2}{g^2}\tilde{a}_{3,3} - 2\frac{(g_{F^3}^{\mathsf{L}})^2}{g^2}(a_{1,1} - a_{1,0}) + e_{4,2}^{\mathsf{L}}\right)s^2\right\} + \ldots\right],$$

(3.83)

where

$$\tilde{a}_{3,3} = a_{3,3} - a_{3,2} + a_{3,1} - a_{3,0}\,,$$
$$\alpha^{\mathsf{L}} = \frac{(g_{\mathrm{YM}}^{\mathsf{L}})^2}{g^4}\,a_{1,1}(a_{1,1} - a_{1,0}) + \frac{(g_{\mathrm{YM}}^{\mathsf{L}})^2}{g^2}(2a_{3,3} - a_{3,2}) + \frac{(g_{F^3}^{\mathsf{L}})^2}{g^2}(a_{1,1} - a_{1,0})\,.$$

(3.84)

Schematic Operator	Total	Generalized	String	Cubic BAS
$\mathrm{Tr}[F^4]$	1	1	0	×
$\mathrm{Tr}[D^2F^4]$	2	1	1	1
$\mathrm{Tr}[D^4F^4]$	3	3	1	1
$\mathrm{Tr}[D^6F^4]$	4	3	2	2

Table 3.1: Number of tunable parameters in the operator coefficients contributing to the MHV amplitude $\mathcal{A}_4[1^+2^+3^-4^-]$ subject to the L or R sector KKBCJ relations (generalized, string, or pure field theory BAS, respectively). The total number of independent MHV operators at that dimension is also listed. The × indicates that $\mathrm{Tr}[F^4]$ is disallowed by the field theory KKBCJ relations.

The **R sector** takes the form

$$
\begin{aligned}
\mathcal{A}_4^{\mathrm{R}}[1^+2^+3^-4^-] =[12]^2\langle 34\rangle^2 &\Bigg[\frac{(g_{\mathrm{YM}}^{\mathrm{R}})^2}{su} - \frac{(g_{F^3}^{R})^2}{\Lambda^4}\frac{t}{s} + \frac{(g_{\mathrm{YM}}^{\mathrm{R}})^2}{g^2\Lambda^4}a_{1,1} + \frac{e_{3,1}^{\mathrm{R}}}{\Lambda^6}\,t \\
&+ \frac{1}{\Lambda^8}\left\{\frac{(g_{\mathrm{YM}}^{\mathrm{R}})^2}{g^2}a_{3,3}s^2 + \alpha^{\mathrm{R}}\,t^2 + e_{4,2}^{\mathrm{R}}\,st\right\} + \dots\Bigg], \\
\mathcal{A}_4^{\mathrm{R}}[1^+3^-2^+4^-] =[12]^2\langle 34\rangle^2 &\Bigg[\frac{(g_{\mathrm{YM}}^{\mathrm{R}})^2}{tu} + \frac{1}{\Lambda^4}\left(\frac{(g_{\mathrm{YM}}^{\mathrm{R}})^2}{g^2}a_{1,1} - (g_{F^3}^{\mathrm{R}})^2\right) + \frac{e_{3,1}^{\mathrm{R}}}{\Lambda^6}s \\
&+ \frac{1}{\Lambda^8}\Bigg\{-\left(\frac{(g_{\mathrm{YM}}^{\mathrm{R}})^2}{g^2}a_{3,3} + \frac{(g_{F^3}^{\mathrm{R}})^2}{g^2}a_{1,1}\right)tu \\
&+ \left(\alpha^{\mathrm{R}} - \frac{(g_{\mathrm{YM}}^{\mathrm{R}})^2}{g^2}a_{3,3} - 2\frac{(g_{F^3}^{\mathrm{R}})^2}{g^2}a_{1,1} + e_{4,2}^{\mathrm{R}}\right)s^2\Bigg\} + \dots\Bigg],
\end{aligned}
\tag{3.85}
$$

where

$$
\alpha^{R} = \frac{(g_{\mathrm{YM}}^{\mathrm{R}})^2}{g^4}a_{1,1}\big(a_{1,1} - a_{1,0}\big) + \frac{(g_{\mathrm{YM}}^{\mathrm{R}})^2}{g^2}\big(2a_{3,3} - a_{3,2} + a_{3,0}\big) + \frac{(g_{F^3}^{\mathrm{R}})^2}{g^2}a_{1,1}\,.
\tag{3.86}
$$

Each of the local (i.e. non-pole) terms in eq. (3.83) or eq. (3.85) correspond to a local operator in the YM + HD effective action. For example,

$$
\begin{aligned}
\mathcal{A}_4^{\mathrm{L}}[1^+2^+3^-4^-] &\supset [12]^2\langle 34\rangle^2 \frac{1}{\Lambda^4}\frac{(g_{\mathrm{YM}}^{\mathrm{L}})^2}{g^2}\big(a_{1,1} - a_{1,0}\big)\,, \\
\mathcal{A}_4^{\mathrm{R}}[1^+2^+3^-4^-] &\supset [12]^2\langle 34\rangle^2 \frac{1}{\Lambda^4}\frac{(g_{\mathrm{YM}}^{\mathrm{R}})^2}{g^2}a_{1,1},
\end{aligned}
\tag{3.87}
$$

comes from the matrix element of (a particular contraction of) $\mathrm{Tr}[F^4]$. As this shows, the generalized KKBCJ allows $\mathrm{Tr}[F^4]$ with independent tunable coefficients, a_{L} and a_{R} given in eq. (3.67),

for the L and R sectors respectively, from the $\partial^2\phi^4$ operators (3.66) in the zeroth-copy model. In contrast, this operator is not allowed by the uncorrected field theory KKBCJ relations (which have $a_{k,r} = 0$). And while $\text{Tr}[F^4]$ does arise the α'-expansion of the open (super)string gluon amplitudes, it does so with a fixed untunable coefficient because $a_{1,1} = -1/(6\pi\alpha')$ and $a_{1,0} = 0$.

In Table 3.1, the row labeled $\text{Tr}[F^4]$ summarizes the above discussion. Similarly, the subsequent rows in the table compare the number of allowed operators at higher order contributing to the YM + HD MHV tree amplitude when subject to the respective KKBCJ constraints. In the count of tunable couplings, we consider $g_{\text{YM}}^{\text{L/R}}$, g and $g_{F^3}^{\text{L/R}}$ fixed by the 3-point amplitudes and we avoid double-counting by taking into account that lower-point parameters often feed into higher-point contributions. The lesson from the Table 3.1 is that our generalized KKBCJ relations allow a broader range of EFT operators in single-copy EFTs but still not all operators are allowed.

For a closer comparison with string theory, the α'-expansion of the 4-gluon MHV tree amplitude of type-I open string theory is

$$\mathcal{A}_4^{\text{open}}[1^+2^+3^-4^-] = g_{\text{YM}}^2[12]^2\langle34\rangle^2\left[\frac{1}{su} - \frac{\pi^2\alpha'^2}{6} + \alpha'^3\zeta(3)t + O(\alpha'^4)\right]. \qquad (3.88)$$

Comparing the leading orders, this corresponds to the limit

$$a_{k,l}, g, \Lambda \to \text{String Kernel}, \quad g_{F^3}^2 \to 0, \quad e_{3,1}^{\text{L}} \to \frac{\zeta_3}{\pi^3}, \ \ldots \qquad (3.89)$$

of the L or R sector MHV amplitudes given in eq. (3.83) and eq. (3.85), where *String Kernel* refers to eq. (3.64).

3.5.3   4-Graviton MHV from of YM + HD

The generalized KLT double-copy formula can be carried out in any choice of KLT basis (and we have explicitly checked the basis-independence) thanks to the generalized KKBCJ relations. For example, we can compute $\mathcal{M}_4$ as

$$\mathcal{M}_4(1234) = \mathcal{A}_4^{\text{L}}(1^+2^+3^-4^-)\frac{1}{f_1(s,t)}\mathcal{A}_4^{\text{R}}(1^+2^+3^-4^-), \qquad (3.90)$$

with f_1 given by eq. (3.62). Using (3.83) and (3.85), we then find

$$
\begin{aligned}
\mathcal{M}_4(1^+2^+3^-4^-) = [12]^4\langle 34\rangle^4 \bigg[&-\frac{\kappa^2}{stu} + \frac{\kappa_\varphi^2+\kappa_B^2}{\Lambda^4}\frac{1}{s} \\
&-\frac{1}{\Lambda^6}\left(\frac{(g_{\text{YM}}^{\text{R}})^2}{g^2}\,e_{3,1}^{\text{L}} + \frac{(g_{\text{YM}}^{\text{L}})^2}{g^2}\,e_{3,1}^{\text{R}} - \frac{\kappa^2}{g^2}\,a_{2,0} \right) \\
&+\frac{1}{\Lambda^8}\left(\kappa_{R^3}^2\frac{tu}{s} + \left(\frac{(g_{\text{YM}}^{\text{R}})^2}{g^2}\,e_{4,2}^{\text{L}} + \frac{(g_{\text{YM}}^{\text{L}})^2}{g^2}\,e_{4,2}^{\text{R}} + \tilde{a}_{\Lambda^8} \right)s \right) \\
&+ O\left(\frac{1}{\Lambda^{10}} \right) \bigg],
\end{aligned}
\tag{3.91}
$$

where we have used the identification of the gravitational coupling κ and the R^3-coupling κ_{R^3} in (3.74) and the non-canonical 4-derivative couplings between the dilaton/axion and the graviton in eq. (3.79). The constant $\tilde{a}_{\Lambda^8}$ is a linear combination of kernel coefficient $a_{k,r}$.

Performing a term-by-term analysis of eq. (3.91), we find

- $O(\Lambda^0)$: the leading term is the tree-level graviton amplitude.

- $O(\Lambda^{-4})$: the axion and dilaton can be exchanged only in the s-channel since they couple to same-helicity gravitons (3.78).

- $O(\Lambda^{-6})$: this local contribution is the matrix element of R^4. It is generated irrespective of the higher-dimension corrections in KKBCJ and the KLT kernel so long as the coefficient $e_{3,1} \neq 0$ of D^2F^4 is non-zero in the L or R sector. Thus, even in the usual field theory double-copy or in the α'-expansion of stringy KLT, R^4 arises from the double-copy of D^2F^4 with the usual leading YM 4-point amplitude.[9] The new feature in the generalized double-copy is that R^4 can be generated from the $a_{2,0}$-controlled 4-derivative correction to the BAS model even in the absence of D^2F^4 in both the L and R sectors of (YM + HD).

- $O(\Lambda^{-8})$: the pole term arises from the factorization into two R^3-vertices. Since they are only $+++$ and $---$, the exchange happens only in the s-channel. In addition there is a local term from ∇^2R^4 at this order and its coefficient is determined by the double-copy of the matrix element $\text{Tr}D^4F^4$ and the usual YM amplitude along with various kernel coefficients $a_{k,r}$ suppressed into the constant $\tilde{a}_{\Lambda^8}$ in eq. (3.91).

There are no other poles in $\mathcal{M}_4(1^+2^+3^-4^-)$ than those shown in eq. (3.91), hence higher-order contributions all arise from local operators. It is perhaps curious to mention that the full residue of

---

[9]While it is true that the MHV matrix element of R^4 mathematically is directly the square of the MHV matrix element of $\text{Tr}F^4$, it is *not* the case that R^4 arises from $\text{Tr}F^4$ in the actual double-copy.

Schematic Operator	MHV	NSD	SD
R^4	1 of 1	0 of 0	0 of 1
$\nabla^2 R^4$	1 of 1	0 of 0	1 of 1
$\nabla^4 R^4$	2 of 2	1 of 1	1 of 2
$\nabla^6 R^4$	2 of 2	0 of 0	1 of 1
$\nabla^8 R^4$	3 of 3	1 of 1	1 of 2
$\nabla^{10} R^4$	3 of 3	1 of 1	2 of 2

Table 3.2: Number of independent local operators out of the total possible contributing to the 4-graviton amplitude: we list how many operators are generated by any version of the KLT double copy (generalized / field theory BAS / string kernel).

the s-channel of the MHV amplitude (3.91) factorizes into the palatable form

$$\lim_{s \to 0} s \, \mathcal{M}_4[1^+ 2^+ 3^- 4^-] = \frac{[12]^4 \langle 34 \rangle^4}{g^2} \left(\frac{(g_{\text{YM}}^{\text{L}})^2}{t} + \frac{(g_{F^3}^{\text{L}})^2 t}{\Lambda^4} \right) \left(\frac{(g_{\text{YM}}^{\text{R}})^2}{t} + \frac{(g_{F^3}^{\text{R}})^2 t}{\Lambda^4} \right) . \qquad (3.92)$$

Upon expanding the above expression, the t^{-2} term corresponds to the exchange of the graviton with the regular Einstein-Hilbert 3-point interactions, the t^2 term corresponds to the exchange with a graviton with two R^3 interactions, and t^0 term corresponds to dilaton-axion exchange.

It is quite interesting to note that while the generalized KKBCJ relations allow for a wider range of higher-derivative operators in the L and R MHV amplitudes, there are (for generic input) no new operators appearing in the 4-point MHV gravity amplitude (see Table 3.1); rather, its Wilson coefficients are merely shifted by the $a_{k,r}$ parameters. For example, in eq.(3.91), we can absorb the nonzero $a_{2,0}$ into $e_{3,1}^{\text{R}}$ as

$$e_{3,1}^{\text{R}} \to e_{3,1}^{\text{R}} + \frac{(g_{\text{YM}}^{\text{R}})^2}{g^2} a_{2,0} . \qquad (3.93)$$

The pattern continues to higher orders; we have explicitly checked up to and including $O(p^{18})$, i.e. $\nabla^{10} R^4$. Table 3.2 summarizes the number of independent local operators that contribute to the MHV amplitude and we find that each one of them is produced in any of the KLT double-copies. In particular, we find at 4-point that the entire effect of the higher-derivative corrections to the double-copy kernel can be absorbed into the R (or L) sector Wilson coefficients of the YM+HD amplitudes. Of course, there are also other combinations of the double-copy spectrum. For example, we can double-copy $\mathcal{A}_4^{\text{L}}(1^+ 2^+ 3^- 4^-)$ with $\mathcal{A}_4^{\text{R}}(1^- 2^- 3^+ 4^+)$ to get the $\mathcal{M}_4(ZZ\bar{Z}\bar{Z})$ amplitude. It is noteworthy (but somewhat trivial at 4-point) that the same shift of Wilson coefficients that absorbs the effect of the $a_{k,r}$-coefficients of the double-copy kernel for the 4-graviton MHV amplitude also does the job for these other helicity combinations obtained from double-copies of the 4-gluon MHV amplitudes.

This phenomenon is reminiscent of the single-valued projection that occurs in the string double-copy [174], but is much more general. While the single-valued projection that occurs in string theory is tied to a particular expansion of higher dimensional operators, our result seems to hold for a large class of EFTs without a clear high energy completion.

3.5.4 SD and NSD Sectors

One can similar perform an analysis of YM with higher-derivative corrections in the Self-Dual (SD, or all-plus) and Next-To-Self-Dual Sector (NSD, or one-minus) at 4-point. Up to the order $D^{10}F^4$ we have checked that the matrix elements of local operators can be written with a common spinor-helicity prefactor times a Mandelstam polynomial:

$$
\begin{aligned}
\text{SD } (+++++): \quad & \frac{1}{\langle 12\rangle\langle 23\rangle\langle 34\rangle\langle 41\rangle} \times P_{\text{SD}}(s,t)\,, \\
\text{NSD } (+++-): \quad & \frac{\langle 4|1.3|4\rangle^2}{\langle 12\rangle\langle 23\rangle\langle 34\rangle\langle 41\rangle} \times P_{\text{NSD}}(s,t)\,,
\end{aligned}
\tag{3.94}
$$

where $\langle 4|1.3|4\rangle = \langle 41\rangle[13]\langle 34\rangle$ and P_{SD} and P_{NSD} are local Mandelstam polynomials. We impose cyclic symmetry for the ansatz of the SD local terms. Including the appropriate pole terms and subjecting the ansatz to the generalized KKBCJ relations (eq. (3.49) and the L or R sector identities eqs. (3.52)-(3.53) and eqs. (3.55)-(3.56)), we find the result for the R-sector SD amplitude is

$$
\begin{aligned}
\mathcal{A}_4^{\text{R}}[1^+2^+3^+4^+] = & \frac{stu}{\langle 12\rangle\langle 23\rangle\langle 34\rangle\langle 41\rangle}\left(\frac{2g_{\text{YM}}^{\text{R}}g_{F^3}^{\text{R}}}{\Lambda^2} + \frac{2g_{\text{YM}}^{\text{R}}g_{F^3}^{\text{R}}}{g^2\Lambda^6}a_{1,1}\,t^2 \right. \\
& \left. - \frac{d_1^{\text{R}}}{2\Lambda^6}(s^2+t^2+u^2) + \frac{d_2^{\text{R}}}{\Lambda^8}\,stu + \dots \right),
\end{aligned}
\tag{3.95}
$$

and the R-sector NSD amplitude is

$$
\mathcal{A}_4^{\text{R}}[1^+2^+3^+4^-] = \frac{\langle 4|1.3|4\rangle^2}{\langle 12\rangle\langle 23\rangle\langle 34\rangle\langle 41\rangle}\left(\frac{g_{\text{YM}}^{\text{R}}g_{F^3}^{\text{R}}}{\Lambda^2} + \frac{g_{\text{YM}}^{\text{R}}g_{F^3}^{\text{R}}}{g^2\Lambda^6}a_{1,1}\,su - \frac{c_1^{\text{R}}}{\Lambda^8}stu + \dots \right).
\tag{3.96}
$$

The leading term in each case arises from the pole diagram with a 3-point vertex of YM and one from F^3 and they have been given previously (see [166] and references therein). The rest of the terms are local and can be rewritten in a manifestly polynomial form in terms of spinor-helicity variables that is less compact. The L-sector SD and NSD amplitudes are similar and, to the orders shown, they are found by simply taking $a_{1,1} \to a_{1,1} - a_{1,0}$ and changing the superscripts R to L.

One can compute the double-copy of various combinations of the MHV, SD, and NSD amplitudes to get all the possible gravity-dilaton-axion amplitudes. In particular, amplitudes with an odd number of external axions are nonvanishing whenever the L and R sector couplings are distinct, as

noticed already at 3-point.

Let us simply do one illustrative example here, the SD graviton amplitude. Using eq. (3.90), we find from eq. (3.95) that

$$
\begin{aligned}
\mathcal{M}_4(1^+2^+3^+4^+) =&\, 4\kappa\kappa_{R^3}\, stu\, \frac{[12][23][34][41]}{\langle 12\rangle\langle 23\rangle\langle 34\rangle\langle 41\rangle} \\
&+ \frac{1}{5g^2\Lambda^8}\Big(g_{F^3}^{\mathrm{L}}g_{\mathrm{YM}}^{\mathrm{L}}d_1^{\mathrm{R}} + g_{F^3}^{\mathrm{R}}g_{\mathrm{YM}}^{\mathrm{R}}d_1^{\mathrm{L}} - 2\kappa\kappa_{R^3}\big(2a_{1,1} - a_{1,0}\big)\Big) \\
&\times \Big([12]^4[34]^4 s + [13]^4[24]^4 t + [14]^4[23]^4 u\Big) + \ldots
\end{aligned}
\tag{3.97}
$$

Let us first comment on the leading term. This is a pole term with two sets of contributions: one from the graviton exchange with a regular vertex from R and another from R^3, contributing $2\kappa\kappa_{R^3}$ to the overall factor. Next, there are scalar exchanges which kinematically take the same form as the graviton exchange: the dilaton exchange comes with coupling κ_φ^2 while the axion exchange contributes $(i\kappa_B)^2$. Thanks to the relation eq. (3.80), the total scalar exchange therefore contributes a coupling $\kappa_\varphi^2 - \kappa_B^2 = 2\kappa\kappa_{R^3}$. Thus, the combined graviton+dilaton+axion exchange accounts precisely for the overall factor $4\kappa\kappa_{R^3}$ in the first line of eq. (3.97).

Next, we notice that there is no contribution corresponding to R^4. There does exist a unique operator R^4 with a nonvanishing matrix element in the SD sector, but it is not produced in the double copy. For $\nabla^2 R^4$, there is likewise a unique SD matrix element and as shown above it *is* produced by the double-copy.

Table 3.2 summarizes the results for higher-derivative operators produced by the double-copy of the 4-point SD and NSD graviton amplitudes. We have computed 4-point amplitudes too with external scalars too, but will not clutter the presentation by presenting them here.

3.6 Generalized KLT at 5-Point

We now analyse the KLT bootstrap equations at 5-point: we set up the problem and present the conditions on the zeroth copy that ensures that the matrix of amplitudes has rank 2. We then solve the equations perturbatively and show that — very importantly — this does not place restrictions on the coefficients $a_{k,r}$ for the 4-point KLT kernel. As an example, we apply the generalized KLT double-copy to YM theory with higher derivative corrections in the SD (all-plus) sector.

3.6.1 5-Point Bootstrap Equations

We use cyclic symmetry and momentum relabeling to write the $(n-1)! = 4! = 24$ doubly color-ordered amplitudes in terms of 8 functions:

$$
\begin{aligned}
m_5[12345|12345] &= g_1[12345], & m_5[12345|13254] &= g_5[12345], \\
m_5[12345|12354] &= g_2[12345], & m_5[12345|13524] &= g_6[12345], \\
m_5[12345|12453] &= g_3[12345], & m_5[12345|14253] &= g_7[12345], \\
m_5[12345|12543] &= g_4[12345], & m_5[12345|15432] &= g_8[12345].
\end{aligned}
\tag{3.98}
$$

Cyclic symmetry requires $g_1[12345] = g_1[51234]$ and likewise for g_6, g_7, and g_8. We do not assume reversal symmetry.

Imposing the minimal rank condition is equivalent to requiring all 3×3 minors to vanish, thus reducing the 24×24 matrix to rank $(n-3)! = 2$. These conditions allow us to analytically solve for g_4, g_5, g_6, g_7, and g_8 in terms of g_1, g_2, and g_3. For example,

$$
\begin{aligned}
g_4[12345] =& \Big(g_1[12345]g_1[12354]g_2[12435] - g_2[12345]g_2[12354]g_2[12435] \\
& - g_1[12354]g_2[51243]g_3[12345] + g_2[12354]g_3[12345]g_3[12435] \Big) \\
& \Big(g_1[12345]g_3[12435] - g_2[12345]g_2[51243] \Big)^{-1}
\end{aligned}
\tag{3.99}
$$

The remaining analytic solutions are given in Appendix B.2. In addition, there are bootstrap equations that relate g_1, g_2, and g_3. One can explicitly check that the BAS amplitudes and the string kernel amplitudes of Ref. [39] solve these equations.

Let us now outline how we set up the ansatz for solving the functions g_i perturbatively in the momentum expansion. The leading order terms are the usual BAS amplitudes and the subleading terms have both local contributions as well as pole terms from factorization into BAS 3-point amplitudes and 4-point local contributions parameterized by the coefficients $a_{k,r}$ in Section 3.4.3. For example, the s_{12}-factorization channel of g_1 is

$$
\begin{aligned}
s_{12}\, g_1[12345]\Big|_{s_{12}=0} &= s_{12}\, m[12345|12345]\Big|_{s_{12}=0} \\
&= g^3\left(\frac{1}{s_{34}} + \frac{1}{s_{45}} \right) + m_3[12P|12P]\, \tilde{m}_4[345P|345P] \\
&= g^3\left(\frac{1}{s_{34}} + \frac{1}{s_{45}} \right) + \frac{g(a_{1,0} - 2a_{1,1})}{\Lambda^4} s_{35} - \frac{g\, a_{2,0}}{\Lambda^6} s_{35}^2 + \dots,
\end{aligned}
\tag{3.100}
$$

where $P = P_{12}$ is on-shell ($P^2 = 0$), $m_3[12P|12P] = g$ and $\tilde{m}_4[345P|345P] = f_1(s_{34}, s_{35})\big|_{\text{local}}$ are the higher-derivative corrections to the 4-point bi-adjoint that are encoded in the function f_1

given in eq. (3.62).

Including all five factorization channels and all possible local counterterms compatible with cyclic symmetry gives the following ansatz for g_1

$$
\begin{aligned}
g_1[12345] =& g^3 \left(\frac{1}{s_{12}s_{34}} + \frac{1}{s_{23}s_{45}} + \frac{1}{s_{34}s_{51}} + \frac{1}{s_{45}s_{12}} + \frac{1}{s_{51}s_{23}} \right) \\
& + \frac{g}{\Lambda^4}(a_{1,0} - 2a_{1,1}) \left(\frac{s_{35}}{s_{12}} + \frac{s_{41}}{s_{23}} + \frac{s_{13}}{s_{45}} + \frac{s_{24}}{s_{51}} + \frac{s_{52}}{s_{34}} \right) + w_1 \\
& - \frac{g a_{2,0}}{\Lambda^6} \left(\frac{s_{35}^2}{s_{12}} + \frac{s_{41}^2}{s_{23}} + \frac{s_{13}^2}{s_{45}} + \frac{s_{24}^2}{s_{51}} + \frac{s_{52}^2}{s_{34}} \right) \\
& + w_1' \left(s_{12} + s_{23} + s_{34} + s_{45} + s_{51} \right) + \dots
\end{aligned}
\tag{3.101}
$$

In the ansatz, the local terms have coefficients w_i.

Remarkably, the 5-point rank 2 bootstrap equations fix the couplings w_1 and w_1' of the 5-point local contact terms completely in terms of the 4-point bi-adjoint, namely

$$
w_1 = 2\frac{g}{\Lambda^4} \left(2a_{1,1} - a_{1,0} \right) \quad \text{and} \quad w_1' = -\frac{g}{\Lambda^6} a_{2,0} \,.
\tag{3.102}
$$

One has to go to cubic order in the Mandelstams in order to find local 5-point operators whose coefficients are not fixed by 4-point coefficients. Starting at $O(p^4)$ (not shown above) we include also parity odd terms, but we have found that none of them are allowed by the bootstrap. We have solved the bootstrap equations up to and including $O(p^6)$.

It is very important that the 5-point bootstrap equations do not place any restrictions on the $a_{k,r}$-parameters that were free in the 4-point solution. This is a very relevant consistency check: if 5-point has constrained 4-point, then we would have needed to go to 6-point to understand if that gave even further constraints. As it is, the lack of such constraints is an important clue that our generalization of the KLT kernel is based on sound principles.

3.6.2 Comparison with String Theory at 5-point

The string KLT amplitudes in Ref. [39] are dimensionless, for example

$$
\begin{aligned}
g_1^{\text{string}}[12345] = & \cot(\pi\alpha' s_{12})\cot(\pi\alpha' s_{34}) + \cot(\pi\alpha' s_{51})\cot(\pi\alpha' s_{34}) \\
& + \cot(\pi\alpha' s_{12})\cot(\pi\alpha' s_{45}) + \cot(\pi\alpha' s_{23})\cot(\pi\alpha' s_{45}) \\
& + \cot(\pi\alpha' s_{23})\cot(\pi\alpha' s_{51}) + 1 \\
= & \frac{1}{\alpha'^2\pi^2}\left(\frac{1}{s_{12}s_{45}} + \frac{1}{s_{23}s_{45}} + \frac{1}{s_{23}s_{51}} + \frac{1}{s_{12}s_{34}} + \frac{1}{s_{51}s_{34}}\right) \\
& + \frac{1}{3}\left(\frac{s_{35}}{s_{12}} + \frac{s_{41}}{s_{23}} + \frac{s_{13}}{s_{45}} + \frac{s_{24}}{s_{51}} + \frac{s_{52}}{s_{34}} - 2\right) + O(\alpha'^2)\,.
\end{aligned}
\tag{3.103}
$$

To compare eqs. (3.101)-(3.102) with eq. (3.103), we therefore multiply g_1 by Λ and then find a match when the $a_{k,r}$ take the values in eq. (3.64) up to and including order $O(p^6)$. At $O(p^6)$ there are four coefficients of local operators that are unrelated to the 4-point $a_{k,r}$'s and the comparison to eq. (3.103) shows that all four coefficients are zero in the string kernel. In the generalized kernel they can take any value.

3.6.3 Example: Higher-Derivative YM to Gravity at 5-Point

Due to the tower of local corrections to the 4-point YM amplitudes in Sections 3.5.2 and 3.5.4, the analysis of the 5-point factorization channels takes a bit more effort. We assume a general ansatz for the pole contribution takes the form

$$
\mathcal{A}_5^{\text{YM}}[1^+2^+3^+4^+5^+] = \frac{1}{\langle 12\rangle\langle 23\rangle\langle 34\rangle\langle 45\rangle\langle 51\rangle}\Big[P_+(s_{ij}) + P_-(s_{ij})\epsilon(1,2,3,4)\Big],
\tag{3.104}
$$

where P_+ and P_- are cyclically invariant polynomials in a basis of independent Mandelstam invariants $\{s_{12}, s_{23}, s_{34}, s_{45}, s_{51}\}$ and

$$
\epsilon(1,2,3,4) = \epsilon_{\mu\nu\rho\sigma}p_1^\mu p_2^\nu p_3^\rho p_4^\sigma = \frac{i}{4}\Big(\langle 12\rangle\langle 34\rangle[23][14] - \langle 14\rangle\langle 23\rangle[12][34]\Big)\,.
\tag{3.105}
$$

Since this ansatz is cyclically invariant, we only need to match a single factorization channel to the known 3- and 4-point amplitudes. For the 45 channel we match to

$$\mathcal{A}_4^{\mathrm{YM}}[1^+2^+3^+(P_{45})^+]\mathcal{A}_3^{\mathrm{YM}}[(-P_{45})^-4^+5^+] = \frac{[45]}{\langle 12\rangle\langle 23\rangle\langle 34\rangle\langle 51\rangle} P_{\mathrm{SD}}(s_{12}, s_{13})\,,$$

$$\mathcal{A}_4^{\mathrm{YM}}[1^+2^+3^+(P_{45})^-]\mathcal{A}_4^{\mathrm{YM}}[(-P_{45})^+4^+5^+] \tag{3.106}$$

$$= \frac{[45]}{\langle 12\rangle\langle 23\rangle\langle 34\rangle\langle 51\rangle}(s_{12}(s_{51} - s_{23}) + s_{23}s_{34})^2 P_{\mathrm{NSD}}(s_{12}, s_{13})\,, \tag{3.107}$$

where P_{SD} and P_{NSD} were defined in eq. (3.94) and their explicit form can be inferred from the L and R sector results for the 4-point SD and NSD amplitudes presented in Section 3.5.4 where $\langle 45\rangle = 0$ for the equality to hold. Combining this with the 5-particle ansatz gives the following residue matching condition:

$$P_+(s_{45} = 0) - \frac{i}{4}(s_{12}(s_{51} - s_{23}) + s_{23}s_{34})P_-(s_{45} = 0)$$

$$= P_{\mathrm{SD}}(s_{12}, s_{13}) + (s_{12}(s_{51} - s_{23}) + s_{23}s_{34})^2 P_{\mathrm{NSD}}(s_{12}, s_{13}). \tag{3.108}$$

Both sides of this equation are polynomials that can be written in terms of the independent Mandelstam invariants $\{s_{12}, s_{23}, s_{34}, s_{51}\}$, so we can match terms on both sides and fix all coefficients in the ansatz.

Next, we have to add contributions of local terms to the ansatz. For example, the two independent SD contributions from $\mathrm{Tr}[F^5]$ are

$$\mathcal{A}_5^{\mathrm{YM}}[1^+2^+3^+4^+5^+] \supset \frac{c_{5,1}}{\Lambda^6}[12][23][34][45][51]$$

$$+ \frac{c_{5,2}}{\Lambda^6}\left([12]^2[34][35][45] + \text{cyclic perms}\right). \tag{3.109}$$

The ansatz of pole terms (fixed by 3- and 4-point input) and all possible local terms is then subject to the L and R generalized KKBCJ relations at 5-point. This is efficiently done in the form of setting all 3×3 matrices

$$\det \begin{bmatrix} m_5[12345|12345] & m_5[12345|12354] & \mathcal{A}_5^{\mathrm{R}}[12345] \\ m_5[12354|12345] & m_5[12354|12354] & \mathcal{A}_5^{\mathrm{R}}[12354] \\ m_5[\alpha_i|12345] & m_5[\alpha_i|12354] & \mathcal{A}_5^{\mathrm{R}}[\alpha_i] \end{bmatrix}, \tag{3.110}$$

to zero. No constraints are placed by these constraints on the lower-point coefficients, but some coefficients of the 5-point local operators are fixed; for example we find $c_{5,1} = 0$ and $c_{5,2} = 0$ for both the L and R sectors. This is summarized in the row labeled $\mathrm{Tr}[F^5]$ in Table 3.3.

The double-copy of $\mathcal{A}[1^+2^+3^+4^+5^+]$ with itself gives the graviton amplitude expression for

Schematic Operator	Total	Bootstrapped	String	FT
$\mathrm{Tr}[F^5]$	2	×	×	×
$\mathrm{Tr}[D^2 F^5]$	5	×	×	×
$\mathrm{Tr}[D^4 F^5]$	14	1	1	1
$\mathrm{Tr}[D^6 F^5]$	28	4	2	2

Table 3.3: Number of operators contributing to $\mathcal{A}_5^{\mathrm{R}}[1^+2^+3^+4^+5^+]$ after imposing the KKBCJ relations in the generalized, string, and BAS form. We also list the total number of independent operators. The × indicates that no operator at that order is allowed.

Schematic Operator	SD
R^5	0 of 1
$\nabla^2 R^5$	0 of 1
$\nabla^4 R^5$	1 of 3
$\nabla^6 R^5$	1 of 3

Table 3.4: Number of tunable parameters in $\mathcal{M}_5[1^+2^+3^+4^+5^+]$ of the given form and number of tuneable parameters compatible with the double copy. Note that the generalized, string and cubic BAS double copy all generate the same set of higher dimension operators.

$\mathcal{M}(1^+2^+3^+4^+5^+)$, which we have computed up to $O(\Lambda^{-14})$. As at 4-point, we find that the same operators are produced by the generalized double-copy kernel as with BAS or strings, however, their coefficients are now in certain cases shifted but the parameters of the kernel.

3.7 Alternative Double-Copy Constructions

We showed in the Introduction how the zeros of the determinant of the rank R_n submatrix of zeroth-copy amplitudes may provide "missing poles" needed for the double copy to work, but that they can also give rise to potentially dangerous spurious poles. No such spurious poles arose in the higher-derivative generalizations of the double-copy kernel at 4- and 5-point studied in Sections 3.4-3.6.

In this section we initiate the study of whether there can be other versions of the double-copy which are not anchored on the leading BAS model. The central property we examine is whether the rank R_n determinant has zeroes in unphysical locations that could lead to spurious singularities in the double-copy amplitudes *unless* additional cancellations take place.

3.7.1 Modification of KLT at 3-Point

In Section 3.3 we classified the most general 3-point bi-adjoint scalar amplitudes

$$m_3[123|123] = g + \lambda_3 \,, \qquad\qquad m_3[123|132] = -g + \lambda_3 \,, \qquad (3.111)$$

where g is the cubic BAS coupling and λ_3 is the coupling associated with the cubic interaction with d^{abc}-contractions; see eq. (3.30). We found that rank 1 at 3-point required one of these two couplings to be zero. Let us now examine what happens at 4-point.

It follows from the 3-particle input that the three independent doubly-ordered amplitudes at 4-point are

$$m_4[1234|1234] = (g + \lambda_3)^2 \left(\frac{1}{s} + \frac{1}{u} \right) \,, \qquad (3.112)$$

$$m_4[1234|1243] = (-g^2 + \lambda_3^2) \frac{1}{s} \,, \qquad (3.113)$$

$$m_4[1234|1432] = (-g + \lambda_3)^2 \left(\frac{1}{s} + \frac{1}{u} \right) \,. \qquad (3.114)$$

For generic non-zero values of g and λ_3, the 6×6 matrix of amplitudes in eq. (3.112) in this model has rank 6; i.e. it is full rank. The determinant is

$$\frac{2048 g^3 \lambda_3^7 \left(3g^2 - \lambda_3^2 \right)}{s^2 t^2 (s+t)^2} \,, \qquad (3.115)$$

and it has no kinematic zeros, so no spurious poles arise at 4-point. However, it does vanish for $g = 0$, $\lambda_3 = 0$, and $\lambda_3 = \pm\sqrt{3}g$ which means that those cases have lower ranks. We find

	Couplings	Matrix Rank	Spurious Singularities?
	$g \neq 0, \lambda_3 \neq 0$	6	No
4-point	$g \neq 0, \lambda_3 = \sqrt{3}g$	5	No
	$g = 0, \lambda_3 \neq 0$	3	No
	$g \neq 0, \lambda_3 = 0$	1	No

The 3rd column asks if there are spurious zeroes in the determinant at the given rank, and in each case at 4-point the answer is no. We proceed to 5-point.

As explained in Section 3.6, the 5-point amplitudes are determined by 8 functions g_1-g_8 and they determine the full 24×24 matrix of zeroth copy amplitudes m_5. We calculate them from the known 3-particle vertices with general g and λ_3, compute the rank, and examine the associated determinants for zeros. The results are summarized as

	Couplings	Matrix Rank	Spurious Singularities?
	$g \neq 0, \lambda_3 \neq 0$	24	Yes
5-point	$g \neq 0, \lambda_3 = \sqrt{3}g$	21	Yes
	$g = 0, \lambda_3 \neq 0$	11	Yes
	$g \neq 0, \lambda_3 = 0$	2	No

Thus, despite first appearances, only the model with $\lambda_3 = 0$, i.e. the BAS model, leads to a double-copy without spurious singularities appearing in the kernel. This is a serious potential obstacle for the double-copy since it means that additional cancellation has to take place among the terms in the KLT sum to avoid spurious poles in the double-copy 5-point amplitude. We discuss such cancellations briefly for the case with $g = 0$ and $\lambda_3 \neq 0$ in Section 3.7.3.

3.7.2 Modification of KLT at 4-Point

Having classified the possible generalizations of the double copy at 3-point, let us now set $g = \lambda_3 = 0$ and examine the possibility for zeroth-copy models with constant 4-point interactions ϕ^4.

There are different ways four bi-adjoint scalars $\phi^{aa'}$ can be contracted with group-invariant tensors. This is simplest to classify using the amplitudes. We know from Section 3.4.1 that three amplitudes determine the full 6×6 matrix and we simply parameterize them with three constants,

$$m_4[1234|1234] = \alpha_1, \quad m_4[1234|1243] = \alpha_2, \quad m_4[1234|1432] = \alpha_3. \qquad (3.116)$$

The resulting matrix ranks at 4-point are summarized below

Couplings	Matrix Rank
$\alpha_1 \neq 0, \alpha_2 \neq 0, \alpha_3 \neq 0$	6
$\alpha_1 \neq 0, \alpha_2 \neq 0, \alpha_3 = -4\alpha_2 - \alpha_1$	5
$\alpha_1 \neq 0, \alpha_2 \neq 0, \alpha_3 = 2\alpha_2 - \alpha_1$	4
$\alpha_1 \neq 0, \alpha_2 = 0, \alpha_3 = -\alpha_1$	3
$\alpha_1 = -2\alpha_2, \alpha_2 \neq 0, \alpha_3 = -2\alpha_2$	2
$\alpha_1 = \alpha_2 = \alpha_3$	1

No kinematically spurious zeros arise in the determinants at 4-point since the amplitudes are constants, so we need to go to 6-point to assess the model further.

At 6-point we find that all cases have spurious singularities in the kernel from zeros in the determinant, *except* the model with $\alpha_1 = \alpha_2 = \alpha_3 \equiv \lambda$. This model is

$$\mathcal{L} = -\frac{1}{2}\left(\partial_\mu \phi^{aa'}\right)^2 + \lambda \, d^{abcd} \tilde{d}^{a'b'c'd'} \phi^{aa'} \phi^{bb'} \phi^{cc'} \phi^{dd'}, \qquad (3.117)$$

and the 120×120 matrix of its tree amplitudes has rank 10.

An appealing feature of a kernel based on the zeroth copy (3.117) is that it double-copies F^4 with itself to R^4; this is not true of the BAS or stringy double-copy. However, by now, we have learned the lesson that higher-point calculations may change our outlook. And this is the case here too: the 5040×5040 matrix of 8-point amplitudes has rank 273 and there are spurious zeros in the 273×273 determinants. Therefore, unless there are additional cancellations at 8-point, this model does not lead to a healthy double-copy.

3.7.3 Cancellation Spurious Singularities

In the previous two subsections, we have encountered examples with spurious poles in the kernel. While they represent a potential problem, it is worth noting that the L and R sector amplitudes must obey the KKBCJ relations defined by the kernel. Does this allow one to cancel the spurious poles in the generalized KLT sum to recover a sensible local tree amplitude as a result of the double-copy? We briefly examine this question here.

As an example where such cancellations do happen, consider the kernel based on the zeroth copy with cubic interactions only with $g = 0$ and $\lambda_3 \neq 0$. A model whose tree amplitudes solve the corresponding rank 3 generalized KKBCJ relations is

$$\mathcal{L}_{\text{int}} = d^{abc} \phi^a \phi^b \phi^c \,, \tag{3.118}$$

and it is easy to see at 5-point that the spurious poles in the kernel do get canceled. The double-copy of this theory with itself is the abelian ϕ^3 model.

Thus encouraged, we tried the same with a less trivial model

$$\mathcal{L}_{\text{int}} = d^{abc} Z^a F^b_{\mu\nu} F^{c\mu\nu} + \text{h.c.} \,, \tag{3.119}$$

for a complex adjoint scalar field Z, but in this case the spurious poles of the kernel were not cancelled at 5-point.

Based on these examples, we note that issues with spurious poles appear to arise for kernels with non-minimal rank, i.e. with rank greater than $(n-3)!$. For the non-minimal rank kernels studied, imposing generalized KKBCJ conditions is in general not enough to ensure a well-defined double copy. From a practical point of view, one could simply disregard the models that do not produce sensible answers under the double copy. However, this approach is somewhat unsatisfactory as it does not provide a nice explanation for why some models work while others do not. A more formal view centered on the double-copy kernel suggests that a valid double-copy product kernel should yield sensible local results for *any* local input amplitude that obeys the generalized KKBCJ

relations associated with that kernel. By this metric, our results suggest that the minimal rank condition might be necessary for a valid double-copy kernel.

We have referred to rank $(n-3)!$ at n-point as minimal rank. This makes sense in the context of BAS+HD where the higher-derivative corrections generically increase the rank to be greater than $(n-3)!$. However, one could of course remove the cubic BAS interactions and ask if there are solutions to the bootstrap equations of rank less than $(n-3)!$. At 4-point, minimal rank is already 1, so we can only go smaller than that by eliminating all 4-point interactions. At 5-point, there will be no factorization channels in the absence of 3-point interactions, hence the leading order is Mandelstam^0, i.e. constant ϕ^5-type interactions. Minimal rank $(n-3)!$ at 5-point is 2, so a non-trivial sub-minimal rank would be 1. One finds that at order Mandelstam^0, there is one unique solution to the rank 1 bootstrap equations at 5-point. Whether the resulting double-copy has physical significance and if the sub-minimal rank is perserved at higher point are questions we leave for future investigations.

3.8 Discussion

In this chapter, we introduced a novel bottom-up approach to the double-copy in the KLT formulation. It was based on the KLT algebra and how it links the identity element ("zeroth copy") to the kernel that determines the multiplication rule. We showed how this gives a KLT bootstrap formalism for the zeroth copy model whose tree amplitudes determine the kernel. At 4- and 5-point we solved the KLT bootstrap equations and found a generalized double-copy kernel based on a low-energy expansion that generalizes the α'-expansion of the string theory KLT kernel. We applied the generalized double-copy to YM theory and χPT. Many interesting questions remain to be studied and we now discuss some of them.

3.8.1 Similarity Transformations

In our examples with the generalized KLT kernel based on BAS+HD, we found that the double-copy contains the same operators as the standard field theory double copy, but with shifts in some of their Wilson coefficients. It is tempting to ask if this shift can be encoded more systematically. To examine this, consider at 4-point performing a *similarity transformation* on the BAS solutions

with superscripts $^{(0)}$:

$$m_4[\beta|\alpha] = Z^{\mathrm{L}}[\alpha]\, Z^{\mathrm{R}}[\beta] m_4^{(0)}[\beta|\alpha]\,,$$
$$\mathcal{A}_4^{\mathrm{L}}[\alpha] = Z^{\mathrm{L}}[\alpha]\mathcal{A}_4^{\mathrm{L}(0)}[\alpha]\,, \tag{3.120}$$
$$\mathcal{A}_4^{\mathrm{R}}[\beta] = Z^{\mathrm{R}}[\beta]\mathcal{A}_4^{\mathrm{R}(0)}[\beta]\,.$$

Note that the amplitudes $\mathcal{A}_4^{\mathrm{L/R}(0)}[\alpha]$ may include whatever higher-derivative corrections are compatible with the BAS KKBCJ relations. In general, there are fewer operators in $\mathcal{A}_4^{\mathrm{L/R}(0)}[\alpha]$ than in $\mathcal{A}_4^{\mathrm{L/R}}[\alpha]$.

It follows from the definition in eq. (3.120) that if $m_4^{(0)}[\beta|\alpha]$ solves the rank $(n-3)!$ bootstrap equations, then so does $m_4[\beta|\alpha]$ (the rank of a matrix does not change when the rows and columns of a matrix are rescaled). Similarly, the single-copy amplitudes $\mathcal{A}_4$ solve the generalized KKBCJ relations whenever $\mathcal{A}_4^{(0)}$ is compatible with the field theory ones, as can be seen from

$$\mathbb{1} \otimes \mathrm{R} = \mathrm{R}: \qquad m_4[\delta|\alpha]\frac{1}{m_4[\beta|\alpha]}\mathcal{A}_n^{\mathrm{R}}[\beta] = \mathcal{A}_n^{\mathrm{R}}[\delta]\,, \tag{3.121}$$

and similarly for the L sector.

When applied to the double-copy, we see that

$$\mathcal{M}_4 = \mathcal{A}_n^{\mathrm{L}}[\alpha]\frac{1}{m_4[\beta|\alpha]}\mathcal{A}_n^{\mathrm{R}}[\beta] = \mathcal{A}_n^{\mathrm{L}(0)}[\alpha]\frac{1}{m_4^{(0)}[\beta|\alpha]}\mathcal{A}_n^{\mathrm{R}(0)}[\beta]\,. \tag{3.122}$$

It may now seem plausible that all double-copies can be equivalently obtained from the field theory BAS kernel. However, one has to be more careful:

1. First of all, one must ensure that the LHS of eq. (3.120) is local; no spurious poles are allowed to arise from the product with the similarity factors.

2. The cyclicity properties of the amplitudes $m_4[\beta|\alpha]$ are ensured if $Z^{\mathrm{L/R}}$ are both cyclic.

3. It is not *a priori* clear that all solutions to the 4-point KLT bootstrap equation are related to the BAS amplitude via a similarity transformation such as the one in the first line of eq. (3.120).

4. With a cyclic choice for $Z^{\mathrm{L/R}}$, one may not be able to produce all possible solutions $\mathcal{A}_n^{\mathrm{L/R}}$ to the generalized KKBCJ relations.

To simultaneously enforce all these properties is non-trivial. In the perturbative context of BAS+HD, one can solve items 1 and 2 by choosing $Z^{\mathrm{L/R}} = 1 + su\, P^{\mathrm{L/R}}$, where $P^{\mathrm{L/R}}$ is a Mandelstam polynomial symmetric in s and u. We can then test whether our generalized solution for m_4

given in Section 3.4.3 for BAS+HD can be reproduced and fix most of the constants in the ansatz $P^{\text{L/R}}$.[10] So this resolves item 3 above. The resulting similarity functions $Z^{\text{L/R}}$ do indeed produce the most general solution to the generalized KKBCJ equations given in Section 3.5.2 for the MHV YM+HD amplitudes (to the orders we have checked), so that addresses item 4. This requires shifts in the YM Wilson coefficients of $\mathcal{A}_n^{\text{L/R}(0)}$ such as the one given in eq. (3.93). This then explains (to the orders checked) why we found no new operators in the double-copy at 4-point and why their coefficients could be understood as shifts of the Wilson coefficients of the L and R copies. Note though that this assumes that the L and R Wilson coefficients are sufficiently generic.

At 5-point and higher, it becomes much more challenging to overcome the potential obstructions from the constraints listed above. Another issue arises if one studies double-copies outside the regime of the low-energy expansion. Then it becomes much harder to ensure the absense of spurious poles. Future explorations may shed light on these questions.

3.8.2 Connection to BCJ Double-Copy

While we have focused on the KLT formula, there is in the field theory ($\alpha' \to 0$) limit an alternative formulation of the double-copy, first introduced by Bern, Carrasco and Johansson (BCJ) [171], based on a trivalent graphical expansion and the principle of *color-kinematics duality* (see the review [175]). One of the primary advantages of this approach is that it has been proposed — and tested in numerous cases — to generalize to loop integrands, making possible otherwise prohibitively difficult high-loop-order calculations in maximal supergravity [176]. Focusing on tree-level, it is natural to ask if the generalized double-copy presented in this chapter has a BCJ-like formulation.

The recent papers [169, 177] incorporate higher-derivative corrections and generalized color-tensors in the BCJ double-copy. This approach makes use of generalized *color weights* $\hat{c}_{s/t/u}$ (see (18) of Ref. [169] for a precise definition) that depend on both color tensors and Mandelstam invariants in such a way that the usual *adjoint-type* color identities remain true. Taking such objects, we can construct a natural zeroth-copy by making the usual BCJ replacement of kinematic numerators with color-factors; at 4-point

$$m_4 = \frac{\hat{c}_s^{(L)} \hat{c}_s^{(R)}}{s} + \frac{\hat{c}_t^{(L)} \hat{c}_t^{(R)}}{t} + \frac{\hat{c}_u^{(L)} \hat{c}_u^{(R)}}{u} \, . \tag{3.123}$$

Similar to the output of the KLT bootstrap described in this chapter, this can be identified as a scattering amplitude of a higher-derivative corrected BAS model, though *a priori* these two

---

[10]We have done this to order $O(p^6)$ as a preliminary test.

approaches are not obviously related. To the orders checked at 4p-point, we find that when eq. (3.123) is expressed as a matrix in L and R color-orderings, the result has rank 1 for all choices of parameters in the generalized color-weights defined in Ref. [169]. In this sense, eq. (3.123) provides a closed form *solution* to the 4-point bootstrap equations, which impose the 4-point kernel is rank 1. Moreover, we have found that up to $O(p^8)$, the parameters in eq. (3.123) can always be chosen to reproduce the most general solution to the KLT bootstrap equations of eq. (3.61). This conjecture was proven at 4-point in Ref. [178]. It remains unknown whether the higher-multiplicity generalized color-factors described in Ref. [177] likewise provide a solution to the bootstrap conditions and whether a BCJ-like double-copy procedure can be devised to reproduce the results of the generalized double-copy (3.90) presented in this chapter. We leave these and related important questions to future work.

3.8.3   Exact Solutions to the Bootstrap Equations: Truncations

The field theory and string zeroth copies are exact solutions to the rank $(n-3)!$ bootstrap equations. We have found generalizations of these that solve the bootstrap equations as an order-by-order low-energy expansion corresponding to adding higher-derivative terms to the BAS model. A natural question is if there are new solutions that solve the bootstrap equations exactly?

To address this, we take the 4-point solution in eqs. (3.61)-(3.62) as the starting point and examine if the low-energy expansion truncates for certain choices of coefficients $a_{i,j}$, i.e. if there are choices of a finite set of non-zero coefficients such that the rank of the 6×6 matrix is exactly 1, rather than solving this constraint order by order in the low-energy expansion. Interestingly, such solutions do exist!

For example, setting $a_{1,1} = 0$ or $a_{1,1} = a_{1,0}$ (equivalently, $a_\mathrm{L} = 0$ or $a_\mathrm{R} = 0$) while taking all other $a_{i,j} = 0$ is an exact solution to the f_2 condition (3.45), moreover, they give local solutions for f_1: specifically for $a_\mathrm{L} = 0$, we have

$$f_1(s,t) = -\frac{g^2 t}{su} - 4\frac{a_\mathrm{R}}{\Lambda^4} t\,, \quad f_2(s,t) = -\frac{g^2}{s} - 4\frac{a_\mathrm{R}}{\Lambda^4} u\,. \tag{3.124}$$

When this is used as input at 5-point, one finds that the 24×24 matrix indeed has rank 2, so the solution truncates consistently; this is true for both solutions $a_\mathrm{L} = 0$ and $a_\mathrm{R} = 0$.[11]

When the contribution from a_R in eq. (3.124) is regarded as a perturbation of the BAS model and the kernel is expanded in small s_{ij}/Λ^2, no spurious poles arise, because this is just like the general perturbative solution in Section 3.4.3. However, if we attempt to regard the solution eq. (3.124) as

---

[11]Similarly, one can include the contribution with coefficient $a_{2,0}$ with no further restrictions in the 4- and 5-point bootstrap. At higher-orders, one finds that certain choices of the $a_{i,j}$'s admit finite truncations.

an *exact* solution with no expansion in s_{ij}/Λ^2, we have to beware of potential spurious poles in the kernel (e.g. in $1/f_1(s,t)$). It is clear that f_1 in eq. (3.124) in addition to the zero at $t = 0$ (which provides the missing t-channel pole in the double-copy) also has a zero that cannot be a physical pole (it is not even a massive pole). This means that amplitudes $\mathcal{A}_4^{\text{L/R}}$ that are double-copied with this kernel must have zeros that cancel the spurious poles; this is similar to the discussion of potential cancellation of spurious poles in Section 3.7.3. Something nice can indeed happen to cancel these poles. To see this, consider the L and R amplitudes for YM+HD in eq. (3.83) and eq. (3.85). Setting $a_{\text{L}} = 0$ (i.e. $a_{1,1} = a_{1,0}$), $g_{F^3} = 0$ and all other higher-derivative contributions to zero, one finds

$$\mathcal{A}_4^{\text{L}}[1^+2^+3^-4^-] = [12]^2\langle 34\rangle^2 \frac{(g_{\text{YM}}^{\text{L}})^2}{su}\,, \qquad \mathcal{A}_4^{\text{R}}[1^+2^+3^-4^-] = (g_{\text{YM}}^{\text{R}})^2[12]^2\langle 34\rangle^2 \left[\frac{1}{su} + \frac{4a_{\text{R}}}{g^2\Lambda^4}\right]$$
(3.125)

When these amplitudes are double-copied using eq. (3.90) with f_1 given by eq. (3.124), the entire a_{R} dependence cancels and the result is simply the pure Einstein gravity amplitude

$$\mathcal{M}_4(1^+2^+3^-4^-) = \kappa^2 \frac{[12]^4\langle 34\rangle^4}{stu}\,.$$
(3.126)

Here eq. (3.74) was used to identify κ. In a sense this is a version of the similarity transformations eq. (3.120) at work for a finite (i.e. non-perturbative) modification of the zeroth and single-copy models. In particular, this example shows that for the choice of kernel given by eq. (3.124), it possible at 4-point to double-copy YM with YM+F^4 to give Einstein gravity $\sqrt{-g}R$ without higher-derivative terms!

Finally, let us note that the solution eq. (3.124) can be written in the form eq. (3.123) with manifestly local generalized color-factors $\hat{c}_{s/t/u}$. The exact solutions to the KLT bootstrap equations, their relation to the BCJ-like formulation [169, 177], and the issues of spurious poles deserve further investigation.

3.8.4   Exact Solutions to the Bootstrap Equations: Z-theory

Any function of the form

$$f_2^{\text{ansatz}}(s,t) = \frac{1}{s}\frac{G_1(s)G_2(t)}{G_3(s+t)}\,,$$
(3.127)

for general G_1, G_2, and G_3 solves the 4-point KLT bootstrap equation eq. (3.45). Eq. (3.127) is not the most general ansatz to the bootstrap equations, but is curious nonetheless. For example, the string solution is in the form of eq. (3.127)) with $G_2(t) = G_3(s+t) = 1$ and $G_1(s) = s/\sin(\alpha's)$. Furthermore, there is another solution to eq. (3.127) motivated by string theory; the double partial

amplitudes of non-abelian Z-theory take the form of eq. (3.127) [179–181]:

$$Z_{1234}[1243] = \frac{1}{s}\frac{\Gamma(1+\alpha's)\Gamma(1+\alpha'u)}{\Gamma(1+\alpha's+\alpha'u)} \ . \tag{3.128}$$

The double partial amplitudes of non-abelian Z-theory can be identified with the disk integrals that appear at tree-level in open string integrands and encode all non-trivial α'-dependence for type-I open-string amplitudes at tree-level. This α'-dependence can be extracted using generalized double copy procedures, where the double copy of Z-theory amplitudes with SYM yields type-I open string amplitudes: "type-I=Z $\otimes$ SYM". In addition to providing another "stringy" solution to the bootstrap equations, one might wonder what physical meaning the minimal rank condition could have for Z-theory amplitudes.

CHAPTER 4

Boundary Correlators in Anti-de Sitter

4.1 Overview

In this chapter, we discuss a novel representation of AdS boundary correlators termed the differential representation. In the differential representation, AdS boundary correlators are expressed as (nonlocal) differential operators acting on a single contact diagram. We are partially motivated by the recent generalization of the ambitwistor string to $AdS_3 \times S^3$ [50], which provides an explicit example of color/kinematics duality in an AdS space.[1] Our conjectures are the natural generalization of the results in Ref. [50] to higher dimensions and the natural extension of the results of Ref. [48] to non-scalar theories.

Using the differential representation, we derive the AdS analogs of color/kinematics duality, focusing on YM. Despite steady effort and significant progress in several directions, a systematic formulation of color/kinematics duality and of the double copy in curved space remains elusive. For example, AdS momentum space might be expected to be the most natural representation when searching for generalizations of amplitude relations as AdS boundary correlation functions in momentum space contain flat-space scattering amplitudes [186]. However, imposing color/kinematics duality on integrated, color-ordered momentum space correlators does not seem to yield BCJ relations [187, 188]. In contrast to AdS momentum space, scalar Witten diagrams in Mellin space are simple and yield correlation functions that exhibit colour-kinematics duality [189, 190]. However, with some notable exceptions, see refs. [191, 192], current state-of-the-art techniques in Mellin space often rely on using supersymmetry to relate scalar correlators to those of spin-1 and spin-2 states [193–197]. However, using the differential representing, we derive novel relations for generic AdS boundary correlators, which are schematically similar to flat space BCJ relations with the suitable replacement of Mandelstam invariants with combinations of conformal generators

---

[1]In flat space, particular BCJ representations of a variety of theories can be derived from ambitwistor string models [182–185].

D_i^{AB}, given in section 4.2:

$$s_I \to \left(\sum_{i \in I} D_i^{AB} \right)^2 .$$ (4.1)

To check our conjecture, we construct the four-point gluon correlator of YM theory in AdS of general dimension and verify that, for a four-dimensional boundary, it obeys these relations

$$(D_1^{AB} + D_2^{AB})^2 A(1, 2, 3, 4) = (D_1^{AB} + D_3^{AB})^2 A(1, 3, 2, 4) .$$ (4.2)

We expect (but do not prove) that these relations are obeyed for general dimensions.

We then discuss the extension of our proposal for color/kinematics duality to a double copy relation for gauge theories. We consider a variety of proposals that appear to be valid in different limits for three-point correlators. We first study a differential double copy procedure that naturally generalizes our proposal for color/kinematics duality in AdS, which seems to yield self-consistent results in AdS$_3$. For higher dimensional AdS spacetimes, we find that the differential double copy leads to a current conserving three-point graviton correlator only if we supplement the YM with specific higher dimensional operators. We also consider other double copy procedures in position space and Mellin space. We reproduce the result of Ref. [198], giving a double copy-like relation for the three-point Mellin amplitude without supersymmetry in the limit $d \to \infty$. Furthermore, we compare our results with the Mellin space double copy construction of Ref. [190], which gives super-graviton AdS boundary correlators on AdS$_5 \times S^5$ in terms of super-gluon AdS boundary correlators on AdS$_5 \times S^3$. We conclude with a heuristic discussion of double copy procedures for various formulations of AdS boundary correlators in the high energy limit.

We conclude the chapter by deriving the one-loop generalization of the differential representation. We find that operator-valued integrals of scalar Witten diagrams can be interpreted as integrals over a non-commutative space. For example, operator-valued integrals obey a generalization of integration-by-parts (IBP) [56, 58, 199–208], which is discussed in Section 4.6.3. After evaluating these operator-valued integrals, the higher loop correlators in AdS become functions of conformal generators acting on contact diagrams. To illustrate the new methodoloy, we compute three-point bubble and triangle Witten diagrams in AdS$_{d+1}$ for $d = 2$ and $d = 2, 3, 4$ dimensions respectively using the differential representation. We compare the former to a more traditional computation performed in position space. To the author's knowledge, closed form expressions for the triangle Witten diagram in general dimension were previously unknown [51].

4.2 AdS Boundary Correlators

In this section, we review certain properties of boundary correlators on AdS_{d+1} background. We are particularly interested in their embedding space form, since they exhibit interesting properties that are analogous to those of flat space scattering amplitudes in momentum space.

4.2.1 Embedding Space

We write AdS boundary correlators as $\mathcal{A}(P_i, Z_i)$, where P_i is a point on the conformal boundary $\partial\mathrm{AdS}_{d+1}$ and Z_i is a polarization vector. In the following, all the quantities we discuss are given in the embedding space. If the external particles have spin, then the AdS boundary correlator $\mathcal{A}$ is also a multilinear function in the polarization vector Z_i. The complete definitions of P_i and Z_i, which are not necessary for the discussion here, are given in appendix C.1. A boundary correlator $\mathcal{A}$ is a homogeneous function in both P_i and Z_i,

$$\mathcal{A}(\lambda P_i, Z_i) = \lambda^{-\Delta_i}\mathcal{A}(P_i, Z_i)\,, \qquad \mathcal{A}(P_i, \lambda Z_i) = \lambda^{l_i}\mathcal{A}(P_i, Z_i)\,, \tag{4.3}$$

where Δ_i is the conformal weight of particle i and l_i is its spin. Note that the conformal weight is defined as the negative of the scaling dimension. AdS boundary correlators are expected to be scalar quantities invariant under the action of the conformal group $\mathrm{SO}(d+1, 1)$, which is isomorphic to the Lorentz group of the embedding space. The conformal generator acting on the i-th particle is

$$D_i^{AB} = P_i^A \frac{\partial}{\partial P_{i,B}} - P_i^B \frac{\partial}{\partial P_{i,A}} + Z_i^A \frac{\partial}{\partial Z_{i,B}} - Z_i^B \frac{\partial}{\partial Z_{i,A}}\,. \tag{4.4}$$

Because the embedding space realizes the conformal transformations linearly, the *conformal Ward identity (CWI)* capturing the conformal invariance of $\mathcal{A}$ is

$$\sum_{i=1}^{n} D_i^{AB}\mathcal{A} = 0\,. \tag{4.5}$$

It resembles the momentum conservation of flat space amplitudes. For an external spinning particle, we can peel off a polarization vector, such that

$$\mathcal{A} = Z_{i,M}\mathcal{A}^M\,. \tag{4.6}$$

111

Written as an embedding space vector, $\mathcal{A}^M$ is transverse to the conformal boundary $\partial\mathrm{AdS}_{d+1}$ if and only if

$$P_{i,M}\mathcal{A}^M = 0. \tag{4.7}$$

See appendix C.1 for more details. Therefore, for $\mathcal{A}(P_i, Z_i)$ to be an AdS boundary correlator, it has to satisfy the *transversality condition*,

$$\mathcal{A}(P_i, Z_i)\Big|_{Z_i \to P_i} = 0, \tag{4.8}$$

which is analogous to the linearized gauge invariance of flat space amplitudes.

In flat space, momentum conservation leads to relations between Mandelstam variables, for example, $s + t + u = 0$ for four-point massless kinematics. We now show how similar relations among conformal generators arise for AdS boundary correlators. We first define for convenience the inner product of conformal generators as

$$D_{ij}^2 \equiv D_i \cdot D_j = \eta_{AC}\eta_{BD}D_i^{AB}D_j^{CD}, \qquad D_i^2 \equiv D_i \cdot D_i. \tag{4.9}$$

Clearly, $D_{ij}^2 = D_{ji}^2$ since D_i commutes with D_j as they act on different variables. D_i^2 is proportional to the quadratic Casimir operator of particle i,

$$\begin{aligned}
-\frac{1}{2}D_i^2 &= \left(P_i \cdot \frac{\partial}{\partial P_i}\right)\left(d + P_i \cdot \frac{\partial}{\partial P_i}\right) + \left(Z_i \cdot \frac{\partial}{\partial Z_i}\right)\left(d - 2 + Z_i \cdot \frac{\partial}{\partial Z_i}\right) \\
&\quad + 2\left(Z_i \cdot \frac{\partial}{\partial P_i}\right)\left(P_i \cdot \frac{\partial}{\partial Z_i}\right) \\
&\cong \Delta_i(\Delta_i - d) + l_i(l_i + d - 2).
\end{aligned} \tag{4.10}$$

When acting on an AdS boundary correlator, or more generally, a conformal partial wave, the second line of the above equation does not contribute due to transversality (4.8). We use $\cong$ to denote "equivalent when acting on a conformal partial wave". Therefore, we can use the eigenvalue of D_i^2 to define the on-shell mass of particle i. A scalar particle is massless if $\Delta_i = d$ while a vector particle is massless if $\Delta_i = d - 1$ (see section 4.2.4 for further comments on this definition). Thus, massless scalar and vector correlators satisfy

$$D_i^2\mathcal{A} = 0 \quad \text{for all } i. \tag{4.11}$$

Massless vector correlators further satisfy the current conservation [209],

$$\frac{\partial}{\partial P_{i,M}}\left[\left(\frac{d}{2}-1+Z_i\cdot\frac{\partial}{\partial Z_i}\right)\frac{\partial}{\partial Z_i^M}-\frac{1}{2}Z_{i,M}\frac{\partial^2}{\partial Z_i\cdot\partial Z_i}\right]\mathcal{A}=0\,.\tag{4.12}$$

Eq. (4.12) assumes that the i-th particle has conformal weight $\Delta_i=d-2+l_i$. Notably, current conservation for graviton boundary correlators requires $\Delta_i=d$, which leads to $-\frac{1}{2}D_i^2\cong 2d$. This is an exception to the naive definition of masslessness described above.

The massless condition and the CWI (4.5) together give rise to very simple relations among conformal generators. As a simple example, we consider the four-point CWI,

$$(D_1^{AB}+D_2^{AB}+D_3^{AB}+D_4^{AB})\mathcal{A}=0\,,\tag{4.13}$$

from which we can derive

$$(D_1+D_2)^2\mathcal{A}=-(D_1+D_2)\cdot(D_3+D_4)\mathcal{A}=(D_3+D_4)^2\mathcal{A}\,.\tag{4.14}$$

For massless AdS boundary correlators, we thus get

$$D_{12}^2\mathcal{A}=D_{34}^2\mathcal{A}\,,\quad\text{or}\quad D_{12}^2\cong D_{34}^2\,.\tag{4.15}$$

Similarly, we can derive that

$$D_{12}^2+D_{13}^2+D_{23}^2\cong 0\,,\tag{4.16}$$

which is the AdS incarnation of the flat space relation $s+t+u=0$. For correlators of higher multiplicity, we define

$$D_I^2\equiv\frac{1}{2}\left(\sum_{a\in I}D_a\right)^2\,.\tag{4.17}$$

Using a slight generalization of eq. (4.14), we can show that

$$D_I^2\cong D_{\bar{I}}^2\,,\tag{4.18}$$

where $\bar{I}$ is the complement of set I in the set of labels of all external particles. Furthermore, we can show that the relations between massless on-shell Mandelstam variables can all be realized as relations between various D_I^2 when acting on a conformal partial wave. One can also prove that [48]

$$[D_I^2,D_{I'}^2]=0\quad\text{if}\quad(I\cap I'=\emptyset)\text{ or }(I\subset I')\text{ or }(I'\subset I)\,.\tag{4.19}$$

We will often be interested in understanding how the inverse of D_I^2 acts on conformal correlators. We will show in the next section that the inverse of D_I^2 acting on a contact diagram can be related to a bulk-bulk propagator in Witten diagram computations. However, one can understand how $(D_I^2)^{-1}$ acts on more generic conformal correlators by decomposing the conformal correlator into conformal partial waves [210]. Conformal partial waves are, by construction, eigenfunctions of D_I^2. Therefore, since any conformal correlator can be expanded as a linear combination of conformal partial waves, one can use such a conformal partial wave decomposition to systematically understand how D_I^2 acts on any conformal correlator. Conformal partial waves beyond four-point were recently considered in refs. [211, 212].

Gauge invariance and on-shell kinematics are crucial for flat space amplitudes to have additional structures, like color/kinematics duality, BCJ amplitude relations, and double copy. Due to the properties listed above, we therefore intuitively expect that embedding space is a promising stage to explore such hidden structures in AdS boundary correlators.

4.2.2 AdS Propagators

In terms of the embedding space coordinates, the scalar equation of motion on the AdS background $X^2 = -1$ is given by

$$\partial_A(G^{AB}\partial_B\phi) - \Delta(\Delta - d)\phi = J \,, \tag{4.20}$$

where J corresponds to scalar source terms. From eq. (4.20), the scalar bulk-boundary propagator is[2]

$$E_\Delta(P_k, X) = \frac{\mathcal{N}_\Delta}{(-2P_k \cdot X)^\Delta} \,, \qquad \mathcal{N}_\Delta = \frac{\Gamma(\Delta)}{2\pi^{d/2}\Gamma(\Delta - d/2 + 1)} \,, \tag{4.21}$$

The assumption that $z \geq 0$ implies $X \cdot P \leq 0$. Another solution is the bulk-bulk propagator, which we write using the split representation

$$G_\Delta(X,Y) = \int_{-i\infty}^{i\infty} \frac{dc}{2\pi i} f_\Delta(c)\Omega_c(X,Y) \tag{4.22}$$

---

[2]We follow here the normalization in [213, 214], which is slightly different from that of [215], for the scalar bulk-boundary propagator. Together with the normalization for the vector-field bulk-boundary propagator in eq. (4.26), they are convenient to simplify certain overall factors for $d \neq 2$ in later sections.

where

$$\Omega_c(X,Y) = -2c^2 \int_{\partial \text{AdS}} dQ E_{d/2+c}(Q,X) E_{d/2-c}(Q,Y)$$

$$f_\Delta = \frac{1}{(\Delta - d/2)^2 - c^2} \,.$$

(4.23)

The bulk-bulk propagator is normalized such that

$$\left[\partial_A (G^{AB} \partial_B) - \Delta(\Delta - d) \right] G_\Delta(X,Y) = -\delta^{d+1}(X,Y) \,.$$

(4.24)

Physically, the split representation corresponds to a decomposition of the AdS bulk-bulk propagator in terms of AdS harmonic functions, $\Omega_c(X,Y)$, which are eigenfunctions of the AdS Laplacian that are divergence free. It is easy to check that eq. (4.22) is the bulk propagator by using that eq. (4.21) is the bulk-boundary propagator and an identity that decomposes the AdS delta function into AdS harmonic functions. The crucial insight of the split representation is that the AdS harmonic functions can be represented as products of bulk-boundary propagators integrated over the boundary. Therefore, the split representation allows us to sew three-point correlators together in a manner reminiscent of BCFW recursions in flat space.

We now turn to the propagator of a gauge boson in AdS. The equations of motion for the spin-1 state are

$$(\nabla^2 - \Delta(\Delta - d) + 1) A^{a,A} = J^{a,A}$$

(4.25)

where $J^{a,A}$ corresponds to vector source terms. From eq. (4.25), the bulk-boundary propagator is

$$E_\Delta^{MA}(P,X) = \left(\eta^{MA} - \frac{X^M P^A}{P \cdot X} \right) \frac{\mathcal{N}_{\Delta,1}}{(-2P \cdot X)^\Delta} \,, \qquad \mathcal{N}_{\Delta,1} = \frac{\Delta}{\Delta - 1} \mathcal{N}_\Delta \,,$$

(4.26)

which is well defined on the AdS hypersurface because $E_\Delta^{MA} X_A = 0$ and $P_M E_\Delta^{MA} = 0$. Crucially, we can write eq. (4.26) in terms of the scalar bulk-boundary propagator using a differential operator, $\mathcal{D}^{MA}$:

$$E_\Delta^{MA} = \frac{\Delta}{\Delta - 1} \mathcal{D}^{MA} E_\Delta, \quad \text{where} \quad \mathcal{D}_\Delta^{MA} = \eta^{MA} + \frac{1}{\Delta} P^A \frac{\partial}{\partial P_M} \,.$$

(4.27)

Another solution to the equations of motion is the bulk-bulk propagator, which we again write using the split-representation,

$$G_\Delta^{AB}(X,Y) = \int_{-i\infty}^{i\infty} \frac{dc}{2\pi i} f_\Delta(c) \Omega_c^{AB}(X,Y)$$

(4.28)

where f_Δ is the same as for a scalar field and

$$\Omega_c^{AB}(X,Y) = -2c^2 \int_{\partial\text{AdS}} dQ\, \eta_{MN} E_{d/2+c}^{MA}(Q,X) E_{d/2-c}^{NB}(Q,Y) \qquad (4.29)$$

Similar to the scalar split representation, the vector split representation also corresponds to a decomposition of the bulk-bulk propagator in terms of spin-1 AdS harmonic functions, $\Omega_c^{AB}(X,Y)$, which is well defined in the bulk embedding because $X_A \Omega_c^{AB}(X,Y) = 0$ and $\Omega_c^{AB}(X,Y) Y_B = 0$. The same property is also satisfied by G_Δ^{AB}. Using eqs. (4.27) and (4.28) in the evaluation of position space correlators prevents the appearance of uncontracted bulk integration variables in the AdS boundary correlators and will allow us to write the correlator manifestly in terms of Z_i, P_i and D-functions.

4.2.3 Vertex Rules for Yang-Mills from the Embedding Space Action

Yang-Mills is a theory of massless spin-1 states in AdS and its Lagrangian is given by

$$\mathcal{L}_{\text{YM}} = -\frac{1}{4} F_{\mu\nu}^a F^{a,\mu\nu} \qquad (4.30)$$

where the indices are contracted with the AdS metric, $F_{\mu\nu}^a = \nabla_\mu A_\nu^a - \nabla_\nu A_\mu^a - g f^{abc} A_\mu^b A_\nu^c$ and, as before, ∇ is the gravitational covariant derivative. While the translation of contact term Feynman graphs between AdS and the embedding space is straightforward, it becomes less so for exchange diagrams of vector and tensor fields for generic theories. Fortunately, the AdS embedding of eq. (4.30) is essentially unchanged. Under the Lorentz gauge, it is given by

$$\mathcal{L} = -\frac{1}{2} G^{AB} G^{CD} \partial_A A_C^a \partial_B A_D^a + g f^{abc} G^{AB} G^{CD} (\partial_A A_C^a) A_B^b A_D^c \qquad (4.31)$$

$$- \frac{g^2}{4} G^{AB} G^{CD} f^{abx} f^{xcd} A_A^a A_C^b A_B^c A_D^d , \qquad (4.32)$$

from which we can read off the three-point and four-point vertices in the embedding space. Einstein's gravity has a similar (though significantly more involved) presentation.

4.2.4 On-Shell and Off-Shell Correlators

As it is well-known, field equations in AdS space generically exhibit two solutions with distinct asymptotics near the boundary,

$$\phi(z,x) = \phi_0(z^{\Delta_0} + \dots) + \phi_1(z^{\Delta_1} + \dots) , \qquad (4.33)$$

where Δ_0 and Δ_1 are the smaller and larger solutions to a second-order equation which relates the $SO(d+1,1)$ quantum numbers of the field and its AdS mass term, respectively. They are distinguished by the fact that a solution with ϕ_0 asymptotics is not normalizable near the boundary while a solution with ϕ_1 asymptotics is normalizable, $\int_{\text{AdS}} d^d x \int_0 dz \sqrt{g} |\phi|^2 < \infty$.[3]

For scalar fields, the traditional definition of AdS mass is related to the conformal weight by the formula

$$\Delta(\Delta - d) = m^2 \ . \tag{4.34}$$

Therefore, for a massless scalar, we find

$$\Delta_1 = \Delta = d \ , \qquad \Delta_0 = d - \Delta = 0 \ . \tag{4.35}$$

A similar consideration for vectors and gravitons in the bulk yields $\Delta = d - 1$ and $\Delta = d$ respectively [43, 44]. It is worth mentioning that there is no invariant meaning to the AdS mass because fields with the same properties and belonging to the same multiplet have different AdS energies [217]. A possible definition of massless fields in AdS is that they occur in the tensor product of two doubleton multiplets, which correspond to massless conformal fields on the boundary [218]; the mass can then be interpreted as a suitable shift of the corresponding quadratic Casimir of $SO(d+1,1)$.[4] For $\mathcal{N} = 8$ supergravity in $\text{AdS}_5 \times S^5$, the corresponding operators are conserved currents in $\mathcal{N} = 4$ sYM theory, belonging to the stress tensor multiplet.

The leading field asymptotics on a surface parallel to the boundary at $z = \epsilon$ serves as a source for gauge-invariant operators of dimension Δ, as

$$S_{\text{boundary}} \sim \int_{\text{AdS}} d^d x \sqrt{-\gamma_\epsilon} \phi(\epsilon, x) \mathcal{O}(\epsilon, x) = \int_{\text{AdS}} d^d x \phi_0(x) \epsilon^{-\Delta} \mathcal{O}(\epsilon, x) \ , \tag{4.36}$$

and $\mathcal{O}(\epsilon, x) = \epsilon^\Delta \mathcal{O}(x)$ render this term independent of ϵ. Thus, by differentiating the effective action with respect to ϕ_0, one evaluates [44] correlation functions of gauge-invariant operators in the boundary theory. From the perspective of the bulk theory, they can be interpreted as correlation functions of the fields with these prescribed asymptotics; we shall refer to them as *on-shell* correlation functions. By analogy with the case of flat space correlation functions with external states not obeying the free equations of motion, we will refer to bulk correlation functions whose asymptotics are not ϕ_0 as *off-shell*.

In general, off-shell correlation functions do not have an immediate boundary interpretation for specific values of the conformal weight. However, they feature prominently in the split represen-

---

[3]Technically, if Δ lies in the range $(d-2)/2 < \Delta < d/2$, either ϕ_0 or ϕ_1 can correspond to the source term. The choice between ϕ_0 and ϕ_1 as the source term simply corresponds to how there are two different quantizations of the bulk scalar field [216].

[4]We thank Murat Günaydin for discussion on this point.

tation of the bulk-bulk propagator. In that form, the propagator is written as a sum of products of bulk-boundary propagators, see e.g. eq. (4.22), and thus higher-point correlators are written as sums of products of lower-point correlators which have at least one leg off-shell in the sense defined above. For scalar fields, one bulk-boundary propagator factor corresponds to the conformal weight Δ of the scalar field while the other corresponds to a weight $d - \Delta$ associated to the normalizable mode of the same scalar field. While the former is a non-normalizable mode and thus leads to an on-shell field, the latter is a normalizable mode of the same field; its usual interpretation is that it defines a particular state in the boundary theory so the correlator with one such insertion may be interpreted as a term in the perturbative expansion of an on-shell correlator in that state. A similar interpretation should hold for correlators with more than one off-shell leg, except that the relevant state corresponds to turning on normalizable modes of several fields. The bulk-bulk propagators of higher-spin fields have support on bulk-boundary propagators with AdS energies beyond those corresponding to the normalizable and non-normalizable modes. They have a less straightforward boundary interpretation, but may perhaps be understood as needed to obtain a representation of the $(d + 1)$-dimensional rotation group.

In flat space, field redefinitions change the correlation functions of fundamental fields, but these changes are projected out of S-matrix elements by the LSZ reduction. It is interesting to ask whether our definition of on-shellness has similar properties. One might expect this to be the case in light of the holographic duality between on-shell correlators and gauge theory correlation functions of gauge-invariant operators. Indeed, the Schwinger-Dyson equation[5]

$$\left\langle \frac{\delta S}{\delta \phi(x)} \phi(x_1) \ldots \phi(x_n) \right\rangle = \sum_{i=1}^{n} \delta(x - x_i) \langle \phi(x_1) \ldots \widehat{\phi}(x_i) \ldots \phi(x_n) \rangle \,, \qquad (4.37)$$

holds in AdS space (and more generally in curved space); since the field sources at x_i, $i = 1, ..., n$ are placed on the boundary while the argument of $\frac{\delta S}{\delta \phi(x)}$ is a bulk point, they cannot coincide so the right-hand side vanishes identically implying that AdS on-shell correlation functions in the sense defined above are invariant under suitable field redefinitions.[6]

The Schwinger-Dyson equation, however, does not hold for off-shell correlation functions. This is easiest to see by looking at a free field theory for $n = 1$; the off-shell two-point function of

---

[5]Here the hat signifies that the field at that position is absent from the correlation function and ϕ denotes a generic field, not necessarily a scalar.

[6]Similar to field redefinitions that leave invariant the S matrix of a flat-space field theory, field redefinitions that leave correlators invariant should not change quadratic term of bulk fields and vanish at the boundary. For example, $\phi_i \mapsto \phi_i' = \sum_j a_{ij} \phi_j +$ nonlinear yields a sum of the original correlation functions weighted by coefficients a_{ij}. This may be easily understood by noticing that the boundary operators sourced by the fields ϕ' are linear combinations of those sourced by the fields ϕ. More generally, it is not difficult to see that, if a nonlinear field redefinition do not change the boundary conditions of a field, then the nonlinear terms are subleading at the boundary and therefore do not change the on-shell correlators.

as defined above does not correlate the conformal weight with the AdS Lagrangian mass term while $\frac{\delta S}{\delta \phi(x)}$ depends on the AdS Lagrangian mass term, so $\langle \frac{\delta S}{\delta \phi(x)} \phi(x_1) \rangle$ cannot be proportional to $\delta(x - x_1)$. This is consistent with the earlier observation that off-shell correlation functions do not have a straightforward gauge theory interpretation. It is interesting that this dependence on the choice of fields cancels out when off-shell correlators are assembled into on-shell ones.

It has been recently shown that it is interesting to consider varying the mass of bulk fields. For example, one can extract the proper time from the event horizon to a black hole singularity by studying how thermal one point functions vary with the mass of the bulk field [219], allowing one to probe the bulk geometry of thermal states beyond the quantum entanglement wedge. Furthermore, analytic continuations in spin and in Δ are famously connected [220, 221] to light ray operators and the OPE inversion formula. Further discussion is beyond the scope of this paper.

4.3 Differential Representation of Boundary Correlators

The *differential representation* of an n-point boundary correlator takes the form[7]

$$\mathcal{A}_n = \hat{\mathcal{A}}_n D_{\Delta_1, \Delta_2, \ldots, \Delta_n} \tag{4.38}$$

where $\hat{\mathcal{A}}_n$ is a collection of local and nonlocal differential operators that contains information on boundary states. For example, for external spinning states, it contains information on their spin and polarization. Regardless of the spin of external states, $\hat{\mathcal{A}}_n$ acts on a scalar contact diagram (D-function),

$$D_{\Delta_1, \Delta_2, \ldots, \Delta_n} = \quad \begin{array}{c} \Delta_3 \quad \Delta_4 \\ \Delta_2 \overbrace{\bigotimes}^{} \vdots \\ \Delta_1 \quad \Delta_n \end{array} \quad = \int_{\text{AdS}} dX \prod_{i=1}^{n} E_{\Delta_i}(X, P_i) \,. \tag{4.39}$$

Here $E_{\Delta_i}(X, P_i) = \frac{1}{(-2P_i \cdot X)^{\Delta_i}}$ is the scalar bulk-boundary propagator.[8] The D-function thus defined provides the support of CWI to the boundary correlator, and plays a role similar to the momentum conservation constraint in the flat space S matrix. Generally, up to subtleties related to the noncommutativity of conformal generators, $\hat{\mathcal{A}}_n$ takes a form similar to the corresponding flat space amplitude. With examples and justification to be detailed in later sections, we claim that a

---

[7]As discussed in the introduction, we assume that our boundary correlators have a perturbative Witten diagram expansion in the bulk. From a holographic point of view, they correspond to correlators in a putative boundary CFT in the strong coupling limit.

[8]In this work, we omit the overall normalization $\mathcal{C}_\Delta$ of a bulk-boundary propagator. Since for a given boundary correlator all bulk-boundary propagators are the same, the omitted factors can only alter the overall normalization.

generic differential correlator $\hat{\mathcal{A}}_n$ can be written as

$$\hat{\mathcal{A}}_n = \sum_{g \in \text{cubic}} C_g \prod_{I \in g} \frac{1}{D_I^2 + M_{I,s}^2} \hat{N}_g \,, \tag{4.40}$$

where $\hat{N}_g$ is a local operator. The summation runs over all the trivalent Witten diagrams. Importantly, the bulk-bulk propagator associated with an internal leg I is given by an inverse differential operator,

$$I \left\{ \begin{array}{c} \end{array} \right. \hspace{-0.5em} \begin{array}{c} \includegraphics \end{array} \hspace{-0.5em} \xrightarrow{} \frac{1}{D_I^2 + M_{I,s}^2} \,, \tag{4.41}$$

where D_I^2 is the quadratic Casimir operator of the AdS symmetry group acting on all external points connected to one end of that internal line and $M_{I,s}^2$ is the eigenvalue of the quadratic Casimir for the representation of the internal state. The inverse differential operator $(D_I^2 + M_{I,s}^2)^{-1}$ will be called a propagator in the context of differential representation. We stress that this form is also expected for theories with quartic and higher-point interaction vertices and, if necessary, such vertices are trivially resolved into trivalent ones by multiplying and dividing by suitable operators. For theories with fields charged under a non-abelian gauge or flavor symmetry, C_g in eq. (4.41) is the color factor associated with the diagram. The (local) operator $\hat{N}_g$, acting directly on the D-function, can be understood as the analog of the flat-space kinematic numerator factor.

To justify eq. (4.40) and in particular the appearance of the nonlocal operators (4.41), we start with the differential representation of the bulk-bulk propagator, which was first proposed for bi-adjoint ϕ^3 theory in Ref. [48]. As the simplest example, we consider the following s-channel scalar Witten diagram

$$\begin{array}{c} \includegraphics \end{array} = \int_{\text{AdS}} dX dY\, E_{\Delta_3}(X, P_3) E_{\Delta_4}(X, P_4) G_\Delta(X, Y) E_{\Delta_1}(Y, P_1) E_{\Delta_2}(Y, P_2) \,, \tag{4.42}$$

and rewrite the bulk-bulk propagator as the inverse of the free-field operator acting on the delta function

$$\mathcal{G}_\Delta(X, Y) = -\frac{1}{\nabla_X^2 - \Delta(\Delta - d)} \delta(X, Y) \,. \tag{4.43}$$

We can now integrate out the bulk point Y and get

$$
\text{(diagram)} = \int_{\text{AdS}} dX E_{\Delta_3}(X, P_3) E_{\Delta_4}(X, P_4)
$$
$$
\times \frac{(-1)}{\nabla^2 - \Delta(\Delta - d)} E_{\Delta_1}(X, P_1) E_{\Delta_2}(X, P_2). \tag{4.44}
$$

When acting on a product of scalar bulk-boundary propagators, the AdS Laplacian ∇^2 can also be written as $\nabla^2 = -D_X \cdot D_X$. Then, the identity

$$
D_X \cdot D_X \Big[E_{\Delta_1}(X, P_1) E_{\Delta_2}(X, P_2) \Big] = D_{12}^2 \Big[E_{\Delta_1}(X, P_1) E_{\Delta_2}(X, P_2) \Big], \tag{4.45}
$$

which is a consequence of the conformal Ward identity, converts the quadratic Casimir operator for the bulk point X to the quadratic Casimir operator for the pair $(1, 2)$ of boundary points. This gives the differential representation of the s-channel Witten diagram:

$$
\text{(diagram)} = \frac{1}{D_{12}^2 + \Delta(\Delta - d)} D_{\Delta_1, \Delta_2, \Delta_3, \Delta_4}. \tag{4.46}
$$

It is exactly analogous to the corresponding scattering amplitude in flat space. The derivation for higher point scalar Witten diagrams is similar. We note that the operators D_I^2 associated with the internal lines all commute with each other, so there is no ordering ambiguity in the propagators of the differential representation.

4.4 BCJ Relations for AdS Boundary Correlators

In this section, we begin by discussing the cubic bi-adjoint scalar (BAS) theory in AdS space. We then use the results we obtain to motivate a generalization of color/kinematics duality and of the BCJ amplitudes relations for certain AdS boundary correlators.

4.4.1 Cubic Bi-Adjoint Scalar in AdS

To motivate the BCJ amplitude relations in an AdS setup, we first consider the simplest theory in AdS that could exhibit color/kinematics duality – cubic BAS in AdS, defined by the Lagrangian

$$
\mathcal{L} = \frac{1}{2}(\nabla\phi)^2 - \frac{g}{6} f^{abc} \tilde{f}^{a'b'c'} \phi^{aa'} \phi^{bb'} \phi^{cc'}. \tag{4.47}
$$

As in flat space, the scalars transform in the bi-adjoint representation of $\mathrm{SU}(N) \times \mathrm{SU}(N')$. Perturbative computations of AdS boundary correlators involve summing cubic Witten diagrams respectively, dressed with appropriate color factors. We will review a particular representation of the cubic BAS boundary correlators given in Ref. [50] for $d = 2$ and in Ref. [48] for general d. We will first consider the four-point formula before generalizing to the n-point case.

First, from the differential representation, the four-point BAS AdS boundary correlator can be represented as

$$\mathcal{A}^{\mathrm{BAS}} = \left(\frac{C_s \tilde{C}_s}{D_{12}^2} + \frac{C_t \tilde{C}_t}{D_{23}^2} + \frac{C_u \tilde{C}_u}{D_{13}^2} \right) \left(\frac{\Gamma(d)}{2\pi^{d/2}\Gamma(d/2+1)} \right)^4 D_{d,d,d,d} \,, \tag{4.48}$$

where the color factors are $C_s = f^{a_1 a_2 x} f^{x a_3 a_4}$, $C_t = f^{a_2 a_3 x} f^{x a_1 a_4}$, $C_u = f^{a_3 a_1 x} f^{x a_2 a_4}$ and similarly for $\tilde{C}_{s,t,u}$. Since we are working with external scalars, we can ignore the Z component of D_i^{AB}. The n-point color-dressed BAS correlator can similarly be written as

$$\mathcal{A}^{\mathrm{BAS}} = \left(\frac{\Gamma(d)}{2\pi^{d/2}\Gamma(d/2+1)} \right)^n \sum_{\mathrm{cubic}\ g} C(g|\alpha_g)\tilde{C}(g|\alpha_g) \prod_{I \in g} \frac{1}{D_I^2} D_{\underbrace{d,d,\ldots,d}_{n}} \,, \tag{4.49}$$

where the sum runs over all cubic graphs, and $C(g|\alpha_g)$ and $\tilde{C}(g|\alpha_g)$ are the color factors, which are the same as flat space, associated with the cubic graph g.

4.4.2 Color/Kinematics Duality for Flat Space Amplitudes

We now take a slight detour and review a streamlined derivation of the flat-space BCJ amplitudes relations before generalizing them to AdS boundary correlators. Although this derivation differs from the one considered in Chapter 3, it is equivalent when there are no higher derivative operators. We will use this perspective on color-kinematics duality in this chapter because it is more suitable for generalization to AdS. In flat space, amplitudes that satisfy color/kinematics duality can be written as a sum over cubic graphs [171],

$$\mathcal{A}_{\mathrm{flat}} = \sum_{\mathrm{cubic}\ g} C(g|\alpha_g) N(g|\alpha_g) \prod_{I \in g} \frac{1}{s_I} \,. \tag{4.50}$$

where both the kinematic numerators (sometimes referred to as BCJ numerators) and color factors obey Jacobi-like relations corresponding to triplets of cubic graphs as shown in figure 4.1,

$$N(g_s|I_1 I_2 I_3 I_4) + N(g_t|I_1 I_4 I_2 I_3) + N(g_u|I_1 I_3 I_4 I_2) = 0 \,,$$
$$C(g_s|I_1 I_2 I_3 I_4) + C(g_t|I_1 I_4 I_2 I_3) + C(g_u|I_1 I_3 I_4 I_2) = 0 \,. \tag{4.51}$$

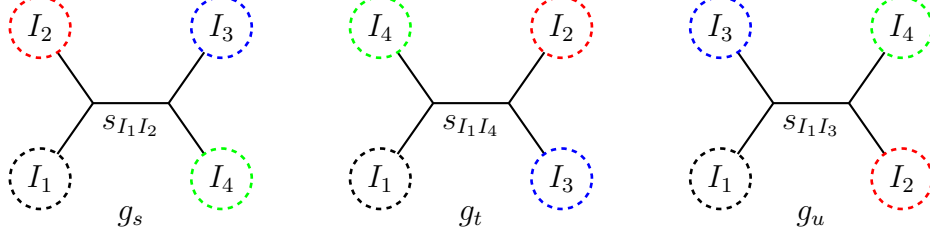For cubic BAS, the numerator $N(g|\alpha_g)$ is simply another the color factor $\tilde{C}(g|\alpha_g)$ so that the Jacobi identity trivially holds. We can expand the color factors in eq. (4.50) into the $(n-2)!$ dimensional Del Duca-Dixon-Maltoni (DDM) basis, consisting of the color factors of the half ladder graphs [222],

$$
C_{1,\alpha(2,3,\ldots,n-1),n} \equiv C\left(\begin{array}{c} \overset{\alpha(2)\ \alpha(3)\qquad\quad \alpha(n-1)}{\underset{1\ \rule{3cm}{0.4pt}\ n}{|\quad|\quad\cdots\quad|}} \end{array}\middle| 1,\alpha,n\right)
$$
$$
= f^{a_1 a_{\alpha(2)} x_2} f^{x_2 a_{\alpha(3)} x_3} \cdots f^{x_{n-2} a_{\alpha(n-1)} a_n}. \tag{4.52}
$$

As an example, we give the decomposition of the following five-point color factor explicitly,

$$
C\left(\begin{array}{c} \overset{3}{2\ \diagdown\!\!\!\diagup\ 4}\\ 1\ \rule{1.5cm}{0.4pt}\ 5 \end{array}\middle| 1,2,3,4,5\right) = f^{a_1 x a_5} f^{x a_2 y} f^{y a_3 a_4}
$$
$$
= C_{1,2,3,4,5} - C_{1,2,4,3,5} - C_{1,3,4,2,5} + C_{1,4,3,2,5}. \tag{4.53}
$$

The decomposition of both color factors in the BAS amplitude leads to the double (color-ordered) partial amplitude denoted as m,

$$
\mathcal{A}_{\text{flat}}^{\text{BAS}} = \sum_{\alpha,\beta \in S_{n-2}} C_{1,\alpha(2,3,\ldots,n-1),n} \, m[1,\alpha,n|1,\beta,n] \, \tilde{C}_{1,\beta(2,3,\ldots,n-1),n}. \tag{4.54}
$$

In general, $m[\alpha|\beta]$ receives contributions from all cubic Feynman diagrams that are planar for both permutations α and β. For a generic amplitude that exhibits color/kinematics duality, the DDM basis decomposition gives

$$
\mathcal{A}_{\text{flat}} = \sum_{\alpha \in S_{n-2}} C_{1,\alpha(2,3,\ldots,n-1),n} A_{\text{flat}}(1,\alpha,n), \tag{4.55}
$$

where $A_{\text{flat}}(1,\alpha,n)$ is the (color-ordered) partial amplitude given by

$$
A_{\text{flat}}(1,\alpha,n) = \sum_{\beta \in S_{n-2}} m[1,\alpha,n|1,\beta,n] N_{1,\beta(2,3,\ldots,n-1),n}. \tag{4.56}
$$

Here $N_{1,\beta,n}$ are DDM-basis numerators associated with half ladder graphs as in eq. (4.52). They also form a basis for all the BCJ numerators. As a consequence of the color structure, we can use the Kleiss-Kuijf relation [223]

$$
A_{\text{flat}}[1,\alpha,n,\beta] = (-1)^{|\beta|} \sum_{\sigma \in \alpha \sqcup\!\sqcup \beta^T} A_{\text{flat}}[1,\sigma,n] \tag{4.57}
$$

Figure 4.1: A triplet of three cubic tree graphs that differ by one propagator.

and cyclicity to expand any partial amplitudes in terms of the DDM basis ones.

We note that the DDM basis is minimal for color factors, but over-complete for partial amplitudes on the support of on-shell massless kinematics. This is reflected by the fact that the rank of $m[\alpha|\beta]$, as a matrix in the DDM basis, is only $(n-3)!$. Crucially, the null vectors of $m[\alpha|\beta]$ translate to BCJ amplitude relations for partial amplitudes,

$$\sum_{\beta \in S_{n-2}} v(\beta) m[1, \beta, n|\alpha] = 0 \quad \longrightarrow \quad \sum_{\beta \in S_{n-2}} v(\beta) A_{\text{flat}}[1, \beta, n] = 0 . \tag{4.58}$$

For example, at four points the $m[\alpha|\beta]$ matrix,

$$\begin{bmatrix} m[1,2,3,4|1,2,3,4] & m[1,2,3,4|1,3,2,4] \\ m[1,3,2,4|1,2,3,4] & m[1,3,2,4|1,3,2,4] \end{bmatrix} = \begin{bmatrix} \frac{1}{s_{12}} + \frac{1}{s_{23}} & -\frac{1}{s_{23}} \\ -\frac{1}{s_{23}} & \frac{1}{s_{13}} + \frac{1}{s_{23}} \end{bmatrix} , \tag{4.59}$$

has a null vector $v = [s_{12}, -s_{13}]$, which leads to the BCJ amplitude relation

$$s_{12} A_{\text{flat}}[1,2,3,4] = s_{13} A_{\text{flat}}[1,3,2,4] . \tag{4.60}$$

More generally, the fundamental BCJ relations can be written as [171]

$$0 = s_{12} A_{\text{flat}}[1,2,\dots,n] + \sum_{j=3}^{n-1} \left(s_{12} + \sum_{k=3}^{j} s_{2k} \right) A_{\text{flat}}[1,3,\dots,j,2,j+1,\dots,n] . \tag{4.61}$$

4.4.3 Color/Kinematics Duality for AdS Boundary Correlators

To define an extension of color/kinematics duality to field theories in AdS space, we need to first assume a suitably general form for their boundary correlators. Motivated by eq. (4.49), a natural generalization of eq. (4.50) is that an AdS boundary correlator $\mathcal{A}$ can be cast into the form

$$\mathcal{A} = \sum_{\text{cubic } g} C(g|\alpha_g) \left(\prod_{I \in g} \frac{1}{D_I^2} \right) \hat{N}(g|\alpha_g) D_{\underbrace{d,d,\dots,d}_{n}} , \tag{4.62}$$

124

where the numerators $\hat{N}(g|\alpha_g)$ are now differential operator-valued, act directly on the D-functions and absorb the normalization factors of the bulk-boundary propagators. Note that we have placed the product of $(D_I^2)^{-1}$ to the left of the kinematic numerators in eq. (4.62) for reasons that will be clarified shortly. A more general form of the boundary correlator replaces the factor $\hat{N}(g|\alpha_g)D_{d,d,...,d}$ by some more general structure $N(g|\alpha_g)$ which may perhaps be written as a linear combination of differential operators acting on D functions.

With the definition (4.62), the kinematic Jacobi relations are taken to be the operator relations,

$$\hat{N}(g_s|I_1I_2I_3I_4) + \hat{N}(g_t|I_1I_4I_2I_3) + \hat{N}(g_u|I_1I_3I_4I_2) = 0 . \tag{4.63}$$

With the more general form of correlators, the kinematic Jacobi relations are functional relations, in close similarity with flat space scattering amplitudes. We will comment briefly on its consequences at the end of section 4.4.4.

Kinematic numerators as differential operators have already appeared in the study of celestial amplitudes in flat space [224–226], so it should not be surprising that it may also happen in AdS space. In this paper, the representation (4.62) is realized manifestly for the NLSM at four and six points.

The kinematic Jacobi relation (4.63) can be relaxed so that the combination of numerator factors on the right-hand side is required to vanish only when acting on functions of the type $D_{\Delta_1, \Delta_2,...}$, as it is the case when the numerator factors are assembled into a correlator. While we have not explicitly verified, it is natural to expect that only this weaker relation is required by the gauge invariance of eq. (4.62). There is no analog of this weaker relation for tree-level flat space amplitudes in momentum space; at loop level, however, this is analogous to the requirement that the kinematic Jacobi relations hold only up to total derivatives.

The leap from eq. (4.49) to eq. (4.62) is partially motivated by a recent generalization of ambitwistor string models to AdS$_3 \times S^3$ [50]. These models can be interpreted as taking the infinite tension limit of a WZW model with AdS$_3 \times S^3$ target space. For a non-abelian spin-1 theory on AdS$_3 \times S^3$, the ambitwistor model in Ref. [50] provides a CHY-like formula for the differential representation of $A(\alpha)$ in a YM-Chern-Simons theory. We expect that these formulas for the differential correlator simplify to eq. (4.62), just as in flat space. Furthermore, we tentatively expect that the AdS$_3 \times S^3$ ambitwistor model generalizes to higher dimensions, at least for the YM sector. Proving these expectations, however, is beyond the scope of this paper. Therefore, we simply take the AdS$_3 \times S^3$ computation as inspiration and conjecture that eqs. (4.51) and (4.62) hold for certain single-colored theories in higher dimensional AdS.

Before we proceed, let us note that our discussion has been restricted to colored theories in AdS. There is a natural generalization of eq. (4.62) to gravitational theories which will be discussed in

section 4.5.

4.4.4 BCJ Relations for AdS Boundary Correlators

We now demonstrate that the color/kinematics dual form (4.62) of the AdS boundary correlators naturally lead to additional relations among the AdS partial correlators. First, we use the color Jacobi identity (4.51) to expand the AdS correlator in the DDM basis,

$$\mathcal{A} = \sum_{\alpha \in S_{n-2}} C_{1,\alpha(2,3,\ldots,n-1),n} \mathcal{A}[1,\alpha,n] \,, \tag{4.64}$$

where $A(1,\beta,n)$ are the AdS partial correlators. We then perform the same expansion for the kinematic numerators, $\hat{N}(g|\alpha)$, now finding

$$\mathcal{A}[1,\alpha,n] = \sum_{\beta \in S_{n-2}} \hat{m}[1,\alpha,n|1,\beta,n] \hat{N}_{1,\beta(2,3,\ldots,n-1),n} D_{\underbrace{d,d,\ldots,d}_{n}} \,, \tag{4.65}$$

where $\hat{m}[\alpha|\beta]$ is the double partial correlator of BAS obtained by simply replace s_I by D_I^2 in the flat space amplitude $m[\alpha|\beta]$. We note that D_I^2 and $D_{I'}^2$ always commute if they belong to the same Feynman diagram since I and I' always satisfy the condition in eq. (4.19). The DDM basis partial correlators form a basis for all partial correlators due to the Kleiss-Kuijf relation (4.57) and cyclicity, which depends on color Lie algebra only.

Similar to flat space amplitudes, eq. (4.65) yields relations among the partial correlators, since the null vectors of $\hat{m}[\alpha|\beta]$ are orthogonal to the vector of partial correlators,

$$\sum_{\beta \in S_{n-2}} \hat{v}(\beta) \hat{m}(1,\beta,n|\alpha) = 0 \quad \longrightarrow \quad \sum_{\beta \in S_{n-2}} \hat{v}(\beta) A(1,\beta,n) = 0 \,, \tag{4.66}$$

cf. eq. (4.58). The null vectors $\hat{v}(\beta)$ in general are themselves differential operators. If $v(\beta)$ is a null vector of $m[\alpha|\beta]$ that is first order in Mandelstam variables, then it is not difficult to see that $\hat{v}(\beta)$ is still a null vector of $\hat{m}[\alpha|\beta]$ after the replacement $s_I \to D_I^2$.[9] We can then conjecture that the rank of $\hat{m}[\alpha|\beta]$ is still $(n-3)!$ on the support of CWI (4.5). In particular, it leads to the

---

[9]The reasoning goes as follows. In flat space, proving BCJ relations requires using on-shell identities to cancel certain numerators with propagators. Now for AdS correlators, CWI works the same as on-shell identites, and cancellation between numerators and denominators will not be affected by non-commutativity since for each term every D_I^2 in the denominator commutes and there is only a single term in the numerator. Of course, finding more generic null vectors is difficult.

conclusion that the partial correlators of the form (4.65) satisfy the fundamental BCJ relations

$$0 = D_{12}^2 \mathcal{A}[1, 2, \ldots, n] + \sum_{j=3}^{n-1} \left(D_{12}^2 + \sum_{k=3}^{j} D_{2j}^2 \right) \mathcal{A}[1, 3, \ldots, j, 2, j+1, \ldots, n] \,, \qquad (4.67)$$

which may formally be obtained from eq. (4.61) through the replacement $s_I \to D_I^2$.

To better understand the above statement, we now consider some explicit examples. From eq. (4.65), the four-point DDM basis partial correlators are given by

$$\begin{bmatrix} \mathcal{A}[1, 2, 3, 4] \\ \mathcal{A}[1, 3, 2, 4] \end{bmatrix} = \underbrace{\begin{bmatrix} \frac{1}{D_{12}^2} + \frac{1}{D_{23}^2} & -\frac{1}{D_{23}^2} \\ -\frac{1}{D_{23}^2} & \frac{1}{D_{13}^2} + \frac{1}{D_{23}^2} \end{bmatrix}}_{\hat{m}} \begin{bmatrix} \hat{N}_{1,2,3,4} \\ \hat{N}_{1,3,2,4} \end{bmatrix} D_{d,d,d,d} \,. \qquad (4.68)$$

We would like to show that

$$\hat{v} = \begin{bmatrix} D_{12}^2 \\ -D_{13}^2 \end{bmatrix} \qquad (4.69)$$

annihilates the vector of partial correlators when acted from the left. To this end, it is sufficient to show that $\hat{v}$ annihilates the $\hat{m}$,

$$D_{12}^2 \hat{m}[1234|\alpha] - D_{13}^2 \hat{m}[1324|\alpha] \cong 0 \quad \text{for } \alpha = \{1, 2, 3, \} \text{ and } \{1, 3, 2, 4\} \,, \qquad (4.70)$$

which can be checked explicitly. For example, fixing $\alpha = \{1, 2, 3, 4\}$, we get

$$D_{12}^2 \hat{m}[1234|1234] - D_{13}^2 \hat{m}[1324|1234]$$
$$\cong D_{12}^2 \left(\frac{1}{D_{12}^2} + \frac{1}{D_{23}^2} \right) - (D_{23}^2 + D_{12}^2) \frac{1}{D_{23}^2} = 1 + D_{12}^2 \frac{1}{D_{23}^2} - 1 - D_{12}^2 \frac{1}{D_{13}^2} = 0 \,. \qquad (4.71)$$

The expressions for $\hat{m}$ are obtained from eq. (1.33) through the replacement $s_{ij} \to D_{ij}^2$, and using the "momentum conservation" identity (4.16). One can repeat the above exercise to show that eq. (4.70) holds for $\alpha = (1, 3, 2, 4)$. Therefore, taking the dot product of eq. (4.69) and eq. (4.68) yields

$$D_{12}^2 \mathcal{A}[1, 2, 3, 4] = D_{13}^2 \mathcal{A}[1, 3, 2, 4] \,. \qquad (4.72)$$

As one of the main results of this paper, we will show that the four-point partial correlators of YM satisfy this relation.

For our second example we consider the five-point BCJ relation

$$0 = D_{12}^2 \mathcal{A}[1, 2, 3, 4, 5] + (D_{12}^2 + D_{23}^2)\mathcal{A}[1, 3, 2, 4, 5] .$$
$$+ (D_{12}^2 + D_{23}^2 + D_{24}^2)\mathcal{A}[1, 3, 4, 2, 5] . \tag{4.73}$$

According to eq. (4.65), it suffices to prove that

$$0 \cong D_{12}^2 \hat{m}[1, 2, 3, 4, 5|1, \alpha, 5] + (D_{12}^2 + D_{23}^2)\hat{m}[1, 3, 2, 4, 5|1, \alpha, 5]$$
$$+ (D_{12}^2 + D_{23}^2 + D_{24}^2)\hat{m}[1, 3, 4, 2, 5|1, \alpha, 5] \tag{4.74}$$

for all $\alpha \in S_3$. Here we choose $\alpha = \{2, 3, 4\}$. It is now straightforward to show that

$$D_{12}^2 \hat{m}[1, 2, 3, 4, 5|1, 2, 3, 4, 5] + (D_{12}^2 + D_{23}^2)\hat{m}[1, 3, 2, 4, 5|1, 2, 3, 4, 5]$$
$$+ (D_{12}^2 + D_{23}^2 + D_{24}^2)\hat{m}[1, 3, 4, 2, 5|1, 2, 3, 4, 5] \tag{4.75}$$
$$\cong D_{12}^2 \left(\frac{1}{D_{12}^2 D_{34}^2} + \frac{1}{D_{12}^2 D_{45}^2} + \frac{1}{D_{45}^2 D_{23}^2} + \frac{1}{D_{23}^2 D_{51}^2} + \frac{1}{D_{15}^2 D_{34}^2} \right)$$
$$- (D_{12}^2 + D_{23}^2)\frac{1}{D_{23}^2} \left(\frac{1}{D_{45}^2} + \frac{1}{D_{15}^2} \right) - (D_{12}^2 + D_{15}^2 - D_{34}^2)\frac{1}{D_{15}^2 D_{34}^2} = 0 ,$$

where we have also used $D_{23}^2 + D_{24}^2 + D_{34}^2 \cong D_{234}^2 \cong D_{15}^2$ for the conformal generators on the second line.

Before proceeding, we note that while the AdS boundary correlators of the form (4.62) naturally give rise to the BCJ relations (4.67), the inverse does not hold. In other words, color/kinematics duality in the AdS boundary correlators might have a different manifestation than eq. (4.62). For example, at four-points, the following correlator,

$$\mathcal{A} = \frac{f^{a_1 a_2 x} f^{a_3 a_4 x}}{D_{12}^2}N_s(Z_i, P_i) + \frac{f^{a_1 a_4 x} f^{a_2 a_3 x}}{D_{23}^2}N_t(Z_i, P_i) + \frac{f^{a_1 a_3 x} f^{a_4 a_2 x}}{D_{13}^2}N_u(Z_i, P_i) , \tag{4.76}$$

where

$$N_s(Z_i, P_i) + N_t(Z_i, P_i) + N_u(Z_i, P_i) = 0 , \tag{4.77}$$

still leads to eq. (4.72). However, eq. (4.76) is not equivalent to eq. (4.62) as $N_{s,t,u}$ need not necessarily be written in the form $\hat{N}_{s,t,u}D_{d,d,d,d}$. In practice, it is easier to verify relations like eq. (4.72) than to directly construct kinematic numerators. While we have argued for the form (4.62), it is nevertheless important to keep an open mind.

4.4.5 Color/Kinematics Duality for YM

In this section, we investigate YM theory in AdS space. Its three- and four-point functions have been discussed in various contexts, both as tests of the AdS/CFT correspondence [215, 227] and as illustrations of the embedding and Mellin space techniques [45, 209, 214, 228, 229]. Here we obtain the explicit position-space representation of the YM 4-point boundary correlator and verify that it satisfies the AdS BCJ relations conjectured in section 4.4. We also construct differential representations of the off-shell three-point YM correlator, recovering the results of Ref. [198] when $\Delta_i = d - 1$.

4.4.5.1 The three-point correlator

To set the stage for the calculation of the four-point correlator, we begin by reviewing and extending existing constructions of the position-space three-point correlator for YM theory in AdS space. We will give give an explicit position-space representation as well as a differential representation for this correlator. The former will be useful for the double copy discussion in section 4.5.

We computed the three-point YM AdS boundary correlator using the Feynman rules discussed in section 4.2.3. The structure of the vertex together with the property $E_\Delta^{MA} X_A = 0$ of the vector bulk-boundary propagator imply that the embedding space projector G^{AB} defined in eq. (??) can simply be replaced with η^{AB}. We will compute the correlator for arbitrary weight Δ_i, as this form will be useful for the four-point calculation in the next section. The three-point correlator is

$$\mathcal{A}_{\Delta_1 \Delta_2 \Delta_3}^{a_1 a_2 a_3} = -f^{a_1 a_2 a_3} Z_{1,M_1} Z_{2,M_2} Z_{3,M_3} \int_{\mathrm{AdS}} dX \tag{4.78}$$
$$\times \left[E_{\Delta_1}^{M_1 A_1}(P_1, X) \eta_{A_2 A_3} \left(\partial_{A_1} E_{\Delta_2}^{M_2 A_2}(P_2, X) E_{\Delta_3}^{M_3 A_3}(P_3, X) - (2 \leftrightarrow 3) \right) + \mathrm{cyclic}(1, 2, 3) \right].$$

Using the expression for $E_\Delta^{M,A}$ in eq. (4.26), $[\mathcal{D}_{\Delta_i}^{M_i A_i}, \partial_B] = 0$, and

$$\partial_A E_{\Delta_i}(P_i, X) = -\frac{\Delta_i P_{i,A}}{(P_i \cdot X)} E_{\Delta_i}(P_i, X) \equiv K_{i,A} E_\Delta(P_i, X) . \tag{4.79}$$

The correlator can be organized as

$$\mathcal{A}_{\Delta_1 \Delta_2 \Delta_3}^{a_1 a_2 a_3} = -f^{a_1 a_2 a_3} \left(\prod_{i=1}^{3} Z_{i,M_i} \mathcal{D}_{\Delta_i}^{M_i A_i} \right) \mathcal{P}_{A_1 A_2 A_3}^{\Delta_1 \Delta_1 \Delta_3}(P_1, P_2, P_3) , \tag{4.80}$$

$$\mathcal{P}_{A_1 A_2 A_3}^{\Delta_1 \Delta_1 \Delta_3}(P_1, P_2, P_3) = \int_{\mathrm{AdS}} dX \left[\eta_{A_2, A_3}(K_2 - K_3)_{A_1} + \mathrm{cyclic}(1, 2, 3) \right] \prod_{i=1}^{3} \frac{\mathcal{N}_{\Delta_i, 1}}{(-2P_i \cdot X)^{\Delta_i}} .$$

It is straightforward to recognize the remaining bulk integrals as three-point D-functions. See

appendix C.2 and Ref. [49] for general definitions and properties of D-functions. Unlike their four-point counterparts that will appear in the next section, embedding space isometries (or, equivalently, AdS isometries) completely fixes their dependence on the boundary points, leaving only the overall numerical factor to be determined.

Accounting for the bulk point dependence in the vectors K_{i,A_j}, the tensor $P_{A_1 A_2 A_3}$ in eq. (4.80) evaluates to

$$
\begin{aligned}
\mathcal{P}^{\Delta_1 \Delta_1 \Delta_3}_{A_1 A_2 A_3}(P_1, P_2, P_3) &= 2\left[\prod_{i=1}^{3} \mathcal{N}_{\Delta_i, 1}\right] \eta_{A_2, A_3}\left(\Delta_2 P_{2, A_1} D_{\Delta_1, \Delta_2+1, \Delta_3} - \Delta_3 P_{3, A_1} D_{\Delta_1, \Delta_2, \Delta_3+1}\right) \\
&\quad + \text{cyclic}(1, 2, 3) \\
&= \pi^{d/2}\left[\prod_{i=1}^{3} \frac{\mathcal{N}_{\Delta_i, 1}}{\Gamma(\Delta_i)}\right]\left[\eta_{A_2 A_3}\left(\frac{P_{2, A_1} P_{13}}{\delta_{13} - \frac{1}{2}} - \frac{P_{3, A_1} P_{12}}{\delta_{12} - \frac{1}{2}}\right) + \text{cyclic}(1, 2, 3)\right] \\
&\quad \times \Gamma\left(\frac{\Delta_1 + \Delta_2 + \Delta_3 - d + 1}{2}\right) \text{PT}(1_{\Delta_1}, 2_{\Delta_2}, 3_{\Delta_3}),
\end{aligned}
\tag{4.81}
$$

where δ_{ij} is defined as

$$
\delta_{ij} = \frac{\Delta_i + \Delta_j - \Delta_k}{2}
\tag{4.82}
$$

for $\{i, j, k\}$ being a permutation of $\{1, 2, 3\}$. We also define for convenience the "Parke-Taylor factor" as

$$
\text{PT}(1_{\Delta_1}, 2_{\Delta_2}, 3_{\Delta_3}) = \frac{\Gamma(\delta_{12} + \frac{1}{2})\Gamma(\delta_{23} + \frac{1}{2})\Gamma(\delta_{13} + \frac{1}{2})}{P_{12}^{\delta_{12} + \frac{1}{2}} P_{23}^{\delta_{23} + \frac{1}{2}} P_{13}^{\delta_{13} + \frac{1}{2}}}.
\tag{4.83}
$$

One may verify that the resulting three-point correlator is both transverse and obeys the conformal Ward identity,

$$
\mathcal{A}^{a_1 a_2 a_3}_{\Delta_1 \Delta_2 \Delta_3}\Big|_{Z_i \to P_i} = 0, \qquad \sum_{i=1}^{3} D_i^{AB} \mathcal{A}^{a_1 a_2 a_3}_{\Delta_1 \Delta_2 \Delta_3} = 0.
\tag{4.84}
$$

The former relation may be understood as a consequence of the manifest transversality of the bulk-boundary vector field propagator while the latter implies that the formalism manifestly preserves conformal invariance and together they imply that the three-point function can be pulled back from the embedding space to AdS [209, 214].

The correlator does not obey the current conservation for generic Δ_i. This is, of course, to be expected as boundary current conservation is a reflection of a bulk gauge symmetry for the vector fields, which fixes $\Delta = d - 1$ for spin-1 fields. Other "massive" vector fields may be interpreted as higher Kaluza-Klein modes and, while corresponding to BPS currents in a supersymmetric

holographic framework, do not exhibit gauge invariance.

The on-shell correlator follows from eqs. (4.81) and (4.80) with $\Delta_i = d - 1$. It can be put in a compact form in terms of the $V_{i,jk}$ and H_{ij} functions introduced in Ref. [209]:

$$V_{i,jk} = \frac{(P_j \cdot Z_i)(P_i \cdot P_k) - (P_k \cdot Z_i)(P_i \cdot P_j)}{P_j \cdot P_k} ,$$

$$H_{ij} = -2\big[(Z_i \cdot Z_j)(P_i \cdot P_j) - (Z_i \cdot P_j)(Z_j \cdot P_i)\big] . \tag{4.85}$$

With the notation $V_1 \equiv V_{1,23}$, $V_2 \equiv V_{2,31}$ and $V_3 \equiv V_{3,12}$, the full YM AdS boundary correlator becomes

$$\mathcal{A}_3^{a_1 a_2 a_3} = -f^{a_1 a_2 a_3} \frac{d\,\Gamma(d-2)}{8\pi^d(d-2)} \frac{N_3}{(P_{12}P_{23}P_{13})^{d/2}} , \tag{4.86}$$

where

$$N_3 = (4\Lambda_1 - V_1 V_2 V_3) - \frac{6}{d}\Lambda_1 \tag{4.87}$$

$$\Lambda_1 = V_1 V_2 V_3 + \frac{1}{2}(V_1 H_{23} + \text{cyclic}) \tag{4.88}$$

This form reproduces the result of Ref. [230]. In section 4.5 we will use this form of the correlator and the analogous one corresponding to massive vectors.

In addition to the position space representation, we also construct a differential representation of the off-shell three-point correlator. Its existence is a nontrivial indication for our conjecture that on-shell YM correlators can be written in the form of eq. (4.64). With the definitions

$$\mathcal{E}_i^{AB} = P_i^A Z_i^B - P_i^B Z_i^A , \tag{4.89}$$

the differential form of $\mathcal{A}_{\Delta_1 \Delta_2 \Delta_3}^{a_1 a_2 a_3}$ is

$$\mathcal{A}_{\Delta_1 \Delta_2 \Delta_3}^{a_1 a_2 a_3} = \frac{f^{a_1 a_2 a_3}\Gamma\left(\frac{\Delta_1 + \Delta_2 + \Delta_3 - d + 1}{2}\right)}{16\pi^d \prod_{i=1}^3 \left[\Gamma(\Delta_i - \frac{d}{2} + 1)(\Delta_i - 1)\right]} \hat{A}_{\Delta_1 \Delta_2 \Delta_3} \text{PT}(1_{\Delta_1}, 2_{\Delta_2}, 3_{\Delta_3}) , \tag{4.90a}$$

$$\hat{A}_{\Delta_1 \Delta_2 \Delta_3} = \Big[(2\delta_{12} - 1)(\mathcal{E}_1 \cdot \mathcal{E}_2)(\mathcal{E}_3 \cdot D_1) + 2(\Delta_1^2 - 2\Delta_1 \Delta_2 + 2\Delta_1 - 1)\text{Tr}(\mathcal{E}_1 \mathcal{E}_2 \mathcal{E}_3)$$

$$+ \text{cyclic}(1, 2, 3)\Big] , \tag{4.90b}$$

where the dot products are defined in the sense of eq. (4.9). In the massless limit $\Delta_i = d - 1$, the

differential representation becomes

$$\mathcal{A}_3^{a_1 a_2 a_3} = f^{a_1 a_2 a_3} \frac{\Gamma(d-2)}{16\pi^d (d-2)^2} \hat{A}_3 \frac{1}{P_{12}^{d/2} P_{23}^{d/2} P_{13}^{d/2}} \,, \tag{4.91a}$$

$$\hat{A}_3 = (d-2)\Big[(\mathcal{E}_1 \cdot \mathcal{E}_2)(\mathcal{E}_3 \cdot D_1) + \text{cyclic}(1,2,3)\Big] - 6(d-2)^2 \text{Tr}(\mathcal{E}_1 \mathcal{E}_2 \mathcal{E}_3) \,. \tag{4.91b}$$

This reproduces the result of Ref. [198]. As assumed in section 4.4, this expression has uniform scaling dimension -1 for each external state.

We note that the factor $\mathcal{E}$ defined in eq. (4.89) may be identified with the numerator of the bulk-boundary propagator for the linearized vector field strength; it is curious that, unlike in flat space, it is natural to organize the three-point YM correlator in terms of this tensor. We moreover note that the contribution of a $\text{Tr}[F^3]$ interaction to the AdS boundary correlator involves the same kinematic terms as the YM expression, just with different numeric coefficients. We will return to this observation in section 4.5.1.

Notably, the off-shell differential correlator in eq. (4.90) depends explicitly on the conformal weight Δ_i of external states, in sharp contrast to the differential form of the NLSM four-point correlator. In particular, it signals that certain manipulations used in the construction of the six- and possibly higher-point NLSM correlators may not have a direct counterpart in AdS YM calculations. For example, one could have derived the results in section **??** using the split representation and how the differential represention of the NLSM four-point correlator is unchanged off-shell. This computation does not generalize to YM since the YM differential representation is not independent of Δ_i. Instead, we must directly compute the correlator as a polynomial in P_i, Z_i, and D-functions.

4.4.5.2 The four-point correlator

We now describe a direct evaluation of the four-point on-shell YM correlator and verify that it satisfies the BCJ relations discussed in section 4.4.4. We follow the computation in Ref. [228] and extend it to obtain an explicit polynomial of boundary coordinates P_i, polarization vectors Z_i and D-functions [49]. There are two topologies of diagrams that contribute – the exchange graphs and the contact diagram – and the color-dressed correlator has the general form

$$\mathcal{A}_4^{a_1 a_2 a_3 a_4} = \mathcal{A}_{\text{contact}}^{a_1 a_2 a_3 a_4} + \mathcal{A}_s^{a_1 a_2 a_3 a_4} + \mathcal{A}_t^{a_1 a_2 a_3 a_4} + \mathcal{A}_u^{a_1 a_2 a_3 a_4} \tag{4.92}$$

$$= \mathcal{A}_{\text{contact}}^{a_1 a_2 a_3 a_4} + \mathcal{A}_s^{a_1 a_2 a_3 a_4} + \Big(\mathcal{A}_s^{a_1 a_2 a_3 a_4}\big|_{1\to2\to3\to1}\Big) + \Big(\mathcal{A}_s^{a_1 a_2 a_3 a_4}\big|_{1\to3\to2\to1}\Big) \,,$$

where on the second line we used the symmetry properties of Witten diagrams.

We start with the contribution from the four-point contact diagram, which can be read-off from

the four-field term in YM Lagrangian (4.31),

$$\mathcal{A}_{\text{contact}}^{a_1 a_2 a_3 a_4} = \left(\underset{1}{\overset{2}{\bigtimes}}\,\underset{4}{\overset{3}{}}\right) = \int_{\text{AdS}} dX\, \mathcal{I}_{A_1 A_2 A_3 A_4}^{a_1 a_2 a_3 a_4} \left[\prod_{j=1}^{4} Z_{i,M_i} E_{d-1}^{M_i A_i} \right], \qquad (4.93)$$

$$\mathcal{I}_{A_1 A_2 A_3 A_4}^{a_1 a_2 a_3 a_4} = g^2 f^{a_1 a_2 x} f^{a_3 a_4 x} (\eta_{A_1 A_3} \eta_{A_2 A_4} - \eta_{A_1 A_4} \eta_{A_2 A_3}) + \text{cyclic}(2,3,4)\,. \qquad (4.94)$$

Using the expression for the vector bulk-boundary propagator $E_{\Delta}^{M_1,A_1}$ in eq. (4.26) and the definition of the D-function in eq. (C.21), it is straightforward to obtain:

$$\mathcal{A}_{\text{contact}}^{a_1 a_2 a_3 a_4} = g^2 \left[\frac{(d-1)\Gamma(d-1)}{2\pi^{d/2}(d-2)\Gamma(d/2)} \right]^4 \mathcal{I}_{A_1 A_2 A_3 A_4}^{a_1 a_2 a_3 a_4} \left[\prod_{i=1}^{4} Z_{i,M_i} \mathcal{D}_{d-1}^{M_i A_i} \right] D_{d-1,d-1,d-1,d-1}\,. \qquad (4.95)$$

Acting with the derivatives in $\mathcal{D}_{d-1}^{M_i,A_i}$ generates a significant number of terms, which can be expressed in terms of D-functions with shifted indices using the identities in appendix C.2.

We now turn to the evaluation of the s-channel exchange diagram. We use the split representation of the the bulk-bulk propagator (4.28) to write the exchange graph as a product of two partly off-shell three-point correlators integrated over a boundary point Q and over the dimension/mass of the field corresponding to that point. The three-point correlators are written in Mellin space; this makes the integral over the boundary point straightforward and converts the product of three-point correlators to a Mellin-space four-point correlator. After the integral over the dimension of the intermediate field is evaluated, an inverse Mellin transform yields the desired position-space correlator. Although the computation strategy may appear somewhat convoluted compared to direct integration in the bulk points, it ultimately allows us to write the four-point correlator as an explicit polynomial of P_i, Z_i, and D-functions. Furthermore, the above computation strategy can be systematically generalized to n-point correlators at tree level [214, 228].[10]

Proceeding to the actual computation and using eq. (4.27), the s-channel contribution to the correlator written in terms of the pre-correlator is

$$\mathcal{A}_{s}^{a_1 a_2 a_3 a_4} = \left(\underset{1}{\overset{2}{}}\,\underset{4}{\overset{3}{}}\right) = g^2 f^{a_1 a_2 x} f^{a_3 a_4 x} \left[\prod_{i=1}^{4} Z_{i,M_i} \mathcal{D}_{d-1}^{M_i A_i} \right] \mathcal{P}_{A_1 A_2 A_3 A_4}^{s}\,, \qquad (4.96)$$

---

[10]As we will see, the main difficulty in going to higher order is explicitly evaluating the contour integrals that appear due to using the split representation. For example, at four-points, the only non-trivial integral that appears is eq. (4.109). However, one can show that the c-contours that appear are always equivalent to the c-contour integrals that appear in evaluating scalar correlators. Such scalar correlators in AdS are trivial to calculate using Mellin space Feynman rules [213]. Therefore, although technically more challenging than flat space, one can algorithmically calculate tree-level YM correlators in AdS in terms of Z_i, P_i and D-functions at n-point without evaluating any integrals.

where $\mathcal{P}_{A_1 A_2 A_3 A_4}$ is an integral over the locations of the two three-point vertices. The split representation of the massless spin-1 propagator in eq. (4.27) expresses it as an integral of the product of two off-shell three-point pre-correlators in eq. (4.81):

$$\mathcal{P}^s_{A_1 A_2 A_3 A_4} = \int_{-i\infty}^{i\infty} \frac{dc}{2\pi i} \frac{-2c^2}{c^2 - (d/2 - 1)^2} \tag{4.97}$$
$$\times \int_{\partial\text{AdS}} dQ \, \eta_{NM} \left[\mathcal{D}^{NA_Q}_{d/2+c} \mathcal{P}^{d-1\,d-1\,d/2+c}_{A_1 A_2 A_Q}(P_1, P_2, Q) \right] \left[\mathcal{D}^{MB_Q}_{d/2-c} \mathcal{P}^{d-1\,d-1\,d/2-c}_{A_3 A_4 B_Q}(P_3, P_4, Q) \right] .$$

The derivatives of the three-point pre-correlators are obtained by simply evaluating the derivatives with respect to an off-shell leg in eq. (4.81),

$$\mathcal{D}^{NA_Q}_{d/2+c} \mathcal{P}^{d-1\,d-1\,d/2+c}_{A_1 A_2 A_Q} = \frac{\left(\frac{d-1}{d-2}\right)^2 \Gamma\left(\frac{3d/2+c-1}{2}\right)}{4\pi^d (d/2 + c - 1)\Gamma(d/2)^2 \Gamma(1+c)} \text{PT}(1_{d-1}, 2_{d-1}, Q_{d/2+c})$$
$$\times \left[(\eta^{A_1 A_2} P_1^N - 2\eta^{A_1 N} P_1^{A_2}) P_{2Q} - (\eta^{A_1 A_2} P_2^N - 2\eta^{A_2 N} P_2^{A_1}) P_{1Q} \right] + (\dots) , \tag{4.98}$$

where $P_{iQ} = -2P_i \cdot Q$ and similarly for $\mathcal{D}^{NA_Q}_{d/2-c} \mathcal{P}^{d-1\,d-1\,d/2-c}_{A_3, A_4, A_Q}$. The terms in $(\dots)$ will vanish when the leg P_1 and P_2 are taken on-shell. More specifically, they are removed as the result of the identity [228]

$$\mathcal{D}^{MA}_\Delta \frac{\partial}{\partial P_A} \mathcal{F}_{\Delta-1}(P) = 0 , \tag{4.99}$$

where $\mathcal{F}_{\Delta-1}(P)$ is any function of weight $\Delta - 1$ in P. Thus in the following we will neglect the $(\dots)$ terms in eq. (4.98).

The two terms on the second line of eq. (4.98) are related by the interchange of labels 1 and 2; the terms in the analogous factor in $\mathcal{D}^{NA_Q}_{d/2-c} \mathcal{P}^{d-1\,d-1\,d/2-c}_{A_3, A_4, A_Q}$ are related by the interchange of labels 3 and 4. Thus, replacing these expressions in eq. (4.97) yields four terms, three of which can be obtained from the fourth through the transformations $1 \leftrightarrow 2$, $3 \leftrightarrow 4$ and $(1, 3) \leftrightarrow (2, 4)$. It is not difficult to find that

$$\int_{\partial\text{AdS}} dQ \, \eta_{NM} \mathcal{D}^{NA_Q}_{d/2+c} P^{d-1\,d-1\,d/2+c}_{A_1 A_2 A_Q} \mathcal{D}^{MB_Q}_{d/2-c} P^{d-1\,d-1\,d/2-c}_{A_3 A_4 B_Q} = \frac{\Gamma\left(\frac{3d/2+c-1}{2}\right)^2 \Gamma\left(\frac{3d/2-c-1}{2}\right)^2}{64\pi^{2d}\Gamma(d/2)^4 \Gamma(1+c)\Gamma(1-c)}$$
$$\times \left(\frac{d-1}{d-2}\right)^4 \left[\frac{P_{13}\, \mathcal{K}^{(P_1 P_2 P_3 P_4)}_{A_1 A_2 A_3 A_4}}{P_{12}^{\frac{3d/2-c-1}{2}} P_{34}^{\frac{3d/2+c-1}{2}}} I\left(\begin{smallmatrix} P_1 & P_2 & P_3 & P_4 \\ \tilde{\Delta}_1 & \tilde{\Delta}_2 & \tilde{\Delta}_3 & \tilde{\Delta}_4 \end{smallmatrix}\right) - \frac{P_{23}\, \mathcal{K}^{(P_2 P_1 P_3 P_4)}_{A_2 A_1 A_3 A_4}}{P_{12}^{\frac{3d/2-c-1}{2}} P_{34}^{\frac{3d/2+c-1}{2}}} I\left(\begin{smallmatrix} P_1 & P_2 & P_3 & P_4 \\ \tilde{\Delta}_2 & \tilde{\Delta}_1 & \tilde{\Delta}_3 & \tilde{\Delta}_4 \end{smallmatrix}\right) \right.$$
$$\left. - \frac{P_{14}\, \mathcal{K}^{(P_1 P_2 P_4 P_3)}_{A_1 A_2 A_4 A_3}}{P_{12}^{\frac{3d/2-c-1}{2}} P_{34}^{\frac{3d/2+c-1}{2}}} I\left(\begin{smallmatrix} P_1 & P_2 & P_3 & P_4 \\ \tilde{\Delta}_1 & \tilde{\Delta}_2 & \tilde{\Delta}_4 & \tilde{\Delta}_3 \end{smallmatrix}\right) + \frac{P_{24}\, \mathcal{K}^{(P_2 P_1 P_4 P_3)}_{A_2 A_1 A_4 A_3}}{P_{12}^{\frac{3d/2-c-1}{2}} P_{34}^{\frac{3d/2+c-1}{2}}} I\left(\begin{smallmatrix} P_1 & P_2 & P_3 & P_4 \\ \tilde{\Delta}_2 & \tilde{\Delta}_1 & \tilde{\Delta}_4 & \tilde{\Delta}_3 \end{smallmatrix}\right) \right], \tag{4.100}$$

where $\mathcal{K}$ and $\tilde{\Delta}_i$ are defined as

$$\mathcal{K}^{(P_1 P_2 P_3 P_4)}_{A_1 A_2 A_3 A_4} = \frac{(\eta_{A_1 A_2} P_1^N - 2\delta^N_{A_1} P_{1,A_2})(\eta_{A_3 A_4} P_{3,N} - 2\eta_{A_3 N} P_{3,A_4})}{P_{13}}, \tag{4.101}$$

$$\tilde{\Delta}_1 = \frac{d/2+c+1}{2}, \quad \tilde{\Delta}_2 = \frac{d/2+c-1}{2}, \quad \tilde{\Delta}_3 = \frac{d/2-c+1}{2}, \quad \tilde{\Delta}_4 = \frac{d/2-c-1}{2}. \tag{4.102}$$

Importantly, $\tilde{\Delta}_i$ satisfy the relation $\sum_{i=1}^{4} \tilde{\Delta}_i = d$. The function $I\left(\begin{smallmatrix} P_1 & P_2 & P_3 & P_4 \\ \tilde{\Delta}_1 & \tilde{\Delta}_2 & \tilde{\Delta}_3 & \tilde{\Delta}_4 \end{smallmatrix}\right)$ is the result of converting a certain four-point contact integral over the boundary to its Mellin representation [228],

$$I\left(\begin{smallmatrix} P_1 & P_2 & P_3 & P_4 \\ \tilde{\Delta}_1 & \tilde{\Delta}_2 & \tilde{\Delta}_3 & \tilde{\Delta}_4 \end{smallmatrix}\right) = \int_{\partial \text{AdS}} dQ \prod_{i=1}^{4} \frac{\Gamma(\tilde{\Delta}_i)}{(-2P_i \cdot Q)^{\tilde{\Delta}_i}} \qquad \left(\text{under the constraint } \sum_{i=1}^{4} \tilde{\Delta}_i = d\right)$$

$$= \pi^{d/2} \int_{-i\infty}^{i\infty} \left[\prod_{1 \leqslant i < j} \frac{d\tilde{\delta}_{ij}}{2\pi i} \Gamma(\tilde{\delta}_{ij}) P_{ij}^{-\tilde{\delta}_{ij}} \right] \left[\prod_{k=1}^{4} \delta\left(\tilde{\Delta}_k - \sum_{l=1, l\neq k}^{4} \tilde{\delta}_{lk}\right) \right], \tag{4.103}$$

where we also assume that the integration variable $\tilde{\delta}_{ij}$ is symmetric in its indices. We note that the four integrals entering eq. (4.100) differ by interchange of $\tilde{\Delta}_i$ with fixed ordering of P_i. Thus, they are different even though $I\left(\begin{smallmatrix} P_1 & P_2 & P_3 & P_4 \\ \tilde{\Delta}_1 & \tilde{\Delta}_2 & \tilde{\Delta}_3 & \tilde{\Delta}_4 \end{smallmatrix}\right)$ is invariant under the interchange of *pairs* $(P_i, \tilde{\Delta}_i)$.

Now that we have converted the integral over the boundary point insertion into Mellin form, we can proceed and perform the contour integral over c. We start with the change of variables,

$$\delta_{12} = \tilde{\delta}_{12} + \frac{3d/2 - c - 1}{2}, \qquad \delta_{34} = \tilde{\delta}_{34} + \frac{3d/2 + c - 1}{2}, \tag{4.104}$$

$$\delta_{13} = \tilde{\delta}_{13} - 1, \qquad \delta_{ij} = \tilde{\delta}_{ij} \quad \text{for all others},$$

for the integral $I_{\tilde{\Delta}_1 \tilde{\Delta}_2 \tilde{\Delta}_3 \tilde{\Delta}_4}$ given in eq. (4.103), together with its images under the specified permutation maps for the other three terms in the sum of eq. (4.100), to align the constraints on the Mellin integration variables, which now become

$$\prod_{k=1}^{4} \delta\left(\tilde{\Delta}_k - \sum_{l=1,, l\neq k}^{4} \tilde{\delta}_{lk}\right) \rightarrow \prod_{k=1}^{4} \delta\left(d - 1 - \sum_{l=1,, l\neq k}^{4} \delta_{lk}\right) \tag{4.105}$$

in all four terms in eq. (4.100). The pre-correlator then has the rather compact expression:

$$\mathcal{P}^s_{A_1 A_2 A_3 A_4} = -\frac{\left(\frac{d-1}{d-2}\right)^4}{32\pi^{3d/2}\Gamma(d/2)^4} \int_{-i\infty}^{i\infty} \left[\prod_{1 \leqslant i < j} \frac{d\delta_{ij}}{2\pi i} \frac{\Gamma(\delta_{ij})}{P_{ij}^{\delta_{ij}}} \right] \left[\prod_{k=1}^{4} \delta\left(d-1- \sum_{l=1, l\neq k}^{4} \delta_{lk}\right) \right] \tag{4.106}$$

$$\times \int_{-i\infty}^{i\infty} \frac{dc}{2\pi i} S(\delta_{12}, c) \left[\mathcal{K}_{A_1 A_2 A_3 A_4} \delta_{13} - (1 \leftrightarrow 2) - (3 \leftrightarrow 4) + \left(\begin{smallmatrix} 1 \leftrightarrow 2 \\ 3 \leftrightarrow 4 \end{smallmatrix}\right) \right],$$

where the permutation map acts on P_i, A_i and the indices of δ_{ij}. For example, under the permutation $1 \leftrightarrow 2$ we exchange $P_1 \leftrightarrow P_2$, $A_1 \leftrightarrow A_2$, $\delta_{13} \leftrightarrow \delta_{23}$ and $\delta_{14} \leftrightarrow \delta_{24}$. The entire c dependence is contained in the function $S(\delta_{12}, c)$,

$$S(\delta_{12}, c) = \left.\frac{l(\delta_{12}, c)l(\delta_{12}, -c)}{(d/2 - 1)^2 - c^2}\right|_{\Delta_{12} = \Delta_{34} = 2d-1}, \tag{4.107}$$

where $l(\delta_{12}, c)$ with generic $\Delta_{12} = \Delta_1 + \Delta_2$ and $\Delta_{34} = \Delta_3 + \Delta_4$ is given by

$$l(\delta_{12}, c) = \frac{\Gamma\left(\delta_{12} - \frac{\Delta_{12} - c - d/2}{2}\right)\Gamma\left(\frac{\Delta_{12} + c - d/2}{2}\right)\Gamma\left(\frac{\Delta_{34} + c - d/2}{2}\right)}{\Gamma(\delta_{12})\Gamma(c)}. \tag{4.108}$$

Choosing the contour such that nonphysical poles do not contribute, the c integral in eq. (4.106) yields

$$\int_{-i\infty}^{i\infty} \frac{dc}{2\pi i} \frac{l(\delta_{12}, c)l(\delta_{12}, -c)}{(d/2 - 1)^2 - c^2} = \Gamma\left(\frac{\Delta_{12} + \Delta_{34} - d}{2}\right) \sum_{l=1}^{m} \frac{\left(\frac{\sum_i \Delta_i - d}{2}\right)_{-l}(\delta_{12})_{-l}}{\left(\frac{\Delta_{12} - d + 1}{2}\right)_{1-l}\left(\frac{\Delta_{12} - 1}{2}\right)_{1-l}}$$

$$= \frac{2\Gamma\left(\frac{\Delta_{12} + \Delta_{34} - d}{2}\right){}_3F_2\left(1, \frac{3 - \Delta_{12}}{2}, \frac{d + 1 - \Delta_{12}}{2}; 2 - \delta_{12}, \frac{d - \Delta_{12} - \Delta_{34} + 4}{2}; 1\right)}{(\delta_{12} - 1)(\Delta_{12} + \Delta_{34} - d - 2)}, \tag{4.109}$$

where $m = \frac{1}{2}(\Delta_{12} - d + 1)$ and $(a)_n$ is the Pochhammer symbol [45, 231]. Although the expression in the second line is derived assuming m is a positive integer, it holds for more generic parameters as a result of analytic continuation.[11] For $d = 4$, we find that

$$\left.\int_{-i\infty}^{i\infty} \frac{dc}{2\pi i} S(\delta_{12}, c)\right|_{d=4} = 12\left[\frac{\Gamma(\delta_{12} - 2)}{3\Gamma(\delta_{12})} + \frac{\Gamma(\delta_{12} - 1)}{2\Gamma(\delta_{12})}\right] = \frac{4}{\delta_{12} - 2} + \frac{2}{\delta_{12} - 1}. \tag{4.110}$$

As we have evaluated the c integral, we are left with the evaluation of the Mellin integrals in eq. (4.106). They can be converted into D-functions using the identity

$$\mathbf{M}^{-1}\left[\prod_{1 \leq i < j}^{4} \frac{\Gamma(\delta_{ij} + l_{ij})}{\Gamma(\delta_{ij})}\right] = \frac{2}{\pi^{d/2}} \frac{\prod_{i=1}^{4}\Gamma(\tilde{\Delta}_i)}{\Gamma\left(\frac{\tilde{\Sigma} - d}{2}\right)}\left[\prod_{1 \leq i < j}^{4} P_{ij}^{l_{ij}}\right] D_{\tilde{\Delta}_1 \tilde{\Delta}_2 \tilde{\Delta}_3 \tilde{\Delta}_4}, \tag{4.111}$$

$$\tilde{\Delta}_i = \Delta_i + \sum_{j=1, j \neq i}^{4} l_{ij}, \qquad \tilde{\Sigma} = \sum_{i=1}^{4} \tilde{\Delta}_i, \quad .$$

---

[11]To arrive at the right-hand side of eq. (4.109), a specific choice of contour for the c integral is required, which is the same one made in eq. (133) of [45].

Here $\mathbf{M}^{-1}$ denotes the inverse Mellin transform,

$$\mathbf{M}^{-1}\Big[f(\delta_{ij})\Big] = \int_{-i\infty}^{i\infty} \left[\prod_{1\leqslant i<j}^{4} \frac{d\delta_{ij}}{2\pi i} \frac{\Gamma(\delta_{ij})}{P_{ij}^{\delta_{ij}}} \right] \left[\prod_{k=1}^{4} \delta\Big(\Delta_k - \sum_{l=1}^{4} \delta_{lk}\Big) \right] f(\delta_{ij}) \,. \tag{4.112}$$

To derive eq. (4.111), it suffices to consider the inverse Mellin transform of

$$\frac{\Gamma(\delta_{12} + l)}{\Gamma(\delta_{12})} \,. \tag{4.113}$$

We first parameterize the delta functions in the inverse Mellin transform (4.112)

$$\delta\Big(\Delta_i - \sum_j \delta_{ij}\Big) = \int_0^\infty \frac{dt_i}{t_i} t_i^{\Delta_i - \sum_j \delta_{ij}} \tag{4.114}$$

and then evaluate the δ_{ij} contour integral using

$$\int_{-i\infty}^{i\infty} \frac{d\delta_{ij}}{2\pi i} \Gamma(\delta_{ij} + l)(t_i t_j P_{ij})^{-\delta_{ij}} = (t_i t_j P_{ij})^l e^{-t_i t_j P_{ij}} \,. \tag{4.115}$$

This leads to

$$\mathbf{M}^{-1}\left[\frac{\Gamma(\delta_{12} + l)}{\Gamma(\delta_{12})} \right] = (P_{12})^l \int_0^\infty \left[\prod_{i=1}^{4} \frac{dt_i}{t_i} \right] t_1^{\Delta_1 + l} t_2^{\Delta_2 + l} t_3^{\Delta_3} t_4^{\Delta_4} \prod_{i<j} e^{-t_i t_j P_{ij}} \,. \tag{4.116}$$

To convert this expression to a D-function, we first insert the identity element

$$\begin{aligned}
1 = &\frac{1}{\Gamma[(\Delta_1 + l)/2 + (\Delta_2 + l)/2 + \Delta_3/2 + \Delta_4/2 - d/2]} \\
&\times \int_0^\infty \frac{dz}{z} z^{-d/2 + (\Delta_1 + l)/2 + (\Delta_2 + l)/2 + \Delta_3/2 + \Delta_4/2} e^{-z}
\end{aligned} \tag{4.117}$$

and then rescale $t_i \to t_i'/\sqrt{z}$. Now we can carry out the z integral as

$$\frac{\pi^{d/2}}{2} \int_0^\infty \frac{dz}{z} z^{-d/2} \exp\left[-z + \frac{1}{z}\Big(\sum_i t_i' P_i\Big)^2 \right] = \int_{\text{AdS}} dX \prod_i e^{2t_i' X \cdot P_i} \,. \tag{4.118}$$

Finally, we perform the t_i' integral as

$$\int_0^\infty \frac{dt_i'}{t_i'} (t_i')^{\Delta_i'} e^{t'(2X \cdot P_i)} = \frac{\Gamma(\Delta_i')}{(-2X \cdot P_i)^{\Delta_i'}} \tag{4.119}$$

to reach our desired result

$$\mathbf{M}^{-1}\left[\frac{\Gamma(\delta_{12}+l)}{\Gamma(\delta_{12})}\right] = \frac{2}{\pi^{d/2}}P_{1,2}^l\frac{\Gamma(\Delta_1+l)\Gamma(\Delta_2+l)\Gamma(\Delta_3)\Gamma(\Delta_4)D_{\Delta_1+l_1,\Delta_2+l_2,\Delta_3,\Delta_4}}{\Gamma[(\Delta_1+l)/2+(\Delta_2+l)/2+\Delta_3/2+\Delta_4/2-d/2]}. \tag{4.120}$$

It is trivial to see that eq. (4.120) generalizes to eq. (4.111).

Specialized to $d = 4$, eqs. (4.110) and (4.111) together can bring the pre-correlator in eq. (4.106) to a linear combination of D-functions weighted by polynomial of P_i, Z_i. An expression valid for generic boundary dimension d can be obtained by using eq. (4.111) together with the sum representation [45] of eq. (4.109). In the following, we focus on $d = 4$. The pre-correlator is given by

$$\mathcal{P}^{\mathrm{s}}_{A_1A_2A_3A_4}\Big|_{d=4} = -\frac{243}{32\pi^8}\left[\frac{P_{13}\mathcal{R}_{A_1A_2A_3A_4}}{P_{12}}D_{3,2,4,3} - \frac{P_{14}\mathcal{R}^{(3\leftrightarrow4)}_{A_1A_2A_3A_4}}{P_{12}}D_{3,2,3,4}\right.$$
$$\left. + \frac{P_{13}\mathcal{R}_{A_1A_2A_3A_4}}{P_{12}^2}D_{2,1,4,3} - \frac{P_{14}\mathcal{R}^{(3\leftrightarrow4)}_{A_1A_2A_3A_4}}{P_{12}^2}D_{2,1,3,4}\right], \tag{4.121}$$

where

$$\mathcal{R}_{A_1A_2A_3A_4} = \mathcal{K}_{A_1A_2A_3A_4} + \begin{pmatrix} 1\leftrightarrow2 \\ 3\leftrightarrow4 \end{pmatrix}, \qquad \mathcal{R}^{(3\leftrightarrow4)}_{A_1A_2A_3A_4} = \mathcal{R}_{A_1A_2A_3A_4}\Big|_{\substack{P_3\leftrightarrow P_4 \\ A_3\leftrightarrow A_4}}. \tag{4.122}$$

Finally, we apply the $\mathcal{D}$-derivatives in eq. (4.96) and express the result in terms of D-functions by repeated use of the identity

$$\frac{\partial D_{\Delta_1,\Delta_2,\Delta_3,\Delta_4}}{\partial P_{1,A}} = \frac{4\Delta_1}{\sum_{i=1}^4\Delta_i-d}\left(\Delta_2P_2^AD_{\Delta_1+1,\Delta_2+1,\Delta_3,\Delta_4} + \Delta_3P_3^AD_{\Delta_1+1,\Delta_2,\Delta_3+1,\Delta_4}\right.$$
$$\left. + \Delta_4P_4^AD_{\Delta_1+1,\Delta_2,\Delta_3,\Delta_4+1}\right). \tag{4.123}$$

It is then straightforward, albeit tedious, to find an explicit expression for the s-channel correlator $\mathcal{A}_s^{a_1a_2a_3a_4}$ as a linear combination of D-functions, from which the t- and u-channel correlators can subsequently be obtained by the relabelings given in eq. (4.92).

The partial correlators can be extracted from eq. (4.92) in the usual way, either by directly going to a trace basis or by using the Jacobi identity

$$f^{a_1a_4x}f^{a_2a_3x} + f^{a_1a_2x}f^{a_3a_4x} + f^{a_1a_3x}f^{a_4a_2x} = 0, \tag{4.124}$$

to pass to the DDM basis,

$$\mathcal{A}_4^{a_1 a_2 a_3 a_4} = f^{a_1 a_2 x} f^{a_3 a_4 x} A_4(1,2,3,4) + f^{a_1 a_3 x} f^{a_2 a_4 x} A_4(1,3,2,4) \,. \qquad (4.125)$$

We are now in a position to verify that the AdS BCJ relation (4.72),

$$D_{12}^2 A_4(1,2,3,4) = D_{13}^2 A_4(1,3,2,4) \,, \qquad (4.126)$$

is satisfied. The conformal generators D_i^{AB} are defined in eq. (4.9). While it is in principle possible, albeit tedious, to do so analytically through judicious use of the D-function identities in appendix C.2.3, we have verified eq. (4.126) numerically at $d = 4$ at random kinematic points with very high precision. The part of the conformal generator that acts on the polarization vectors Z_i is crucial for the AdS BCJ relations to hold.

The fact that the four-point AdS BCJ relation is satisfied suggests that it may be possible to put the four-point YM AdS boundary correlator in the form put forth in eq. (4.64). Similar to the three-point YM AdS boundary correlator, we expect that the four-point BCJ representation will match the flat space result up to possible additional terms that result from the non-commutativity of factors in the AdS kinematic numerators. Algorithms for efficiently computing such differential representations are left to future investigation.

4.5 Towards a Bosonic Double Copy in AdS Space

In this section, we discuss possible double copy procedures in AdS space. We first analyze a "differential" double copy that is analogous to the celestial double copy in flat space. The differential turns out to yield consistent AdS boundary correlators for $d = 2$, in agreement with expectations based on the $\text{AdS}_3 \times \text{S}_3$ ambitwistor string [50], but issues develop in higher dimensions even at three-points. We then study the double copy in position space and find that the most naive construction holds for three-point correlators only in the limit of large AdS dimension, thus recovering results of Ref. [198]. Finally, we discuss limiting cases in which connections between AdS boundary correlators and flat space amplitudes should expose double-copy structures in momentum and Mellin space.

4.5.1 A Differential Double Copy

In section 4.4 we suggested that the NLSM and YM AdS boundary correlators can be written as sums of differential operators acting on a single contact diagram,

$$\mathcal{A} = \sum_{\text{cubic } g} C(g|\alpha_g) \left(\prod_{I \in g} \frac{1}{D_I^2} \right) \hat{N}(g|\alpha_g) D_{d,d,d,\dots} \,, \tag{4.127}$$

and that, as in flat space, color/kinematics duality identifies the algebraic properties of the color factor with those of the kinematic numerators $\hat{N}$ when acting on the contact diagram. Given such a differential representation, the most natural attempt at an AdS double copy procedure is to simply replace the color factors, $C(g|\alpha_g)$, with their associated kinematic numerators, $\hat{N}(g|\alpha_g)$. However, direct counting of the conformal weight for each external state suggests that certain modifications are necessary. Indeed, for YM theory, we assumed in section 4.127 and explicitly demonstrated in section 4.4.5.1 that the conformal weight of the kinematic numerators $\hat{N}$ with respect to every external state is -1. Combining this with the d conformal weight of $D_{d,d,d,\dots}$ for each of its external points implies that the action of two kinematic numerators leads to a $d-2$ overall conformal weight for each external state of the putative differential double copy. Thus, in addition to replacing the color factors with kinematic numerators, to obtain the requisite conformal weight $\Delta = d$ it is necessary to also increase the conformal weight of each of the external legs of the contact diagram by two units. The full double copy procedure should then amount to the replacements

$$\begin{aligned} C(g|\alpha_g) &\to \hat{N}(g|\alpha_g) \,, \\ D_{d,d,d,\dots} &\to D_{d+2,d+2,d+2,\dots} \,, \end{aligned} \tag{4.128}$$

where $\hat{N}$ here might differ from the one in eq. (4.127) by some operators that annihilate $D_{d,d,d,\dots}$. Remarkably, the ambitwistor string construction of Ref. [50] strongly suggests that spin-2 $\text{AdS}_3 \times S^3$ boundary correlators can be derived by applying the substitution rules in eq. (4.128). Specifically, one would apply eq. (4.128) to the differential representation (4.127) of correlators in a YM-Chern-Simons theory deformed by a specific linear combination of certain higher-dimension operators. The generalization of this double copy procedure from $d = 2$ to arbitrary d turns out to be more subtle than one might naively expect.[12]

To see this, it suffices to consider the differential double copy at three points. We derived the differential form of the three-point AdS YM correlator in section 4.4.5.1. The normalization

---

[12]There are subtleties even in $d = 2$ related to how gravitons do not obey eq. (4.11); the equation of motion for a free graviton in AdS is $(-\frac{1}{2}D_X^2 + 2)h^{AB} = 0$, rather than $D_X^2 h^{AB} = 0$. This implies that the $1/D_I^2$ factors in eq. (4.127) should also be shifted in order to interpret these factors as propagators in the associated Witten diagrams. However, the formulas of Ref. [50] seem to suggest that this shift is not necessary.

of the bulk-boundary vector-field propagator in eq. (4.26) is singular for $d = 2$; so to have a smooth analytic continuation in dimension for the purpose of this discussion, we will change it by removing the offending factor of $(\Delta - 1)^{-1} = (d - 2)^{-1}$. We will also deform the YM theory with the operator $\mathrm{Tr}[F^3]$ with an arbitrary (Wilson) coefficient g_{F^3}.

With these preparations and up to an overall constant which is finite for all positive values of d, the differential form of the YM+$g_{F^3}\mathrm{Tr}[F^3]$ three-point correlator is

$$\hat{N}_3^{g_{F^3}} \propto \left[1 + 6g_{F^3}(d-2)^2\right]\left[(\mathcal{E}_2 \cdot \mathcal{E}_2)(\mathcal{E}_3 \cdot D_1) + \text{cyclic}\right]$$
$$+ 6(d-2)\left[-1 + 2g_{F^3}(d-2)(d+2)\right]\mathrm{Tr}(\mathcal{E}_1\mathcal{E}_2\mathcal{E}_3) \tag{4.129}$$

where $\mathcal{E}$ is defined in eq. (4.89). We note that our $\mathrm{Tr}[F^3]$ contribution is consistent with that in [232] at $d = 3$. The differential double-copy proposal then suggests that the corresponding AdS double-copy boundary correlator is

$$\mathcal{M}_3^{\mathrm{DC}} \propto \hat{N}_3^{g_{F^3}} \hat{N}_3^{g'_{F^3}} D_{d+2,d+2,d+2} , \tag{4.130}$$

with independent g_{F^3} and g'_{F^3} coefficients to allow for a general heterotic double copy [22].

In $d = 2$, the double copy works straightforwardly. This is due to additional linear relations between $V_1V_2V_3$ and Λ_1 in eq. (4.87). Consequently, in $d = 2$ we have

$$\hat{N}_3^{g_{F^3}} D_{2,2,2} \propto \frac{V_1V_2V_3}{P_{12}P_{23}P_{13}} , \qquad \hat{N}_3^{g_{F^3}} \hat{N}_3^{g'_{F^3}} D_{4,4,4} \propto \frac{(V_1V_2V_3)^2}{(P_{12}P_{23}P_{13})^2} . \tag{4.131}$$

It is also easy to check that both expressions in eq. (4.131) satisfy current conservation for $d = 2$ and therefore can be interpreted as an AdS three-graviton correlator. This result is a non-trivial generalization of Ref. [50], which only studied YM-Chern-Simons theory in AdS deformed by a fixed linear combination of higher-dimension operators while here the Wilson coefficient g_{F^3} is arbitrary. In fact, to give nonzero contribution at $d = 2$, it needs to be proportional to $(d - 2)^{-2}$. We see that, just as in flat space, the AdS$_3$ double copy appears to be compatible with pure YM theory deformed by certain higher derivative operators, such as $\mathrm{Tr}[F^3]$, with arbitrary Wilson coefficients [166].

For $d > 2$, the current conservation of $\mathcal{M}_3^{\mathrm{DC}}$ requires g_{F^3} to take specific values. If we follow eq. (4.130), there are only two solutions,

$$g_{F^3} = -\frac{1}{6(d-2)^2} , \qquad g'_{F^3} = \frac{d}{6(d-2)^2(3d-4)} ;$$
$$g_{F^3} = \frac{2d-3}{6(d-2)^2} , \qquad g'_{F^3} = -\frac{1}{6(d-2)^2} . \tag{4.132}$$

which impose that one of the $\hat{N}_3^{g_{F3}}$ is proportional to $\mathrm{Tr}(\mathcal{E}_1\mathcal{E}_2\mathcal{E}_3)$. The resultant gravity correlator is a linear combination of the Einstein-Hilbert term and certain higher derivatives operators. Moreover, we can modify eq. (4.130) to make it symmetric with respect to g_{F3} and g'_{F3}, $\mathcal{M}_3^{\mathrm{DC}} \propto (\hat{N}_3^{g_{F3}}\hat{N}_3^{g'_{F3}} + \hat{N}_3^{g'_{F3}}\hat{N}_3^{g_{F3}})D_{d+2,d+2,d+2}$. Then the current conservation leads to a unique solution with $g_{F3} = -\frac{1}{6(d-2)^2}$ and $g'_{F3} = \frac{5d-6}{6(d-2)^2(3d-2)}$.

We have seen that to realize the AdS double-copy construction requires certain generalizations of the flat space case. A possible approach to understanding it may be higher-dimensional generalizations of the ambitwistor string theory of Ref. [50]. Possible obstacles relate to the stringy realization of the massless spectrum in $\mathrm{AdS}_5 \times S^5$, see refs. [233, 234]. In flat space, the interplay between gauge invariance and color/kinematics duality guarantees that the result of the double copy exhibits diffeomorphism invariance. Thus, an alternative approach could rely on a thorough exploration of the analogous interplay for AdS boundary correlators.

4.5.2 Position-Space Three-Point Double Copy and Comments on Mellin-Space Double Copy

Recent results suggest that the differential double copy (4.128) may not be the only double copy procedure applicable to AdS boundary correlators. To gain some insight into the possible structure of alternative double copy relations between gauge and gravity theories in AdS space, it is useful to examine the simple example of the three-point AdS boundary correlator in position space. A supersymmetric version of the Mellin-space double copy was given at 4-points in Ref. [190].

Using the three-point Feynman rule following from the Einstein-Hilbert action in AdS space (with cosmological constant $\Lambda = -d(d-1)/2$) and following the same computational strategy as for the YM AdS boundary correlator, we found that the three-graviton AdS boundary correlator is

$$\mathcal{M}_3 = \frac{d^2\,\Gamma(d)}{16\pi^d(d+1)^3} \frac{M_3}{(P_{12}P_{13}P_{23})^{1+d/2}}\,, \tag{4.133}$$

$$M_3 = f_1\Lambda_1^2 + f_2\Lambda_1 V_1 V_2 V_3 + f_3(V_1 V_2 V_3)^2 + f_4\Lambda_2 + f_5\Lambda_3$$

where V_i, $H_{i,j}$, and Λ_1 are defined in eqs. (4.85), Λ_2 and Λ_3 are

$$\Lambda_2 = H_{1,2}H_{2,3}H_{3,1}\,, \tag{4.134}$$

$$\Lambda_3 = V_1 V_2 H_{1,3}H_{2,3} + \text{cyclic}\,.$$

and the functions $f_{1,...5}$ are

$$f_1 = 16 - \frac{16}{d} - \frac{8}{d^2}\,, \qquad\qquad f_2 = -8 - \frac{8}{d} + \frac{24}{d^2} + \frac{16}{d^3}\,,$$

$$f_3 = 1 + \frac{4}{d} - \frac{4}{d^2} - \frac{16}{d^3}\,, \qquad f_4 = \frac{8}{d}\,, \qquad f_5 = \frac{4}{d^2} + \frac{8}{d^3}\,. \tag{4.135}$$

This expression for $\mathcal{M}_3$ agrees with Ref. [230] up to some notational translation:

$$\Lambda_1^{\text{(here)}} = -(-2P_1 \cdot P_2)(-2P_2 \cdot P_3)(-2P_3 \cdot P_1)\Lambda_1^{\text{(there)}}\,,$$

$$(V_1 V_2 V_3)^{\text{(here)}} = -(-2P_1 \cdot P_2)(-2P_2 \cdot P_3)(-2P_3 \cdot P_1)(V_1 V_2 V_3)^{\text{(there)}}\,,$$

$$\Lambda_2^{\text{(here)}} = (-2P_1 \cdot P_2)^2(-2P_2 \cdot P_3)^2(-2P_3 \cdot P_1)^2\Lambda_2^{\text{(there)}}\,,$$

$$\Lambda_3^{\text{(here)}} = (-2P_1 \cdot P_2)^2(-2P_2 \cdot P_3)^2(-2P_3 \cdot P_1)^2\Lambda_3^{\text{(there)}}\,. \tag{4.136}$$

It is not difficult to see the numerator M_3 above and the analogous quantity N_3 in the three-point YM correlator in eq. (4.87) are related by

$$\lim_{d\to\infty} M_3 = \lim_{d\to\infty} (N_3)^2\,, \tag{4.137}$$

That is, to leading order in the expansion in the large dimension of the AdS space, the three-graviton correlator equals the square of the three-gluon correlator in eq (4.87), in agreement with Ref. [198].

We note that, for three-point correlators, the position-space factors M_3 and N_3 coincide (up to possible *overall* normalization factors) with the corresponding Mellin-space amplitudes. With this observation, eq. (4.137) above also implies that simple squaring relations between gauge and gravity three-point amplitudes may hold in Mellin space only in the large-d limit. In contrast, Ref. [190] reports such a squaring relation for the scalar components of the super-gluon and super-graviton multiplet at $d = 4$. The difference is presumably due to the action of supercharges which introduces a nontrivial dependence on the conformal weight.

We will refrain from conjecturing the generalization of this relation to higher-point correlators or how it might be formulated for the differential form of correlators. It is however difficult not to note, as was also noted in [189], certain similarities between the large-dimension limit above and the relation between flat space S-matrix and AdS boundary correlators. Indeed, it was argued in Ref. [45, 213, 235] that these two quantities are closely related; a formulation of this connection which holds for amplitudes of massive fields is [235]

$$m_1^a T(k_i) = \lim_{\Delta_i \to \infty} \frac{\Delta_1^a}{\mathcal{N}} M\left(\gamma_{ij} = \frac{\Delta_i \Delta_j}{\sum_{k=1}^{n} \Delta_k}\left(1 + \frac{k_i \cdot k_j}{m_i m_j}\right)\right) \tag{4.138}$$

where M is a Mellin-space amplitude, γ_{ij} are Mellin variables obeying the standard constraints, T is a flat space amplitude, k_i are flat-space momenta, $a = \frac{n(d-1)}{2} - d - 1$ and

$$\mathcal{N} = \frac{\pi^d}{2} \Gamma\left(\frac{\sum_{i=1}^n \Delta_i - d}{2} \right) \prod_{i=1}^n \frac{\sqrt{\mathcal{N}_{\Delta_i}}}{\Gamma(\Delta_i)}, \qquad \mathcal{N}_\Delta = \frac{\Gamma(\Delta)}{2\pi^{d/2}\Gamma(\Delta - d/2 + 1)} \ . \tag{4.139}$$

It clearly implies that, at least in the limit of large AdS energies, the Mellin-space amplitude exhibits a double-copy structure which is inherited from the corresponding flat space S-matrix element. The large-Δ limit may be realized either by considering very massive particles or, as in the three-point example discussed above, by taking the space-time dimension to be large. It would be interesting to understand better in what sense $\mathrm{AdS}_{d\to\infty}$ may be interpreted as flat space. More involved relations [45, 213, 236] connecting Mellin-space and flat space amplitudes are also suggestive of a double-copy structure in this limit.

Taking at face value the observation that we may assume the dimension to be large, let us discuss another limit on AdS boundary correlators that points to a double-copy structure in AdS momentum space.

4.5.3 An Argument for Double Copy at High Energies

The AdS Poincaré patch that we have been using exhibits translational invariance – and thus conserved momentum – in the directions parallel to the boundary. It is therefore natural to consider momentum-space AdS boundary correlators – i.e. Fourier-transforms of AdS boundary correlators along the boundary coordinates. Properties of momentum-space correlation functions of gauge-invariant operators have been discussed from dual gauge theory perspective in refs. [237–240].

A hard high energy scattering process (i.e. a scattering process for which the momentum transfer is large) may be expected to be localized in a small region of the space. Thus, for weakly-curved spaces, the scattering effectively occurs in flat space. An important point, emphasized in refs. [241, 242] and used there to provide a connection between the soft high-energy string theory S-matrix elements and the hard S-matrix elements of gauge theories, is that the momenta of particles in the scattering region are not the same as the momenta at infinity/boundary. Rather than the boundary momentum p, it is the momentum $\tilde{p}$ in the local inertial frame,

$$\tilde{p}_a = e_a^\mu p_\mu \tag{4.140}$$

with the vielbein e_μ^a and $p_\mu \sim \partial/\partial x^\mu$, that governs the local scattering process. Moreover, since the propagation from the boundary to the interaction region probes a large region of the curved space, the asymptotic states are captured by the curved-space bulk-boundary propagators.

Thus, if the extent of the scattering region is not too large, the correlation function labeled by boundary momenta is schematically

$$\mathcal{M}_{\Delta_1\dots\Delta_n}(p) = \langle \mathcal{O}_{\Delta_1}(p_1) \dots \mathcal{O}_{\Delta_n}(p_n) \rangle = \int_M \mathcal{M}_{\text{flat}}(\tilde{p}) \prod_{i=1}^n E_{\Delta_i} \ , \tag{4.141}$$

where E_{Δ_i} are the bulk-boundary propagators labeled by boundary momenta for the fields dual to the operators $\mathcal{O}_{\Delta_i}$, $\mathcal{M}_{\text{flat}}$ is the flat space amplitude for these fields and M is the entire space (e.g. AdS$_5\times$X). For tree-level boundary correlators the integration runs over the coordinates that are not Fourier-transformed (e.g. in AdS it is only the transverse direction). The asymptotic states for fields with spin naturally carry tangent space indices, so their bulk-boundary propagators are similarly labeled.

The Poincaré patch the metric is

$$ds^2 = \frac{R^2}{z^2} \left(\eta_{\mu\nu} dx^\mu dx^\nu + dr^2 \right) \ . \tag{4.142}$$

In these coordinates, the boundary is at $z = 0$ and the momentum in the local inertial frame is

$$\tilde{p} = \frac{z}{R} p \ . \tag{4.143}$$

Thus, for any finite boundary momentum p, the local momentum is large if the scattering occurs away from the boundary. One may extend the range of validity of this approximation by taking the boundary momenta to be parametrically large, but the scattering region is required to have a relatively small extent in the AdS transverse direction. Therefore, the double-copy structure of the flat space gravitational amplitudes, formally written as $\mathcal{M}_{\text{flat}}(\tilde{p}) = \text{DC}[\mathcal{A}_{\text{L, flat}}(\tilde{p}), \mathcal{A}_{\text{L, flat}}(\tilde{p})]$, implies that in the regime eq. (4.141) holds the transverse-space integrand of AdS boundary correlators also have certain double-copy properties. For graviton asymptotic states:

$$\mathcal{M}_{\Delta_1\dots\Delta_n}(p) = \int_M \text{DC}[\mathcal{A}_{\text{L, flat}}^{M_1\dots M_n}(\tilde{p}), \mathcal{A}_{\text{L, flat}}^{N_1\dots N_n}(\tilde{p})] \prod_{i=1}^n E_{\Delta_i}^{M_i N_i, A_i B_i} Z_{i, A_i B_i} \ , \tag{4.144}$$

where graviton Z_i are polarization tensors, $E_{\Delta_i}^{M_i N_i, A_i B_i}$ are graviton bulk-boundary propagators and $\mathcal{A}_{L,R}$ are the left and right gauge theory amplitudes entering the flat space double copy.

Inspection of the bulk-boundary propagators reveals that these properties may be further enhanced in the limit of large AdS dimension or large Δ. As discussed in section 4.2.3, the vector-field propagator may be written as a differential operator acting on the scalar propagator, *cf.*

eq. (4.27). The graviton propagator has a similar form

$$E_\Delta^{MN,AB} = \mathcal{D}^{MN,AB} E_\Delta \,, \tag{4.145}$$

$$\mathcal{D}^{MN,AB} = \eta^{MA}\eta^{NB} + \frac{1}{\Delta}\left(\eta^{MA}P^B\frac{\partial}{\partial P_N} + \eta^{NB}P^A\frac{\partial}{\partial P_M}\right) + \frac{1}{\Delta(\Delta+1)}P^A P^B \frac{\partial^2}{\partial P_M \partial P_N} \,.$$

In the limit of large Δ or for massless fields in the limit of large AdS dimension, this operator may also be written as

$$E_{\Delta\to\infty}^{MN,AB} = \mathcal{D}^{MN,AB} E_{\Delta\to\infty} = \mathcal{D}^{MA}\mathcal{D}^{NB} E_{\Delta\to\infty} = \mathcal{D}^{NB}\mathcal{D}^{MA} E_{\Delta\to\infty} \tag{4.146}$$

$$\mathcal{D}^{MA} = \eta^{MA} + \frac{1}{\Delta}P^A\frac{\partial}{\partial P_M} \,. \tag{4.147}$$

Even though $\mathcal{D}$ contains terms with a manifest Δ^{-1} which might seem possible to ignore in the large-Δ limit, the derivatives with respect to the bulk point provide an additional factor $\mathcal{O}(\Delta)$ which render this term finite in this limit. The factorization of $\mathcal{D}^{MN,AB}$ relies on dropping various terms $\mathcal{O}(\Delta^{-1})$ after the derivatives are evaluated. Thus, in the high energy (from the boundary perspective) and large large AdS dimension, the integrand of the momentum-space gravitational AdS boundary correlator can be written as the square of a differential operator acting on scalar bulk-boundary propagators:

$$\mathcal{M}_{\Delta_1\dots\Delta_n}(p) = \int_M \mathrm{DC}[\mathcal{A}_{\mathrm{L,\,flat}}^{M_1\dots M_n}(\tilde{p}), \mathcal{A}_{\mathrm{L,\,flat}}^{N_1\dots N_n}(\tilde{p})]\prod_{i=1}^n Z_{i,A_i}\mathcal{D}^{M_i,A_i}Z_{i,B_i}\mathcal{D}^{N_i,B_i}\,E_{\Delta_i\to\infty}\,. \tag{4.148}$$

A single power of this differential operator,

$$\mathcal{A}_{\Delta_1\dots\Delta_n}(p) = \int_M \mathcal{A}_{\mathrm{flat}}^{M_1\dots M_n}(\tilde{p})\prod_{i=1}^n Z_{i,A_i}\mathcal{D}^{M_i,A_i}\,E_{\Delta_i\to\infty} \tag{4.149}$$

where we suppressed color indices, is a color-dressed gauge theory AdS boundary correlator. While in general the weight of vector fields and gravitons is different, their differences are sub-leading in the large dimension or large energy limit so $E_{\Delta_i\to\infty}$ are the same in both eq. (4.148) and eq. (4.149).

Similar reasoning suggests AdS boundary correlators with other asymptotic states can be double-copied in the same sense as outlined here. Fourier-transforming the boundary momenta provides a possible connection to the position-space representation of AdS boundary correlators. It would be very interesting to understand whether a more direct relation can be formulated.

4.6 The Differential Representation at One Loop

We now generalize the differential representation of scalar AdS correlators beyond tree-level by introducing the notion of operator-valued integration. Note that a similar higher loop generalization of the differential representation is also given in Ref. [243].

4.6.1 Operator-Valued Integration

We motivate our construction using the triangle Witten diagram

$$\mathcal{A}_3^{\triangle} = \parbox{3cm}{} \quad . \tag{4.150}$$

Given the position space representation of $\mathcal{A}_3^{\triangle}$,

$$
\begin{aligned}
\mathcal{A}_3^{\triangle} = \int_{\text{AdS}} & dX_1 dX_2 dX_3 G_d(X_1, X_2) G_d(X_2, X_3) \\
& \times G_d(X_1, X_3) \prod_{i=1}^{3} E_d(X_i, P_i)
\end{aligned}
\tag{4.151}
$$

we replace $G_d(X_2, X_3)$ with its split-representation
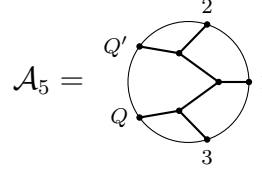
$$
\begin{aligned}
G_\Delta(X_2, X_3) = \int_{-i\infty}^{i\infty} & \frac{dc}{2\pi i} (-2c^2) \int_{\partial\text{AdS}} dQ dQ' \\
& \times \frac{\delta^d(Q, Q')}{D_Q^2 - \Delta(d - \Delta)} E_{\frac{d}{2}+c}(X_2, Q) E_{\frac{d}{2}-c}(X_3, Q') \ .
\end{aligned}
\tag{4.152}
$$

with $\Delta = d$. Upon making this replacement, the triangle Witten diagram simplifies to the form

$$
\begin{aligned}
\mathcal{A}_3^{\triangle} = \int_{-i\infty}^{i\infty} & \frac{dc}{2\pi i} (-2c^2) \int_{\partial\text{AdS}} dQ dQ' \delta(Q, Q') \\
& \times \frac{1}{D_Q^2} \mathcal{A}_5(P_1, P_2, P_3, Q, Q')
\end{aligned}
\tag{4.153}
$$

where $\mathcal{A}_5$ is a 5-point tree-level Witten diagram. So far, we have simply rewritten the loop diagram as a spectral integral over a tree diagram, as is standard [244]. We now write the tree diagram in

the differential representation

$$\mathcal{A}_5 = \quad \tag{4.154}$$

$$= \frac{1}{D_{Q3}^2}\frac{1}{D_{Q31}^2}\mathcal{C}_5^c(P_1, P_2, P_3, Q, Q') \,.$$

where the c superscript indicates that the conformal dimensions associated with Q and Q' external states in Eq. (4.154) are $\Delta_Q = d/2 + c$ and $\Delta_{Q'} = d/2 - c$ respectively. Combining Eqs. (4.153) and (4.154), we find

$$\begin{aligned}
\mathcal{A}_3^\triangle &= \int_{-i\infty}^{i\infty} \frac{dc}{2\pi i}(-2c^2) \int_{\partial\mathrm{AdS}} dQ dQ' \delta(Q, Q') \\
&\times \frac{1}{D_Q^2}\frac{1}{D_{Q3}^2}\frac{1}{D_{Q31}^2}\mathcal{C}_5^c(P_1, P_2, P_3, Q, Q') \,.
\end{aligned} \tag{4.155}$$

This is the differential representation of the triangle one-loop Witten diagram.

The above manipulations can be performed on any one-loop Witten diagram. One simply uses the split representation, Eq. (4.152), to convert the one-loop, n-point Witten diagram to a tree-level $(n+2)$-point Witten diagram in the differential representation [245]. For example, repeating the above manipulations for bubble and box Witten diagrams, one finds

$$\mathcal{A}_3^{\mathrm{Bubble}} = \int_{-i\infty}^{i\infty} \frac{dc}{2\pi i}(-2c^2) \int_{\partial\mathrm{AdS}} dQ dQ' \delta(Q, Q')\frac{1}{D_Q^2}\frac{1}{D_{Q3}^2}\mathcal{C}_5^c(P_i, Q, Q') \tag{4.156}$$

and

$$\mathcal{A}_4^{\mathrm{Box}} = \int_{-i\infty}^{i\infty} \frac{dc}{2\pi i}(-2c^2) \int_{\partial\mathrm{AdS}} dQ dQ' \delta(Q, Q')\frac{1}{D_Q^2 D_{Q1}^2 D_{Q12}^2 D_{Q123}^2}\mathcal{C}_6^c(P_i, Q, Q') \,. \tag{4.157}$$

Notably, the first lines of Eqs. (4.155)-(4.157) are universal. In contrast, the second lines are unique to the Witten diagram and analogous to the corresponding Feynman diagram under the replacement of the internal loop momentum with D_Q^{AB}.

We interpret the universal integrals over c, Q and Q' in the first lines of Eqs. (4.155)-(4.157) as the AdS analog of $\int dl^\mu$. We refer to such scalar integrals collectively as an operator-valued integral

and formally define the operator-valued integral of an operator-valued integrand, $\hat{\mathcal{I}}(D_Q, D_i)$, as

$$
\int [\mathcal{D}D_Q]\hat{\mathcal{I}}(D_Q, D_i) \equiv \int_{\partial\text{AdS}} dQ\, dQ'\, \delta^d(Q, Q')
$$
$$
\times \int_{-i\infty}^{i\infty} \frac{dc}{2\pi i}(-2c^2)\hat{\mathcal{I}}(D_Q, D_i)\mathcal{C}_{n+2}^c(P_i, Q, Q')
$$

(4.158)

where $\mathcal{C}_{n+2}^c(Q, Q', P_i)$ is an $(n+2)$-point contact diagram,

$$
\mathcal{C}_{n+2}^c(Q, Q', P_i) = \int_{\text{AdS}} dX\, E_{\frac{d}{2}+c}(Q, X)E_{\frac{d}{2}-c}(Q', X)\prod_{i=1}^{n} E_{\Delta_i}(P_i, X)\,.
$$

(4.159)

Again, the c superscript refers to how the conformal dimensions of the Q and Q' states depend on c. Our notation is meant to suggest that we should interpret Eq. (4.158) as an integral over D_Q. Using this notation, the triangle Witten diagram is

$$
\mathcal{A}_3^\triangle = \int [\mathcal{D}D_Q]\frac{1}{D_Q^2}\frac{1}{D_{Q3}^2}\frac{1}{D_{Q31}^2}\,,
$$

(4.160)

and similarly for the bubble and box differential representations. The operator-valued integrals evaluate to functions of conformal generators of external states acting on contact diagrams, $\mathcal{C}_n$.

The operator-valued integral notation is interesting because it simplifies expressions and provides a representation of Witten diagrams analogous to Feynman diagrams. However, the utility of the operator-valued integral goes beyond aesthetics. We show in Sections 4.6.2 and 4.6.3 that certain identities of scalar integrals generalize to operator-valued integrals and can be leveraged to simplify the evaluation of specific Witten diagrams.

4.6.2 Explicit Calculations at Three-Point

The differential representation is particularly useful for performing direct integration of one-loop Witten diagrams. This is most apparent at three-point where a number of simplifications occur, specifically a form of tensor-reduction. For Feynman integrals, tensor reduction implies that three-point, one-loop integrals obey the identity

$$
0 = \int d^{d+1}l\, f(l^2)(l \cdot p_i)^N(l \cdot p_j)^M\big|_{p_i^2=0}
$$

(4.161)

for any integers N, M such that $M \geq 0$, $N \geq 0$ and $N + M > 0$ [246]. For three-point Witten diagrams, we conjecture an analogous identity holds if $\Delta = d$ for all external states:

$$0 = \int [\mathcal{D}D_Q]\hat{f}(D_Q^2)(D_Q \cdot D_i)^N (D_Q \cdot D_j)^M|_{n=3} \tag{4.162}$$

with the same conditions on N and M, for all possible orderings of the differential operators in the integrand. Eq. (4.162) is much more non-trivial than its flat-space analog. Even if one assumes tensor reduction is applicable to operator-valued integrals, conformal generators can in principle be contracted using the structure constants of the AdS isometry group as well as dot products. Using formulas in Appendix C.3, we explicitly checked Eq. (4.162) holds for $N + M \leq 10$.

We can prove Eq. (4.162) for the special case that $N = 0$. We first note that when $(D_Q \cdot D_1)^N$ acts on $D_{\Delta_Q, \Delta_1, \ldots}$, the result takes the form

$$\begin{aligned} &(D_Q \cdot D_1)^N D_{\Delta_Q, d \ldots} \\ &= \sum a_{n,k}(Q \cdot P_1)^k D_{\Delta_Q+k, d+k, \ldots} \end{aligned} \tag{4.163}$$

where $D_{\Delta_Q+k, d+k, \ldots}$ is the D-function, defined as

$$\begin{aligned} D_{\Delta_Q, \Delta_1, \ldots} = \\ \int_{\text{AdS}} dX (-2X \cdot P_1)^{-\Delta_Q} (-2X \cdot P_n)^{-\Delta_1} \ldots . \end{aligned} \tag{4.164}$$

To solve for $a_{n,k}$, we use the relation

$$\begin{aligned} (D_Q \cdot D_1)[(Q \cdot P_1)^k D_{\Delta_Q+k, d+k, \ldots}] = \\ - 8(\Delta_Q + k)(d + k)(Q \cdot P_1)^{k+1} D_{\Delta_Q+k+1, d+k+1, \ldots} \\ - 4(\Delta_Q + k)(d/2 + k)(Q \cdot P_1)^k D_{\Delta_Q+k, d+k, \ldots} \end{aligned} \tag{4.165}$$

which provides a recursion relation for the $a_{n,k}$ coefficients,

$$a_{n,k} = a_{n-1,k-1} f_{k-1} + a_{n-1,k} g_k \tag{4.166}$$

where

$$\begin{aligned} f_k &= -8(\Delta_Q + k)(d + k) \, , \\ g_k &= -4(\Delta_Q + k)(d/2 + k) \, , \\ a_{0,0} &= 1 \, , \\ a_{n,k} &= 0 \text{ if } k > n \text{ or } k < 0 \, . \end{aligned} \tag{4.167}$$

We now take the expression in Eq. (4.168) and integrate over Q using Eq. (C.50). We find the result

$$\int_{\text{AdS}} dQ \sum_{k=0}^{n} a_{n,k} (Q \cdot P_i)^k D_{\Delta_Q+k,d+k,\ldots}$$
$$= \pi^{d/2} D_{\Delta_Q,d,\ldots} \sum_{k=0}^{n} \left(\frac{1}{2}\right)^{-k} a_{n,k} \frac{\Gamma(d/2+k)}{\Gamma(d+k)} \ . \tag{4.168}$$

To show this expression is zero, substitute the identity in Eq. (4.166) for all $a_{n,k}$. There are now two sums over $g_k \times (\ldots)$ and $f_{k-1} \times (\ldots)$ respectively. Substituting in the definitions of g_k and f_k in Eq. (4.167), these two sums cancel. Therefore, the expression in Eq. (4.168) vanishes. Unfortunately, proving Eq. (4.162) for non-zero N and M is much more difficult than the $N = 0$ case. We will sketch a proof strategy here. Similar to the $N = 0$ case, one would first establish an ansatz for $(D_Q \cdot D_1)^N (D_Q \cdot D_2)^M D_{\Delta_Q,d,d,\ldots}$ as a sum of terms of the form

$$(Q \cdot P_1)^{k_1} (Q \cdot P_2)^{k_2} (P_1 \cdot P_2)^{k_3} D_{\Delta_Q+k_1+k_2,d+k_1+k_3,d+k_2+k_3,\ldots} \ . \tag{4.169}$$

One would then establish a recursion relation among coefficients similar to Eq. (4.165) and perform an integral over Q using Eq. (C.51). Unlike the $N = 0$ case, one would also need to subsequently integrate over the bulk coordinate X using the closed form expression of the 3-point D-function. After integrating over Q and X, the hope is that the recursion relations between coefficients would be enough to show that the terms in the sum cancel among themselves, similar to what happens in the $N = 0$ case.

Eq. (4.162) can be leveraged to dramatically simplify the calculation of certain three-point Witten diagrams. As an illustrative example, consider the three-point bubble diagram:

$$\mathcal{A}_3^{\text{Bubble}} = \tag{4.170}$$

where the conformal dimension of the state running in the loop, Δ_l, is left unfixed. We restrict this computation to $d = 2$ as this Witten diagram diverges for $d \geq 3$. The differential representation of $\mathcal{A}_3^{\text{Bubble}}$ is

$$\int [\mathcal{D}D_Q] \frac{1}{(D_Q^2 - \Delta_l(d - \Delta_l))(D_{Q3}^2 - \Delta_l(d - \Delta_l))} \ . \tag{4.171}$$

Since $\Delta_3 = d = 2$, we find that $D_3^2 = 0$. Performing a Taylor Series in $D_Q \cdot D_3$, one finds that all terms vanish due to Eq. (4.162) except the leading term. Therefore, the bubble Witten diagram

simplifies to

$$\int [\mathcal{D}D_Q] \frac{1}{(D_Q^2 - \Delta_l(2 - \Delta_l))^2} \ . \tag{4.172}$$

Substituting the definition of the operator-valued integral and using [45, 247]

$$\frac{\Gamma(d/2)\Gamma(d/2 + c)\Gamma(d/2 - c)}{4\pi^{d/2}\Gamma(d)\Gamma(1 - c)\Gamma(1 + c)} = \int_{\partial \text{AdS}} dQ E_{d/2+c}(Q, X) E_{d/2-c}(Q, X) \ , \tag{4.173}$$

we reduce the integral to a single contour integral which can be evaluated using the residue theorem. The final result for $\mathcal{A}_3^{\text{Bubble}}$ is

$$\int_{-i\infty}^{i\infty} \frac{dc}{(2\pi)^2 i} \frac{\Gamma(1 + c)\Gamma(1 - c)\mathcal{C}_3}{\Gamma(c)\Gamma(-c)(1 - c^2 - \Delta_l(2 - \Delta_l))^2} = \frac{1}{8\pi(\Delta_l - 1)} \mathcal{C}_3 \ . \tag{4.174}$$

We can cross-check this result by an explicit computation in position space. To simplify the computation, we consider the more general case that P_3^A is in the bulk and then take the limit that P_3^A approaches the boundary, writing

$$\mathcal{A}_3^{\text{Bubble}} = \lim_{P_3 \to \partial \text{AdS}} (z_3)^{-2} \int_{\text{AdS}} dX_1 dX_2 E(P_1, X_1) E(P_2, X_1)(G_{\Delta_l}(X_1, X_2))^2 G(X_2, P_3) \ . \tag{4.175}$$

We consider the split-representation of the $d = 2$ bulk-to-bulk propagator in Eq. (4.22) and the bubble,

$$G_{\Delta_l}(X_1, X_2)^2 = \int_{-i\infty}^{i\infty} \frac{dc}{2\pi i} B_c^{\Delta_l} \Omega_c(X_1, X_2) \ , \tag{4.176}$$

where $B(c)$ was derived in Ref. [248],

$$B_c^{\Delta_l} = \frac{\psi(\Delta_l - \frac{1+c}{2}) - \psi(\Delta_l - \frac{1-c}{2})}{8\pi c} \ . \tag{4.177}$$

$\Omega_c(X_1, X_2)$ is the AdS harmonic functions, which can be defined in terms of the bulk-to-bulk propagator:

$$\Omega_c(X_1, X_2) = c(G_{d/2+c}(X_1, X_2) - G_{d/2-c}(X_1, X_2)) \ . \tag{4.178}$$

Using orthogonality of AdS conformal partial waves, we find that

$$\int_{\text{AdS}} dX_2 (G_{\Delta_l}(X_1, X_2))^2 G(X_2, P_3) = \int_{-i\infty}^{i\infty} \frac{dc}{2\pi i} \frac{B_c^{\Delta_l}}{1 - c^2} \Omega_c(X_1, P_3) \ . \tag{4.179}$$

Substituting Eq. (4.179) into Eq. (4.175) and rewriting the conformal partial wave as a sum of

$G_{d/2\pm c}(X_1, X_2)$, the one-loop correlator simplifies to

$$\lim_{z_{-3}\to 0} z_3^{-2} \int_{-i\infty}^{i\infty} \frac{dc}{2\pi i} \frac{cB_c^{\Delta_l}}{1-c^2} \int dX_1 E(P_1, X_1)$$
$$E(P_2, X_1)(G_{1+c}(X_1, P_3) - G_{1-c}(X_1, P_3)) \tag{4.180}$$

This integral can be evaluated using the residue theorem, but the contour is different for each term due to distinct behavior at $|z| \to \infty$. The $G_{1\pm c}(X_1, P_3)$ term corresponds to a contour which includes the residue at $c = \pm 1$. The final result is

$$\mathcal{A}_3^{\text{Bubble}} = \frac{1}{8\pi(\Delta_l - 1)} \mathcal{C}_3 \, . \tag{4.181}$$

As expected, we find that the operator-valued integration result in Eq. (4.174) matches the result derived from direct integration in position space in Eq. (4.181). Given that $\mathcal{A}_3^{\text{Bubble}}$ is a one-loop diagram in AdS$_3$, it was surprisingly straightforward to evaluate. The key to the above computation was using the split representation of the bubble diagram in Eqs. (4.176) and (4.177). Unfortunately, this computation strategy does not generalize to more complicated one-loop Witten diagrams, such as the triangle Witten diagram.

We can use the differential representation to evaluate more complex Witten diagrams, such as the triangle Witten diagram. We fix the conformal dimension of states running in the loop to $\Delta_l = d$ for simplicity. The relevant operator-valued integral is then Eq. (4.160). We again take a Taylor series of the operator-valued integrand, except now in $D_Q \cdot D_1$ and $D_Q \cdot D_2$. All terms vanish except the leading term due to Eq. (4.162). The final result can be converted into a single scalar integral, which can again be evaluated using residue theorem. Evaluating the integral, we found

$$\mathcal{A}_3^{\triangle}|_{d=2} = \frac{1}{32\pi} \mathcal{C}_3, \quad \mathcal{A}_3^{\triangle}|_{d=4} = \frac{13}{1536\pi^2} \mathcal{C}_3 \, ,$$
$$\mathcal{A}_3^{\triangle}|_{d=3} = \frac{7\pi^2 - 36\zeta(3) - 6}{1296\pi^2} \mathcal{C}_3 \, , \tag{4.182}$$

and that the integral is divergent for $d \geq 5$, similar to flat space. Evaluating the c-integral for odd d is slightly harder than even d because an infinite number of residues contribute that need to be re-summed.

4.6.3 Generalized IBP Relations

In flat space, IBP is an important tool for computing Feynman integrals [56, 58, 199–208]. We now give a partial generalization of IBP for operator-valued integrals. We first note that the operator

valued integral should be invariant under arbitrary conformal transformations of Q and Q', which implies

$$\mathcal{I} = \int [\mathcal{D}D_Q] e^{v\cdot(D_Q + D_{Q'})} \hat{\mathcal{I}} \,, \tag{4.183}$$

where v is a tensor, is independent of v. We now rewrite the above operator-valued integral as

$$\mathcal{I} = \int [\mathcal{D}D_Q] \hat{\mathcal{I}}' e^{-v\cdot(\sum_{i=1}^{n} D_i)} \tag{4.184}$$

where $\hat{\mathcal{I}}'$ is $\hat{\mathcal{I}}$ with the replacement

$$D_a^{AB} \to e^{v\cdot(D_Q + D_{Q'})} D_a^{AB} e^{-v\cdot(D_Q + D_{Q'})} \,. \tag{4.185}$$

for all $a \in \{Q, 1, \ldots, n\}$. If v is a constant tensor, then the above shift only acts non-trivially on D_Q and dependence on $D_{Q'}$ disappears. Let us now take v to be an infinitesimal in Eq. (4.184). Since the result is independent of v, the component linear in v must vanish, which imposes non-trivial linear relations among operator-valued integrals. The collection of identities derivable from this procedure does not necessarily span the space of all linear identities obeyed by operator-valued integrals, but is enough to illustrate that there are non-trivial relations which mimic their flat-space counter-parts.

For example, we can apply the above procedure to the triangle Witten diagram. We assume v is an infinitesimal constant, so the replacement rule simplifies to

$$D_Q^{AB} \to D_Q^{AB} + f_{CD,EF}^{AB} D_Q^{CD} v^{EF} \,. \tag{4.186}$$

where $f_{CD,EF}^{AB}$ is a structure constant of the AdS isometry group. The above procedure ultimately implies the operator-valued integrand

$$\hat{\mathcal{I}} = \frac{v_{AB} f_{CD,EF}^{AB}}{D_Q^2 D_{Q1}^2 D_{Q12}^2} \left((D_Q^{CD} D_1^{EF}) \frac{1}{D_{Q1}^2} \right.$$

$$\left. + (D_Q^{CD} D_{12}^{EF}) \frac{1}{D_{Q12}^2} \right) - \frac{1}{D_Q^2 D_{Q1}^2 D_{Q12}^2} (v \cdot \sum_{i=1}^{3} D_i), \tag{4.187}$$

integrates to zero for external states with arbitrary conformal dimension. Unlike the operator-valued integrands previously considered, the differential operators in each term do not always commute and there are contractions of conformal generators with structure constants. Furthermore, the constant tensor v explicitly breaks conformal symmetry, so the CWI must be applied with care [249].

CHAPTER 5

Conclusion

In this dissertation, I have discussed novel structures in amplitudes and AdS boundary correlators. I leveraged wall-crossing to systematically study the boundary structure of the positive kinematic region of amplitudes in $\mathcal{N} = 4$ pSYM. I then generalized the double copy to a wide range of EFTs. I concluded by applying the differential representation, a novel framework for computing boundary correlators in AdS, to generalizing color-kinematics duality and certain techniques for computing flat space one-loop amplitudes to AdS boundary correlators.

The methodology of this dissertation was to consider scattering in "simple" theories, such as $\mathcal{N} = 4$ pSYM, and then generalize to theories where computations are more difficult, such as in AdS. Since computations in the simple theories are tractable, it is easier to identify hidden structures. One can then directly test whether such structures generalize beyond the simple models, such as to AdS. The structures studied in this dissertation were the positive kinematic region, color-kinematics duality, and the double-copy. Remarkably, I found that color-kinematics duality generalizes to AdS boundary correlators, at least at 4-point. However, I also found that a naive double-copy formula does not generalize to YM and GR in AdS.

An obvious next step for the research program proposed in this dissertation is studying whether there is an analog of the positive kinematic region for planar AdS boundary correlators. The AdS analog of the positive kinematic region would presumably encode the dynamics of multi-particle exchange states, similar to flat-space. However, studying the AdS analog of the positive kinematic region would require studying 4-point correlators; the kinematic structure of 3-point correlators seems too simple to encode any interesting multi-particle dynamics, at least at one-loop. While this dissertation only studied the higher loop computation of 3-point AdS boundary correlators, the operator-valued integral technology provides a path to computing such correlators in the near future.

APPENDIX A

Background on Cluster Algebras

A.1 Introduction to cluster algebras

In this appendix, we give a brief introduction to cluster algebras [119, 250–252]. Thorough introductions are refs. [253–256], while those looking for a review that focuses on the connection with scattering amplitudes are referred to ref. [15]. Cluster algebras were initially motivated by the notion of total positivity. For example, one major motivating question was how much information is generically needed to prove that minors of a given matrix are positive. Due to non-linear relations between minors, this question quickly becomes very hard from a brute force approach of writing out all relations between minors and solving these polynomials directly. The advent of cluster algebras gave a different approach.

Suppose you are given a $2 \times n$ matrix and asked to find the minimal information needed to determine whether all 2×2 minors are positive. The problem is non-trivial due to quadratic relations between minors called plucker relations:

$$\frac{1}{\langle i, k \rangle} \left(\langle i, j \rangle \langle k, l \rangle + \langle i, l \rangle \langle j, k \rangle \right) = \langle j, l \rangle \quad i < j < k < l \,. \tag{A.1}$$

A brute force approach would be to calculate *all* quadratic relations of the form eq. (A.1) at once and find some minimal subset directly. This computation would be problematic for even the best
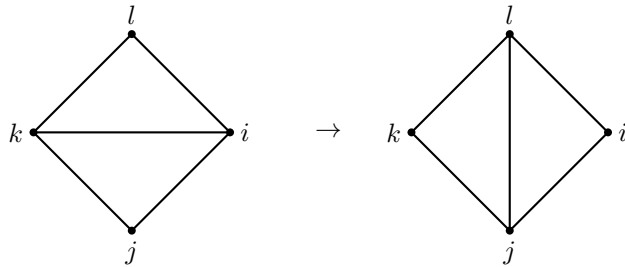
Figure A.1: A visual representation of the plucker relations for $Gr(2, n)$.
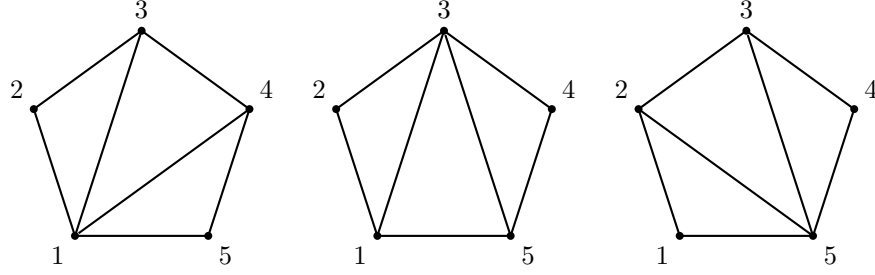
Figure A.2: The first triangulation of the 5-gon corresponds to the parameterization in eq. (A.3). Each minor in eq. (A.3) corresponds to an edge. The remaining triangulated 5-gons correspond to the mutation pattern that leads to $\langle 2, 5 \rangle$.

computers. We instead take a cluster algebra approach and find a preferred set of coordinates on the space of minors. To do so, we note that eq. (A.1) can be visually interpreted as a mutation on the triangulation of a 4-gon with edges, i, j, k, l, as visualized in fig. A.1. Therefore, at $n = 4$, a natural set of preferred minors is

$$\langle 1, 2 \rangle, \ \langle 2, 3 \rangle, \ \langle 3, 4 \rangle, \ \langle 1, 4 \rangle, \ \langle 1, 3 \rangle . \tag{A.2}$$

We can calculate the remaining coordinate, $\langle 2, 4 \rangle$, using eq. (A.1), interpreting eq. (A.1) as a mutation on the 4-gon. Going beyond $n = 4$, it is natural to start with coordinates that can be associated with the triangulation of an n-gon and interpret eq. (A.1) as a mutation on this triangulated n-gon, just as we did for the triangulated 4-gon. For example, consider $n = 5$ and the initial coordinates:

$$\langle 1, 2 \rangle, \ \langle 2, 3 \rangle, \ \langle 3, 4 \rangle, \ \langle 4, 5 \rangle, \ \langle 1, 5 \rangle, \ \langle 1, 3 \rangle, \ \langle 1, 4 \rangle \tag{A.3}$$

which are associated with the first triangulation in fig. A.2. Suppose we want to write $\langle 2, 5 \rangle$ in terms of our initial coordinates. We first perform a "mutation" on $\langle 1, 4 \rangle$, finding

$$\langle 3, 5 \rangle = \frac{1}{\langle 1, 4 \rangle} (\langle 1, 3 \rangle \langle 4, 5 \rangle + \langle 3, 4 \rangle \langle 1, 5 \rangle) \tag{A.4}$$

and a new triangulation where $\langle 1, 4 \rangle$ is replaced with $\langle 3, 5 \rangle$. We then perform a mutation on $\langle 1, 3 \rangle$, finding

$$\langle 2, 5 \rangle = \frac{1}{\langle 1, 3 \rangle} (\langle 3, 5 \rangle \langle 1, 2 \rangle + \langle 2, 3 \rangle \langle 1, 5 \rangle) \tag{A.5}$$

Therefore, assuming that all our initial minors in eq. (A.3) are positive, then $\langle 2, 5 \rangle$ must be positive as well. One can repeat the above calculation for any minor not in eq. (A.3), showing that all minors are positive if our initial minors in eq. (A.3) are positive. Note that we never mutate the edges that define the boundary of the n-gon. These are called frozen variables as they appear in
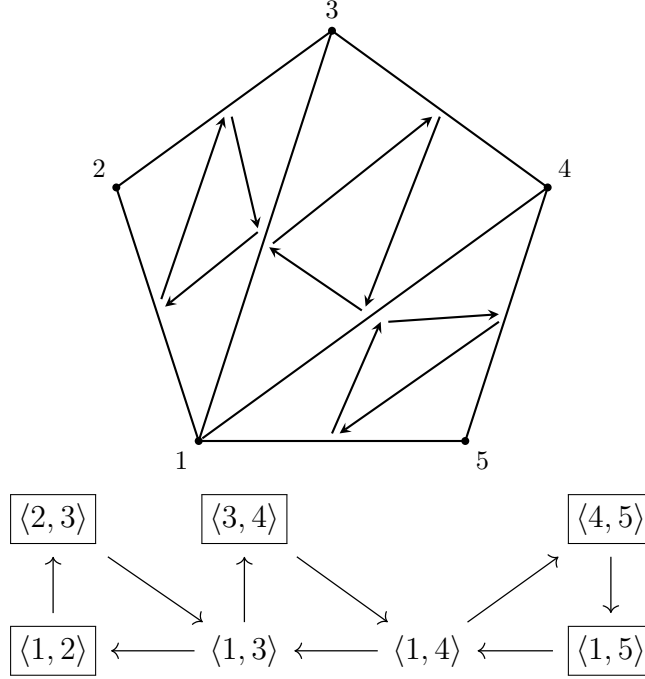
Figure A.3: A triangulation of a 5-gon and its dual quiver representation. The boxed elements in the quiver correspond to frozen nodes.

the Plucker relations but do not themselves mutate.

The above discussion focuses on the positivity of a $Gr(2,n)$ matrix. However, we will ultimately be interested in $Gr(4,n)/T$, where T acts on individual columns by a re-scaling:

$$Z_i^A \to t_i Z_i^A \ . \tag{A.6}$$

where i and A index the columns and rows respectively. Therefore, it is natural to consider the same question as above, except now for $Gr(2,n)/T$. Our minors, $\langle i,j \rangle$, are no longer suitable coordinates as they are not invariant under T. Instead, we must develop a new set of coordinates, $\hat{y}$-variables, for a given triangulation that are invariant under T transformations. Again consider the coordinates in eq. (A.3). Two natural combinations of minors invariant under T are

$$\hat{y}_1 = \frac{\langle 2,3 \rangle \langle 1,4 \rangle}{\langle 1,2 \rangle \langle 3,4 \rangle}, \quad \hat{y}_2 = \frac{\langle 3,4 \rangle \langle 1,5 \rangle}{\langle 1,3 \rangle \langle 4,5 \rangle} \ . \tag{A.7}$$

These variables form a natural set of coordinates on the compactified space $\overline{Gr(2,n)/T}$. To see their importance, lets interpret $\overline{Gr(2,n)/T}$ as the positive region of some manifold. Each triangulation, with its own $\hat{y}_i$ variables, corresponds to a different "corner" of $\overline{Gr(2,n)/T}$, as visualized for $n=5$ in fig. 1.1.

The above strategy of finding an initial "cluster" of coordinates and developing a sequence of coordinate transforms turns out to be very versatile. Generalizing beyond $Gr(2, n)$, one can systematically develop the notion of a cluster algebra. Instead of a triangulation, we associate to each cluster a quiver with exchange matrix $B_{i,j}$:

$$B_{i,j} = \begin{cases} n & \text{if there are } n \text{ arrows from } i \text{ to } j \\ -n & \text{if there are } n \text{ arrows from } j \text{ to } i \\ 0 & \text{if there are no arrows between } j \text{ and } i \end{cases} . \tag{A.8}$$

Each triangulation of an n-gon for $Gr(2, n)$ maps onto a triangulation in the following way

- Each edge in the n-gon triangulation corresponds to a node in the quiver. The edges corresponding to the boundary of the n-gon are frozen nodes that never mutate

- For each triangle in the n-gon triangulation, we draw a clock-wise orientated cycle in Q connecting the vertices associated with the bounding edges.

For example, a visualization of the quiver associated with the first triangulation in fig. A.2 is given in fig. A.3. Given a mutation, the minors generalizes to cluster variables that mutate as

$$\mu_k x_i = \begin{cases} \frac{1}{x_i}(\prod_{j \to i} x_j + \prod_{j \leftarrow i} x_j) & i = k \\ x_i & i \neq k \end{cases} \tag{A.9}$$

If we perform a mutation on node k, the quiver, and corresponding exchange matrix, mutate according to the rules

- Reverse all arrows going in or out of k,

- For each sub-path of the form $i \to k \to j$, add the arrow $i \to j$,

- Remove any two cycles that have formed.

One can explicitly check that eq. (A.9) and the preceding quiver mutation rules are a self consistent generalization of those given for $Gr(2, n)$. Finally, the $\hat{y}$ coordinates also have a natural generalization as

$$\hat{y}_i = \prod_j x_j^{-B_{i,j}}, \tag{A.10}$$

and mutate as

$$\mu_j \hat{y}_i = \begin{cases} \frac{1}{\hat{y}_i} & i = j \\ \hat{y}_i(1 + \hat{y}_j^{\text{Sign}(B_{i,j})})^{B_{i,j}} & i \neq j \end{cases} . \tag{A.11}$$

We will denote the positive space parameterized by x_i coordinates as $\mathcal{A}$ and the space parameterized by $\hat{y}_i$ coordinates as $\mathcal{X}$. The relation between $\mathcal{A}$ and $\mathcal{X}$ is still under active research and not completely understood.

Cluster algebras have many remarkable properties, such as the Laurent phenomenon. The cluster variable of any quiver can be written as a Laurent polynomial of x_i of some initial cluster. For example, consider the cluster algebra associated with $Gr(2,5)$. One can show that any $\langle i', j' \rangle$ can be written as a Laurent polynomial of $\langle i, j \rangle$ in eq. (A.3). To learn about other amazing properties of cluster algebras, the reader is referred to refs. [253, 254].

A.2   Differentiating x-variables with frozen nodes

Like $\hat{y}$-variables, x-variables will also obey additional relations when there are fewer frozen nodes. To see this, again consider the A_3 cluster algebra with initial quiver:

$$x_1 \longrightarrow x_2 \longleftarrow x_3 \ .$$

Without any frozen nodes, all x-variables in the cluster algebra are

$$
\begin{aligned}
\{ &x_1, \quad x_2, \quad x_3 \\
&\frac{x_2+1}{x_1}, \quad \frac{x_1 x_3 + x_2^2 + 2x_2 + 1}{x_1 x_2 x_3} \\
&\frac{x_2+1}{x_3}, \quad \frac{x_1 x_3 + x_2 + 1}{x_1 x_2} \\
&\frac{x_1 x_3 + x_2 + 1}{x_2 x_3}, \quad \frac{x_1 x_3 + 1}{x_2} \} \ .
\end{aligned}
\tag{A.12}
$$

The minimal multiplicative basis of the x-variables is rank 7:

$$
\begin{aligned}
\{ &x_1, \quad x_2, \quad x_3 \\
&x_2 + 1, \quad x_1 x_3 + x_2^2 + 2x_2 + 1, \\
&x_1 x_3 + 1, \quad x_1 x_3 + x_2 + 1 \} \ .
\end{aligned}
\tag{A.13}
$$

However, suppose we include the additional frozen node, z, so the initial quiver is now:

$$
\tag{A.14}
$$

$$z \qquad x_1 \longrightarrow x_2 \longleftarrow x_3 \ .$$

All x-variables in the cluster algebra are now

$$
\begin{aligned}
\{ z, \quad & x_1, \quad x_2, \quad x_3 \\
& \frac{x_2 + z}{x_1}, \quad \frac{x_1 x_3 z + z x_2^2 + (1 + z^2) x_2 + z}{x_1 x_2 x_3} \\
& \frac{x_2 z + 1}{x_3}, \quad \frac{x_1 x_3 z + x_2 + z}{x_1 x_2} \\
& \frac{x_1 x_3 + x_2 z + 1}{x_2 x_3}, \quad \frac{x_1 x_3 + 1}{x_2} \},
\end{aligned}
\tag{A.15}
$$

so the multiplicative basis for x-variables is now rank 10:

$$
\begin{aligned}
\{ z, \quad & x_1, \quad x_2, \quad x_3, \\
& x_2 + z, \quad x_1 x_3 z + z x_2^2 + (1 + z^2) x_2 + z, \\
& x_1 x_3 + 1, \quad x_1 x_3 z + x_2 + z, \\
& x_2 z + 1, \quad x_1 x_3 + x_2 z + 1 \}.
\end{aligned}
\tag{A.16}
$$

Comparing eqs. (A.12) and (A.15), one can clearly see that adding the frozen node, z, removes relations between the x-variables. Therefore, adding more frozen nodes disentangles the x-variables.

Remarkably, the frozen nodes of a principle quiver are enough to ensure that all the x-variables are maximally disentangled. To see this, note that the x-variables of a cluster algebra with *completely arbitrary frozen nodes* can be always be written in the form,

$$
x = x^{\vec{g}} F(\hat{y}_i) \times (\text{monomial of frozen variables}) ,
\tag{A.17}
$$

where $\vec{g}$ and $F(\hat{y}_i)$ are defined in eq. (2.8). The exact formula for computing the monomial of frozen x-variables is unimportant for our purposes and the reader is referred to appendix B of ref. [101] for details. From eq. (A.17), we see that the x-variable of a cluster algebra with arbitrary frozen nodes is the same as the x-variable of cluster algebra with a principal quiver up to a monomial of frozen x-variables. Therefore, one multiplicative basis of the $\hat{y}$-variables of a cluster algebra with arbitrary frozen nodes is the multiplicative basis of $\hat{y}$-variables of a cluster algebra with a principal quiver in addition to all the frozen x-variables.

To see this result explicitly, again consider the A_3 cluster algebra. We now consider a cluster algebra with the principal quiver:

$$
\begin{array}{ccccc}
y_1 & & y_2 & & y_3 \\
\downarrow & & \downarrow & & \downarrow \\
x_1 & \longrightarrow & x_2 & \longleftarrow & x_3 \; .
\end{array}
$$

A complete basis of all F-polynomials is

$$
\begin{aligned}
f_1 &= 1 + \hat{y}_1 \,, \\
f_2 &= 1 + \hat{y}_2 \,, \\
f_3 &= 1 + \hat{y}_3 \,, \\
f_4 &= 1 + \hat{y}_1 + \hat{y}_1 \hat{y}_2 \,, \\
f_5 &= 1 + \hat{y}_3 + \hat{y}_3 \hat{y}_2 \,, \\
f_6 &= 1 + \hat{y}_1 + \hat{y}_3 + \hat{y}_3 \hat{y}_1 + \hat{y}_3 \hat{y}_2 \hat{y}_1 \,.
\end{aligned}
\tag{A.18}
$$

We can now apply the basis in eq. (A.18) to the quiver in (A.14), where

$$
\hat{y}_1 = \frac{z}{x_2}, \quad \hat{y}_2 = x_1 x_3, \quad \hat{y}_3 = \frac{1}{z x_2} \,.
\tag{A.19}
$$

Substituting eq. (A.19) into eq. (A.18) and including the x-variables of the initial quiver in (A.14) yields the multiplicative basis

$$
\begin{aligned}
&\{ z, \ x_1, \ x_2, \ x_3 \,, \\
f_1 &= \frac{x_2 + z}{x_2} \,, \\
f_2 &= x_1 x_3 + 1 \,, \\
f_3 &= \frac{z x_2 + 1}{z x_2} \,, \\
f_4 &= \frac{x_1 x_3 z + x_2 + z}{x_2} \,, \\
f_5 &= \frac{x_1 x_3 + x_2 z + 1}{z x_2} \,, \\
f_6 &= \frac{z x_1 x_3 + z x_2^2 + (1 + z^2) x_2 + z}{z x_2^2} \} \,.
\end{aligned}
\tag{A.20}
$$

Eq. (A.20) corresponds to a complete multiplicative basis for the x-variables in eq. (A.15). A complete multiplicative basis for the $\hat{y}$-variables consists of the f_i in eq. (A.20), the $\hat{y}_i$ in eq. (A.19) and z.

A.3   Review: $A_{1,1}$ cluster algebra

In this appendix, we consider the cluster algebra and scattering diagram associated with the principal quiver,

$$
\begin{array}{ccc}
y_{-1} & & y_0 \\
\downarrow & & \downarrow \\
x_{-1} & \!\!\!\Longrightarrow\!\!\! & x_0 \ ,
\end{array}
$$

reviewing the results in refs. [36, 101, 102]. We perform repeated mutations on the nodes associated with x_{-1} and x_0, starting with the x_{-1} node,
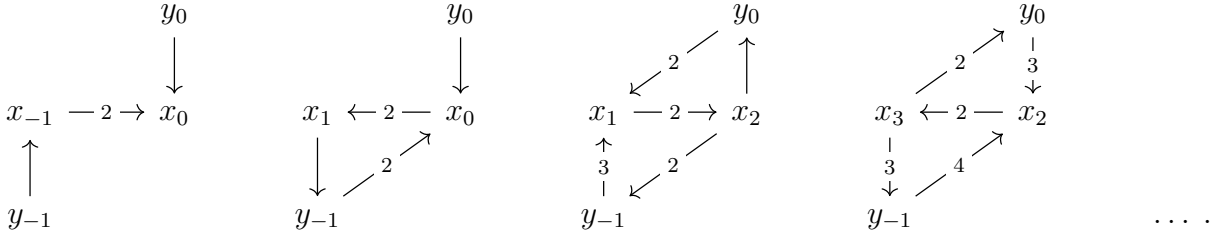
After a sequence of $2n$ mutations where $n > 0$, the quiver takes the form
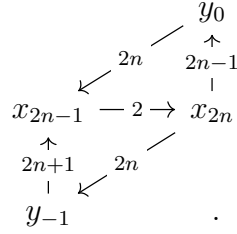
Using cluster mutations and the above representation of the quiver after $2n$ mutations, we defined a recursive solution for x_i in this model, finding:

$$
\begin{aligned}
x_{2n-1}x_{2n-3} &= \left(y_{-1}^{2n-1}y_0^{2n-2} + x_{2n-2}^2\right), \\
x_{2n}x_{2n-2} &= \left(y_{-1}^{2n}y_0^{2n-1} + x_{2n-1}^2\right).
\end{aligned}
\tag{A.21}
$$

This form of the mutation relations is still too complicated to solve analytically due to being inherently nonlinear. Instead, we identify a new variable,

$$
\mathcal{P} = \frac{y_{-1}}{x_{-1}x_0} + \frac{x_0}{x_{-1}} + \frac{x_{-1}y_{-1}y_0}{x_0} \ ,
\tag{A.22}
$$

such that

$$
x_{2n-1} = x_{2n-2}\mathcal{P} - x_{2n-3}\mathcal{F}, \quad \mathcal{F} = y_{-1}y_0 \ .
\tag{A.23}
$$
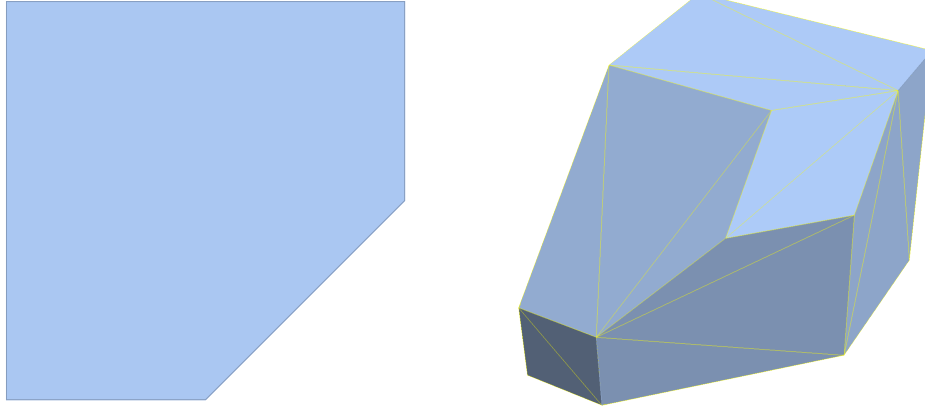
Figure A.4: Cluster polytopes corresponding to A_2 (left) and A_3 (right).

$\mathcal{P}$ is not an element of the cluster algebra, but a cluster-like variable associated with the limiting ray. For further discussion of $\mathcal{P}$, the reader is referred to ref. [36]. Only eq. (A.23) is important for our purposes, which one can explicitly check.

We can solve eq. (A.23) by first writing down the associated generating function:

$$G_{i>0}(t) = \frac{x_0 - x_{-1}\mathcal{F}t}{1 - \mathcal{P}t + \mathcal{F}t^2} = \sum_{n=0}^{\infty} x_i t^i \, , \tag{A.24}$$

and then finding a closed-form expression for the derivatives of $G_{n>0}(t)$:

$$x_i = \frac{1}{2^{i+2}}[(x_{-1} + B_+\sqrt{\triangle})(\mathcal{P} + \sqrt{\triangle})^{i+1} + (x_{-1} - B_+\sqrt{\triangle})(\mathcal{P} - \sqrt{\triangle})^{i+1}] \, ,$$
$$B_+ = \frac{2x_0 - x_{-1}\mathcal{P}}{\triangle} \, , \tag{A.25}$$
$$\triangle = \mathcal{P}^2 - 4\mathcal{F} \, .$$

Using our closed form expressions for x_i in eq. (A.25), it is trivial to calculate closed form expressions for $\hat{y}_i$ after 2n mutations:

$$\hat{y}_{2n-1} = y_0^{2n} y_{-1}^{2n+1} x_{2n}^{-2}, \quad \hat{y}_{2n} = y_0^{1-2n} y_{-1}^{-2n} x_{2n-1}^{2} \, . \tag{A.26}$$

A.4 Review: cluster polytopes

Instead of investigating the scattering diagram, much research has focused on a closely related object, *the cluster polytope*. Every scattering diagram is dual to a polytope where vertices correspond to cones, facets to g-vectors, and edges to walls. More concretely, one can define a polytope using

facet vectors:

$$\{Y \in \mathbb{P}^N | Y \cdot W_i \geq 0 \text{ for all } i\} \, . \tag{A.27}$$

For a cluster polytope, the facet vectors, W_i, match onto the g-vectors

$$W_i = (c_i, \vec{g}_i) \tag{A.28}$$

where the constants, c_i, are chosen such that the polytope has the correct vertex and facet structure. As an example, fig. A.4 shows the cluster polytopes associated with A_2 and A_3 [128]. The fan and polytope interpretation are equivalent and simply correspond to different visualizations of the same combinatorial data.

Given a set of tropical functions, f_i, an obvious question is how to derive the cluster polytope associated with the corresponding fan without calculating all the c_i in eq. (A.28). The answer is remarkably simple. For each f_i, we associate a corresponding polytope, P_i, by taking the convex hull of exponent vectors for each term. As an example, consider the following Laurent polynomials,

$$\begin{aligned} f_1 = 1 + x &\rightarrow \{(0,0), \ (0,1)\} \\ f_2 = 1 + x + xy &\rightarrow \{(0,0), \ (0,1), \ (1,1)\} \, , \end{aligned} \tag{A.29}$$

where we have listed the vertices of the corresponding polytopes. We then consider the Minkowski sum of all such polytopes. Alternatively, we simply take the product of all such f_i and find the associated P using the same procedure

$$f_1 f_2 = (1 + x)(1 + x + xy) \rightarrow \{(0,0), \ (1,0), \ (1,1), \ (2,0), \ (2,1)\} \, . \tag{A.30}$$

A proof of this procedure is provided in ref. [32].

A.5 Comparison to the origin clusters of ref. [102]

In this appendix, we compare our techniques and results to those of ref. [102]. The general computation strategy of ref. [102] revolved around studying clusters with quivers of the form
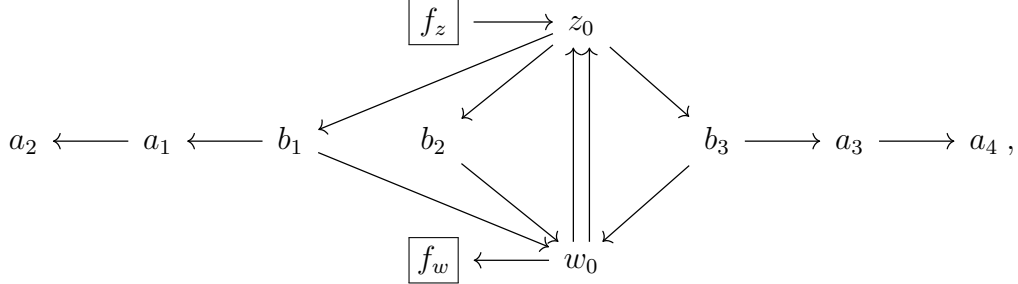
where we have suppressed all frozen variables disconnected from the $A_{1,1}$ subalgebra. Such clusters were called origin clusters. The authors then used the generating function of the $A_{1,1}$ subalgebra in eq. (A.25) to motivate three algebraic functions:

$$\frac{w_0 - B_w\sqrt{\triangle}}{w_0 + B_w\sqrt{\triangle}}, \quad \frac{z_0 - B_z\sqrt{\triangle}}{z_0 + B_z\sqrt{\triangle}}, \quad \frac{\mathcal{P} - \sqrt{\triangle}}{\mathcal{P} + \sqrt{\triangle}}, \tag{A.31}$$

where

$$z_1 = \frac{b_1 b_2 b_3 - f_w z_0^2}{w_0}, \quad w_1 = \frac{b_1 b_2 b_3 - f_z w_0^2}{z_0},$$

$$B_w = \frac{2w_1 - w_0 \mathcal{P}}{\triangle}, \quad B_z = \frac{2z_1 - z_0 \mathcal{P}}{\triangle}, \tag{A.32}$$

$$\mathcal{P} = \frac{f_z w_0 + z_1}{z_0}, \quad \triangle = \mathcal{P}^2 - 4 f_w f_z.$$

The multiplicative functions in eq. (A.31) are simply an alternative multiplicative basis for the $\hat{y}_{\gamma_i}^{\pm}$ of the $A_{1,1}$ subalgebra found in section 2.2.3. The authors ultimately studied 32 origin clusters for each limiting ray apparently relevant for $\mathcal{N} = 4$ pSYM.

Including the rational x-variables associated with the origin cluster, this method ultimately yields a multiplicative basis for the $\hat{y}_{\gamma_i}^0$ of the two asymptotic chambers associated with each origin cluster. Mutating w_0 (z_0) first leads to the first (second) asymptotic chamber after an infinite number of mutations on the $A_{1,1}$ subalgebra. Notably, this technique only allows one to probe the $\hat{y}_{\gamma_i}^0$ of asymptotic chambers adjacent to a limiting wall. To see this, note that the generalized mutation identified in section 2.2.3 applies to the $A_{1,1}$ subalgebra when asymptotically close to the limiting ray. Since a generalized mutation corresponds to a limiting wall, the asymptotic chamber must be adjacent to a limiting wall. However, many asymptotic chambers are not adjacent to a limiting

wall. For example, consider the asymptotic scattering diagram in fig. 2.7, which is associated with the limiting ray of the $A_{2,1}$ cluster algebra. There are two asymptotic chambers, C_2 and C_5, that are not adjacent to the limiting wall. To probe the $\hat{y}_{\gamma_i}^0$ of such asymptotic chambers, one must either find a generating function for the sequences of cones that do not explicitly contain an $A_{1,1}$ sub-algebra or use the wall-crossing techniques developed in this paper. Excluding these asymptotic chambers when calculating the multiplicative basis for $\hat{y}_{\gamma_i}$ leads to a truncated asymptotic symbol alphabet. For example, excluding asymptotic chambers C_2 and C_5 of $A_{2,1}$ leads to the truncated alphabet,

$$\hat{y}_{\gamma_1}^0, \ \hat{y}_{\gamma_2}^0, \ \hat{y}_{\gamma_3}^0, \ \frac{1 + \hat{y}_{\gamma_1}^0 \hat{y}_{\gamma_2}^0 \hat{y}_{\gamma_3}^0}{1 + \hat{y}_{\gamma_1}^0}, \ 1 - \hat{y}_{\gamma_2}^0 \hat{y}_{\gamma_3}^0 \ , \tag{A.33}$$

in comparison to the full alphabet in eq. (2.53).

Interestingly, the $\hat{y}_{\gamma_i}$ of asymptotic chambers adjacent to the limiting wall are enough to derive the algebraic letters that have appeared in explicit computations. Rather, the known 18 algebraic letters that appear in the 8-point 2-loop NHMV amplitude are monomials of algebraic variables in the form of eq. (A.31). However, there is no obvious reason why additional algebraic letters could not appear at higher loop orders.

APPENDIX B

Explicit Expressions for Generalized KLT Double Copy

B.1 Pions, Special Galileons and Born-Infeld Photons

In Section 3.5 we discuss in detail which higher-derivative Yang-Mills operators that can be double-copied and what corrections they map to in the resulting theory of gravity. This is of course not the only effective field theory that can be double-copied via the formalism introduced in Section 3.2. A far simpler theory is a non-linear sigma model of pions, also known as chiral perturbation theory, whose 4-point amplitude at leading order is

$$\mathcal{A}_4^0[1234] = \frac{t}{f_\pi^2}, \tag{B.1}$$

where f_π is the pion decay constant.

To find double-copy-compatible corrections, we start with an ansatz[1],

$$\mathcal{A}_4[1234] = \frac{t}{f_\pi^2} + \frac{b_{1,1}s^2 + b_{1,2}st + b_{1,3}t^2}{\Lambda^4} + \frac{b_{2,1}s^3 + b_{2,2}s^2t + b_{2,3}st^2 + b_{2,4}t^3}{\Lambda^6}$$
$$+ \frac{b_{3,1}s^4 + b_{3,2}s^3t + b_{3,3}s^2t^2 + b_{3,4}st^3 + b_{3,5}t^4}{\Lambda^8} + O\left(\frac{1}{\Lambda^{10}}\right), \tag{B.2}$$

with appropriate superscripts on the parameters $b_{i,j}$ for the left and right KKBCJ-compatible amplitudes.

Since we are dealing with a scalar theory, every other color-ordering is a simple relabeling of (B.2). As a result the (right) KKBCJ relations of Section 3.4 can be rewritten as consistency

---

[1]While it is *a priori* possible that the amplitude begins with a constant contribution at order Λ^0, such a term is forbidden by the leading order BCJ relations.

conditions on the (right) amplitude such as,

$$\mathcal{A}_4[1234] = m[1234|1432]\, m[1243|1432]^{-1}\mathcal{A}_4[1243]\,, \tag{B.3}$$

where $\mathcal{A}_4[1243]$ is given by a $3 \leftrightarrow 4$ relabelling of $\mathcal{A}_4[1234]$.

Solving such consistency conditions using $m[\alpha|\beta]$ given in Section 3.4, gives us the final NLSM amplitudes,

$$\mathcal{A}_4^{\mathrm{R}}[1234] = \frac{t}{(f_\pi^{\mathrm{R}})^2} + \frac{a_{1,1}stu}{(f_\pi^{\mathrm{R}})^2\, g^2\Lambda^4} + \frac{b_{2,4}^{\mathrm{R}}\, t(s^2 + t^2 + u^2)}{2\Lambda^6} - \frac{b_{3,3}^{\mathrm{R}}\, st^2u}{\Lambda^8} + O\left(\frac{1}{\Lambda^{10}}\right),\tag{B.4}$$

$$\mathcal{A}_4^{\mathrm{L}}[1234] = \frac{t}{(f_\pi^{\mathrm{L}})^2} + \frac{(a_{1,1} - a_{1,0})stu}{(f_\pi^{\mathrm{L}})^2\, g^2\Lambda^4} + \frac{b_{2,4}^{\mathrm{L}}\, t(s^2 + t^2 + u^2)}{2\Lambda^6} - \frac{b_{3,3}^{\mathrm{L}}\, st^2u}{\Lambda^8} + O\left(\frac{1}{\Lambda^{10}}\right).\tag{B.5}$$

Note that all corrections that are quadratic in Mandelstam variables are disallowed. This is important in Born-Infeld theory as we discuss below.

To construct Born-Infeld amplitudes in all helicity sectors, we will also need the self-dual, next-to-self-dual and MHV Yang-Mills amplitudes that are compatible with the KLT kernel developed in Section 3.4. These are given in (3.95), (3.96) and (3.85).

We now construct higher derivative corrections to the special Galileon and Born-Infeld amplitudes,

$$\mathcal{M}_4^{\mathrm{sGal}}(1234) = -\frac{stu}{(f_\pi^{\mathrm{L}})^2\,(f_\pi^{\mathrm{R}})^2\, g} - \frac{(b_{2,4}^{\mathrm{L}}\,(f_\pi^{\mathrm{L}})^2 + b_{2,4}^{\mathrm{R}}\,(f_\pi^{\mathrm{R}})^2)stu(s^2 + t^2 + u^2)}{2\,(f_\pi^{\mathrm{L}})^2\,(f_\pi^{\mathrm{R}})^2\, g^2\,\Lambda^6}$$

$$+ \frac{((b_{3,3}^{\mathrm{L}}\,(f_\pi^{\mathrm{L}})^2 + b_{3,3}^{\mathrm{R}}\,(f_\pi^{\mathrm{R}})^2)g^2 + a_{2,0}\Lambda^4)\, s^2t^2u^2}{(f_\pi^{\mathrm{L}})^2\,(f_\pi^{\mathrm{R}})^2\, g^4\,\Lambda^8} + O\left(\frac{1}{\Lambda^{10}}\right),\tag{B.6}$$

$$\mathcal{M}_4^{\mathrm{BI}}(1^+2^+3^-4^-) = [12]^2\langle34\rangle^2\left[-\frac{(g_{\mathrm{YM}}^{\mathrm{R}})^2}{(f_\pi^{\mathrm{L}})^2\, g^2} + \frac{(g_{F^3}^{\mathrm{R}})^2\, tu}{(f_\pi^{\mathrm{L}})^2\, g^2\Lambda^4} - \frac{(g_{\mathrm{YM}}^{\mathrm{R}})^2\, b_{2,4}^{\mathrm{L}}\,(s^2 + t^2 + u^2)}{2g^2\Lambda^6}\right.$$

$$\left.- \frac{\left(e_{3,1}^{R}\, g^2 - a_{2,0}\,(g_{\mathrm{YM}}^{\mathrm{R}})^2\right)stu}{(f_\pi^{\mathrm{L}})^2\, g^4\Lambda^6} + O\left(\frac{1}{\Lambda^8}\right)\right],\tag{B.7}$$

$$\mathcal{M}_4^{\mathrm{BI}}(1^+2^+3^+4^-) = [12]^2[3|1|4\rangle^2\left[-\frac{g_{F^3}^{\mathrm{R}}g_{\mathrm{YM}}^{\mathrm{R}}}{(f_\pi^{\mathrm{L}})^2\, g^2\Lambda^2} - \frac{g_{F^3}^{\mathrm{R}}\, g_{\mathrm{YM}}^{\mathrm{R}}\, b_{2,4}^{\mathrm{L}}\,(s^2 + t^2 + u^2)}{2g^2\Lambda^8}\right.$$

$$\left.- \frac{(c_1^{R}g^2 - a_{2,0}g_{F^3}^{\mathrm{R}}g_{\mathrm{YM}}^{\mathrm{R}})stu}{(f_\pi^{\mathrm{L}})^2\, g^4\,\Lambda^8} + O\left(\frac{1}{\Lambda^{10}}\right)\right],\tag{B.8}$$

$$\mathcal{M}_4^{\mathrm{BI}}(1^+2^+3^+4^+) = \frac{s^2tu^2}{\langle12\rangle\langle23\rangle\langle34\rangle\langle41\rangle}\left[-\frac{2g_{F^3}^{\mathrm{R}}g_{\mathrm{YM}}^{\mathrm{R}}}{(f_\pi^{\mathrm{L}})^2\, g^2\Lambda^2} + \frac{(d_1^{R}g^2 - 4a_{1,1}g_{F^3}^{\mathrm{R}}g_{\mathrm{YM}}^{\mathrm{R}})\,(s^2 + t^2 + u^2)}{4\,(f_\pi^{\mathrm{L}})^2\, g^4\Lambda^6}\right]$$

$$+ O\left(\frac{1}{\Lambda^8}\right).\tag{B.9}$$

One of the applications of this analysis is determining whether or not duality symmetry is anomalous. Born-Infeld theory is known to have an electromagnetic duality at tree-level which manifests on the scattering amplitudes as an optical helicity conservation rule. In order for the symmetry to be non-anomalous at 1-loop, duality-violating amplitudes should be removable by the addition of local counterterms for e.g. a Λ^{-6} counterterm at 4-point. This was found to be true [257], though the 1-loop regularization scheme was incompatible with the double-copy, i.e. the local counterterms necessary to restore the symmetry were not produced by the double-copy [167]. It is interesting that the more nuanced approach to higher-derivative corrections in the double-copy explored in this paper results in (B.8) and (B.9) which also lack Λ^{-6} corrections, in keeping with the previous analysis.

At 5-point, higher-derivative corrections added to the kernel do not change a previously noted [135] result that the first BCJ-compatible correction to χPT occurs at 14-derivative order. In particular, this means that the WZW term is incompatible with the generalized KKBCJ constraints.

B.2 Analytic Expressions for the 5-Point Bootstrap

We arrange the 24×24 matrix $m[a|b]$ according to the following ordering of the permutations of momenta $2, 3, 4, 5$:

$$\begin{aligned}
\{&12345, 12354, 12435, 12453, 12534, 12543, 13245, 13254, \\
&13425, 13452, 13524, 13542, 14235, 14253, 14325, 14352, \\
&14523, 14532, 15234, 15243, 15324, 15342, 15423, 15432\}\,.
\end{aligned} \tag{B.10}$$

As described in Section 3.6.1, the 5-point bootstrap equations can be solved for g_4-g_8 in terms of g_1, g_3, and g_3. The following are the results, we indicate which minors are set to set to zero to obtain each relation using the notation that

$$\text{Minor}_3[r_1, r_2, r_3; c_1, c_2, c_3], \tag{B.11}$$

denotes the 3×3 minor with rows r_1, r_2, r_3 and columns c_1, c_2, c_3 with labels refering to the basis (B.10). We use cyclic symmetry of g_1 to simplify the results as well as momentum relabeling.

From $\text{Minor}_3[1, 2, 3; 1, 2, 4]$ we get

$$\begin{aligned}
g_4[12345] = &\Big(g_1[12345]g_1[12354]g_2[12534] - g_2[12345]g_2[12354]g_2[12534] \\
&\quad - g_1[12345]g_2[41253]g_3[12354] + g_2[12345]g_3[12345]g_3[12534]\Big) \\
&\Big(g_1[12354]g_3[12534] - g_2[12354]g_2[41253]\Big)^{-1}.
\end{aligned} \tag{B.12}$$

From $\text{Minor}_3[1, 2, 7; 1, 2, 3]$ we get

$$
\begin{aligned}
g_5[12345] =& \Big(g_1[13245]g_1[13254]g_3[51234] - g_1[13254]g_2[45123]g_2[51324] \\
& - g_2[13245]g_2[13254]g_3[51234] + g_2[13245]g_2[45123]g_3[25413] \Big) \\
& \Big(g_1[13245]g_3[25413] - g_2[13254]g_2[51324] \Big)^{-1}.
\end{aligned}
\tag{B.13}
$$

From $\text{Minor}_3[1, 2, 3; 1, 2, 11]$ we get

$$
\begin{aligned}
g_6[12345] =& \Big(g_1[12345]g_1[12354]g_3[35124] - g_1[12345]g_3[12435]g_3[41235] \\
& - g_2[12345]g_2[12354]g_3[35124] + g_2[12345]g_2[51243]g_3[41235] \Big) \\
& \Big(g_1[12354]g_2[51243] - g_2[12354]g_3[12435] \Big)^{-1}.
\end{aligned}
\tag{B.14}
$$

From $\text{Minor}_3[1, 2, 3; 1, 2, 14]$ we get

$$
\begin{aligned}
g_7[12345] =& \Big(g_1[12345]g_1[12354]g_5[12435] - g_1[12345]g_3[12435]g_5[23541] \\
& - g_2[12345]g_2[12354]g_5[12435] + g_2[12345]g_2[51243]g_5[23541] \Big) \\
& \Big(g_1[12354]g_2[51243] - g_2[12354]g_3[12435] \Big)^{-1}.
\end{aligned}
\tag{B.15}
$$

where g_5 is as given in (B.13). From $\text{Minor}_3[1, 2, 3; 1, 2, 24]$ we get

$$
\begin{aligned}
g_8[12345] =& \Big(g_1[12345]g_1[12354]g_4[43512] - g_1[12345]g_3[12435]g_4[54123] \\
& - g_2[12345]g_2[12354]g_4[43512] + g_2[12345]g_2[51243]g_4[54123] \Big) \\
& \Big(g_1[12354]g_2[51243] - g_2[12354]g_3[12435] \Big)^{-1}.
\end{aligned}
\tag{B.16}
$$

where g_4 is as given in (B.12).

The perturbative solutions for the g functions are

$$
\begin{aligned}
g_1[12345] =& g^3 \left(\frac{1}{s_{12}s_{34}} + \frac{1}{s_{23}s_{45}} + \frac{1}{s_{34}s_{51}} + \frac{1}{s_{45}s_{12}} + \frac{1}{s_{51}s_{23}} \right) \\
& + \frac{g}{\Lambda^4}(a_{1,0} - 2a_{1,1}) \left(\frac{s_{35}}{s_{12}} + \frac{s_{41}}{s_{23}} + \frac{s_{13}}{s_{45}} + \frac{s_{24}}{s_{51}} + \frac{s_{52}}{s_{34}} + 1 \right) \\
& - \frac{g a_{2,0}}{\Lambda^6} \left(\frac{s_{35}^2}{s_{12}} + \frac{s_{41}^2}{s_{23}} + \frac{s_{13}^2}{s_{45}} + \frac{s_{24}^2}{s_{51}} + \frac{s_{52}^2}{s_{34}} \right) + O\left(\frac{1}{\Lambda^5} \right),
\end{aligned}
\tag{B.17}
$$
$$
g_2[12345] = g^3 \left(-\frac{1}{s_{12}s_{45}} - \frac{1}{s_{23}s_{45}} \right)
$$

$$+ \frac{g}{\Lambda^4} \left((2a_{1,1} - a_{1,0}) \frac{s_{13}}{s_{45}} + a_{1,0} \left(\frac{s_{35}}{s_{12}} + \frac{s_{14}}{s_{23}} \right) + a_{1,1} \left(\frac{s_{45}}{s_{12}} + \frac{s_{45}}{s_{23}} - 2 \right) \right)$$

$$+ \frac{ga_{2,0}}{\Lambda^6} \left(\frac{s_{13}^2}{s_{45}} - \frac{s_{14}s_{15}}{s_{23}} - \frac{s_{34}s_{35}}{s_{12}} - 2s_{13} \right) + O\left(\frac{1}{\Lambda^5} \right), \tag{B.18}$$

$$g_3[12345] = g^3 \left(-\frac{1}{s_{12}s_{45}} \right)$$

$$+ \frac{g}{\Lambda^4} \left(a_{1,0} \left(\frac{s_{13}}{s_{45}} + \frac{s_{35}}{s_{12}} - 1 \right) + a_{1,1} \left(\frac{s_{45}}{s_{12}} + \frac{s_{12}}{s_{45}} \right) \right)$$

$$+ \frac{ga_{2,0}}{\Lambda^6} \left(-\frac{s_{13}s_{23}}{s_{45}} - \frac{s_{34}s_{35}}{s_{12}} + s_{14} + s_{25} \right) + O\left(\frac{1}{\Lambda^5} \right), \tag{B.19}$$

$$g_4[12345] = g^3 \left(\frac{1}{s_{12}s_{45}} + \frac{1}{s_{12}s_{34}} \right)$$

$$+ \frac{g}{\Lambda^4} \left((a_{1,0} - 2a_{1,1}) \frac{s_{35}}{s_{12}} + a_{1,0} \left(-\frac{s_{13}}{s_{45}} - \frac{s_{25}}{s_{34}} \right) + a_{1,1} \left(-\frac{s_{12}}{s_{45}} - \frac{s_{12}}{s_{34}} + 2 \right) \right)$$

$$+ \frac{ga_{2,0}}{\Lambda^6} \left(\frac{s_{15}s_{25}}{s_{34}} + \frac{s_{13}s_{23}}{s_{45}} - \frac{s_{35}^2}{s_{12}} + 2s_{35} \right) + O\left(\frac{1}{\Lambda^5} \right), \tag{B.20}$$

$$g_5[12345] = g^3 \left(\frac{1}{s_{23}s_{45}} \right)$$

$$+ \frac{g}{\Lambda^4} \left(a_{1,0} \left(1 - \frac{s_{14}}{s_{23}} - \frac{s_{13}}{s_{45}} \right) + a_{1,1} \left(-\frac{s_{23}}{s_{45}} - \frac{s_{45}}{s_{23}} \right) \right)$$

$$+ \frac{ga_{2,0}}{\Lambda^6} \left(\frac{s_{14}s_{45}}{s_{23}} - \frac{s_{13}s_{12}}{s_{45}} + \frac{s_{14}^2}{s_{23}} + s_{12} + 2s_{24} \right) + O\left(\frac{1}{\Lambda^5} \right), \tag{B.21}$$

$$g_6[12345] = \frac{g}{\Lambda^4} a_{1,0} + \frac{ga_{2,0}}{\Lambda^6} \left(s_{13} + 2s_{14} - s_{23} + s_{24} \right) + O\left(\frac{1}{\Lambda^5} \right), \tag{B.22}$$

$$g_7[12345] = -\frac{g}{\Lambda^4} a_{1,0} - \frac{ga_{2,0}}{\Lambda^6} \left(s_{13} + 2s_{14} - s_{23} + s_{24} \right) + O\left(\frac{1}{\Lambda^5} \right), \tag{B.23}$$

$$g_8[12345] = g^3 \left(\frac{1}{s_{12}s_{34}} + \frac{1}{s_{23}s_{45}} + \frac{1}{s_{34}s_{51}} + \frac{1}{s_{45}s_{12}} + \frac{1}{s_{51}s_{23}} \right)$$

$$+ \frac{g}{\Lambda^4} (a_{1,0} - 2a_{1,1}) \left(\frac{s_{35}}{s_{12}} + \frac{s_{41}}{s_{23}} + \frac{s_{13}}{s_{45}} + \frac{s_{24}}{s_{51}} + \frac{s_{52}}{s_{34}} + 1 \right)$$

$$- \frac{ga_{2,0}}{\Lambda^6} \left(\frac{s_{35}^2}{s_{12}} + \frac{s_{41}^2}{s_{23}} + \frac{s_{13}^2}{s_{45}} + \frac{s_{24}^2}{s_{51}} + \frac{s_{52}^2}{s_{34}} \right) + O\left(\frac{1}{\Lambda^5} \right). \tag{B.24}$$

APPENDIX C

Background on Anti-de Sitter

C.1   Embedding space formalism

The AdS_{d+1} background can be realized as a space-like hypersurface in the $(d+2)$ dimensional flat spacetime $\mathbb{R}^{d+1,1}$. Under Cartesian coordinates $X^A = (X^{\mathsf{a}}, X^d, X^{d+1})$, the hypersurface is given by the equation

$$(X^0)^2 + (X^1)^2 + \cdots + (X^{d-1})^2 + (X^d)^2 - (X^{d+1})^2 = -R^2\,. \tag{C.1}$$

The Poincaré coordinates of AdS_{d+1} are given by the following parametrization,

$$X^{\mathsf{a}} = \frac{R}{z} x^{\mathsf{a}}\,, \qquad X^d = \frac{R}{z} \frac{1 - x^2 - z^2}{2}\,, \qquad X^{d+1} = \frac{R}{z} \frac{1 + x^2 + z^2}{2}\,, \tag{C.2}$$

such that for $R = \text{constant}$ we have

$$ds^2_{\text{AdS}_{d+1}} = g_{\mu\nu} dx^\mu dx^\nu = \frac{R^2}{z^2} \left(dz^2 + dx_{\mathsf{a}} dx^{\mathsf{a}} \right)\,. \tag{C.3}$$

We can also view eq. (C.2) as a coordinate transformation from the Cartesian coorinates X^A to the coordinates (R, z, x^{a}), under which metric of $\mathbb{R}^{d+1,1}$ becomes

$$ds^2_{\mathbb{R}^{2,d}} = -dR^2 + ds^2_{\text{AdS}_{d+1}}\,. \tag{C.4}$$

In fact, (R, z, x^{a}) are Gaussian normal coordinates adapted to the AdS hypersurface and the $g_{\mu\nu}$ in eq. (C.3) is the induced metric.

When we study a scalar field ϕ on AdS_{d+1}, it is convenient to extend its definition to the entire embedding space. However, we need to make sure that the dynamics does not depend on the

variation normal to the AdS hypersurface. It is not difficult to show that

$$\eta^{AB}\partial_A\phi\partial_B\phi = -(\partial_R\phi)^2 + g^{\mu\nu}\partial_\mu\phi\partial_\nu\phi\,, \qquad \frac{1}{R}X^A\partial_A\phi = \partial_R\phi\,. \tag{C.5}$$

We can thus define

$$G_{AB} = \eta_{AB} - \frac{X_A X_B}{X^2} = g^{\mu\nu}\frac{\partial X_A}{\partial x^\mu}\frac{\partial X_B}{\partial x^\nu}\,, \tag{C.6}$$

such that

$$G^{AB}\partial_A\phi\partial_B\phi = g^{\mu\nu}\partial_\mu\phi\partial_\nu\phi\,. \tag{C.7}$$

One can also prove that the AdS Laplacian is given by

$$\partial_A(G^{AB}\partial_B) = -\frac{1}{2}D_X^2 = \nabla^2_{\text{AdS}}\,. \tag{C.8}$$

The matrix form of G_{AB} under the (R, z, x^{a}) coordinates is

$$G_{AB} \xrightarrow{\text{transformation (C.2)}} \begin{pmatrix} 0 & 0 \\ 0 & g_{\mu\nu} \end{pmatrix}\,, \tag{C.9}$$

namely, G^{AB} is indeed a projector to AdS$_{d+1}$. One can easily show that G_{AB} is idempotent and transverse to the normal vector X^A,

$$G_A{}^B G_B{}^C = G_A{}^C\,, \qquad G_{AB}X^B = 0\,. \tag{C.10}$$

Geometrically, G_{AB} is the first fundamental form associated to the hypersurface (C.1). From now on, we fix $R = 1$ for the AdS hypersurface, such that the AdS integration measure becomes

$$\int_{\text{AdS}} dX \equiv \int_{\text{AdS}} \frac{\delta(R-1)R^{d+1}dRdzd^d x}{z^{d+1}} = \int_{\text{AdS}} \frac{dzdx^d}{z^{d+1}}\,. \tag{C.11}$$

Thus we can perform integration-by-parts for $\partial/\partial X^A$ if it appears in the integrand as $\frac{\partial}{\partial X^A}(G^{AB}\cdots)$ or $G^{BA}\frac{\partial}{\partial X^A}(\cdots)$, since the projector G^{AB} removes $\frac{\partial}{\partial R}$ so the measure remains invariant.

A tensor $H_{A_1 A_2 \ldots A_n}$ in the embedding space defines a tensor on AdS if it is *transverse* to the AdS hypersurface,

$$X^{A_i} H_{A_1 A_2 \ldots A_n} = 0\,, \qquad 1 \leqslant i \leqslant n\,. \tag{C.12}$$

174

The AdS tensor can be recovered through the projection

$$h_{\mu_1\mu_2...\mu_n} = \frac{\partial X^{A_1}}{\partial x^{\mu_1}} \frac{\partial X^{A_2}}{\partial x^{\mu_2}} \cdots \frac{\partial X^{A_n}}{\partial x^{\mu_n}} H_{A_1 A_2...A_n}. \tag{C.13}$$

From this equation and the relation (C.6) between $g_{\mu\nu}$ and G_{AB}, we can show that the contraction between two AdS tensors can be uplifted into the embedding space,

$$h_{\mu_1\mu_2...\mu_n} g^{\mu_i\nu_j} f_{\nu_1\nu_2...\nu_m} = H_{A_1 A_2...A_n} G^{A_i B_j} F_{B_1 B_2...B_m} = H_{A_1 A_2...A_n} \eta^{A_i B_j} F_{B_1 B_2...B_m}, \tag{C.14}$$

where the second equality is due to the transversality. Conditions like being symmetric and traceless of an AdS tensor can be directly imposed on its embedding space uplift. A more formal discussion on this topic can be found in ref. [229].

The conformal boundary of AdS is located at $z \to 0$. We can represent a boundary point x_i^{a} by a projective null vector in the embedding space,

$$P_i = \left(x_i^{\mathsf{a}}, \frac{1 - x_i^2}{2}, \frac{1 + x_i^2}{2}\right). \tag{C.15}$$

Obviously we have $P_i^2 = 0$ and we identify $P_i \sim \lambda P_k$. A polarization vector ϵ_i^{a} on the boundary can also be represented in the embedding space,

$$Z_i = \left(\epsilon_i^{\mathsf{a}}, -\epsilon_i \cdot x_i, \epsilon_i \cdot x_i\right), \tag{C.16}$$

such that $P_i \cdot Z_i = 0$ and $Z_i \cdot Z_i = \epsilon_i^2 = 0$. A tensor current $F_{A_1 A_2...A_n}(P)$ defined on the null cone $P^2 = 0$ is physical only if it is homogeneous and transverse,

$$F_{A_1 A_2...A_n}(\lambda P) = \lambda^{-\Delta} F_{A_1 A_2...A_n}(P), \qquad P^{A_i} F_{A_1 A_2...A_n}(P) = 0, \quad 1 \leqslant i \leqslant n. \tag{C.17}$$

Finally, we list a few useful relations that connect the embedding space and physical space expressions,

$$\begin{aligned} -2X \cdot P_i &= z + z^{-1}(x - x_i)^2, & -2P_i \cdot P_j &= (x_i - x_j)^2, \\ P_i \cdot Z_j &= \epsilon_j \cdot (x_i - x_j), & Z_i \cdot Z_j &= \epsilon_i \cdot \epsilon_j, \end{aligned} \tag{C.18}$$

where X is a bulk point defined as in eq. (C.2).

C.2 Contact diagrams in AdS

Contact diagrams of scalar operators play a crucial role in flat space scattering amplitudes. Crucially, the delta function that imposes momentum conservation on an n-point scattering amplitudes arises from the contact diagram of an n-point scalar vertex

$$
\begin{aligned}
\mathcal{A}_{\text{contact}}^{\text{flat}} &= \int d^d x \prod_i e^{ip_i x} \\
&= \delta^d \left(\sum_i p_i^\mu \right)
\end{aligned}
\tag{C.19}
$$

The contact diagrams of n-point scalar vertex operators play an analogous role in AdS, giving the AdS analog of the flat space delta function. The contact diagram associated with the vertex $\prod_i \phi_i$ in AdS is

$$
\mathcal{A}_{\text{contact}}^n = \left(\prod_{i=1}^n \frac{\Gamma(\Delta_i)}{2\pi^{d/2}\Gamma(\Delta_i - d/2 + 1)} \right) D_{\Delta_1 \dots \Delta_n}
\tag{C.20}
$$

where

$$
D_{\Delta_1 \dots \Delta_n} = \int_{\text{AdS}} dX \prod_{i=1}^n \frac{1}{(-2P_i \cdot X)^{\Delta_i}}
\tag{C.21}
$$

is the D-function. Any tree-level position space correlator in AdS will be a polynomial in D-functions, Z-variables and P-variables. Similar to how all flat space scattering amplitudes contain a universal momentum conserving delta function, each term in the polynomial expansion of the position space correlator contains its own D-function. A major challenge for evaluating position space correlators in AdS is finding representations of D-functions amiable to numeric approximation.

C.2.1 Three-point D-functions

The D-functions that appear in three-point correlators can be integrated directly:

$$
\begin{aligned}
D_{\Delta_1 \Delta_2 \Delta_3} &= \int_{\text{AdS}} dX \prod_{i=1}^3 \frac{1}{(-2P_i \cdot X)^{\Delta_i}} \\
&= \frac{\pi^{d/2}}{2 \prod_i \Gamma(\Delta_i)} \Gamma\left(\frac{\Delta_1 + \Delta_2 + \Delta_3 - d}{2} \right) \prod_{i<j} \frac{\Gamma(\delta_{ij})}{(-2P_i \cdot P_j)^{\delta_{ij}}} \\
\delta_{ij} &= \frac{1}{2}(\Delta_i + \Delta_j - \Delta_k) \, .
\end{aligned}
\tag{C.22}
$$

The three-point D-function is the one which has a rational dependence on coordinates; higher point D-functions are rather non-trivial functions.

C.2.2   Exact solution of four-point D-functions

In this section, we review a derivation of an exact solution to the four-point D-function in terms of derivatives of polylogarithms. Advantages (and disadvantages) of alternative methods are discussed at the end.

To find a numerically tractable representation of eq. (C.21), we first rewrote the D-function into a Feynman parameterization:

$$D_{\Delta_1,\Delta_2,\Delta_3,\Delta_4} = \frac{\pi^{d/2}\Gamma(\frac{\Sigma-d}{2})\Gamma(\frac{\Sigma}{2})}{2\prod_i \Gamma(\Delta_i)} \int \frac{\prod_j \alpha_j^{\Delta_j-1}\delta(\sum_i \alpha_i - 1)}{(\sum_{k,l}\alpha_k\alpha_l P_{k,l})^{\Sigma/2}}, \tag{C.23}$$

where $\Sigma = \Delta_1 + \Delta_2 + \Delta_3 + \Delta_4$. Our goal is to find an exact solution for the integral in eq. (C.23) that can be used for numerical analysis in Mathematica. We first solve for the integral in eq. (C.23) for the simplest case when $\Delta_i = 1$ for all i's, which we denote as $B(P_{ij})$. It is nothing but the four-mass box integral [53, 258],

$$
\begin{aligned}
B(P_{ij}) &= \int \frac{\prod_j d\alpha_j \delta(\sum_i \alpha_i - 1)}{\left(\sum_{k,l}\alpha_k\alpha_l P_{k,l}\right)} \\
&= \frac{1}{\sqrt{\Delta'}}\left[\frac{1}{2}\log\left(\frac{u_+u_-}{(1-u_+)^2(1-u_-)^2}\right)\log\frac{u_+}{u_-} \right. \\
&\quad \left. - \mathrm{Li}_2(1-u_+) + \mathrm{Li}_2(1-u_-) - \mathrm{Li}_2\left(1-\frac{1}{u_-}\right) + \mathrm{Li}_2\left(1-\frac{1}{u_+}\right)\right],
\end{aligned}
\tag{C.24}
$$

where

$$\Delta' = X^2 + Y^2 + Z^2 - 2XY - 2YZ - 2ZX, \qquad X = P_{12}P_{34}, \qquad Y = P_{13}P_{24},$$

$$u_\pm = \frac{Y+X-Z\pm\sqrt{\Delta'}}{2Y}, \qquad\qquad\qquad Z = P_{14}P_{23}. \tag{C.25}$$

Note that eq. (C.24) is simply the standard four-mass box integral whose solution has been known for 20 odd years.[1] We then identify a simply relation between derivatives of $B(P_{ij})$ and

---

[1] The same integral was evaluated in eq. (39) in ref. [259], but their solution appears to have a typo. One can test the relative sign of individual terms in a given convention by checking whether the resulting D-function obeys the properties given in appendix C.2.3.

$D_{\Delta_1, \Delta_2, \Delta_3, \Delta_4}$ to find a generic solution for four-point D-functions:

$$
\frac{\pi^{d/2}(-1)^{\sum_{i<j} c_{ij}} \Gamma(\frac{\Sigma'-d}{2})\Gamma(\frac{\Sigma'}{2})}{2\Gamma(2+\sum_{i<j} c_{ij})(\prod_i \Gamma(\Delta_i'))} \left[\prod_{i<j} \left(\frac{\partial}{\partial P_{ij}} \right)^{c_{ij}} \right] B(P_{ij})
$$
$$
= \frac{\pi^{d/2} \Gamma(\frac{\Sigma'-d}{2})\Gamma(\frac{\Sigma'}{2})}{2(\prod_i \Gamma(\Delta_i'))} \int \frac{\prod_a d\alpha_a \alpha_a^{\Delta_a'-1} \delta(\sum_b \alpha_b - 1)}{\left(\sum_{i,j} \alpha_i \alpha_j P_{ij} \right)^{\Sigma'/2}} \tag{C.26}
$$
$$
= D_{\Delta_1', \Delta_2', \Delta_3', \Delta_4'} \,,
$$

where $\Delta_i' = \sum_{j \neq i} c_{ij} + 1$ and $\Sigma' = \sum_i \Delta_i'$. Equations (C.24) and (C.26) together provide a closed form expressions for arbitrary four-point D-functions in terms of derivatives of polylogarithms. Unfortunately, although this representation is advantageous in that it provides an *exact* representation of the D-function in terms of polylogarithms, the D-function expressions become cumbersome very quickly, even for symbolic computation programs such as Mathematica. We ultimately used numeric differentiation algorithms in combination with eqs. (C.24) and (C.26) to solve for the D-functions at arbitrary kinematic points. These results were cross-checked with more direct numeric integrations of eq. (C.23).

Finding numerically tractable representations of D-functions is generically quite hard. For example, although standard Mellin integral representations of the D-function can be integrated numerically with high precision, defining the actual contour for integration is somewhat subtle. While the Mellin representation of Feynman integrals is largely understood, the problem seems to be slightly more technically challenging for the D-functions corresponding to AdS contact diagrams. One might hope that numeric integration in the Feynman representation would offer a more realistic approach, as it suffers from no contour ambiguities. Unfortunately, direct numeric integration of Feynman parameterized integrals is often unstable for arbitrary kinematics and Δ_i unless sophisticated weighted Monte-Carlo sampling techniques are applied. For example, see ref. [260].

C.2.3 D-function identities

When computing NLSM and YM AdS boundary correlators, we have used some D-function identities to simplify the results. In this appendix, we derive these identities starting from the conformal Ward identity. We start with the four-point case,

$$
(D_1^{AB} + D_2^{AB} + D_3^{AB} + D_4^{AB}) D_{\Delta_1, \Delta_2, \Delta_3, \Delta_4} = 0 \,. \tag{C.27}
$$

We can act respectively $(D_1 + D_3)^{AB}$ and $(D_2 + D_4)^{AB}$ onto this equation, giving

$$(2D_{13}^2 + D_1^2 + D_3^2)D_{\Delta_1,\Delta_2,\Delta_3,\Delta_4} = -(D_1 + D_3)_{AB}(D_2 + D_4)^{AB}D_{\Delta_1,\Delta_2,\Delta_3,\Delta_4} ,$$
$$(2D_{24}^2 + D_2^2 + D_4^2)D_{\Delta_1,\Delta_2,\Delta_3,\Delta_4} = -(D_2 + D_4)_{AB}(D_1 + D_3)^{AB}D_{\Delta_1,\Delta_2,\Delta_3,\Delta_4} . \qquad \text{(C.28)}$$

Since $(D_1 + D_3)$ commutes with $(D_2 + D_4)$ and $D_i^2 = -2m_i^2 = -2\Delta_i(\Delta_i - d)$ when acting on a conformal partial wave, we get

$$(D_{23}^2 - m_2^2 - m_3^2)D_{\Delta_1,\Delta_2,\Delta_3,\Delta_4} = (D_{14}^2 - m_1^2 - m_4^2)D_{\Delta_1,\Delta_2,\Delta_3,\Delta_4} . \qquad \text{(C.29)}$$

In particular, when $\Delta_i = \Delta$, we have

$$D_{13}^2 D_{\Delta,\Delta,\Delta,\Delta} = D_{24}^2 D_{\Delta,\Delta,\Delta,\Delta} . \qquad \text{(C.30)}$$

The above relation can be easily generalized to n-points,

$$\left(D_I^2 - \sum_{i\in I} m_i^2\right)D_{\Delta_1,\Delta_2,\dots,\Delta_n} = \left(D_{\bar{I}}^2 - \sum_{i\in\bar{I}} m_i^2\right)D_{\Delta_1,\Delta_2,\dots,\Delta_n} , \qquad \text{(C.31)}$$

where $I \cup \bar{I} = \{1, 2, \dots, n\}$ and $I \cap \bar{I} = \emptyset$.

We can also carry out the derivatives in eq. (C.29) explicitly to obtain relations involving boundary positions. For example, we can use

$$-\frac{1}{2}D_{13}^2 D_{\Delta_1,\Delta_2,\Delta_3,\Delta_4} = 4\Delta_1\Delta_3(P_1 \cdot P_3)D_{\Delta_1+1,\Delta_2,\Delta_3+1,\Delta_4} + \Delta_1\Delta_3 D_{\Delta_1,\Delta_2,\Delta_3,\Delta_4} , \qquad \text{(C.32)}$$

and a similar equation for D_{24}^2 to show that

$$(P_1 \cdot P_3)D_{\Delta+1,\Delta,\Delta+1,\Delta} = (P_2 \cdot P_4)D_{\Delta,\Delta+1,\Delta,\Delta+1} \quad \text{for } \Delta_i = \Delta . \qquad \text{(C.33)}$$

One can also show that acting D_{12}^2 and D_{13}^2 consecutively gives

$$\frac{1}{4}D_{12}^2 D_{13}^2 D_{\Delta_1,\Delta_2,\Delta_3,\Delta_4} = 16\Delta_1(\Delta_1 + 1)\Delta_2\Delta_3(P_1 \cdot P_2)(P_1 \cdot P_3)D_{\Delta_1+2,\Delta_2+1,\Delta_3+1,\Delta_4} \qquad \text{(C.34)}$$
$$+ 4\Delta_1(\Delta_1 + 1)\Delta_2\Delta_3\Big[(P_1 \cdot P_2)D_{\Delta_1+1,\Delta_2+1,\Delta_3,\Delta_4} + (2 \leftrightarrow 3)\Big]$$
$$- 4\Delta_1\Delta_2\Delta_3(P_2 \cdot P_3)D_{\Delta_1,\Delta_2+1,\Delta_3+1,\Delta_4} + \Delta_1^2\Delta_2\Delta_3 D_{\Delta_1,\Delta_2,\Delta_3,\Delta_4} ,$$

which is symmetric under the $2 \leftrightarrow 3$ exchange. This also means that $D_{\Delta_1,\Delta_2,\Delta_3,\Delta_4}$ lives in the kernel of $[D_{12}^2, D_{13}^2]$, namely, $[D_{12}^2, D_{13}^2]D_{\Delta_1,\Delta_2,\Delta_3,\Delta_4} = 0$.

Next, we act D_1^{AB} onto eq. (C.27) and then use eq. (C.29) to eliminate D_{14}^2. This gives

$$(D_{12}^2 + D_{13}^2 + D_{23}^2)D_{\Delta_1,\Delta_2,\Delta_3,\Delta_4} + (m_4^2 - m_1^2 - m_2^2 - m_3^2)D_{\Delta_1,\Delta_2,\Delta_3,\Delta_4} = 0. \tag{C.35}$$

When $\Delta_i = \Delta$, we get

$$(D_{12}^2 + D_{13}^2 + D_{23}^2)D_{\Delta,\Delta,\Delta,\Delta} = 2\Delta(\Delta - d)D_{\Delta,\Delta,\Delta,\Delta}. \tag{C.36}$$

This equation also implies the identity

$$(P_1 \cdot P_2)D_{\Delta+1,\Delta+1,\Delta,\Delta} + (P_1 \cdot P_3)D_{\Delta+1,\Delta,\Delta+1,\Delta}$$
$$+ (P_2 \cdot P_3)D_{\Delta,\Delta+1,\Delta+1,\Delta} = -\frac{4\Delta - d}{4\Delta}D_{\Delta,\Delta,\Delta,\Delta}. \tag{C.37}$$

In the on-shell limit $\Delta = d$, we thus derive the relation

$$(D_{12}^2 + D_{13}^2 + D_{23}^2)D_{d,d,d,d,} = 0, \tag{C.38}$$

which resembles the relation $s + t + u = 0$ for flat space Mandelstam variables.

The above identities can also be derived using integration-by-parts relations. Below we show the derivation of eq. (C.29). Our calculation will be given in the embedding space, which is in parallel with the one in the physical space [49]. To start with, we define

$$D_{\partial\Delta_1,\Delta_2,\partial\Delta_3,\Delta_4} \equiv \int_{\text{AdS}} dX\, G^{AB} \left[\frac{\partial}{\partial X^A} \frac{1}{(-2P_1 \cdot X)^{\Delta_1}} \right] \frac{1}{(-2P_2 \cdot X)^{\Delta_2}}$$
$$\times \left[\frac{\partial}{\partial X^B} \frac{1}{(-2P_3 \cdot X)^{\Delta_3}} \right] \frac{1}{(-2P_4 \cdot X)^{\Delta_4}}$$
$$= 4\Delta_1\Delta_3(P_1 \cdot P_3)D_{\Delta_1+1,\Delta_2,\Delta_3+1,\Delta_4} + \Delta_1\Delta_3 D_{\Delta_1,\Delta_2,\Delta_3,\Delta_4}. \tag{C.39}$$

We then use the identity

$$\partial_A G^{AB} \partial_B \left[\frac{1}{(-2P_1 \cdot X)^{\Delta_1}} \frac{1}{(-2P_3 \cdot X)^{\Delta_3}} \right] = 2G^{AB} \frac{\partial}{\partial X^A} \frac{1}{(-2P_1 \cdot X)^{\Delta_1}} \frac{\partial}{\partial X^B} \frac{1}{(-2P_3 \cdot X)^{\Delta_3}}$$
$$+ \frac{m_1^2 + m_3^2}{(-2P_1 \cdot X)^{\Delta_1}(-2P_3 \cdot X)^{\Delta_3}} \tag{C.40}$$

to write eq. (C.39) as

$$D_{\partial\Delta_1,\Delta_2,\partial\Delta_3,\Delta_4} + \frac{1}{2}(m_1^2 + m_3^2)D_{\Delta_1,\Delta_2,\Delta_3,\Delta_4}$$

$$= \frac{1}{2} \int_{\text{AdS}} dX (\partial_A G^{AB} \partial_B) \left[\frac{1}{(-2P_1 \cdot X)^{\Delta_1}} \frac{1}{(-2P_3 \cdot X)^{\Delta_3}} \right] \frac{1}{(-2P_2 \cdot X)^{\Delta_2}} \frac{1}{(-2P_4 \cdot X)^{\Delta_4}}$$

$$= \frac{1}{2} \int_{\text{AdS}} dX (\partial_A G^{AB} \partial_B) \left[\frac{1}{(-2P_2 \cdot X)^{\Delta_2}} \frac{1}{(-2P_4 \cdot X)^{\Delta_4}} \right] \frac{1}{(-2P_1 \cdot X)^{\Delta_1}} \frac{1}{(-2P_3 \cdot X)^{\Delta_3}}$$

$$= D_{\Delta_1, \partial \Delta_2, \Delta_3, \partial \Delta_4} + \frac{1}{2}(m_2^2 + m_4^2) D_{\Delta_1, \Delta_2, \Delta_3, \Delta_4} , \qquad (C.41)$$

where integration-by-parts has been used to obtain the second equation. This leads to the identity

$$4\Delta_1 \Delta_3 (P_1 \cdot P_3) D_{\Delta_1+1, \Delta_2, \Delta_3+1, \Delta_4} + \frac{1}{2}(2\Delta_1 \Delta_3 + m_1^2 + m_3^2) D_{\Delta_1, \Delta_2, \Delta_3, \Delta_4}$$

$$= 4\Delta_2 \Delta_4 (P_2 \cdot P_4) D_{\Delta_1, \Delta_2+1, \Delta_3, \Delta_4+1} + \frac{1}{2}(2\Delta_2 \Delta_4 + m_2^2 + m_4^2) D_{\Delta_1, \Delta_2, \Delta_3, \Delta_4} . \qquad (C.42)$$

When $\Delta_i = \Delta$, we can recover $(P_1 \cdot P_3) D_{\Delta+1, \Delta, \Delta+1, \Delta} = (P_2 \cdot P_4) D_{\Delta, \Delta+1, \Delta, \Delta+1}$. Now using eq. (C.32) to replace $P_i \cdot P_j$ by D_{13}^2 immediately leads to

$$(D_{23}^2 - m_2^2 - m_3^2) D_{\Delta_1, \Delta_2, \Delta_3, \Delta_4} = (D_{14}^2 - m_1^2 - m_4^2) D_{\Delta_1, \Delta_2, \Delta_3, \Delta_4} . \qquad (C.43)$$

C.3 Useful Integral Identities

In this appendix, we discuss how we checked that Eq. (4.162) holds. Crucially, first note that $\hat{f}(D_Q^2)$ becomes $\hat{f}(d^2/4 - c^2)$ upon acting on $\mathcal{C}_5(P_i, Q, Q')$ in Eq. (4.158) and is therefore independent of Q. However, non-trivial dependence on Q emerges upon acting $(D_Q \cdot D_i)^N (D_Q \cdot D_j)^M$ on $\mathcal{C}_5(P_i, Q, Q')$. We explicitly checked that the resulting expression vanishes upon integrating over Q for $N + M \leq 10$.

We review the computation strategy to integrate over Q. We find that the integrand contains terms whose Q-dependence takes the generic form

$$I_{a_1, a_2, \dots} = \int_{\partial \text{AdS}} dQ \frac{\prod_i (-2Q \cdot P_i)^{a_i}}{(-2Q \cdot X)^{d + \sum_i a_i}} . \qquad (C.44)$$

We first consider the simplest specialization of Eq. (C.44):

$$I_a = \int_{\partial \text{AdS}} dQ \frac{(-2Q \cdot P_1)^a}{(-2Q \cdot X)^{d+a}} . \qquad (C.45)$$

Using the identity

$$\frac{\Gamma[a]}{f^a} = \int_0^\infty \frac{dv}{v} v^a e^{-vf} , \qquad (C.46)$$

we can rewrite Eq. (C.45) as

$$\left(\frac{\partial}{\partial\alpha}\right)^a \int_{\partial\text{AdS}} dQ \int_0^\infty \frac{dv}{v} \frac{v^{d+a}e^{2Q\cdot(vX-\alpha P_1)}}{\Gamma[d+a]}\Big|_{\alpha=0} \, . \tag{C.47}$$

Finally, using the identity

$$\int_{\partial\text{AdS}} dQ e^{2Q\cdot T} = \frac{\pi^{d/2}}{|T|^{d/2}} e^{-|T|} \tag{C.48}$$

the integral over Q in Eq. (C.47) yields

$$\left(\frac{\partial}{\partial\alpha}\right)^a \int \frac{v^{d+a-1}\pi^{d/2}e^{-\sqrt{v\alpha(-2X\cdot P_1)-v^2}}dv}{\Gamma[d+a](v\alpha(-2X\cdot P_1)-v^2)^{d/4}}\Big|_{\alpha=0} \tag{C.49}$$

which simplifies to

$$I_a = (-2P_1\cdot X)^a \pi^{d/2} \frac{\Gamma[\frac{d}{2}+a]}{\Gamma[d+a]} \, . \tag{C.50}$$

This computation strategy generalizes to all integrals of the form Eq. (C.44). Writing the result in a tensor version of Eq. (C.44), the integral yields

$$\begin{aligned} I^{A_1,\dots,A_n} &= \int dQ \frac{Q^{A_1}\dots Q^{A_n}}{(-2Q\cdot X)^{d+n}} \, , \\ &= \frac{\pi^{d/2}\Gamma(d/2+n)}{\Gamma(d+n)} X^{A_1}\dots X^{A_n} - \text{Traces} \end{aligned} \tag{C.51}$$

where traces are subtracted using η^{AB}.

Eq. (C.51) was originally given in Ref. [247] by taking derivatives of the integral

$$\begin{aligned} I(X) &= \int dQ \frac{1}{(-2Q\cdot X)^d} \\ &= \frac{\pi^{d/2}\Gamma(d/2)}{\Gamma(d)} \frac{1}{(-X^2)^{d/2}} \, . \end{aligned} \tag{C.52}$$

in the bulk coordinate X^A. We have reproduced this formula here by direct integration to avoid subtleties that are relevant when taking derivatives in bulk or boundary coordinates in embedding space [261].

Bibliography

[1]   Stephen J. Parke and T. R. Taylor. "An Amplitude for n Gluon Scattering". In: *Phys. Rev. Lett.* 56 (1986), p. 2459. DOI: `10.1103/PhysRevLett.56.2459`.

[2]   Freddy Cachazo, Peter Svrcek, and Edward Witten. "MHV vertices and tree amplitudes in gauge theory". In: *JHEP* 09 (2004), p. 006. DOI: `10.1088/1126-6708/2004/09/006`. arXiv: `hep-th/0403047`.

[3]   Ruth Britto, Freddy Cachazo, and Bo Feng. "New recursion relations for tree amplitudes of gluons". In: *Nucl. Phys. B* 715 (2005), pp. 499–522. DOI: `10.1016/j.nuclphysb.2005.02.030`. arXiv: `hep-th/0412308`.

[4]   Ruth Britto et al. "Direct proof of tree-level recursion relation in Yang-Mills theory". In: *Phys. Rev. Lett.* 94 (2005), p. 181602. DOI: `10.1103/PhysRevLett.94.181602`. arXiv: `hep-th/0501052`.

[5]   Nima Arkani-Hamed and Jaroslav Trnka. "The Amplituhedron". In: *JHEP* 10 (2014), p. 030. DOI: `10.1007/JHEP10(2014)030`. arXiv: `1312.2007 [hep-th]`.

[6]   Steven Weinberg. "Infrared photons and gravitons". In: *Phys. Rev.* 140 (1965), B516–B524. DOI: `10.1103/PhysRev.140.B516`.

[7]   T. W. B. Kibble. "Coherent Soft-Photon States and Infrared Divergences. I. Classical Currents". In: *J. Math. Phys.* 9.2 (1968), pp. 315–324. DOI: `10.1063/1.1664582`.

[8]   T. W. B. Kibble. "Coherent soft-photon states and infrared divergences. ii. mass-shell singularities of green's functions". In: *Phys. Rev.* 173 (1968), pp. 1527–1535. DOI: `10.1103/PhysRev.173.1527`.

[9]   John M. Cornwall and George Tiktopoulos. "Infrared Behavior of Nonabelian Gauge Theories". In: *Phys. Rev. D* 13 (1976), p. 3370. DOI: `10.1103/PhysRevD.13.3370`.

[10]   Clifford Cheung et al. "On-Shell Recursion Relations for Effective Field Theories". In: *Phys. Rev. Lett.* 116.4 (2016), p. 041601. DOI: `10.1103/PhysRevLett.116.041601`. arXiv: `1509.03309 [hep-th]`.

[11] Alexander B. Goncharov et al. "Classical Polylogarithms for Amplitudes and Wilson Loops". In: *Phys. Rev. Lett.* 105 (2010), p. 151605. DOI: 10.1103/PhysRevLett.105.151605. arXiv: 1006.5703 [hep-th].

[12] Davide Gaiotto et al. "Pulling the straps of polygons". In: *JHEP* 12 (2011), p. 011. DOI: 10.1007/JHEP12(2011)011. arXiv: 1102.0062 [hep-th].

[13] A. B. Goncharov. "Multiple polylogarithms, cyclotomy and modular complexes". In: *arXiv e-prints*, arXiv:1105.2076 (May 2011), arXiv:1105.2076. arXiv: 1105.2076 [math.AG].

[14] Nima Arkani-Hamed et al. *Grassmannian Geometry of Scattering Amplitudes*. Cambridge University Press, 2016. ISBN: 9781107086586, 9781316572962. DOI: 10.1017/CBO9781316091548. arXiv: 1212.5605 [hep-th]. URL: http://www.cambridge.org/us/academic/subjects/physics/theoretical-physics-and-mathematical-physics/grassmannian-geometry-scattering-amplitudes?format=HB&isbn=9781107086586.

[15] John Golden et al. "Motivic Amplitudes and Cluster Coordinates". In: *JHEP* 01 (2014), p. 091. DOI: 10.1007/JHEP01(2014)091. arXiv: 1305.1617 [hep-th].

[16] Claude Duhr. "Mathematical aspects of scattering amplitudes". In: *Theoretical Advanced Study Institute in Elementary Particle Physics: Journeys Through the Precision Frontier: Amplitudes for Colliders*. 2015, pp. 419–476. DOI: 10.1142/9789814678766_0010. arXiv: 1411.7538 [hep-ph].

[17] A.B. Goncharov. "Geometry of Configurations, Polylogarithms, and Motivic Cohomology". In: *Advances in Mathematics* 114.2 (1995), pp. 197–318. ISSN: 0001-8708. DOI: https://doi.org/10.1006/aima.1995.1045. URL: http://www.sciencedirect.com/science/article/pii/S0001870885710456.

[18] Simon Caron-Huot et al. "Six-Gluon amplitudes in planar $\mathcal{N} = 4$ super-Yang-Mills theory at six and seven loops". In: *JHEP* 08 (2019), p. 016. DOI: 10.1007/JHEP08(2019)016. arXiv: 1903.10890 [hep-th].

[19] Lance J. Dixon et al. "Heptagons from the Steinmann Cluster Bootstrap". In: *JHEP* 02 (2017), p. 137. DOI: 10.1007/JHEP02(2017)137. arXiv: 1612.08976 [hep-th].

[20] Zhenjie Li and Chi Zhang. "The three-loop MHV octagon from $\overline{Q}$ equations". In: *JHEP* 12 (2021), p. 113. DOI: 10.1007/JHEP12(2021)113. arXiv: 2110.00350 [hep-th].

184

[21] Aidan Herderschee. "Algebraic branch points at all loop orders from positive kinematics and wall crossing". In: *JHEP* 07 (2021), p. 049. DOI: 10.1007/JHEP07(2021)049. arXiv: 2102.03611 [hep-th].

[22] Huan-Hang Chi et al. "Generalizations of the double-copy: the KLT bootstrap". In: *JHEP* 03 (2022), p. 077. DOI: 10.1007/JHEP03(2022)077. arXiv: 2106.12600 [hep-th].

[23] Pranav Diwakar et al. "BCJ amplitude relations for Anti-de Sitter boundary correlators in embedding space". In: *JHEP* 10 (2021), p. 141. DOI: 10.1007/JHEP10(2021)141. arXiv: 2106.10822 [hep-th].

[24] Aidan Herderschee. "A New Framework for Higher Loop Witten Diagrams". In: (Dec. 2021). arXiv: 2112.08226 [hep-th].

[25] Aidan Herderschee, Seth Koren, and Timothy Trott. "Massive On-Shell Supersymmetric Scattering Amplitudes". In: *JHEP* 10 (2019), p. 092. DOI: 10.1007/JHEP10(2019)092. arXiv: 1902.07204 [hep-th].

[26] Aidan Herderschee, Seth Koren, and Timothy Trott. "Constructing $\mathcal{N} = 4$ Coulomb branch superamplitudes". In: *JHEP* 08 (2019), p. 107. DOI: 10.1007/JHEP08(2019)107. arXiv: 1902.07205 [hep-th].

[27] Aidan Herderschee et al. "On Positive Geometry and Scattering Forms for Matter Particles". In: *JHEP* 06 (2020), p. 030. DOI: 10.1007/JHEP06(2020)030. arXiv: 1912.08307 [hep-th].

[28] Aidan Herderschee and Fei Teng. "Open associahedra and scattering forms". In: *JHEP* 12 (2020), p. 134. DOI: 10.1007/JHEP12(2020)134. arXiv: 2008.06418 [hep-th].

[29] Aidan Herderschee, Radu Roiban, and Fei Teng. "On the differential representation and color-kinematics duality of AdS boundary correlators". In: *JHEP* 05 (2022), p. 026. DOI: 10.1007/JHEP05(2022)026. arXiv: 2201.05067 [hep-th].

[30] Alan Shih-Kuan Chen, Henriette Elvang, and Aidan Herderschee. "Emergence of String Monodromy in Effective Field Theory". In: (Dec. 2022). arXiv: 2212.13998 [hep-th].

[31] Alan Shih-Kuan Chen, Henriette Elvang, and Aidan Herderschee. "Bootstrapping the String KLT Kernel". In: (Feb. 2023). arXiv: 2302.04895 [hep-th].

[32] Nima Arkani-Hamed, Song He, and Thomas Lam. "Stringy canonical forms". In: *JHEP* 02 (2021), p. 069. DOI: 10.1007/JHEP02(2021)069. arXiv: 1912.08707 [hep-th].

[33] Ashoke Sen. "String Field Theory as World-sheet UV Regulator". In: *JHEP* 10 (2019), p. 119. DOI: `10.1007/JHEP10(2019)119`. arXiv: `1902.00263 [hep-th]`.

[34] Edward Witten. "The Feynman $i\epsilon$ in String Theory". In: *JHEP* 04 (2015), p. 055. DOI: `10.1007/JHEP04(2015)055`. arXiv: `1307.5124 [hep-th]`.

[35] Nima Arkani-Hamed, Hugh Thomas, and Jaroslav Trnka. "Unwinding the Amplituhedron in Binary". In: *JHEP* 01 (2018), p. 016. DOI: `10.1007/JHEP01(2018)016`. arXiv: `1704.05069 [hep-th]`.

[36] Nima Arkani-Hamed, Thomas Lam, and Marcus Spradlin. "Non-perturbative geometries for planar $\mathcal{N} = 4$ SYM amplitudes". In: (Dec. 2019). arXiv: `1912.08222 [hep-th]`.

[37] Igor Prlina, Marcus Spradlin, and Stefan Stanojevic. "All-loop singularities of scattering amplitudes in massless planar theories". In: *Phys. Rev. Lett.* 121.8 (2018), p. 081601. DOI: `10.1103/PhysRevLett.121.081601`. arXiv: `1805.11617 [hep-th]`.

[38] H. Kawai, D. C. Lewellen, and S. H. H. Tye. "A Relation Between Tree Amplitudes of Closed and Open Strings". In: *Nucl. Phys.* B269 (1986), pp. 1–23. DOI: `10.1016/0550-3213(86)90362-7`.

[39] Sebastian Mizera. "Inverse of the String Theory KLT Kernel". In: *JHEP* 06 (2017), p. 084. DOI: `10.1007/JHEP06(2017)084`. arXiv: `1610.04230 [hep-th]`.

[40] Walter D. Goldberger and Ira Z. Rothstein. "An Effective field theory of gravity for extended objects". In: *Phys. Rev. D* 73 (2006), p. 104029. DOI: `10.1103/PhysRevD.73.104029`. arXiv: `hep-th/0409156`.

[41] Zvi Bern et al. "Black Hole Binary Dynamics from the Double Copy and Effective Theory". In: *JHEP* 10 (2019), p. 206. DOI: `10.1007/JHEP10(2019)206`. arXiv: `1908.01493 [hep-th]`.

[42] Juan Martin Maldacena. "The Large N limit of superconformal field theories and supergravity". In: *Adv. Theor. Math. Phys.* 2 (1998), pp. 231–252. DOI: `10.1023/A:1026654312961`. arXiv: `hep-th/9711200`.

[43] S. S. Gubser, Igor R. Klebanov, and Alexander M. Polyakov. "Gauge theory correlators from noncritical string theory". In: *Phys. Lett. B* 428 (1998), pp. 105–114. DOI: `10.1016/S0370-2693(98)00377-3`. arXiv: `hep-th/9802109`.

[44] Edward Witten. "Anti-de Sitter space and holography". In: *Adv. Theor. Math. Phys.* 2 (1998), pp. 253–291. DOI: `10.4310/ATMP.1998.v2.n2.a2`. arXiv: `hep-th/9802150`.

[45] Joao Penedones. "Writing CFT correlation functions as AdS scattering amplitudes". In: *JHEP* 03 (2011), p. 025. DOI: `10.1007/JHEP03(2011)025`. arXiv: `1011.1485 [hep-th]`.

[46] Leonard Susskind. "The World as a hologram". In: *J. Math. Phys.* 36 (1995), pp. 6377–6396. DOI: `10.1063/1.531249`. arXiv: `hep-th/9409089`.

[47] Gerard 't Hooft. "Dimensional reduction in quantum gravity". In: *Conf. Proc. C* 930308 (1993), pp. 284–296. arXiv: `gr-qc/9310026`.

[48] Lorenz Eberhardt, Shota Komatsu, and Sebastian Mizera. "Scattering equations in AdS: scalar correlators in arbitrary dimensions". In: *JHEP* 11 (2020), p. 158. DOI: `10.1007/JHEP11(2020)158`. arXiv: `2007.06574 [hep-th]`.

[49] Eric D'Hoker et al. "Graviton exchange and complete four point functions in the AdS / CFT correspondence". In: *Nucl. Phys. B* 562 (1999), pp. 353–394. DOI: `10.1016/S0550-3213(99)00525-8`. arXiv: `hep-th/9903196`.

[50] Kai Roehrig and David Skinner. *Ambitwistor Strings and the Scattering Equations on $AdS_3 \times S^3$*. July 2020. arXiv: `2007.07234 [hep-th]`.

[51] In principle, the triangle Witten can be derived by direct integration for even d using $6j$-symbols [244], but actually evaluating this integral is troublesome.

[52] A. V. Kotikov. "Differential equations method: New technique for massive Feynman diagrams calculation". In: *Phys. Lett. B* 254 (1991), pp. 158–164. DOI: `10.1016/0370-2693(91)90413-K`.

[53] Zvi Bern, Lance J. Dixon, and David A. Kosower. "Dimensionally regulated pentagon integrals". In: *Nucl. Phys. B* 412 (1994), pp. 751–816. DOI: `10.1016/0550-3213(94)90398-0`. arXiv: `hep-ph/9306240`.

[54] Ettore Remiddi. "Differential equations for Feynman graph amplitudes". In: *Nuovo Cim. A* 110 (1997), pp. 1435–1452. DOI: `10.1007/BF03185566`. arXiv: `hep-th/9711188`.

[55] T. Gehrmann and E. Remiddi. "Differential equations for two loop four point functions". In: *Nucl. Phys. B* 580 (2000), pp. 485–518. DOI: `10.1016/S0550-3213(00)00223-6`. arXiv: `hep-ph/9912329`.

[56] K. G. Chetyrkin and F. V. Tkachov. "Integration by Parts: The Algorithm to Calculate beta Functions in 4 Loops". In: *Nucl. Phys. B* 192 (1981), pp. 159–204. DOI: `10.1016/0550-3213(81)90199-1`.

[57] A. V. Smirnov. "Algorithm FIRE – Feynman Integral REduction". In: *JHEP* 10 (2008), p. 107. DOI: 10.1088/1126-6708/2008/10/107. arXiv: 0807.3243 [hep-ph].

[58] A. V. Smirnov and F. S. Chuharev. "FIRE6: Feynman Integral REduction with Modular Arithmetic". In: *Comput. Phys. Commun.* 247 (2020), p. 106877. DOI: 10.1016/j.cpc.2019.106877. arXiv: 1901.07808 [hep-ph].

[59] Clifford Cheung, Julio Parra-Martinez, and Allic Sivaramakrishnan. "On-shell correlators and color-kinematics duality in curved symmetric spacetimes". In: *JHEP* 05 (2022), p. 027. DOI: 10.1007/JHEP05(2022)027. arXiv: 2201.05147 [hep-th].

[60] Enrico Herrmann et al. "Positive geometry, local triangulations, and the dual of the Amplituhedron". In: *JHEP* 01 (2021), p. 035. DOI: 10.1007/JHEP01(2021)035. arXiv: 2009.05607 [hep-th].

[61] Ryota Kojima and Cameron Langer. "Sign Flip Triangulations of the Amplituhedron". In: *JHEP* 05 (2020), p. 121. DOI: 10.1007/JHEP05(2020)121. arXiv: 2001.06473 [hep-th].

[62] C. Anastasiou et al. "Planar amplitudes in maximally supersymmetric Yang-Mills theory". In: *Phys. Rev. Lett.* 91 (2003), p. 251602. DOI: 10.1103/PhysRevLett.91.251602. arXiv: hep-th/0309040.

[63] Zvi Bern, Lance J. Dixon, and Vladimir A. Smirnov. "Iteration of planar amplitudes in maximally supersymmetric Yang-Mills theory at three loops and beyond". In: *Phys. Rev. D* 72 (2005), p. 085001. DOI: 10.1103/PhysRevD.72.085001. arXiv: hep-th/0505205.

[64] Luis F. Alday and Juan Martin Maldacena. "Gluon scattering amplitudes at strong coupling". In: *JHEP* 06 (2007), p. 064. DOI: 10.1088/1126-6708/2007/06/064. arXiv: 0705.0303 [hep-th].

[65] Luis F. Alday, Davide Gaiotto, and Juan Maldacena. "Thermodynamic Bubble Ansatz". In: *JHEP* 09 (2011), p. 032. DOI: 10.1007/JHEP09(2011)032. arXiv: 0911.4708 [hep-th].

[66] Gang Yang. "A simple collinear limit of scattering amplitudes at strong coupling". In: *JHEP* 03 (2011), p. 087. DOI: 10.1007/JHEP03(2011)087. arXiv: 1006.3306 [hep-th].

[67] Andreas Brandhuber, Paul Heslop, and Gabriele Travaglini. "MHV amplitudes in N=4 super Yang-Mills and Wilson loops". In: *Nucl. Phys. B* 794 (2008), pp. 231–243. DOI: 10.1016/j.nuclphysb.2007.11.002. arXiv: 0707.1153 [hep-th].

[68] Luis F. Alday et al. "An Operator Product Expansion for Polygonal null Wilson Loops". In: *JHEP* 04 (2011), p. 088. DOI: 10.1007/JHEP04(2011)088. arXiv: 1006.2788 [hep-th].

[69] Simon Caron-Huot. "Notes on the scattering amplitude / Wilson loop duality". In: *JHEP* 07 (2011), p. 058. DOI: 10.1007/JHEP07(2011)058. arXiv: 1010.1167 [hep-th].

[70] Burkhard Eden et al. "The super-correlator/super-amplitude duality: Part I". In: *Nucl. Phys. B* 869 (2013), pp. 329–377. DOI: 10.1016/j.nuclphysb.2012.12.015. arXiv: 1103.3714 [hep-th].

[71] Benjamin Basso, Amit Sever, and Pedro Vieira. "Spacetime and Flux Tube S-Matrices at Finite Coupling for N=4 Supersymmetric Yang-Mills Theory". In: *Phys. Rev. Lett.* 111.9 (2013), p. 091602. DOI: 10.1103/PhysRevLett.111.091602. arXiv: 1303.1396 [hep-th].

[72] Song He et al. "Feynman Integrals and Scattering Amplitudes from Wilson Loops". In: *Phys. Rev. Lett.* 126 (2021), p. 231601. DOI: 10.1103/PhysRevLett.126.231601. arXiv: 2012.15042 [hep-th].

[73] Song He et al. "The Wilson-loop d log representation for Feynman integrals". In: *JHEP* 05 (2021), p. 052. DOI: 10.1007/JHEP05(2021)052. arXiv: 2012.13094 [hep-th].

[74] Song He, Zhenjie Li, and Qinglin Yang. "Notes on cluster algebras and some all-loop Feynman integrals". In: (Mar. 2021). arXiv: 2103.02796 [hep-th].

[75] Francis Brown and Claude Duhr. "A double integral of dlog forms which is not polylogarithmic". In: (June 2020). arXiv: 2006.09413 [hep-th].

[76] Lance J. Dixon, James M. Drummond, and Johannes M. Henn. "Analytic result for the two-loop six-point NMHV amplitude in N=4 super Yang-Mills theory". In: *JHEP* 01 (2012), p. 024. DOI: 10.1007/JHEP01(2012)024. arXiv: 1111.1704 [hep-th].

[77] Lance J. Dixon, Matt von Hippel, and Andrew J. McLeod. "The four-loop six-gluon NMHV ratio function". In: *JHEP* 01 (2016), p. 053. DOI: 10.1007/JHEP01(2016)053. arXiv: 1509.08127 [hep-th].

[78] Simon Caron-Huot et al. "Bootstrapping a Five-Loop Amplitude Using Steinmann Relations". In: *Phys. Rev. Lett.* 117.24 (2016), p. 241601. DOI: 10.1103/PhysRevLett.117.241601. arXiv: 1609.00669 [hep-th].

[79] James Drummond et al. "Cluster adjacency and the four-loop NMHV heptagon". In: *JHEP* 03 (2019), p. 087. DOI: 10.1007/JHEP03(2019)087. arXiv: 1812.04640 [hep-th].

[80] Simon Caron-Huot et al. "The Cosmic Galois Group and Extended Steinmann Relations for Planar $\mathcal{N} = 4$ SYM Amplitudes". In: *JHEP* 09 (2019), p. 061. DOI: 10.1007/JHEP09(2019)061. arXiv: 1906.07116 [hep-th].

[81] John Golden and Marcus Spradlin. "The differential of all two-loop MHV amplitudes in $\mathcal{N}$ = 4 Yang-Mills theory". In: *JHEP* 09 (2013), p. 111. DOI: 10.1007/JHEP09(2013)111. arXiv: 1306.1833 [hep-th].

[82] Lance J. Dixon et al. "Hexagon functions and the three-loop remainder function". In: *JHEP* 12 (2013), p. 049. DOI: 10.1007/JHEP12(2013)049. arXiv: 1308.2276 [hep-th].

[83] John Golden and Marcus Spradlin. "A Cluster Bootstrap for Two-Loop MHV Amplitudes". In: *JHEP* 02 (2015), p. 002. DOI: 10.1007/JHEP02(2015)002. arXiv: 1411.3289 [hep-th].

[84] John Golden et al. "Cluster Polylogarithms for Scattering Amplitudes". In: *J. Phys. A* 47.47 (2014), p. 474005. DOI: 10.1088/1751-8113/47/47/474005. arXiv: 1401.6446 [hep-th].

[85] James M. Drummond, Georgios Papathanasiou, and Marcus Spradlin. "A Symbol of Uniqueness: The Cluster Bootstrap for the 3-Loop MHV Heptagon". In: *JHEP* 03 (2015), p. 072. DOI: 10.1007/JHEP03(2015)072. arXiv: 1412.3763 [hep-th].

[86] Lance J. Dixon and Matt von Hippel. "Bootstrapping an NMHV amplitude through three loops". In: *JHEP* 10 (2014), p. 065. DOI: 10.1007/JHEP10(2014)065. arXiv: 1408.1505 [hep-th].

[87] Lance J. Dixon et al. "The four-loop remainder function and multi-Regge behavior at NNLLA in planar N = 4 super-Yang-Mills theory". In: *JHEP* 06 (2014), p. 116. DOI: 10.1007/JHEP06(2014)116. arXiv: 1402.3300 [hep-th].

[88] Simon Caron-Huot and Song He. "Jumpstarting the All-Loop S-Matrix of Planar N=4 Super Yang-Mills". In: *JHEP* 07 (2012), p. 174. DOI: 10.1007/JHEP07(2012)174. arXiv: 1112.1060 [hep-th].

[89] Song He, Zhenjie Li, and Chi Zhang. "Two-loop Octagons, Algebraic Letters and $\bar{Q}$ Equations". In: *Phys. Rev. D* 101.6 (2020), p. 061701. DOI: 10.1103/PhysRevD.101.061701. arXiv: 1911.01290 [hep-th].

[90] Song He, Zhenjie Li, and Chi Zhang. "The symbol and alphabet of two-loop NMHV amplitudes from $\bar{Q}$ equations". In: *JHEP* 03 (2021), p. 278. DOI: 10.1007/JHEP03(2021)278. arXiv: 2009.11471 [hep-th].

[91] Song He and Zhenjie Li. "A note on letters of Yangian invariants". In: *JHEP* 02 (2021), p. 155. DOI: 10.1007/JHEP02(2021)155. arXiv: 2007.01574 [hep-th].

[92] Jorge Mago et al. "Symbol alphabets from plabic graphs". In: *JHEP* 10 (2020), p. 128. DOI: 10.1007/JHEP10(2020)128. arXiv: 2007.00646 [hep-th].

[93] J. Mago et al. "Symbol alphabets from plabic graphs II: rational letters". In: *JHEP* 04 (2021), p. 056. DOI: 10.1007/JHEP04(2021)056. arXiv: 2012.15812 [hep-th].

[94] Tristan Dennen et al. "Landau Singularities from the Amplituhedron". In: *JHEP* 06 (2017), p. 152. DOI: 10.1007/JHEP06(2017)152. arXiv: 1612.02708 [hep-th].

[95] Igor Prlina et al. "All-Helicity Symbol Alphabets from Unwound Amplituhedra". In: *JHEP* 05 (2018), p. 159. DOI: 10.1007/JHEP05(2018)159. arXiv: 1711.11507 [hep-th].

[96] Igor Prlina et al. "Boundaries of Amplituhedra and NMHV Symbol Alphabets at Two Loops". In: *JHEP* 04 (2018), p. 049. DOI: 10.1007/JHEP04(2018)049. arXiv: 1712.08049 [hep-th].

[97] Song He, Lecheng Ren, and Yong Zhang. "Notes on polytopes, amplitudes and boundary configurations for Grassmannian string integrals". In: *JHEP* 04 (2020), p. 140. DOI: 10.1007/JHEP04(2020)140. arXiv: 2001.09603 [hep-th].

[98] Nima Arkani-Hamed, Song He, and Thomas Lam. "Cluster configuration spaces of finite type". In: (May 2020). arXiv: 2005.11419 [math.AG].

[99] Nima Arkani-Hamed, Thomas Lam, and Marcus Spradlin. "Positive configuration space". In: (Mar. 2020). arXiv: 2003.03904 [math.CO].

[100] Niklas Henke and Georgios Papathanasiou. "Singularities of eight- and nine-particle amplitudes from cluster algebras and tropical geometry". In: *JHEP* 10 (2021), p. 007. DOI: 10.1007/JHEP10(2021)007. arXiv: 2106.01392 [hep-th].

[101] Niklas Henke and Georgios Papathanasiou. "How tropical are seven- and eight-particle amplitudes?" In: *JHEP* 08 (2020), p. 005. DOI: 10.1007/JHEP08(2020)005. arXiv: 1912.08254 [hep-th].

[102] James Drummond et al. "Algebraic singularities of scattering amplitudes from tropical geometry". In: *JHEP* 04 (2021), p. 002. DOI: 10.1007/JHEP04(2021)002. arXiv: 1912.08217 [hep-th].

[103] Maxim Kontsevich and Yan Soibelman. "Wall-crossing structures in Donaldson-Thomas invariants, integrable systems and Mirror Symmetry". In: *Lect. Notes Union. Mat. Ital.* 15 (2014). Ed. by Ricardo Castano-Bernard et al., pp. 197–308. DOI: `10.1007/978-3-319-06514-4_6`. arXiv: `1303.3253 [math.AG]`.

[104] Mark Gross and Bernd Siebert. "From real affine geometry to complex geometry". In: *arXiv Mathematics e-prints*, math/0703822 (Mar. 2007), math/0703822. arXiv: `math/0703822 [math.AG]`.

[105] Maxim Kontsevich and Yan Soibelman. "Affine structures and non-archimedean analytic spaces". In: *arXiv Mathematics e-prints*, math/0406564 (June 2004), math/0406564. arXiv: `math/0406564 [math.AG]`.

[106] Nathan Reading. "A combinatorial approach to scattering diagrams". In: *arXiv e-prints*, arXiv:1806.05094 (June 2018), arXiv:1806.05094. arXiv: `1806.05094 [math.CO]`.

[107] Nathan Reading. "Scattering fans". In: *arXiv e-prints*, arXiv:1712.06968 (Dec. 2017), arXiv:1712.06968. arXiv: `1712.06968 [math.CO]`.

[108] Mark Gross et al. "Canonical bases for cluster algebras". In: *arXiv e-prints*, arXiv:1411.1394 (Nov. 2014), arXiv:1411.1394. arXiv: `1411.1394 [math.AG]`.

[109] Davide Gaiotto, Gregory W. Moore, and Andrew Neitzke. "Wall-crossing, Hitchin systems, and the WKB approximation". In: *Advances in Mathematics* 234 (2013), pp. 239–403. ISSN: 0001-8708. DOI: `https://doi.org/10.1016/j.aim.2012.09.027`. URL: `https://www.sciencedirect.com/science/article/pii/S0001870812003593`.

[110] Davide Gaiotto, Gregory W. Moore, and Andrew Neitzke. "Framed BPS States". In: *Adv. Theor. Math. Phys.* 17.2 (2013), pp. 241–397. DOI: `10.4310/ATMP.2013.v17.n2.a1`. arXiv: `1006.0146 [hep-th]`.

[111] Evgeny Andriyash et al. "Wall-crossing from supersymmetric galaxies". In: *JHEP* 01 (2012), p. 115. DOI: `10.1007/JHEP01(2012)115`. arXiv: `1008.0030 [hep-th]`.

[112] Jan Manschot, Boris Pioline, and Ashoke Sen. "Wall Crossing from Boltzmann Black Hole Halos". In: *JHEP* 07 (2011), p. 059. DOI: `10.1007/JHEP07(2011)059`. arXiv: `1011.1258 [hep-th]`.

[113] Clay Córdova and Andrew Neitzke. "Line Defects, Tropicalization, and Multi-Centered Quiver Quantum Mechanics". In: *JHEP* 09 (2014), p. 099. DOI: `10.1007/JHEP09(2014)099`. arXiv: `1308.6829 [hep-th]`.

[114] Davide Gaiotto, Gregory W. Moore, and Edward Witten. "Algebra of the Infrared: String Field Theoretic Structures in Massive $\mathcal{N} = (2,2)$ Field Theory In Two Dimensions". In: (June 2015). arXiv: 1506.04087 [hep-th].

[115] Mark Gross, Paul Hacking, and Sean Keel. "Mirror symmetry for log Calabi-Yau surfaces I". In: *arXiv e-prints*, arXiv:1106.4977 (June 2011), arXiv:1106.4977. arXiv: 1106.4977 [math.AG].

[116] Davide Gaiotto, Gregory W. Moore, and Andrew Neitzke. "Spectral networks". In: *Annales Henri Poincare* 14 (2013), pp. 1643–1731. DOI: 10.1007/s00023-013-0239-7. arXiv: 1204.4824 [hep-th].

[117] Lotte Hollands and Andrew Neitzke. "Spectral Networks and Fenchel–Nielsen Coordinates". In: *Lett. Math. Phys.* 106.6 (2016), pp. 811–877. DOI: 10.1007/s11005-016-0842-x. arXiv: 1312.2979 [math.GT].

[118] Lotte Hollands and Omar Kidwai. "Higher length-twist coordinates, generalized Heun's opers, and twisted superpotentials". In: *Adv. Theor. Math. Phys.* 22 (2018), pp. 1713–1822. DOI: 10.4310/ATMP.2018.v22.n7.a2. arXiv: 1710.04438 [hep-th].

[119] Sergey Fomin and Andrei Zelevinsky. "Cluster algebras IV: Coefficients". In: *arXiv Mathematics e-prints*, math/0602259 (Feb. 2006), math/0602259. arXiv: math/0602259 [math.RA].

[120] Melissa Sherman-Bennett. "Combinatorics of $\mathcal{X}$-variables in finite type cluster algebras". In: *arXiv e-prints*, arXiv:1803.02492 (Mar. 2018), arXiv:1803.02492. arXiv: 1803.02492 [math.CO].

[121] Nathan Reading. *A fan for every cluster*. https://math.berkeley.edu/~williams/FominTalks/Reading.pdf. Accessed: 2020–12-05. 2018.

[122] Nima Arkani-Hamed et al. "Binary Geometries, Generalized Particles and Strings, and Cluster Algebras". In: (Dec. 2019). arXiv: 1912.11764 [hep-th].

[123] Nima Arkani-Hamed. *Master Class: Spacetime and Quantum Mechanics, Positive Geometries and Cluster Algebras*. https://youtu.be/xOusuMq83Rg. Youtube, 2020.

[124] Chris Fraser. "Braid group symmetries of Grassmannian cluster algebras". In: *arXiv e-prints*, arXiv:1702.00385 (Feb. 2017), arXiv:1702.00385. arXiv: 1702.00385 [math.CO].

[125] Henriette Elvang and Yu-tin Huang. "Scattering Amplitudes". In: (Aug. 2013). arXiv: 1308.1697 [hep-th].

[126]   Dmitry Galakhov et al. "Wild Wall Crossing and BPS Giants". In: *JHEP* 11 (2013), p. 046. DOI: 10.1007/JHEP11(2013)046. arXiv: 1305.5454 [hep-th].

[127]   David Speyer and Lauren K. Williams. "The tropical totally positive Grassmannian". In: *arXiv Mathematics e-prints*, math/0312297 (Dec. 2003), math/0312297. arXiv: math/0312297 [math.CO].

[128]   James Drummond et al. "Tropical fans, scattering equations and amplitudes". In: (Feb. 2020). arXiv: 2002.04624 [hep-th].

[129]   David A. McGady and Laurentiu Rodina. "Higher-spin massless S-matrices in four-dimensions". In: *Phys. Rev. D* 90.8 (2014), p. 084048. DOI: 10.1103/PhysRevD.90.084048. arXiv: 1311.2938 [hep-th].

[130]   Clifford Cheung et al. "A Periodic Table of Effective Field Theories". In: *JHEP* 02 (2017), p. 020. DOI: 10.1007/JHEP02(2017)020. arXiv: 1611.03137 [hep-th].

[131]   Laurentiu Rodina. "Uniqueness from gauge invariance and the Adler zero". In: *JHEP* 09 (2019), p. 084. DOI: 10.1007/JHEP09(2019)084. arXiv: 1612.06342 [hep-th].

[132]   Nima Arkani-Hamed, Laurentiu Rodina, and Jaroslav Trnka. "Locality and Unitarity of Scattering Amplitudes from Singularities and Gauge Invariance". In: *Phys. Rev. Lett.* 120.23 (2018), p. 231602. DOI: 10.1103/PhysRevLett.120.231602. arXiv: 1612.02797 [hep-th].

[133]   Nima Arkani-Hamed, Tzu-Chen Huang, and Yu-tin Huang. "Scattering Amplitudes For All Masses and Spins". In: (Sept. 2017). arXiv: 1709.04891 [hep-th].

[134]   Laurentiu Rodina. "Scattering Amplitudes from Soft Theorems and Infrared Behavior". In: *Phys. Rev. Lett.* 122.7 (2019), p. 071601. DOI: 10.1103/PhysRevLett.122.071601. arXiv: 1807.09738 [hep-th].

[135]   Henriette Elvang et al. "Soft Bootstrap and Supersymmetry". In: *JHEP* 01 (2019), p. 195. DOI: 10.1007/JHEP01(2019)195. arXiv: 1806.06079 [hep-th].

[136]   Clifford Cheung et al. "Vector Effective Field Theories from Soft Limits". In: *Phys. Rev. Lett.* 120.26 (2018), p. 261602. DOI: 10.1103/PhysRevLett.120.261602. arXiv: 1801.01496 [hep-th].

[137]   Henriette Elvang. "Bootstrap and Amplitudes: A Hike in the Landscape of Quantum Field Theory". In: (July 2020). arXiv: 2007.08436 [hep-th].

[138]   Edward Witten. "Perturbative gauge theory as a string theory in twistor space". In: *Commun. Math. Phys.* 252 (2004), pp. 189–258. DOI: `10.1007/s00220-004-1187-3`. arXiv: `hep-th/0312171`.

[139]   Sabrina Pasterski, Shu-Heng Shao, and Andrew Strominger. "Flat Space Amplitudes and Conformal Symmetry of the Celestial Sphere". In: *Phys. Rev. D* 96.6 (2017), p. 065026. DOI: `10.1103/PhysRevD.96.065026`. arXiv: `1701.00049 [hep-th]`.

[140]   Clifford Cheung, Anton de la Fuente, and Raman Sundrum. "4D scattering amplitudes and asymptotic symmetries from 2D CFT". In: *JHEP* 01 (2017), p. 112. DOI: `10.1007/JHEP01(2017)112`. arXiv: `1609.00732 [hep-th]`.

[141]   Sabrina Pasterski, Shu-Heng Shao, and Andrew Strominger. "Gluon Amplitudes as 2d Conformal Correlators". In: *Phys. Rev. D* 96.8 (2017), p. 085006. DOI: `10.1103/PhysRevD.96.085006`. arXiv: `1706.03917 [hep-th]`.

[142]   Daniel Kapec et al. "Semiclassical Virasoro symmetry of the quantum gravity $\mathcal{S}$-matrix". In: *JHEP* 08 (2014), p. 058. DOI: `10.1007/JHEP08(2014)058`. arXiv: `1406.3312 [hep-th]`.

[143]   Sabrina Pasterski, Andrew Strominger, and Alexander Zhiboedov. "New Gravitational Memories". In: *JHEP* 12 (2016), p. 053. DOI: `10.1007/JHEP12(2016)053`. arXiv: `1502.06120 [hep-th]`.

[144]   Andrew Strominger. "Lectures on the Infrared Structure of Gravity and Gauge Theory". In: (Mar. 2017). arXiv: `1703.05448 [hep-th]`.

[145]   Nima Arkani-Hamed et al. "Celestial Amplitudes from UV to IR". In: (Dec. 2020). arXiv: `2012.04208 [hep-th]`.

[146]   Nima Arkani-Hamed et al. "Scattering Forms and the Positive Geometry of Kinematics, Color and the Worldsheet". In: *JHEP* 05 (2018), p. 096. DOI: `10.1007/JHEP05(2018)096`. arXiv: `1711.09102 [hep-th]`.

[147]   L.D. Landau. "On analytic properties of vertex parts in quantum field theory". In: *Nuclear Physics* 13.1 (1959), pp. 181–192. ISSN: 0029-5582. DOI: `https://doi.org/10.1016/0029-5582(59)90154-3`. URL: `https://www.sciencedirect.com/science/article/pii/0029558259901543`.

[148]   Ömer Gürdoğan and Matteo Parisi. "Cluster patterns in Landau and Leading Singularities via the Amplituhedron". In: (May 2020). arXiv: `2005.07154 [hep-th]`.

[149]   Nima Arkani-Hamed et al. "Causal Diamonds, Cluster Polytopes and Scattering Amplitudes". In: (2019). arXiv: `1912.12948 [hep-th]`.

[150] Nima Arkani-Hamed et al. *Work in Progress*.

[151] Freddy Cachazo et al. "Scattering Equations: From Projective Spaces to Tropical Grassmannians". In: *JHEP* 06 (2019), p. 039. DOI: `10.1007/JHEP06(2019)039`. arXiv: `1903.08904 [hep-th]`.

[152] Freddy Cachazo and Jairo M. Rojas. "Notes on Biadjoint Amplitudes, $\mathrm{Trop}\,G(3,7)$ and $X(3,7)$ Scattering Equations". In: *JHEP* 04 (2020), p. 176. DOI: `10.1007/JHEP04(2020)176`. arXiv: `1906.05979 [hep-th]`.

[153] Francisco Borges and Freddy Cachazo. "Generalized Planar Feynman Diagrams: Collections". In: (Oct. 2019). arXiv: `1910.10674 [hep-th]`.

[154] Freddy Cachazo, Bruno Umbert, and Yong Zhang. "Singular Solutions in Soft Limits". In: *JHEP* 05 (2020), p. 148. DOI: `10.1007/JHEP05(2020)148`. arXiv: `1911.02594 [hep-th]`.

[155] Freddy Cachazo et al. "Planar Matrices and Arrays of Feynman Diagrams". In: (Dec. 2019). arXiv: `1912.09422 [hep-th]`.

[156] Freddy Cachazo and Nick Early. "Minimal Kinematics: An all k and n peek into $\mathrm{Trop}^+G(k,n)$". In: (Mar. 2020). arXiv: `2003.07958 [hep-th]`.

[157] Freddy Cachazo and Nick Early. "Planar Kinematics: Cyclic Fixed Points, Mirror Superpotential, k-Dimensional Catalan Numbers, and Root Polytopes". In: (Oct. 2020). arXiv: `2010.09708 [math.CO]`.

[158] Walter D. Goldberger and Alexander K. Ridgway. "Radiation and the classical double copy for color charges". In: *Phys. Rev. D* 95.12 (2017), p. 125010. DOI: `10.1103/PhysRevD.95.125010`. arXiv: `1611.03493 [hep-th]`.

[159] Chia-Hsien Shen. "Gravitational Radiation from Color-Kinematics Duality". In: *JHEP* 11 (2018), p. 162. DOI: `10.1007/JHEP11(2018)162`. arXiv: `1806.07388 [hep-th]`.

[160] Clifford Cheung, Ira Z. Rothstein, and Mikhail P. Solon. "From Scattering Amplitudes to Classical Potentials in the Post-Minkowskian Expansion". In: *Phys. Rev. Lett.* 121.25 (2018), p. 251101. DOI: `10.1103/PhysRevLett.121.251101`. arXiv: `1808.02489 [hep-th]`.

[161] David A. Kosower, Ben Maybee, and Donal O'Connell. "Amplitudes, Observables, and Classical Scattering". In: *JHEP* 02 (2019), p. 137. DOI: `10.1007/JHEP02(2019)137`. arXiv: `1811.10950 [hep-th]`.

[162] Zvi Bern et al. "Scattering Amplitudes and the Conservative Hamiltonian for Binary Systems at Third Post-Minkowskian Order". In: *Phys. Rev. Lett.* 122.20 (2019), p. 201603. DOI: 10.1103/PhysRevLett.122.201603. arXiv: 1901.04424 [hep-th].

[163] Andrea Antonelli et al. "Energetics of two-body Hamiltonians in post-Minkowskian gravity". In: *Phys. Rev. D* 99.10 (2019), p. 104004. DOI: 10.1103/PhysRevD.99.104004. arXiv: 1901.07102 [gr-qc].

[164] N. Emil J. Bjerrum-Bohr, Taro V. Brown, and Humberto Gomez. "Scattering of Gravitons and Spinning Massive States from Compact Numerators". In: *JHEP* 04 (2021), p. 234. DOI: 10.1007/JHEP04(2021)234. arXiv: 2011.10556 [hep-th].

[165] Gabriel Luz Almeida, Stefano Foffa, and Riccardo Sturani. "Classical Gravitational Self-Energy from Double Copy". In: *JHEP* 11 (2020), p. 165. DOI: 10.1007/JHEP11(2020)165. arXiv: 2008.06195 [gr-qc].

[166] Johannes Broedel and Lance J. Dixon. "Color-kinematics duality and double-copy construction for amplitudes from higher-dimension operators". In: *JHEP* 10 (2012), p. 091. DOI: 10.1007/JHEP10(2012)091. arXiv: 1208.0876 [hep-th].

[167] Henriette Elvang et al. "Electromagnetic Duality and D3-Brane Scattering Amplitudes Beyond Leading Order". In: (June 2020). arXiv: 2006.08928 [hep-th].

[168] Ian Low, Laurentiu Rodina, and Zhewei Yin. "Double Copy in Higher Derivative Operators of Nambu-Goldstone Bosons". In: *Phys. Rev. D* 103.2 (2021), p. 025004. DOI: 10.1103/PhysRevD.103.025004. arXiv: 2009.00008 [hep-th].

[169] John Joseph M. Carrasco et al. "Simple encoding of higher derivative gauge and gravity counterterms". In: *Phys. Rev. Lett.* 125 (2020), p. 251602. DOI: 10.1103/PhysRevLett.125.251602. arXiv: 1910.12850 [hep-th].

[170] Laura A. Johnson, Callum R. T. Jones, and Shruti Paranjape. "Constraints on a Massive Double-Copy and Applications to Massive Gravity". In: *JHEP* 02 (2021), p. 148. DOI: 10.1007/JHEP02(2021)148. arXiv: 2004.12948 [hep-th].

[171] Z. Bern, J. J. M. Carrasco, and Henrik Johansson. "New Relations for Gauge-Theory Amplitudes". In: *Phys. Rev.* D78 (2008), p. 085011. DOI: 10.1103/PhysRevD.78.085011. arXiv: 0805.3993 [hep-ph].

[172] David J. Gross et al. "Heterotic String Theory. 2. The Interacting Heterotic String". In: *Nucl. Phys. B* 267 (1986), pp. 75–124. DOI: 10.1016/0550-3213(86)90146-X.

[173] Michael B. Green and John H. Schwarz. "Anomaly Cancellation in Supersymmetric D=10 Gauge Theory and Superstring Theory". In: *Phys. Lett. B* 149 (1984), pp. 117–122. DOI: 10.1016/0370-2693(84)91565-X.

[174] Stephan Stieberger and Tomasz R. Taylor. "Closed String Amplitudes as Single-Valued Open String Amplitudes". In: *Nucl. Phys.* B881 (2014), pp. 269–287. DOI: `10.1016/j.nuclphysb.2014.02.005`. arXiv: `1401.1218 [hep-th]`.

[175] Zvi Bern et al. "The Duality Between Color and Kinematics and its Applications". In: (Sept. 2019). arXiv: `1909.01358 [hep-th]`.

[176] Zvi Bern et al. "Ultraviolet Properties of $\mathcal{N} = 8$ Supergravity at Five Loops". In: *Phys. Rev.* D98.8 (2018), p. 086021. DOI: `10.1103/PhysRevD.98.086021`. arXiv: `1804.09311 [hep-th]`.

[177] John Joseph M. Carrasco, Laurentiu Rodina, and Suna Zekioglu. "Composing Effective Prediction at Five Points". In: (Apr. 2021). arXiv: `2104.08370 [hep-th]`.

[178] Quentin Bonnefoy et al. "The seeds of EFT double copy". In: *JHEP* 05 (2022), p. 042. DOI: `10.1007/JHEP05(2022)042`. arXiv: `2112.11453 [hep-th]`.

[179] Johannes Broedel, Oliver Schlotterer, and Stephan Stieberger. "Polylogarithms, Multiple Zeta Values and Superstring Amplitudes". In: *Fortsch. Phys.* 61 (2013), pp. 812–870. DOI: `10.1002/prop.201300019`. arXiv: `1304.7267 [hep-th]`.

[180] Carlos R. Mafra, Oliver Schlotterer, and Stephan Stieberger. "Complete N-Point Superstring Disk Amplitude II. Amplitude and Hypergeometric Function Structure". In: *Nucl. Phys.* B873 (2013), pp. 461–513. DOI: `10.1016/j.nuclphysb.2013.04.022`. arXiv: `1106.2646 [hep-th]`.

[181] John Joseph M. Carrasco, Carlos R. Mafra, and Oliver Schlotterer. "Semi-abelian Z-theory: NLSM+ϕ^3 from the open string". In: *JHEP* 08 (2017), p. 135. DOI: `10.1007/JHEP08(2017)135`. arXiv: `1612.06446 [hep-th]`.

[182] Lionel Mason and David Skinner. "Ambitwistor strings and the scattering equations". In: *JHEP* 07 (2014), p. 048. DOI: `10.1007/JHEP07(2014)048`. arXiv: `1311.2564 [hep-th]`.

[183] Nathan Berkovits. "Infinite Tension Limit of the Pure Spinor Superstring". In: *JHEP* 03 (2014), p. 017. DOI: `10.1007/JHEP03(2014)017`. arXiv: `1311.4156 [hep-th]`.

[184] Tim Adamo, Eduardo Casali, and David Skinner. "Ambitwistor strings and the scattering equations at one loop". In: *JHEP* 04 (2014), p. 104. DOI: `10.1007/JHEP04(2014)104`. arXiv: `1312.3828 [hep-th]`.

[185] Eduardo Casali et al. "New Ambitwistor String Theories". In: *JHEP* 11 (2015), p. 038. DOI: `10.1007/JHEP11(2015)038`. arXiv: `1506.08771 [hep-th]`.

[186] Soner Albayrak and Savan Kharel. "Towards the higher point holographic momentum space amplitudes". In: *JHEP* 02 (2019), p. 040. DOI: `10.1007/JHEP02(2019)040`. arXiv: `1810.12459 [hep-th]`.

[187] Soner Albayrak, Savan Kharel, and David Meltzer. "On duality of color and kinematics in (A)dS momentum space". In: (Dec. 2020). arXiv: `2012.10460 [hep-th]`.

[188] Connor Armstrong, Arthur E. Lipstein, and Jiajie Mei. "Color/kinematics duality in AdS_4". In: *JHEP* 02 (2021), p. 194. DOI: `10.1007/JHEP02(2021)194`. arXiv: `2012.02059 [hep-th]`.

[189] Luis F. Alday et al. "Gluon Scattering in AdS from CFT". In: (Mar. 2021). arXiv: `2103.15830 [hep-th]`.

[190] Xinan Zhou. "Double Copy Relation for AdS". In: (June 2021). arXiv: `2106.07651 [hep-th]`.

[191] Charlotte Sleight and Massimo Taronna. "On the consistency of (partially-)massless matter couplings in de Sitter space". In: (June 2021). arXiv: `2106.00366 [hep-th]`.

[192] Charlotte Sleight and Massimo Taronna. "Spinning Mellin Bootstrap: Conformal Partial Waves, Crossing Kernels and Applications". In: *Fortsch. Phys.* 66.8-9 (2018), p. 1800038. DOI: `10.1002/prop.201800038`. arXiv: `1804.09334 [hep-th]`.

[193] Leonardo Rastelli and Xinan Zhou. "Mellin amplitudes for $AdS_5 \times S^5$". In: *Phys. Rev. Lett.* 118.9 (2017), p. 091602. DOI: `10.1103/PhysRevLett.118.091602`. arXiv: `1608.06624 [hep-th]`.

[194] Xinan Zhou. "On Superconformal Four-Point Mellin Amplitudes in Dimension $d > 2$". In: *JHEP* 08 (2018), p. 187. DOI: `10.1007/JHEP08(2018)187`. arXiv: `1712.02800 [hep-th]`.

[195] Leonardo Rastelli and Xinan Zhou. "How to Succeed at Holographic Correlators Without Really Trying". In: *JHEP* 04 (2018), p. 014. DOI: `10.1007/JHEP04(2018)014`. arXiv: `1710.05923 [hep-th]`.

[196] Luis F. Alday and Xinan Zhou. "All Holographic Four-Point Functions in All Maximally Supersymmetric CFTs". In: *Phys. Rev. X* 11.1 (2021), p. 011056. DOI: `10.1103/PhysRevX.11.011056`. arXiv: `2006.12505 [hep-th]`.

[197] Luis F. Alday and Xinan Zhou. "All Tree-Level Correlators for M-theory on $AdS_7 \times S^4$". In: *Phys. Rev. Lett.* 125.13 (2020), p. 131604. DOI: `10.1103/PhysRevLett.125.131604`. arXiv: `2006.06653 [hep-th]`.

[198] Lorenz Eberhardt, Shota Komatsu, and Sebastian Mizera. *Work in Progress; Talk at QCD meets Gravity VI*.

[199] Sebastian Mizera. "Status of Intersection Theory and Feynman Integrals". In: *PoS* MA2019 (2019), p. 016. arXiv: 2002.10476 [hep-th].

[200] Hjalte Frellesvig et al. "Decomposition of Feynman Integrals by Multivariate Intersection Numbers". In: *JHEP* 03 (2021), p. 027. DOI: 10.1007/JHEP03(2021)027. arXiv: 2008.04823 [hep-th].

[201] S. Laporta. "High precision calculation of multiloop Feynman integrals by difference equations". In: *Int. J. Mod. Phys. A* 15 (2000), pp. 5087–5159. DOI: 10.1016/S0217-751X(00)00215-7. arXiv: hep-ph/0102033.

[202] A. von Manteuffel and C. Studerus. *Reduze 2 - Distributed Feynman Integral Reduction*. Jan. 2012. arXiv: 1201.4330 [hep-ph].

[203] Andreas von Manteuffel and Robert M. Schabinger. "A novel approach to integration by parts reduction". In: *Phys. Lett. B* 744 (2015), pp. 101–104. DOI: 10.1016/j.physletb.2015.03.029. arXiv: 1406.4513 [hep-ph].

[204] Philipp Maierhöfer, Johann Usovitsch, and Peter Uwer. "Kira—A Feynman integral reduction program". In: *Comput. Phys. Commun.* 230 (2018), pp. 99–112. DOI: 10.1016/j.cpc.2018.04.012. arXiv: 1705.05610 [hep-ph].

[205] Pierpaolo Mastrolia and Sebastian Mizera. "Feynman Integrals and Intersection Theory". In: *JHEP* 02 (2019), p. 139. DOI: 10.1007/JHEP02(2019)139. arXiv: 1810.03818 [hep-th].

[206] Hjalte Frellesvig et al. "Decomposition of Feynman Integrals on the Maximal Cut by Intersection Numbers". In: *JHEP* 05 (2019), p. 153. DOI: 10.1007/JHEP05(2019)153. arXiv: 1901.11510 [hep-ph].

[207] Hjalte Frellesvig et al. "Vector Space of Feynman Integrals and Multivariate Intersection Numbers". In: *Phys. Rev. Lett.* 123.20 (2019), p. 201602. DOI: 10.1103/PhysRevLett.123.201602. arXiv: 1907.02000 [hep-th].

[208] Sebastian Mizera and Andrzej Pokraka. "From Infinity to Four Dimensions: Higher Residue Pairings and Feynman Integrals". In: *JHEP* 02 (2020), p. 159. DOI: 10.1007/JHEP02(2020)159. arXiv: 1910.11852 [hep-th].

[209] Miguel S. Costa et al. "Spinning Conformal Correlators". In: *JHEP* 11 (2011), p. 071. DOI: 10.1007/JHEP11(2011)071. arXiv: 1107.3554 [hep-th].

[210] F. A. Dolan and H. Osborn. "Conformal partial waves and the operator product expansion". In: *Nucl. Phys. B* 678 (2004), pp. 491–507. DOI: `10.1016/j.nuclphysb.2003.11.016`. arXiv: `hep-th/0309180`.

[211] Ilija Buric et al. "Gaudin Models and Multipoint Conformal Blocks: General Theory". In: (Apr. 2021). arXiv: `2105.00021 [hep-th]`.

[212] Ilija Buric et al. "From Gaudin Integrable Models to d-dimensional Multipoint Conformal Blocks". In: *Phys. Rev. Lett.* 126.2 (2021), p. 021602. DOI: `10.1103/PhysRevLett.126.021602`. arXiv: `2009.11882 [hep-th]`.

[213] A. Liam Fitzpatrick et al. "A Natural Language for AdS/CFT Correlators". In: *JHEP* 11 (2011), p. 095. DOI: `10.1007/JHEP11(2011)095`. arXiv: `1107.1499 [hep-th]`.

[214] Miguel F. Paulos. "Towards Feynman rules for Mellin amplitudes". In: *JHEP* 10 (2011), p. 074. DOI: `10.1007/JHEP10(2011)074`. arXiv: `1107.1504 [hep-th]`.

[215] Daniel Z. Freedman et al. "Correlation functions in the CFT(d) / AdS(d+1) correspondence". In: *Nucl. Phys. B* 546 (1999), pp. 96–118. DOI: `10.1016/S0550-3213(99)00053-X`. arXiv: `hep-th/9804058`.

[216] Igor R. Klebanov and Edward Witten. "AdS / CFT correspondence and symmetry breaking". In: *Nucl. Phys. B* 556 (1999), pp. 89–114. DOI: `10.1016/S0550-3213(99)00387-9`. arXiv: `hep-th/9905104`.

[217] M. Gunaydin and N. Marcus. "The Unitary Supermultiplet of $N = 8$ Conformal Superalgebra Involving Fields of Spin ≤ 2". In: *Class. Quant. Grav.* 2 (1985), p. L19. DOI: `10.1088/0264-9381/2/2/002`.

[218] M. Gunaydin, D. Minic, and Marco Zagermann. "4D doubleton conformal theories, CPT and IIB string on $AdS_5 \times S^5$". In: *Nucl. Phys. B* 534 (1998). [Erratum: Nucl.Phys.B 538, 531–531 (1999)], pp. 96–120. DOI: `10.1016/S0550-3213(98)00543-4`. arXiv: `hep-th/9806042`.

[219] Matan Grinberg and Juan Maldacena. "Proper time to the black hole singularity from thermal one-point functions". In: *JHEP* 03 (2021), p. 131. DOI: `10.1007/JHEP03(2021)131`. arXiv: `2011.01004 [hep-th]`.

[220] Simon Caron-Huot. "Analyticity in Spin in Conformal Theories". In: *JHEP* 09 (2017), p. 078. DOI: `10.1007/JHEP09(2017)078`. arXiv: `1703.00278 [hep-th]`.

[221] David Simmons-Duffin, Douglas Stanford, and Edward Witten. "A spacetime derivation of the Lorentzian OPE inversion formula". In: *JHEP* 07 (2018), p. 085. DOI: `10.1007/JHEP07(2018)085`. arXiv: `1711.03816 [hep-th]`.

[222] Vittorio Del Duca, Lance J. Dixon, and Fabio Maltoni. "New color decompositions for gauge amplitudes at tree and loop level". In: *Nucl. Phys.* B571 (2000), pp. 51–70. DOI: 10.1016/S0550-3213(99)00809-3. arXiv: hep-ph/9910563 [hep-ph].

[223] Ronald Kleiss and Hans Kuijf. "Multi - Gluon Cross-sections and Five Jet Production at Hadron Colliders". In: *Nucl. Phys. B* 312 (1989), pp. 616–644. DOI: 10.1016/0550-3213(89)90574-9.

[224] Eduardo Casali and Andrea Puhm. "Double Copy for Celestial Amplitudes". In: *Phys. Rev. Lett.* 126.10 (2021), p. 101602. DOI: 10.1103/PhysRevLett.126.101602. arXiv: 2007.15027 [hep-th].

[225] Eduardo Casali and Atul Sharma. "Celestial double copy from the worldsheet". In: *JHEP* 05 (2021), p. 157. DOI: 10.1007/JHEP05(2021)157. arXiv: 2011.10052 [hep-th].

[226] Nikhil Kalyanapuram. "Gauge and Gravity Amplitudes on the Celestial Sphere". In: *Phys. Rev. D* 103.8 (2021), p. 085015. DOI: 10.1103/PhysRevD.103.085015. arXiv: 2012.04579 [hep-th].

[227] Gordon Chalmers et al. "R current correlators in N=4 superYang-Mills theory from anti-de Sitter supergravity". In: *Nucl. Phys. B* 540 (1999), pp. 247–270. DOI: 10.1016/S0550-3213(98)00758-5. arXiv: hep-th/9805105.

[228] Savan Kharel and George Siopsis. "Tree-level Correlators of scalar and vector fields in AdS/CFT". In: *JHEP* 11 (2013), p. 159. DOI: 10.1007/JHEP11(2013)159. arXiv: 1308.2515 [hep-th].

[229] Miguel S. Costa, Vasco Gonçalves, and João Penedones. "Spinning AdS Propagators". In: *JHEP* 09 (2014), p. 064. DOI: 10.1007/JHEP09(2014)064. arXiv: 1404.5625 [hep-th].

[230] Alexander Zhiboedov. "A note on three-point functions of conserved currents". In: (June 2012). arXiv: 1206.6370 [hep-th].

[231] Eric D'Hoker, Daniel Z. Freedman, and Leonardo Rastelli. "AdS / CFT four point functions: How to succeed at z integrals without really trying". In: *Nucl. Phys. B* 562 (1999), pp. 395–411. DOI: 10.1016/S0550-3213(99)00526-X. arXiv: hep-th/9905049.

[232] Simon Caron-Huot and Yue-Zhou Li. "Helicity basis for three-dimensional conformal field theory". In: (Feb. 2021). arXiv: 2102.08160 [hep-th].

[233] Matthias R. Gaberdiel and Rajesh Gopakumar. "The Worldsheet Dual of Free Super Yang-Mills in 4D". In: (May 2021). arXiv: 2105.10496 [hep-th].

[234] Matthias R. Gaberdiel and Rajesh Gopakumar. "The String Dual to Free $\mathcal{N} = 4$ Super Yang-Mills". In: (Apr. 2021). arXiv: 2104.08263 [hep-th].

[235] Miguel F. Paulos et al. "The S-matrix bootstrap. Part I: QFT in AdS". In: *JHEP* 11 (2017), p. 133. DOI: 10.1007/JHEP11(2017)133. arXiv: 1607.06109 [hep-th].

[236] Yue-Zhou Li. "Notes on flat-space limit of AdS/CFT". In: (June 2021). arXiv: 2106.04606 [hep-th].

[237] Oluf Tang Engelund and Radu Roiban. "Correlation functions of local composite operators from generalized unitarity". In: *JHEP* 03 (2013), p. 172. DOI: 10.1007/JHEP03(2013)172. arXiv: 1209.0227 [hep-th].

[238] Adam Bzowski, Paul McFadden, and Kostas Skenderis. "Conformal n-point functions in momentum space". In: *Phys. Rev. Lett.* 124.13 (2020), p. 131602. DOI: 10.1103/PhysRevLett.124.131602. arXiv: 1910.10162 [hep-th].

[239] Adam Bzowski, Paul McFadden, and Kostas Skenderis. "Conformal correlators as simplex integrals in momentum space". In: *JHEP* 01 (2021), p. 192. DOI: 10.1007/JHEP01(2021)192. arXiv: 2008.07543 [hep-th].

[240] Sachin Jain et al. "Double copy structure of parity-violating CFT correlators". In: (Apr. 2021). arXiv: 2104.12803 [hep-th].

[241] Joseph Polchinski and Matthew J. Strassler. "Hard scattering and gauge / string duality". In: *Phys. Rev. Lett.* 88 (2002), p. 031601. DOI: 10.1103/PhysRevLett.88.031601. arXiv: hep-th/0109174.

[242] Richard C. Brower et al. "The Pomeron and gauge/string duality". In: *JHEP* 12 (2007), p. 005. DOI: 10.1088/1126-6708/2007/12/005. arXiv: hep-th/0603115.

[243] Humberto Gomez, Renann Lipinski Jusinskas, and Arthur Lipstein. "Cosmological scattering equations at tree-level and one-loop". In: *JHEP* 07 (2022), p. 004. DOI: 10.1007/JHEP07(2022)004. arXiv: 2112.12695 [hep-th].

[244] Junyu Liu et al. "d-dimensional SYK, AdS Loops, and $6j$ Symbols". In: *JHEP* 03 (2019), p. 052. DOI: 10.1007/JHEP03(2019)052. arXiv: 1808.00612 [hep-th].

[245] Radu Roiban has pointed out that this representation of Witten diagrams is very reminiscent of the Q-cut representation of Feynman diagrams [262].

[246] Tensor reduction implies that for the integral in Eq. (4.161) to not vanish, it must be proportional to $p_i \cdot p_j$. However, $p_i \cdot p_j$ vanishes for massless external kinematics at three-point.

[247] David Simmons-Duffin. "Projectors, Shadows, and Conformal Blocks". In: *JHEP* 04 (2014), p. 146. DOI: 10.1007/JHEP04(2014)146. arXiv: 1204.3894 [hep-th].

[248] Dean Carmi, Lorenzo Di Pietro, and Shota Komatsu. "A Study of Quantum Field Theories in AdS at Finite Coupling". In: *JHEP* 01 (2019), p. 200. DOI: 10.1007/JHEP01(2019)200. arXiv: 1810.04185 [hep-th].

[249] For example, due to the presense of the constant tensor v, $D_{12}(v \cdot D_1)\mathcal{C}_4$ is *not* equal to $D_{34}(v \cdot D_1)\mathcal{C}_4$.

[250] Sergey Fomin and Andrei Zelevinsky. "Cluster algebras I: Foundations". In: *arXiv Mathematics e-prints*, math/0104151 (Apr. 2001), math/0104151. arXiv: math/0104151 [math.RT].

[251] Sergey Fomin and Andrei Zelevinsky. "Cluster algebras II: Finite type classification". In: *Inventiones Mathematicae* 154.1 (Oct. 2003), pp. 63–121. DOI: 10.1007/s00222-003-0302-y. arXiv: math/0208229 [math.RA].

[252] Arkady Berenstein, Sergey Fomin, and Andrei Zelevinsky. "Cluster algebras III: Upper bounds and double Bruhat cells". In: *arXiv Mathematics e-prints*, math/0305434 (May 2003), math/0305434. arXiv: math/0305434 [math.RT].

[253] Lauren K. Williams. "Cluster algebras: an introduction". In: *arXiv e-prints*, arXiv:1212.6263 (Dec. 2012), arXiv:1212.6263. arXiv: 1212.6263 [math.RA].

[254] Sergey Fomin, Lauren Williams, and Andrei Zelevinsky. "Introduction to Cluster Algebras. Chapters 1-3". In: *arXiv e-prints*, arXiv:1608.05735 (Aug. 2016), arXiv:1608.05735. arXiv: 1608.05735 [math.CO].

[255] Sergey Fomin, Lauren Williams, and Andrei Zelevinsky. "Introduction to Cluster Algebras. Chapters 4-5". In: *arXiv e-prints*, arXiv:1707.07190 (July 2017), arXiv:1707.07190. arXiv: 1707.07190 [math.CO].

[256] Sergey Fomin, Lauren Williams, and Andrei Zelevinsky. "Introduction to Cluster Algebras. Chapter 6". In: *arXiv e-prints*, arXiv:2008.09189 (Aug. 2020), arXiv:2008.09189. arXiv: 2008.09189 [math.AC].

[257] Henriette Elvang et al. "All-Multiplicity One-Loop Amplitudes in Born-Infeld Electrodynamics from Generalized Unitarity". In: *JHEP* 03 (2020), p. 009. DOI: 10.1007/JHEP03(2020)009. arXiv: 1906.05321 [hep-th].

[258] Ansgar Denner, U. Nierste, and R. Scharf. "A Compact expression for the scalar one loop four point function". In: *Nucl. Phys. B* 367 (1991), pp. 637–656. DOI: 10.1016/0550-3213(91)90011-L.

[259] Massimo Bianchi et al. "Instantons in supersymmetric Yang-Mills and D instantons in IIB superstring theory". In: *JHEP* 08 (1998), p. 013. DOI: 10.1088/1126-6708/1998/08/013. arXiv: hep-th/9807033.

[260] Michael Borinsky. "Tropical Monte Carlo quadrature for Feynman integrals". In: (Aug. 2020). arXiv: 2008.12310 [math-ph].

[261] For example, although the function $P_1^2 f(P_i)$ is zero everywhere as boundary correlators are only defined when $P_i^2 = 0$, its derivative is non-zero. Ignoring this subtlety can lead to contradictions when using derivatives to find identities among D-functions.

[262] Christian Baadsgaard et al. "New Representations of the Perturbative S-Matrix". In: *Phys. Rev. Lett.* 116.6 (2016), p. 061601. DOI: 10.1103/PhysRevLett.116.061601. arXiv: 1509.02169 [hep-th].